Application of the cyclobutane scaffold to the preparation and study of new foldamers, cell penetrating peptides and MRI contrast agents

José Antonio Olivares Montia

Universitat Autònoma de Barcelona

Application of the cyclobutane scaffold to the preparation and study of new foldamers, cell penetrating peptides and MRI contrast agents

José Antonio Olivares Montia

Tesi Doctoral

Estudi de Doctorat en Química

Supervised by:

Prof. Rosa Mª Ortuño Mingarro

Dr. Ona Illa Soler

Departament de Química

Facultat de Ciències

2018

Memòria presentada per aspirar al Grau de Doctor per **José Antonio Olivares Montia**

This thesis is presented for Graduation as Doctor by **José Antonio Olivares Montia**

Vist i plau,

Read and approved,

Prof. Rosa Mª Ortuño Mingarro

Dr. Ona Illa Soler

Bellaterra, 27 de Setembre de 2018

Bellaterra, 27th of September 2018

Acknowledgements

This thesis has been carried out in the *Departament de Química* of the *Universitat Autònoma de Barcelona (UAB)* under the direction of Professor Rosa Mª Ortuño and Doctor Ona Illa. I sincerely would like to thank both of them the opportunity to work in their group and collaborate in several projects that resulted in this thesis. I want to thank Rosa and Ona for the confidence placed in me and for their scientific advice. I want to specially thank Ona for her personal support during the development of this thesis.

Thanks to the *UAB* for the financial support received through a *Personal Investigador en Formació (PIF)* grant, which was very appreciated to carry out this thesis.

I would like to thank Dr. Míriam Royo for giving me the chance to work for six months in her group in the Combinatorial Chemistry Unit at Parc Científic of Barcelona (UQC-PCB). Also, I wish to specially thank Imma and Vida for teaching me different methodologies and techniques about peptide science during this collaboration. Moreover, I want to thank Dani, Joseju, Sonia, Natalia and Patricia for their advices, help and support during the stay.

Furthermore, I want to thank Prof. Carme Nogués and Dr. Nerea Gaztelumendi in the Departament de Biologia Cel·lular, de Fisiologia i d'Immunologia at the Universitat Autònoma of Barcelona, for carrying the biological studies with *HeLa* cells. Specially, I want to thank Nerea for her effort, dedication and patience during the experiments.

Additionally, I would like to thank Dr. Luis Rivas and Dr. Mª Angeles Abengozar of Centro de Investigaciones Biologicas-CSIC (PIB-CSIC) in Madrid for the development of the biological tests with *Leishmania* parasites. Also, I want to thank Luis for giving me the opportunity to visit his group and work with them for a week.

I want to thank Dr. Pau Nolis of the *Servei de Ressonància Magnètica Nuclear* (*SeRMN*) of the *Universitat Autònoma de Barcelona* for carrying out structural studies of different molecules.

In addition, I would like to thank Dr. Oriol Porcar for performing the studies related to the complexation of metals as potential contrast agents under the supervision of Dr. Eva Jacab Toth, in the Centre de Biophysique Moléculaire (CBM) in Orléans, France. I want to thank Eva for her collaboration in the field.

I would like to extend my thanks to all labmates I have been working with, Carme, Jimena, Bernat, Oriol, Jennifer, Jordi, Ramon, Ester, Carlos, Marc, Agustí, Jose, Marina, Xavi and Guillem for the scientific discussions and the laughs spent together.

Moreover, I want to thank my family, specially my parents for their unconditional support before and during the development of this thesis. Finally, I want to thank Laura for helping me during the hardest times and listening to all the problems and difficulties found while performing this thesis. Without her affection and support I could not overcome them.

Part of the results reported in this thesis have been published in the following scientific article:

- **The relevance of the relative configuration in the folding of hybrid peptides containing β-cyclobutane amino acids and γ-amino-L-proline residues.**

  Ona Illa, José Antonio Olivares, Pau Nolis, Rosa M. Ortuño.
  Tetrahedron, **2017**, *73*, 6283-6295.

Other articles with the rest of the results are under preparation and will be published as soon as possible.

Table of contents

1.1 Table of abbreviations

Alloc	1-Allyloxycarbonyl
Boc	*tert*-Butyloxycarbonyl
CA	Contrast Agent
CBAA	Cyclobutane Amino Acid
Cbz	Benzyloxycarbonyl
CEST	Chemical Exchange Saturation Transfer
CF	5(6)-Carboxyfluorescein
CL	Cutaneous Leishmaniasis
CPPs	Cell Penetrating Peptides
DAPI	2-(4-Amidinophenyl)-1*H*-indole-6-carboxamidine
DCL	Diffuse Cutaneous Leishmaniasis
DCM	Dichloromethane
DIC	*N*,*N*'-Diisopropylcarbodiimide
DIPEA	*N*,*N*-Diisopropylethylamine
DMAP	4-Dimethylaminopyridine
DMF	Dimethylformamide
DNA	Deoxyribonucleic Acid
ee	Enantiomeric excess
Fmoc	9-Fluorenylmethyloxycarbonyl
GABA	γ-Aminobutyric Acid
GAG	Glycosaminoglycan
HIV-1	Human Immunodeficiency Virus-1
HPLC	High Performance Liquid Chromatography
HPLC-MS	High Performance Liquid Chromatography-Mass Spectrometry
HSQC	Heteronuclear Single Quantum Coherence Spectroscopy
HSV-1	Herpes Simplex Virus Type 1
LR	Leishmaniasis Recidivans
MAP	Model Amphipathic Peptide
MCL	Mucocutaneous Leishmaniasis

MCPs	Metallocarboxypeptidase Inhibitors
MEM	Minimum Essential Media
MRI	Magnetic Resonance Imaging
MTT	3-(4,5-Dimethylthiazol-2-yl)-2,5-Diphenyltetrazolium Bromide
NFS	Nephrogenic Systemic Fibrosis
NMR	Nuclear Magnetic Resonance
NMRD	Nuclear Magnetic Relaxation Dispersion
NOESY	Nuclear Overhauser Effect Spectroscopy
PARACEST	Paramagnetic Chemical Exchange Saturation Transfer
PBS	Phosphate-Buffered Saline
PI	Propidium Iodide
PKDL	Post-Kala-Azar Dermal Leishmaniasis
ppm	Parts per million
PyBOP	(Benzotriazol-1-yloxy)-tripyrrolidinophosphonium hexafluorophospate
ROESY	Rotating Frame Nuclear Overhauser Effect Spectroscopy
RPMI	Roswell Park Memorial Institute
SD	Standard Deviation
SMCC	Succinimidyl 4-(*N*-maleimidomethyl)-cyclohexane-1-carboxylate
SPS	Solid Phase Synthesis
TAT	Trans-acting Activator of Transcription
TBAI	Tetrabutylammonium Iodide
TFA	Trifluoroacetic Acid
THF	Tetrahydrofuran
TIS	Triisopropylsilane
TMS	Trimethylsilyl
TOCSY	Total Correlation Spectroscopy
r.t.	Room temperature
VL	Visceral Leishmaniasis
WHO	World Health Organization

1.2 Preface

In this thesis, different systems containing a β- or γ-substituted cyclobutane scaffold have been synthesized and studied as foldamers, as cell penetrating peptides (CPP) or as contrast agents. Despite having different structures not directly related between them, the same synthetic strategies and techniques have been used to prepare the different compounds.

The thesis has been structured with a general introduction with some precedents from our research group, followed by the general objectives (Chapter 2). The results of the present thesis are presented in three different chapters (Chapters 3-5), which are divided in different sections. General conclusions are reported in Chapter 6 and the experimental methodologies can be found in Chapter 7.

- **Chapter 3**. Six families of peptides with different stereochemistry built with a cyclobutane containing amino acid (CBAA) in combination with γ-amino-L-proline were synthesized. The study of their folding ability was carried out by using high resolution NMR techniques in order to detect the formation of hydrogen bonds that could induce secondary structures. The information obtained in this chapter was very useful to design new cell penetrating peptides.

- **Chapter 4**. Different new peptides were synthesized by solid phase synthesis techniques and studied as potential penetrating agents in two biological systems: *HeLa* cells and *Leishmania* parasites. The best cell penetrating peptides were conjugated with a drug to study their effect in *Leishmania* parasites.

- **Chapter 5**. A new linear ligand containing a cyclobutane-based diamine was synthesized and complexed with different metal ions. The thermodynamic stability and the hydration number of these complexes were studied by means of different techniques. Their potential as new contrast agents for magnetic resonance imaging (MRI) was studied by different NMR methodologies.

2. General introduction and objectives

2. General introduction and objectives

2.1 Introduction

In the last decade, our research group "Synthesis, Structure and Chemical Reactivity (SERQ)" has been interested in the use of cyclobutane scaffolds as chiral platforms and conformational restriction elements for the synthesis of several new chiral compounds and their use in a wide diversity of applications. The presence of this highly constricting four-membered ring in the molecules provides both rigidity and two chiral centers of known and tunable absolute configuration that can be modified at will. Diverse enantioselective synthetic routes and methodologies were developed to achieve these compounds in an enantioselective manner.

Essentially, two differently disubstituted cyclobutane moieties have been used to prepare the compounds in our research group: the 1,2- or β-substituted cyclobutanes (Figure 1), and the 1,3- or γ-substituted ones (Figure 2). The β-substituted cyclobutane-combining compounds are prepared through a photochemical reaction between ethylene and maleic anhydride and the resulting meso adduct can be easily desymmetrized by a chemoenzymatic reaction. After that, several selective manipulations of the functional groups and epimerization of certain chiral centers allowed the synthesis of all possible stereoisomers.[1,2]

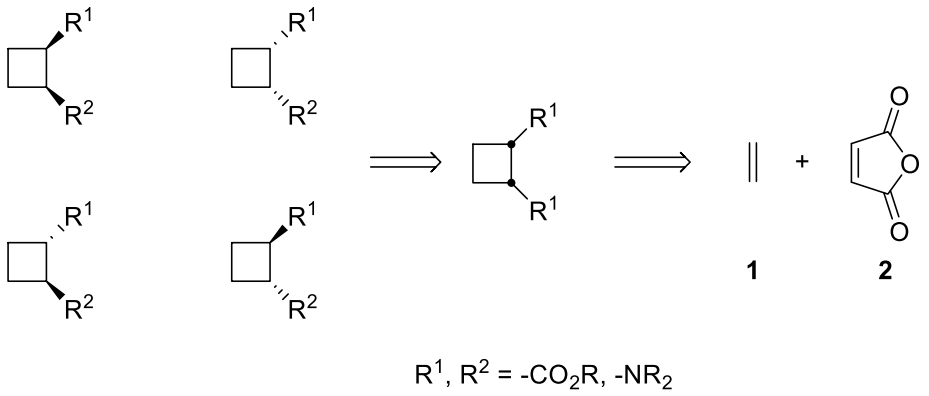

Figure 1. Schematic representation of all possible 1,2-disubstituted cyclobutane-based stereoisomers and their synthetic precursors.

The γ-substituted cyclobutane-based compounds are prepared using (-)-verbenone (**3**) or (-)-α-pinene (**4**) as starting materials (Figure 2), which can be commercially obtained with a reasonable price in an enantiopure form. Both compounds can be oxidized and selectively functionalized leading to different target compounds.[3] Unlike 1,2-disubstituted compounds, only *cis*-1,3-disubstituted cyclobutane moieties can be easily obtained to build chiral compounds from the chiral pool.

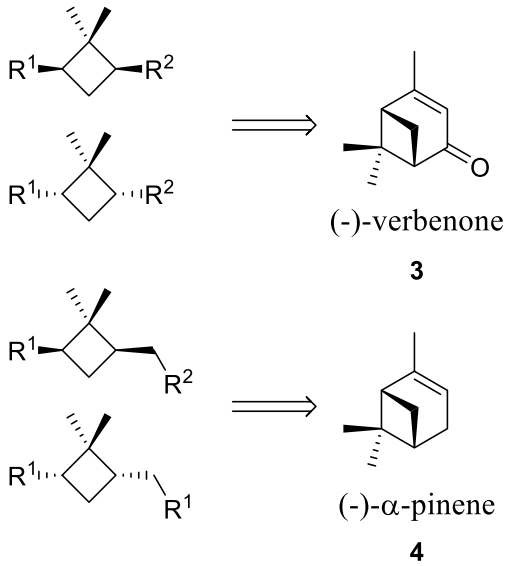

Figure 2. Schematic representation of 1,3-disubstituted cyclobutane-based compounds and their synthetic precursors.

The introduction of conformational restriction elements into molecules with inherent biological activity is essential to achieve interactions with the target receptors and to increase their metabolic stability and activity.[4,5,6] One of the main research lines of our group is the synthesis of cyclobutane-based amino acids (CBAA) and their use as building blocks. The rigidity provided by the cyclobutane scaffold and its well-defined conformation have been key properties for their application in different Chemistry and Biology areas. Some examples of cyclobutane-based compounds related to the fields of this thesis are explained in the introduction of each chapter.

Figure 3 shows some examples containing compounds with the β-substituted cyclobutane unit as building block, such as **5** which was studied as a metallocarboxypeptidase inhibitor (MCPs).[7] Cyclobutane-based thiourea **6** was studied as chiral organocatalysts in the Michael reaction.[8] Furthermore, applications of the cyclobutane scaffold focused in the field of materials can be found in organobridged silsesquioxanes **7** and **8**,[9] organogelator **9** [10] or bolaamphiphile surfactant **10** and other amphiphile surfactants.[11,12]

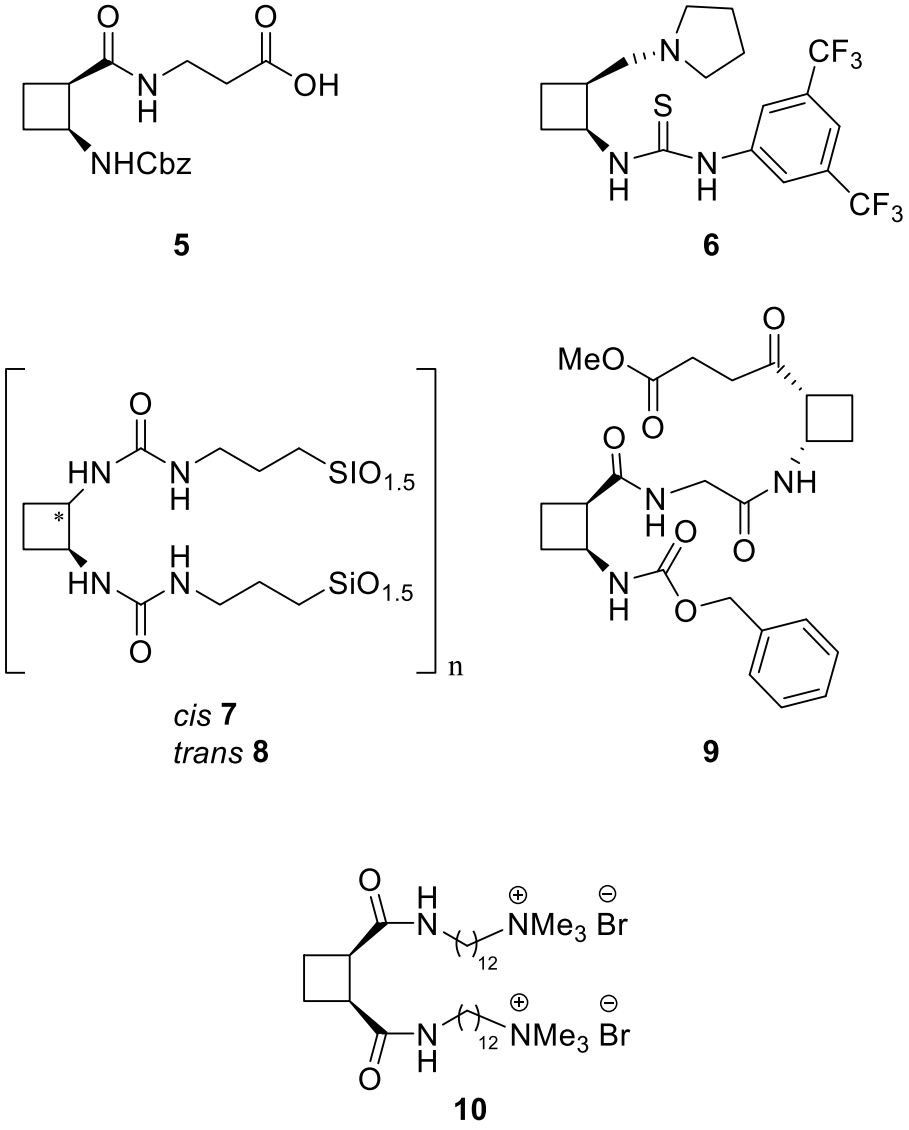

Figure 3. Structures of some examples of different β-substituted cyclobutane-based compounds synthesized in our group.

Figure 4 shows some examples containing the γ-substituted cyclobutane as building block. Diamine **11** performed as ruthenium nanoparticles stabilizer,[13] while amino acid **12** is a good example of a zwitterionic surfactant.[14] Tripeptide **13** works fine as organocatalyst in several asymmetric aldol reactions.[15] The final example is a C_3-symmetric peptide dendrimer **14** which could be applied in the field of chiral materials after further elongation and functionalization.[16]

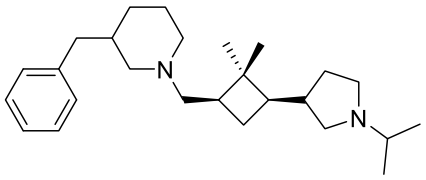

11

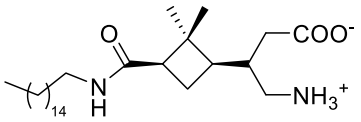

12

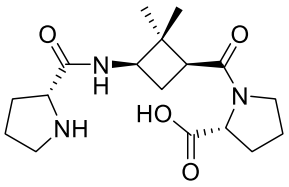

13

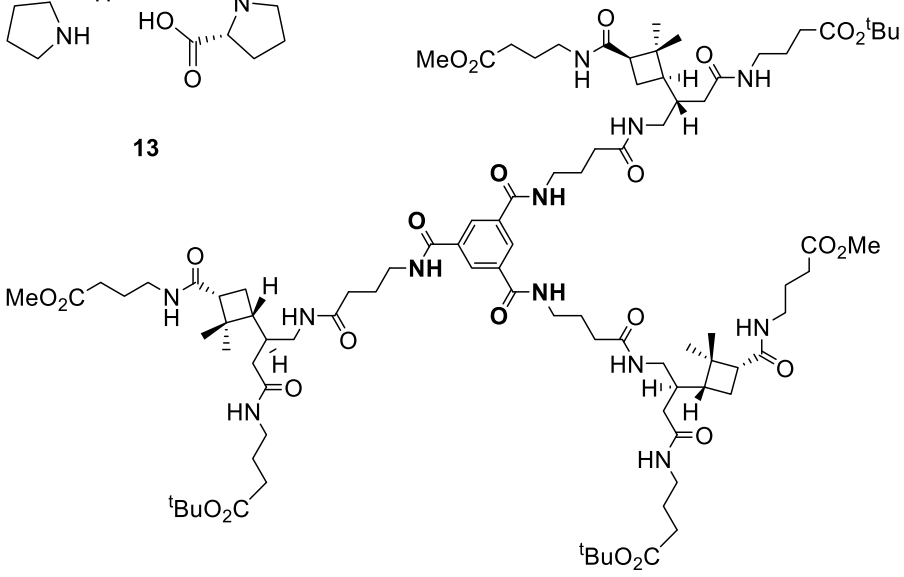

14

Figure 4. Structures of some examples of different γ-substituted cyclobutane-based compounds synthesized in our group.

2.2 Objectives

In this thesis, the chiral cyclobutane scaffold studied in our research group is used to build various compounds with different applications. Peptides as foldamers are synthesized and studied to understand the required folding patterns to develop and design new penetrating agents like cell penetrating peptides (CPPs). Moreover, using the previously acquired synthetic skills and similar cyclobutane platforms, a new ligand to bind Gd^{3+} is studied as contrast agent for Magnetic Resonance Imaging.

Taking into account this brief explanation, the main goals of this thesis are:

I. Objective 1: The synthesis of short CBAA,γ-amino-L-proline peptides: folding studies by high resolution NMR.

II. Objective 2: Synthesis of γ-CBAA,γ-amino-L-proline peptides as cell penetrating agents: studies in HeLa cells and *Leishmania* parasites.

III. Objective 3: The synthesis and physicochemical studies of a new Gd^{3+} complex of open-chain ligand as potential new MRI contrast agent.

3. Synthesis of Short Hybrid Cyclobutane-γ-amino-L-Proline Peptides: Folding Studies by High Resolution NMR

3. Synthesis of Short Hybrid Cyclobutane-γ-amino-L-Proline Peptides: Folding Studies by High Resolution NMR

3.1 Introduction

For several years, peptide chemistry has been studying the impact of the structural organization of peptides and proteins on their function. One of the most interesting areas is the use of peptides containing α-amino acids as potential drugs for treating diseases.[17] However, the instability of peptides containing α-amino acids towards enzymatic degradation has limited the synthesis and study of compounds with a potential pharmacology application. The need to find an alternative to overcome this problem while keeping in equilibrium some critical factors like stability, affinity, specificity and efficacy present in the natural peptides is one of the scientific hits.[18,19,20] Moreover, the necessity to mimic well known secondary structures that are only present in α-peptides is one of the most important research topic in the field. For this reason, the synthesis of peptides consisting of α-amino acids combined with unnatural ω-amino acids (ω is used for any other position that is not α such as β, γ, δ…) and totally ω,ω-peptides, could be a good solution. For example, the appearance of peptide-based foldamers,[21,22] which are synthetic oligomers containing unnatural amino acids or equivalent building blocks, has allowed the preparation of folded structures that mimic natural occurring ones: helices, strands, turns and ribbons, amongst others (Figure 5).[23,24,25] These structures are commonly generated by intra-molecular non-covalent interactions, mainly hydrogen bonds. Foldamers can be classified either by their secondary structure or by the backbone type.

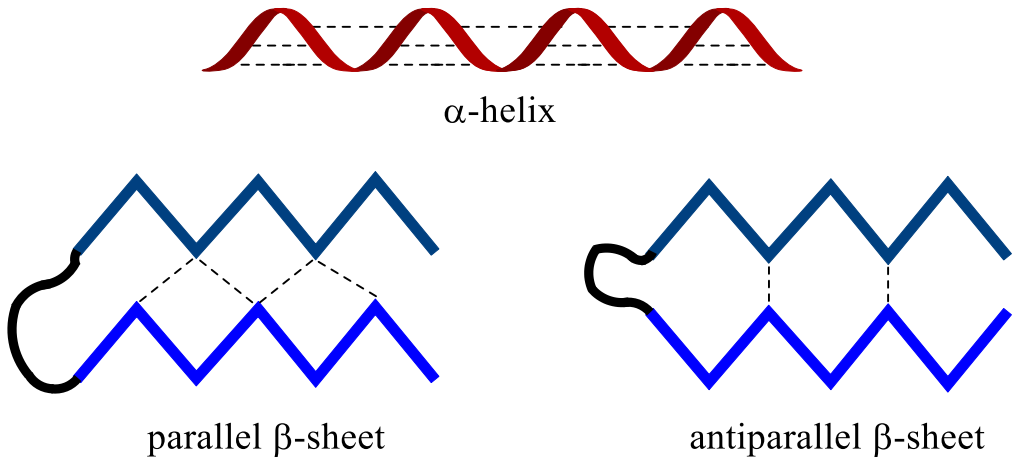

Figure 5. Representation of α-helix and β-sheets secondary structures.

β-Peptides (Figure 6) are probably the most extensively studied foldamers due to three main factors: their resemblance to α-peptides, the wide range of stabilized secondary structures that they can adopt and the different applications found.[26,27,28] For example, Gellman and co-workers studied the interactions of β-peptide **15** with phospholipids working as an antimicrobial agent.[29] This peptide mimicked the structure of a natural peptide adopting a 12-helical conformation, which was defined by a network of 12-membered ring C=O (*i*)→NH (*i*+*3*) hydrogen bonds. Ruetz and coworkers designed and synthesized a whole family of β-peptides (**16-19**) able to cross the cytoplasmic membrane and act as Trojan carriers, which transport and release drugs to the desired zone of the body.[30]

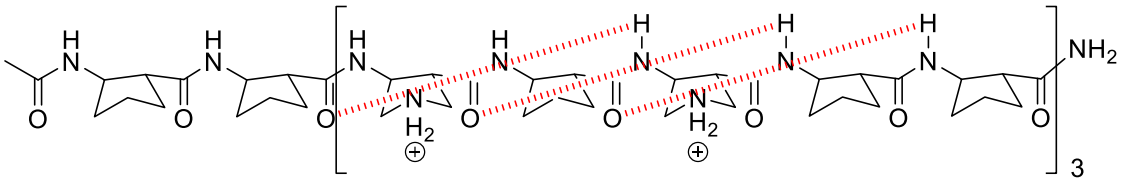

15

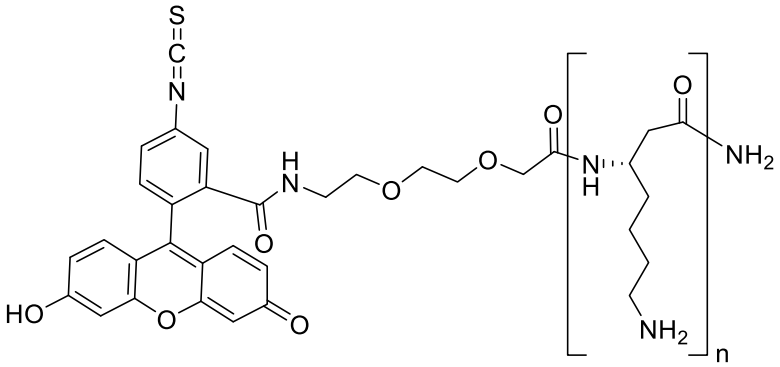

16: n=3
17: n=4
18: n=5
19: n=6

Figure 6. Examples of structures of β-peptides foldamers found in the bibliography. Red-dashed lines represent hydrogen bonds.

γ-Peptides represent the next step for the generation of new families of foldamers based on the amide backbone, but only few examples of them have been reported in the bibliography (Figure 7).[31,32,33] Hanessian and co-workers demonstrated that γ-amino acids could be used to build γ-peptides that adopt helical (**20**) and reverse turn (**21**) structures.[31]

Years later, Royo and collaborators designed different families of foldamers based on *cis*-γ-amino-L-proline (**22**).[33] The introduction of cyclic monomers as building blocks reduces the increased number of conformational freedom of γ-peptides, compared to α- and β-peptides. At the same time, the use of these monomers increases the stability of regular secondary structures.[34,35]

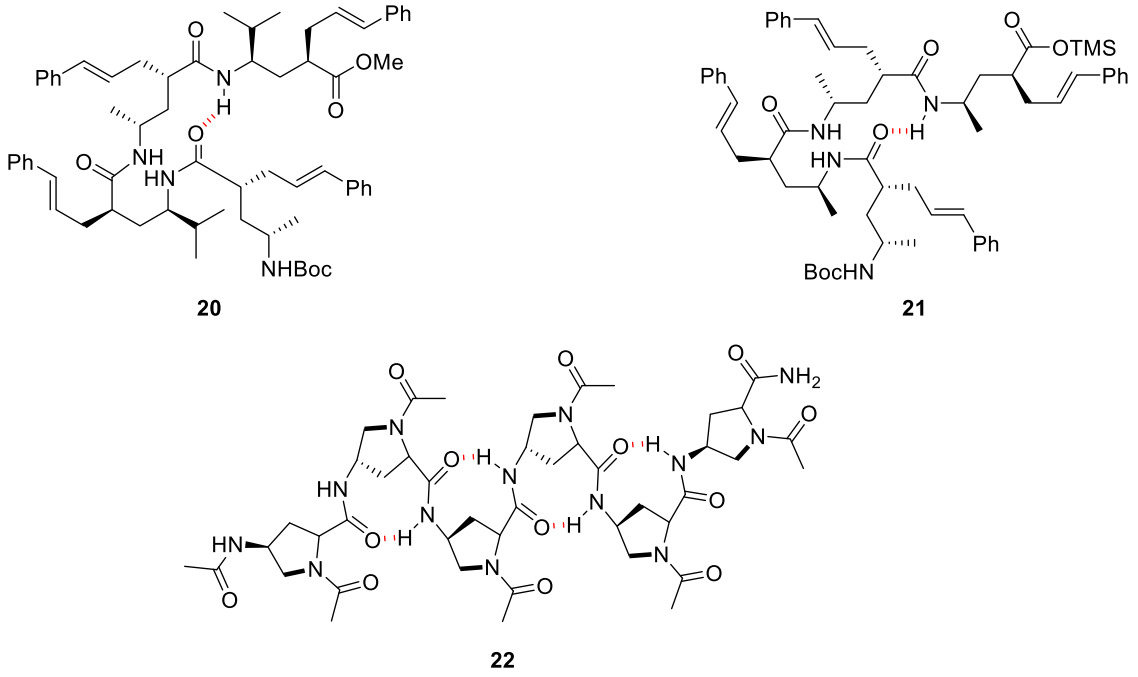

Figure 7. Examples of **s**tructures of γ-peptides foldamers found in the bibliography. Red-dashed lines represent hydrogen bonds.

Otherwise, if novel folding patterns are sought, other approaches may be entailed. Hybrid peptides can be obtained by alternate combination of the stereoisomer of the desired amino acid or with other α- or ω-amino acids.[36,37,38,39,40] Correspondence between α,ω- and ω,ω-sequences may be obtained if the number of backbone atoms are considered. This equivalence can be used to design and synthesize custom hybrid foldamers, since hydrogen-bonding patterns are directly associated to specific structural motifs (Figure 8).[41]

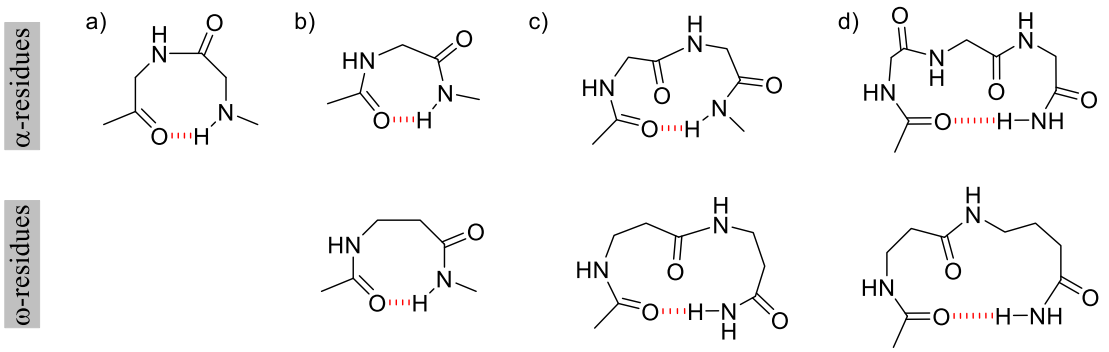

Figure 8. Schematic illustration of turns in all α-residue segments (*top*) and their equivalence in ω-residues (*bottom*). In parenthesis are the number of bonds present in α-residue segments a) δ-turn (C_8). b) γ-turn (C_7). c) β-turn (C_{10}). d) α-turn (C_{13}). Red-dashed lines represent hydrogen bonds.

Thus, n-membered hydrogen bonds could be constructed as suggested by the following hybrid dipeptide sequences as proposed by Balaram (Figure 9).[42]

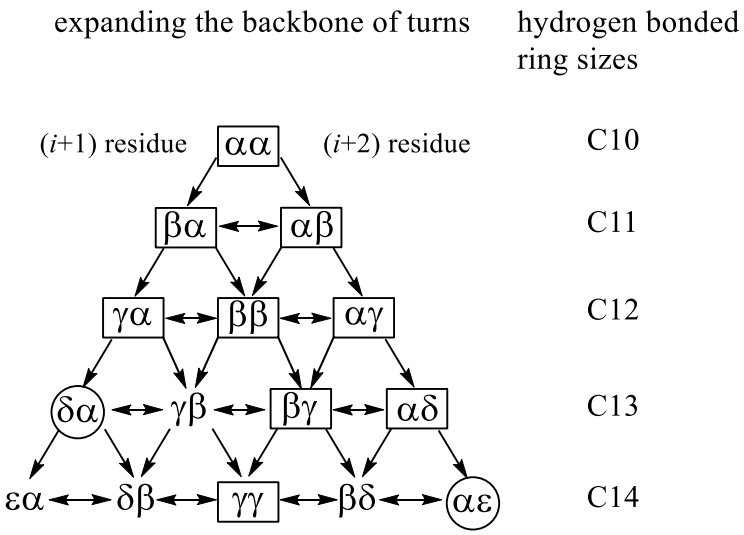

Figure 9. Hydrogen-bonded ring sizes that can be generated, in principle, from hybrid dipeptide sequences, the hydrogen-bond directionality being the same as in normal all α-polypeptide structures. Turns encircled with rectangles have been characterized in single crystals by X-ray diffraction. Turns established only by NMR are indicated with circles.

Our group has previously worked with the cyclobutane scaffold as building block for generating foldamers with a wide range of applications. Homopeptides containing all *cis*-β-CBAA (from di- to octapeptides) were synthesized and studied, observing the formation of an intraresidue six-membered hydrogen-bonded ring (6-strand).[43,44] On the other hand, a 12-helix arrangement was described by Aitken and co-workers for all-*trans*-β-CBAA hexa- and octapeptides.[45] Moreover, Dr. Gorrea developed and studied short peptides made of various combinations of the *cis* and *trans* isomers of this amino acid. The presence of a *trans* amino acid at the *N*-terminus of the peptide revealed the predominance of an eight-member hydrogen-bonded ring while the existence of a *cis* amino acid at the *N*-terminus of the peptide resulted in the formation of a six-member hydrogen-bonded ring (Figure 10).[46] Moreover, exhaustive NMR and computational studies of β-CBAA-containing oligopeptides demonstrated that the established chirality of the monomeric residues, present at any position of the sequence, controls and determines the most stable folding conformation.

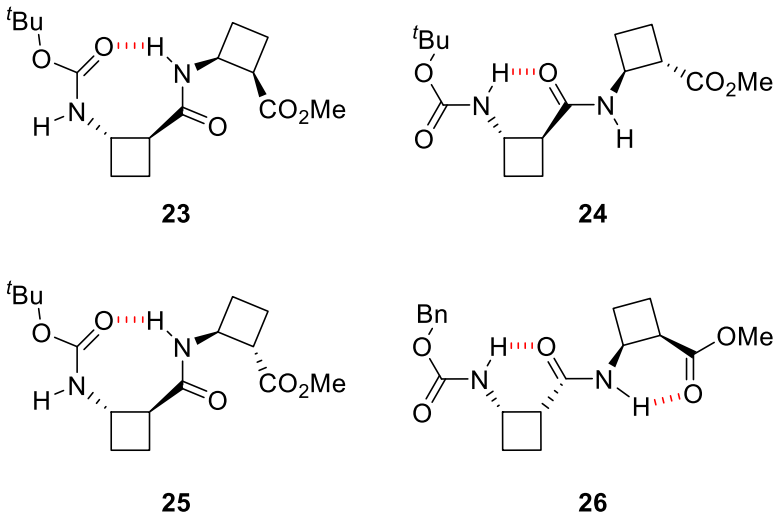

Figure 10. Folding patterns of previously studied β-CBAA-containing oligopeptides. Red-dashed lines represent hydrogen bonds.

The *cis*-CBAA promotes two conformers that produce zig-zag structures from six- and eight-membered hydrogen-bonded rings, Z6 and Z8, while the *trans* form act as a promoter to form a helical eight-membered hydrogen-bonded ring, H8 (Figure 11).[47,48]

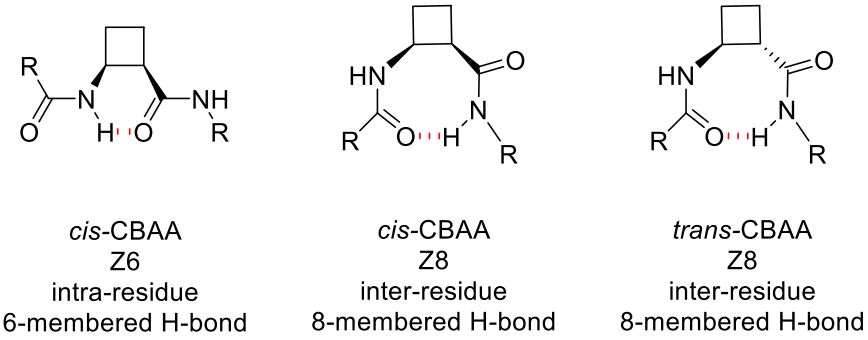

Figure 11. Intra- and inter-residue hydrogen bonds in peptides that incorporate either *cis*-β-CBAA or *trans*-β-CBAA. Red-dashed lines represent hydrogen bonds.

Hybrid oligomers containing β-CBAA conjugated in alternation with glycine, β-alanine or γ-amino butyric acid (GABA) have also been prepared. Results showed a different effect on the final folding depending on the used spacer, being able to modulate the preferential conformation of these hybrid peptides, which could be tuned from a β-sheet-like folding for those containing a glycine or a GABA residue, to a helical folding for those with a β-alanine between cyclobutane residues (Figure 12).[49] Hybrid peptides containing glycine and GABA residues showed the intra-residue 6-membered hydrogen bond (Figure 12a and 12c). Some of these β-CBAA and the peptides in which they have been used as skeleton have been found useful for diverse applications such as: functional organofibers,[50] organogelators,[10,51] neuropeptide Y inhibitors[52] and surfactants.[11,53]

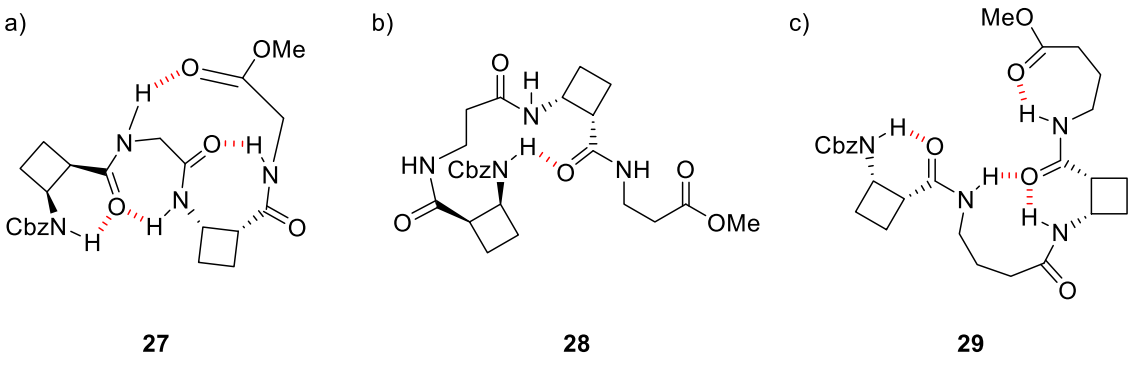

Figure 12. Folding patterns of previously studied β-CBAA-containing oligopeptides in alternation with glycine (a), β-alanine (b) and GABA (c). Red-dashed lines represent hydrogen bonds.

Regarding peptides containing γ-CBAAs, oligomers were built in alternation with GABA, following the previous study with β-CBAAs, and their folding patterns were studied.[54] The study revealed no defined conformation in contrast with those observed for peptides containing β-CBAAs, probably due to the rigidity and sterically demanding moiety used in these cases (Figure 13).

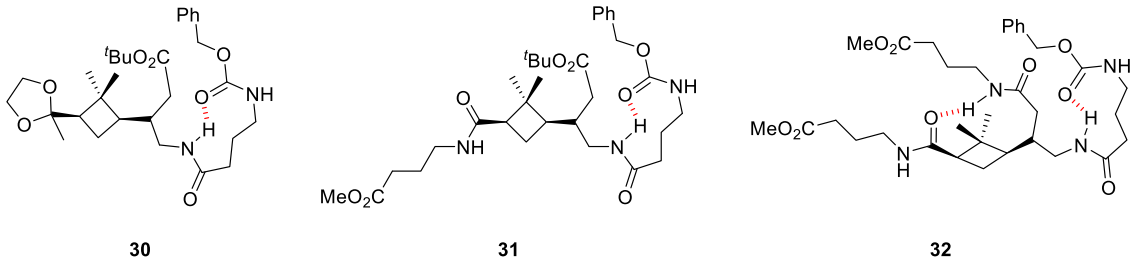

Figure 13. Folding patterns of previously studied γ-CBAA-containing oligopeptides in alternation with 1 (**30**), 2 (**31**) or 3 (**32**) GABA residues. Red-dashed lines represent hydrogen bonds.

Some years ago, our group carried out a detailed structural study with hybrid peptides combining in alternation the cyclobutane moiety with N^{α}-Boc-protected *cis*-γ-amino-L-proline. [55] Proline is a naturally occurring amino acid which is conformationally constrained due to the pyrrolidine ring, inducing well defined secondary structures in peptides that contain it. γ-Amino-L-proline is a derivative of natural proline, which can be used in the synthesis of peptide foldamers acting either as α-amino acid[56] or as γ-amino acid. [33,57] The additional amino group not involved in the peptide bond formation may be functionalized with the introduction of side-chains.

The high resolution NMR study revealed the presence of a hydrogen bond promoting the formation of a strong intra-residue 7-membered ring within the proline residues and an inter-residue hydrogen bond was observed between the carbonyl of the *tert*-butyl carbamate group and the NH of the subsequent γ-CBAA residue (Figure 14).[57]

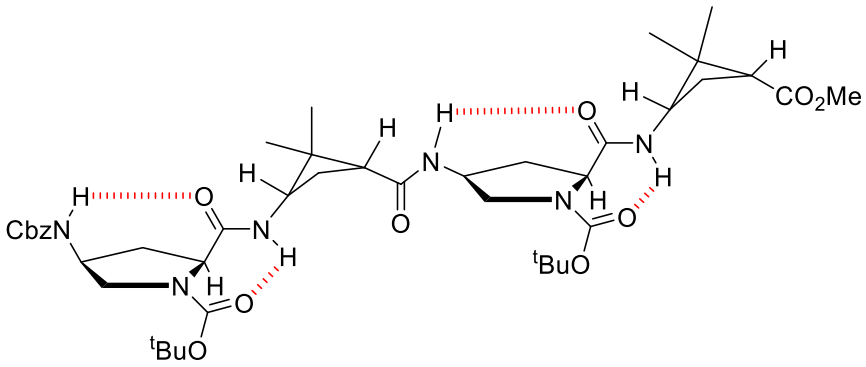

Figure 14. Intra- and inter-residue hydrogen bonds described in hybrid peptides consisting of γ-CBAAs and *cis*-γ-amino-L-proline joined in alternation.

Regarding their application, proline- and γ-aminoproline-based peptides have been reported to have excellent cell penetrating abilities. Further details will be discussed in Chapter 4 of this thesis.

3.2 Objectives

In this part of the thesis, the synthesis of six families of hybrid peptides containing *cis*- or *trans*-γ-amino-L-proline and β- or γ-cyclobutane amino acids of various relative and absolute configurations was proposed (Figure 15). The relevance of the relative configuration of the β- and γ-amino acids in the folding propensity of the resulting peptides would be studied and analyzed by means of high resolution NMR spectroscopy.

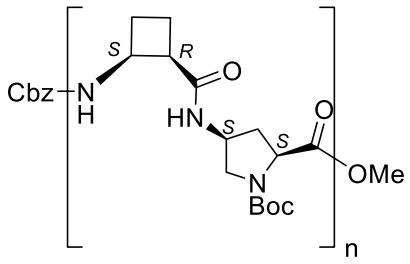

n = 1, β-*cis*,γ-*cis* **33**
n = 2, β-*cis*,γ-*cis* **34**

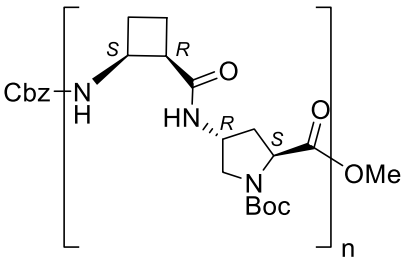

n = 1, β-*cis*,γ-*trans* **35**
n = 2, β-*cis*,γ-*trans* **36**

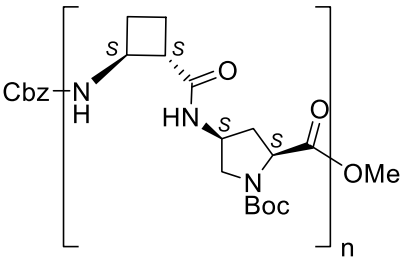

n = 1, β-*trans*,γ-*cis* **37**
n = 2, β-*trans*,γ-*cis* **38**

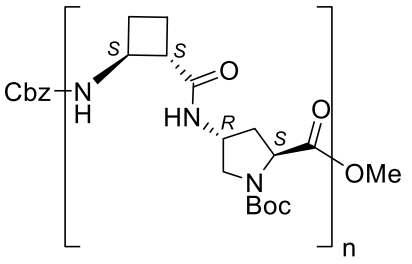

n = 1, β-*trans*,γ-*trans* **39**
n = 2, β-*trans*,γ-*trans* **40**

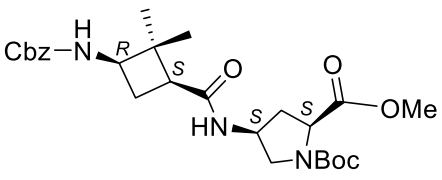

γ-*cis*,γ-*cis* **41**

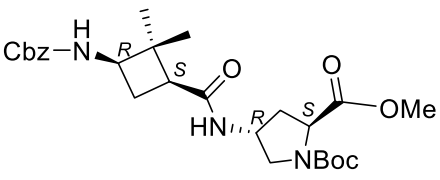

γ-*cis*,γ-*trans* **42**

Figure 15. Structures of the six proposed families of hybrid peptides to be studied as foldamers.

The objectives of this part were:

- The synthesis of the required monomers with suitable protections to be used for the synthesis of the peptides.
- The synthesis of the hybrid peptides shown in Figure 15.
- The study of their behavior as foldamers and the kind of interactions that could promote their arrangement depending on the relative and absolute configuration of the monomers.

3.3 Results and discussion

The results of this chapter of the thesis are presented in two different parts. First, the synthesis of the new hybrid CBAA,γ-amino-L-proline peptides to be studied as foldamers is detailed (section 3.3.1). Later, the studies of folding propensity explored through different high resolution ^{1}H NMR spectroscopy are described (section 3.3.2).

3.3.1 Synthesis of new hybrid peptides as foldamers

Taking into account the previously reported research in our group preparing enantiopure foldamers,[44-54,57] the proposed structures were envisaged through the retrosynthetic pathways shown in Scheme 1 and Scheme 2, depending on the CBAA used as building block.

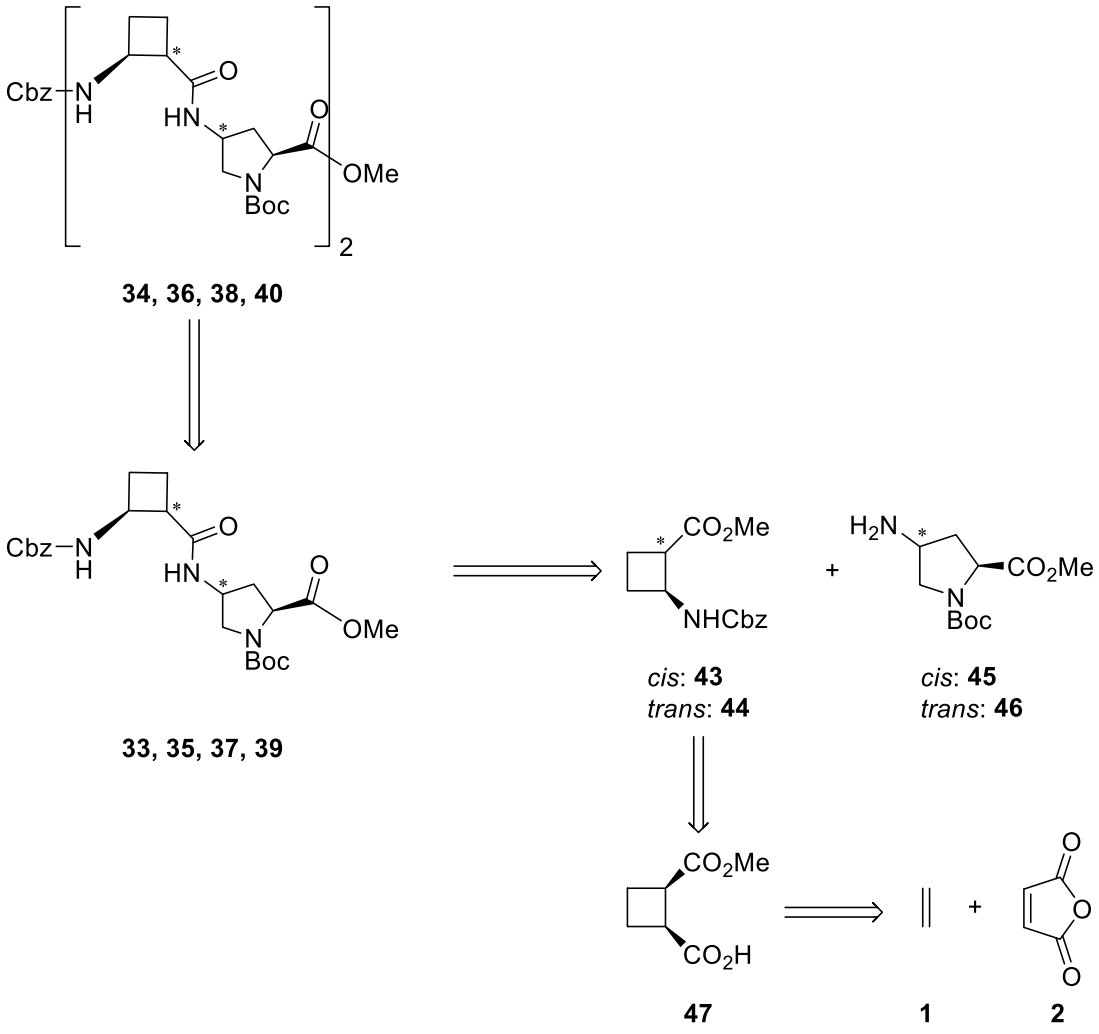

Scheme 1. General retrosynthetic analysis of β-CBAA-based hybrid peptides.

β-*cis*- (**43**) and β-*trans*- (**44**) cyclobutane-based amino acids were previously synthesized in our laboratory.[58,59] They derive, after several transformations, from a [2+2] cycloaddition between ethylene (**1**) and maleic anhydride (**2**). γ-Amino-L-proline in its both enantiopure forms *cis* (**45**) and *trans* (**46**), were commercially available as hydrochloride salt.

On the other hand, γ-cis-CBAA (**48**) was prepared in our group to be part of another series of γ-CBAA,γ-amino-*cis*-/*trans*-L-proline peptides. It was synthesized through several reactions starting with the oxidative cleavage of (-)-verbenone (**3**).

The synthetic routes for all compounds and the corresponding intermediates are explained in the next pages.

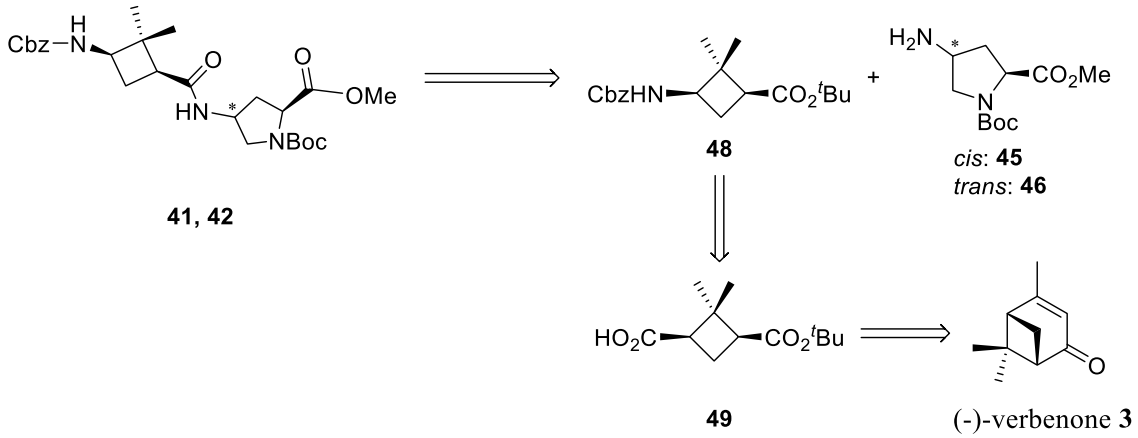

Scheme 2. General retrosynthetic analysis of γ-CBAA-based hybrid peptides.

3.3.1.1 Synthesis of partially protected β-*cis*-cyclobutane amino acid 52

Protected β-*cis*-CBAA **52** can be afforded after a synthetic route of five steps in a 42% overall yield. The synthetic pathway is described in Scheme 3.

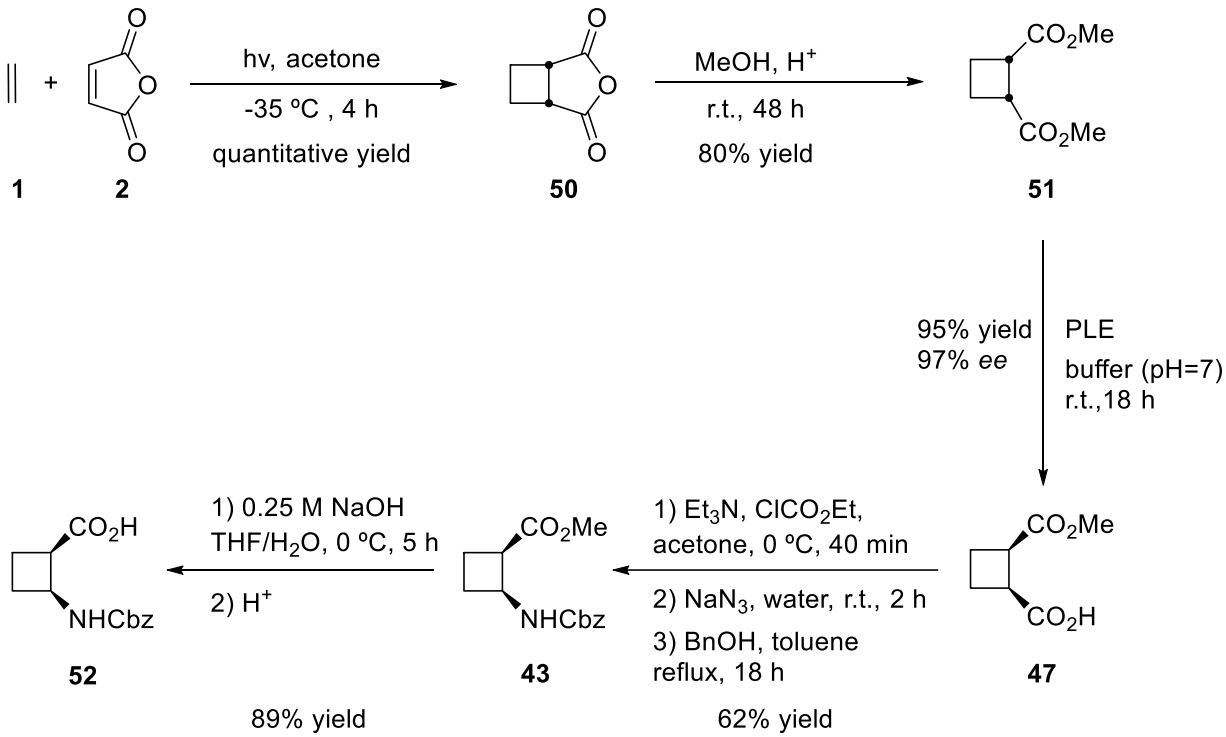

Scheme 3. Synthetic route for amino acid **52**.

The first step was the formation of the cyclobutane ring in quantitative yield by a [2+2] photochemical cycloaddition reaction from ethylene (**1**) and maleic anhydride (**2**).[60] This reaction occurred at -30 ºC in a Pyrex reactor in the presence of acetone acting both as solvent and as photosensitizer. The system was saturated with ethylene and irradiated during 4 hours using a medium pressure 400 W mercury lamp. Then, *meso* diester **51** was synthesized through Fischer esterification of the photoadduct **50** in 80% yield. Finally, optically active hemiester **47** was obtained through pig liver esterase-induced enantioselective hydrolysis of **51**, in >97% *ee* and 95% chemical yield.[61] The fully orthogonally protected amino acid **43** was prepared stepwise by treatment of **47** with ethyl chloroformate and triethylamine, followed by reaction with sodium azide. The resultant acyl azide was heated to reflux in the presence of benzyl alcohol.

The *in situ* formation of an isocyanide through a Curtius rearrangement and subsequent reaction with the alcohol, led to the desired carbamate **43** in 62% yield. Finally, a saponification reaction followed by an acidification afforded protected amino acid **52** in 89% yield.

3.3.1.2 Synthesis of protected β-*trans*-cyclobutane amino acid 59

Protected β-*trans*-CBAA **59** could be prepared after 5 or 9 steps, depending on the chosen synthetic route in a 12-18% overall yield from hemi ester **47**. The synthetic pathway is described in Schemes 4 and 5.

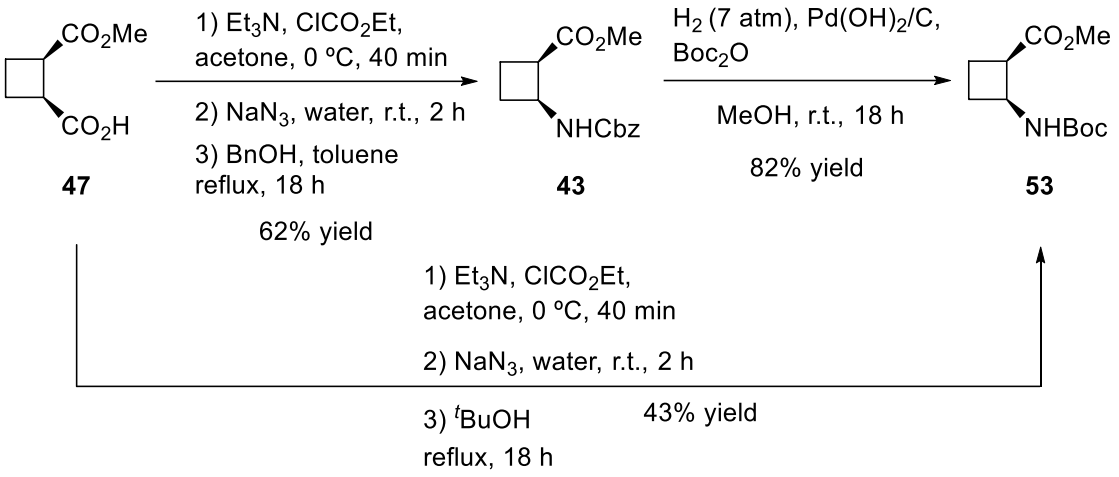

Scheme 4. Synthetic route for intermediate amino acid **53**.

Orthogonally diprotected amino acid **53** could be obtained using two different strategies. The first one was accomplished by a catalytic hydrogenation of amino acid **43** in the presence of di-*tert*-butyl dicarbonate with an overall yield of 51%. The second one was performed through a Curtius rearrangement in neat *tert*-butanol, but a lower yield of 43% was obtained due to the poor nucleophilic character of the alcohol.

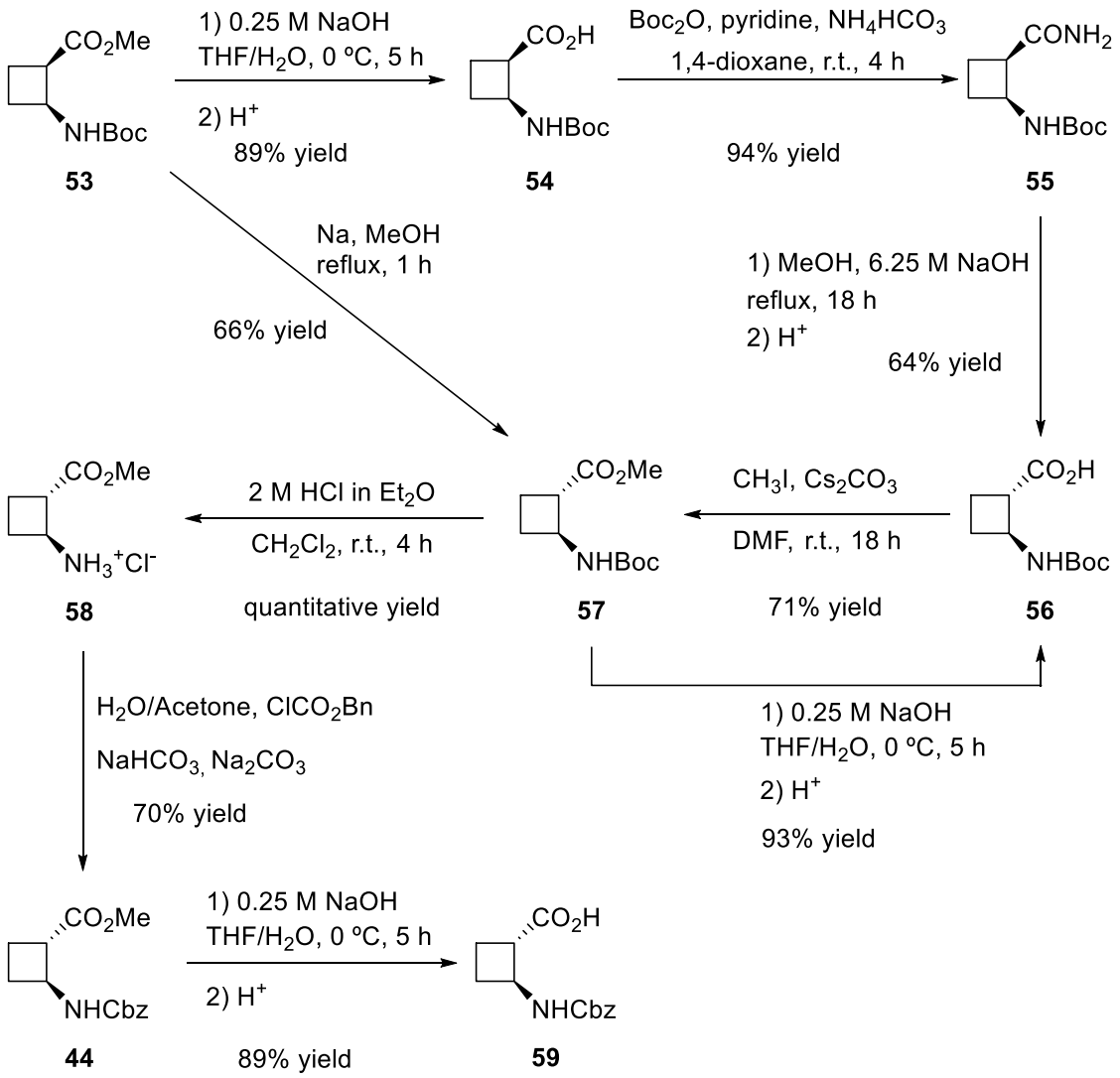

Scheme 5. Synthetic route for amino acid **59**.

The preparation of the protected β–*trans*-amino acid **57** could be easily achieved by the transformation of the methyl ester **53** into the unprotected amide **55** and subsequent epimerization of the carbonyl α-position. Afterwards, the basic hydrolysis of the amide allowed the formation of the *trans*-carboxylic acid **56** in 64% yield.[62] The protected amino acid **57** was achieved by methylation of **56** using methyl iodide and Cs_2CO_3 as a base in 71% yield. The overall yield for this synthetic route was 38%. Furthermore, another methodology to carry out the direct epimerization of the carbonyl α-position of ester **53** generating sodium methoxide *in situ* was described by Aitken and co-workers.[59] In this case, amino acid **57** was obtained directly in 66% yield.

After that, an acidolysis of the *N*-Boc protecting group followed immediately by a protection of the amine as benzyl carbamate led to orthogonally diprotected amino acid **44**. This protection was achieved by reacting **58** with benzyl chloroformate in the presence of $NaHCO_3$ and Na_2CO_3 in a water-acetone mixture. Finally, the saponification of methyl ester followed by acidification afforded β-*trans*-amino acid **59**.

3.3.1.3 Synthesis of dipeptides 33, 35, 37 and 39

Hybrid β-CBAA,γ-amino-L-proline dipeptides were synthesized by means of a coupling reaction between the corresponding β-CBAA *cis*-(**52**) or *trans*-(**59**) and the chosen commercially available γ-amino-L-proline *cis*-(**45**) or *trans*-(**46**). The synthetic route for all the families of peptides is shown in Scheme 6.

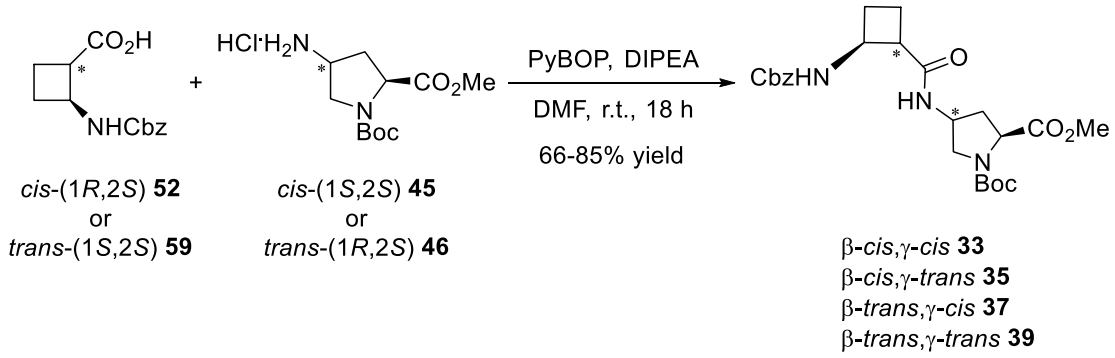

Scheme 6. Synthetic route to obtain β-CBAA-based dipeptides **33**, **35**, **37**, and **39**.

The coupling reaction was performed using PyBOP as coupling agent and DIPEA as base, obtaining β-*cis*,γ-*cis* **33** in 85%, β-*cis*,γ-*trans* **35** in 84%, β-*trans*,γ-*cis* **37** in 77% and β-*trans*,γ-*trans* **39** in 66% yield, respectively.

3.3.1.4 Synthesis of tetrapeptides 34, 36, 38 and 40

Hybrid β-CBAA,γ-amino-L-proline tetrapeptides were synthesized by means of a coupling reaction between the corresponding acid **60**-**63** with its equivalent amine **64-67.**

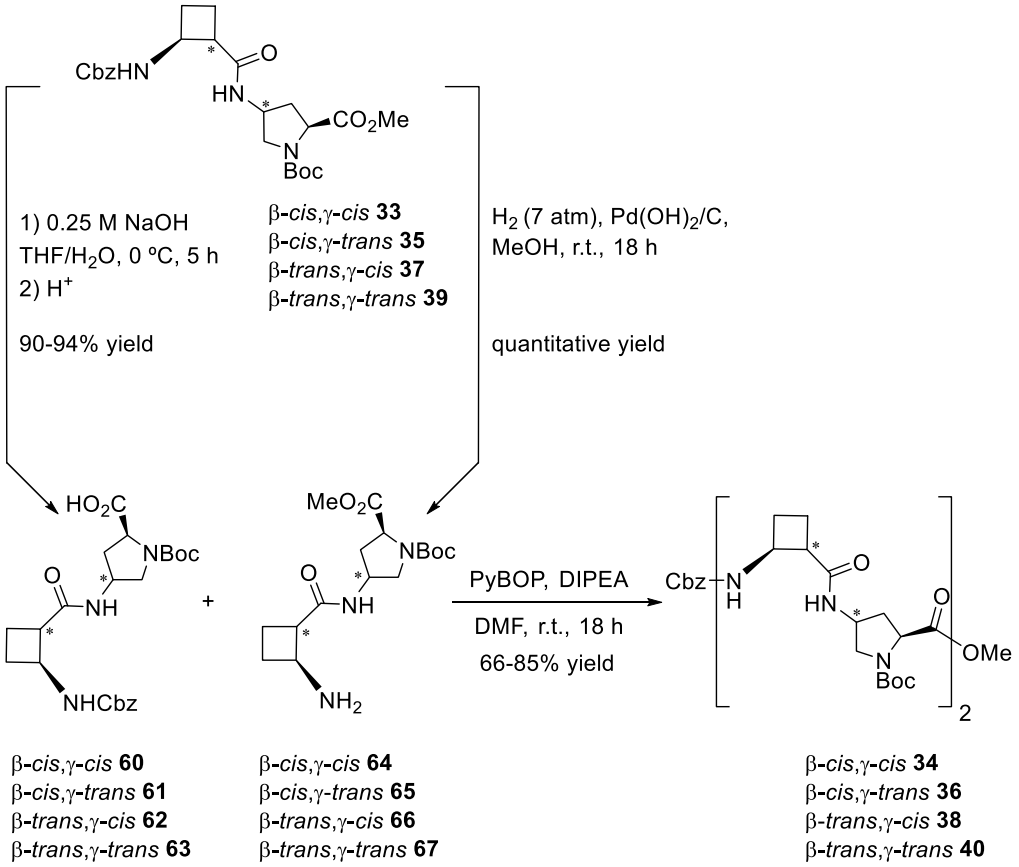

Scheme 7. Synthetic route to obtain β-CBAA-based tetrapeptides **34**, **36**, **38**, and **40**.

The unprotected carboxylic acid peptide series **60**-**63** were synthesized by performing a saponification of the methyl ester present in the γ-amino-L-proline residue of dipeptides **33**, **35**, **37** and **39** in 90-94% yield, respectively. On the other hand, an amine deprotection by catalytic hydrogenation of the benzyl carbamate present in **33**, **35**, **37** and **39** gave the unprotected amine series **64**-**67** in quantitative yield. Finally, a coupling reaction between each desired pair of acid **60**-**63** and amine **64**-**67** using PyBOP as coupling agent and DIPEA as base afforded β-*cis*,γ-*cis* **34** in 42%, β-*cis*,γ-*trans* **36** in 53%, β-*trans*,γ-*cis* **38** in 65% and β-*trans*,γ-*trans* **40** in 69% yield, respectively.

3.3.1.5 Synthesis of protected γ-*cis*-cyclobutane amino acid 70

Protected γ-*cis*-CBAA **70** could be achieved in 62% overall yield in 5 steps from enantiopure and commercially available (-)-verbenone **3**. The synthetic route is described in Scheme 8.

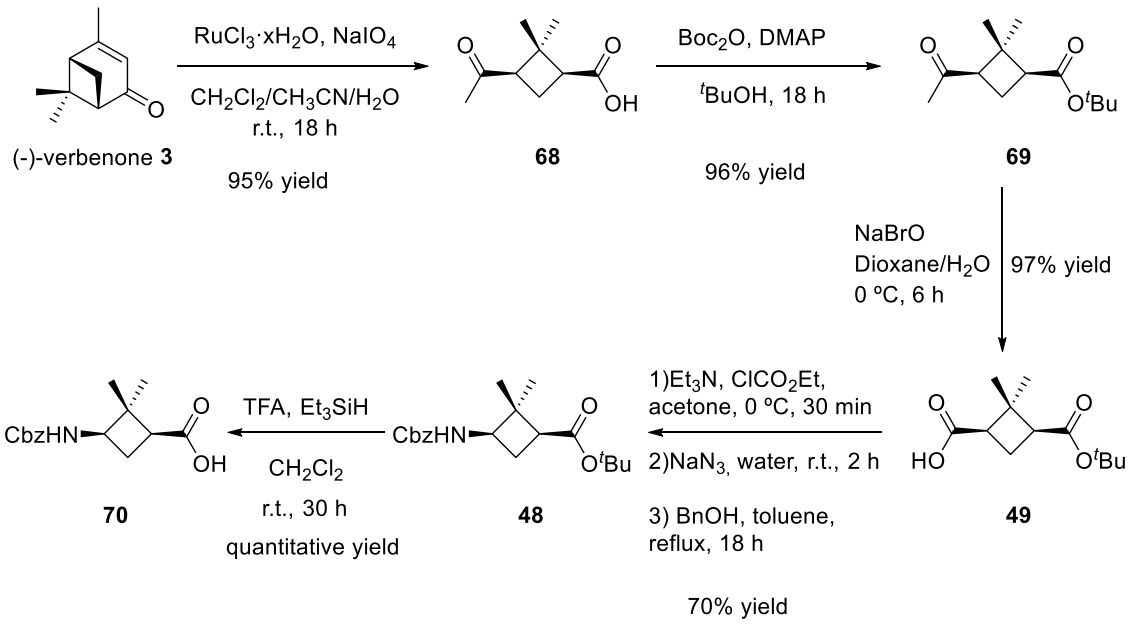

Scheme 8. Synthetic route for amino acid **70**.

In the first step of the synthesis of **70**, a catalytic oxidation of (-)-verbenone **3** led to (-)-*cis*-pinononic acid **68** in 95% yield without epimerization. Then, the carboxylic acid was protected as a *tert*-butyl ester in 96% yield using di-*tert*-butyl dicarbonate and a catalytic amount of DMAP. In the following step, the methyl ketone **69** was submitted to a Lieben degradation to afford carboxylic acid **49** in 97% yield. Subsequently, **49** was transformed into benzyl carbamate **48** through a 3-step procedure including a Curtius rearrangement in 70% yield. Finally, an acidolysis reaction of **48** in the presence of triethylsilane provided amino acid **70** in quantitative yield.[3]

3.3.1.6 Synthesis of dipeptides 41 and 42

Hybrid γ-CBAA,γ-amino-L-proline dipeptides were synthesized by means of a coupling reaction between the γ-*cis*-CBAA **70** and the chosen commercially available γ-amino-L-proline *cis*-(**45**) or *trans*-(**46**). The synthetic route for all families of peptides is shown in Scheme 9.

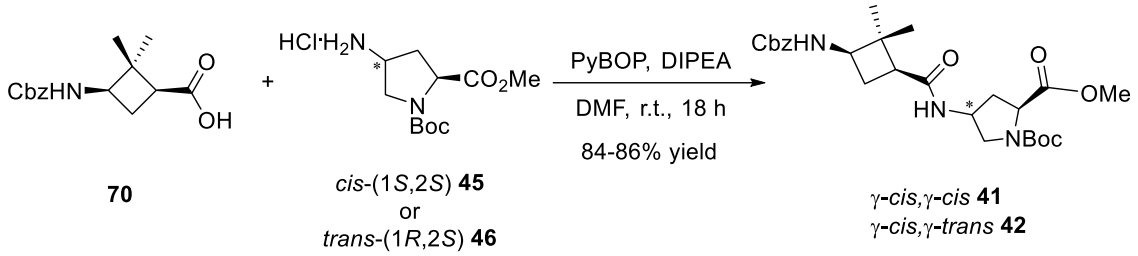

Scheme 9. Synthetic route to obtain γ-CBAA-based dipeptides **41** and **42**.

The coupling reaction was performed using PyBOP as coupling agent and DIPEA as base, obtaining γ-*cis*,γ-*cis*-**41** in 86% and γ-*cis*,γ-*trans*-**42** in 84% yield, respectively.

3.3.2 High-resolution NMR study of hybrid β- or γ-CBAA,γ-amino-L-proline peptides

As stated before, with the aim to understand the folding pattern of the synthesized hybrid peptides, high resolution NMR studies were carried out. To perform this study, the first step was to assign each of the protons that the molecule contains and, secondly, to determine the disposition of the molecule to define secondary structures generated by the formation of hydrogen bonds.

For this reason, in collaboration with Dr. Pau Nolis from the *NMR Service* at the Universitat Autònoma de Barcelona, the following experiments were carried out for each of the compounds synthesized:

1. ^{1}H-NMR spectrum
2. ^{13}C-NMR spectrum
3. Multiplicity edited HSQC-NMR spectrum
4. NOESY-NMR spectrum
5. 1D selective NOESY experiments
6. ROESY-NMR spectrum
7. 1D selective ROESY experiments
8. TOCSY-NMR spectrum
9. 1D selective TOCSY experiments

As it is commonly done for any small molecule, ^{1}H-, ^{13}C- and HSQC-NMR experiments were used to identify most of the C and H atoms present in the compounds. On the other hand, NOESY-NMR, ROESY-NMR and TOCSY-NMR experiments were used to establish intra- and inter-residue connectivities.

3.3.2.1 Structural study in solution of β,γ-dipeptides

The NMR characterization of the four diastereomic β,γ-dipeptides **33**, **35**, **37** and **39** was performed using a 600 MHz spectrometer, in two different solvents, $CDCl_3$ and DMSO-d_6, respectively, at 298 K and at a 35 mM concentration. The existence of rotamers was expected to be observed when using protected peptides with *tert*-butyloxycarbonyl groups due to the rotation of these moieties.[57] It is worth mentioning that the conformation studies with the peptides bearing deprotected γ-amino-L-proline residues could not be performed due to their insolubility.

Regarding the β,γ-dipeptides, the NMR spectra showed the splitting of most of the signals for all the dipeptides, implying the presence of two conformers in solution. The exact conformer ratio varied depending on which was the studied isomer and on the solvent used but in all cases the conformational ratio was close to 3:2. This ratio was assigned to the rotation of the *tert*-butyloxycarbonyl groups.

Particularly, ^{1}H- and ^{13}C-NMR signals belonging to the γ-amino-L-proline residue showed a larger splitting (appeared at more different chemical shifts) compared to those corresponding to the cyclobutane residue signals, which were only slightly or not affected at all depending on the diastereomer and solvent considered. For instance, focusing on the spectra recorded in DMSO-d_6, the most remarkable splitting was seen for protons corresponding to the *tert*-butyl group on the carbamate, the methyl of the ester group and the NH_{15} of the amide bond (Figure 16). The ^{1}H-NMR spectra in $CDCl_3$ are shown in Annex 9.1

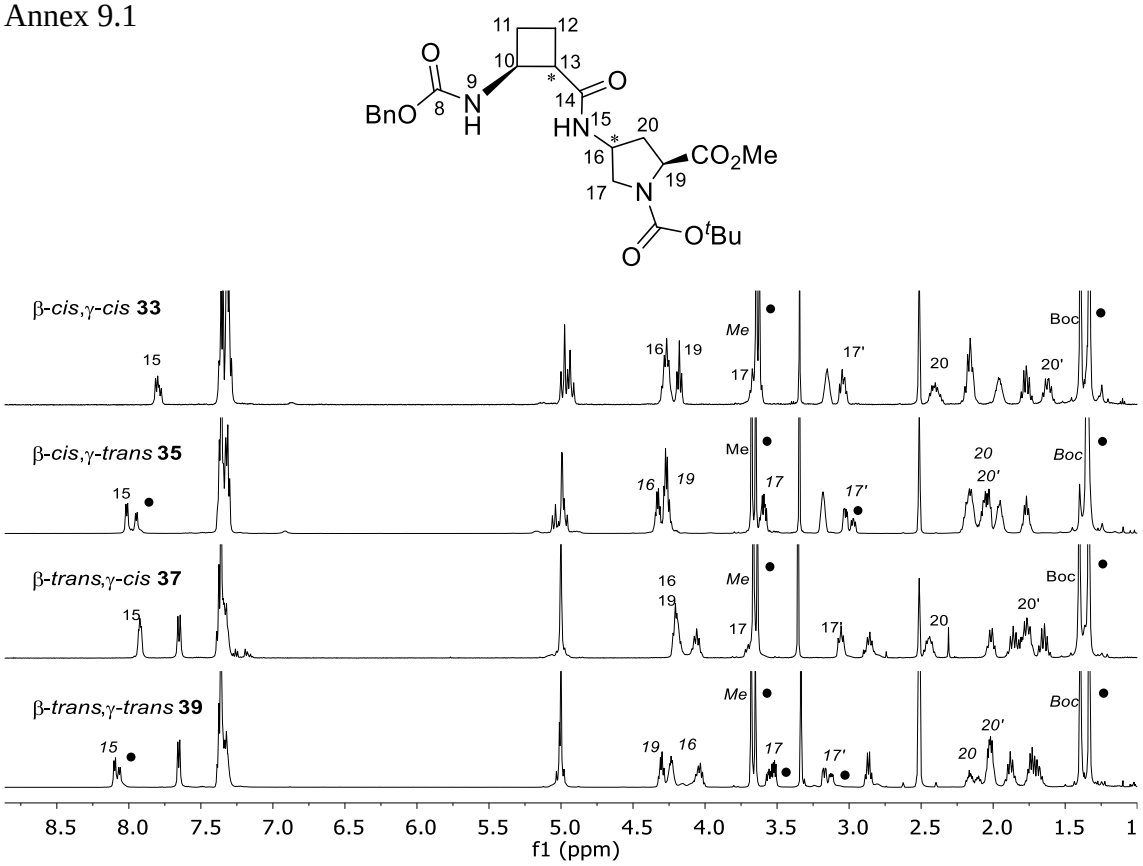

Figure 16. ^{1}H-NMR spectra of dipeptides **33**, **35**, **37** and **39** in DMSO-d_6 at 298 K. Protons of the γ-amino-L-proline residue are indicated, in italics those corresponding to the *trans* residues. The dots indicate the minor conformer observed for certain signals.

Concerning the spatial distribution of β,γ-dipeptides, it was of crucial importance to study sequential NOEs from residue *i* to residue *i-1*. For these studies, $CDCl_3$ was used as solvent to obtain more interesting information on their folding, as it is well known to be less hydrogen-bond disrupting than DMSO-d_6.

Figure 17 shows the 1D NOESY experiments when inverting the amide proton NH_{15}, observing a different NOE pattern depending on whether the cyclobutane residue was substituted with a *cis* or a *trans* relative configuration. A strong sequential NH_{15}-H_{13} NOE was detected when a β-*cis*-CBAA moiety **33** and **35** was present, while a strong sequential NOE between NH_{15}-H_{10} was observed for β-*trans*-CBAA containing peptides **37** and **39**, with the NH_{15}-H_{13} NOE becoming weaker.

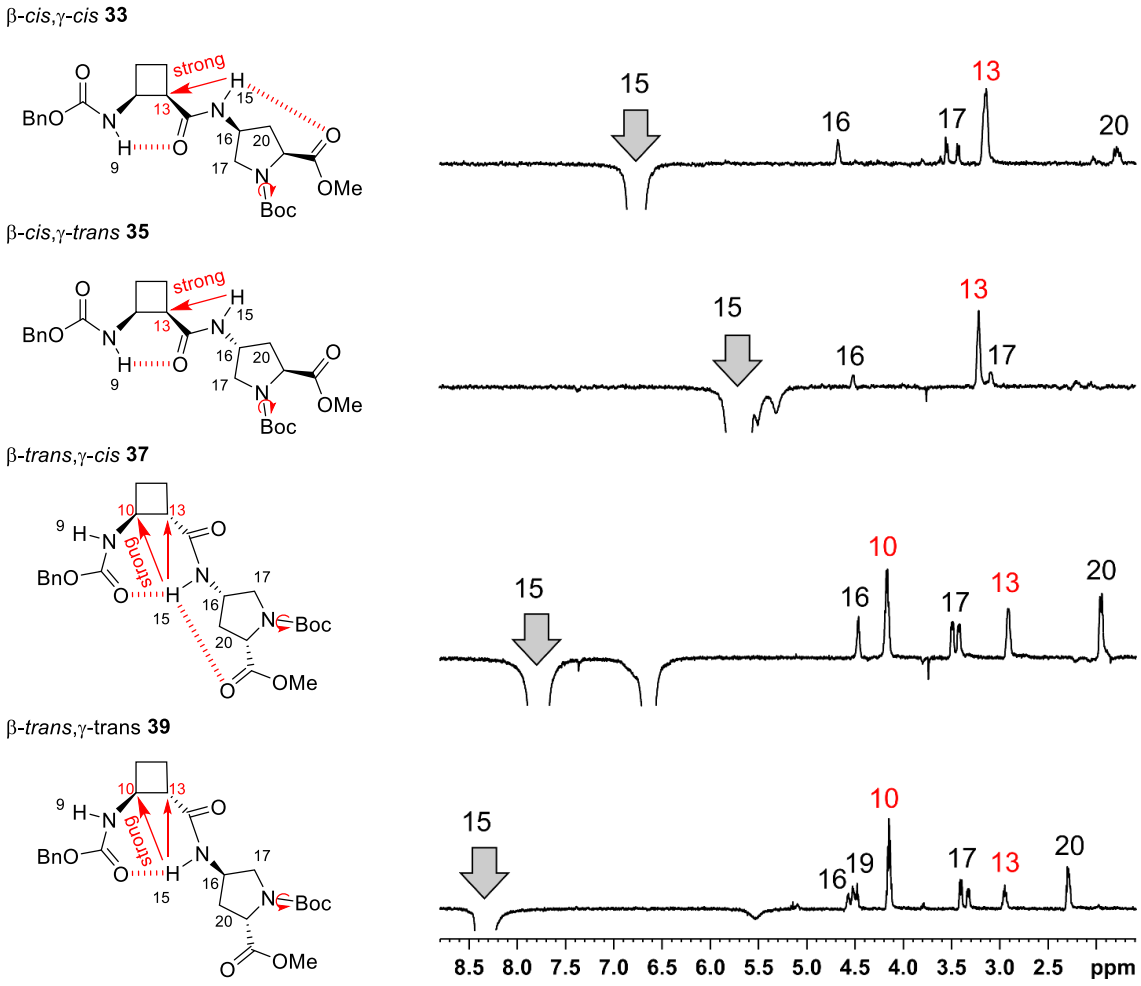

Figure 17. 1D selective NOESY experiments (600 MHz) when inverting the NH_{15} of the γ-amino-L-proline residue of dipeptides **33**, **35**, **37** and **39**, respectively, in $CDCl_3$.

These characteristic patterns imply a prevalence of a six-membered intra-residue hydrogen-bonded ring for the β-*cis*-CBAA and an eight-membered inter-residue hydrogen-bonded ring for the β-*trans*-CBAA.

Following with the previous paragraph, *trans*-cyclobutane containing dipeptides **37** and **39** presented a very characteristic highly deshielded position for NH_{15} (between 8.0-8.5 ppm) compared to *cis*-cyclobutane containing dipeptides **33** and **35** (<7.0 ppm). Both facts were perfectly in agreement with the disposition necessary for an eight-membered hydrogen-bonded ring, as previously stated for peptides built only with β-CBAA.[46,47]

Interestingly, some noticeable differences in chemical shifts of various protons were detected when comparing the diastereomer containing a *cis*-γ-amino-L-proline residue with its analog containing a *trans*-γ-amino-L-proline residue (See Figure 17 for chemical shifts). These differences in chemical shifts implied different hydrogen bonding in the studied peptides. For example, the higher chemical shift displacement of the NH_{15} in **33** (6.7 ppm) with respect to NH_{15} in **35** (5.7 ppm), suggested the formation of an intra-residue seven-membered hydrogen-bonded ring in the *cis*-γ-amino-L-proline residue between NH_{15} and CO_{21}, which is geometrically not possible when having the *trans*-γ-amino-L-proline residue (See Figure 14 for a representation of the hydrogen bonds). Similarly, a 0.5 ppm chemical shift displacement of the NH_{15} proton between **37** (7.8 ppm) and **39** (8.3 ppm) was attributed to the presence of a seven-membered intra-residue hydrogen-bonded ring (NH_{15}-CO_{21}) when the *cis*-γ-amino-L-proline residue was present and which competes with the previously described an inter-residue eight-membered hydrogen-bonded ring (NH_{15}-CO_8). Thereby, the existence of a bifurcated hydrogen bond promoted by the NH_{15} of **37**, which was demonstrated in the 1D NOESY experiment, was assured (Figure 17). The important exchange peak chemical shift (6.6 ppm) for β-*trans*, γ-*cis* **37** matched with that of NH_{15} in **33**, where the seven-membered ring arose. These intra-residue interactions were previously observed and described in the study of the hybrid peptides based on this isomer of γ-amino-L-proline and γ-CBAA residues.[57]

On the other hand, experiments using a highly polar solvent like DMSO-d_6, which is able to compete with intramolecular hydrogen bond formation, showed that NOE patterns change when dealing with *trans*-CBAA containing dipeptides **37** and **39** (Figure 18). By the time NH_{15}-H_{10} NOE became weaker, NH_{15}-H_{13} became stronger. This could be interpreted as the rigidity of the structure was somehow softened and extended by the interaction of DMSO-d_6 with the intra-residue hydrogen bond (NH_{15}-CO_8).

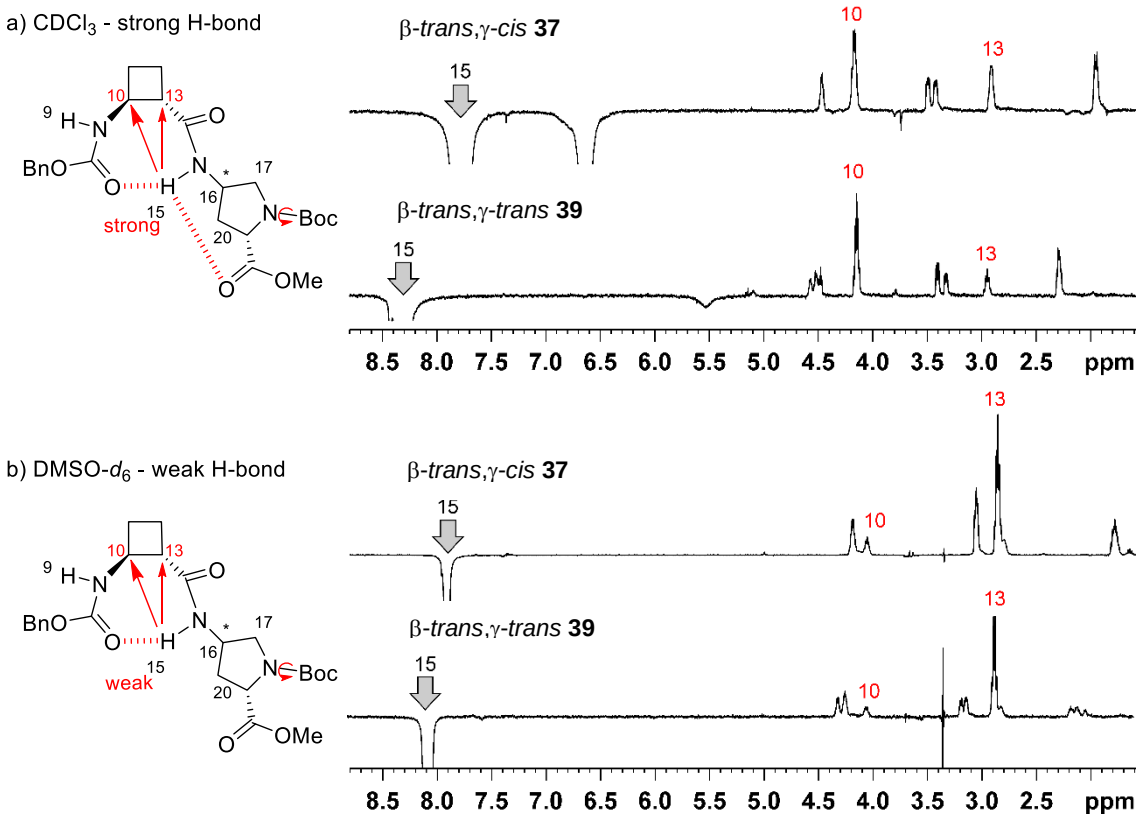

Figure 18. Solvent-dependence comparison of NOE signals (600 MHz) of dipeptides **37** and **39** in $CDCl_3$ and DMSO-d_6.

3.3.2.2 Structural study in solution of β,γ-tetrapeptides

The NMR study of tetrapeptides **34**, **36**, **38** and **40** presented several difficulties. Firstly, they were poorly soluble in $CDCl_3$, therefore the NMR study was performed in DMSO-d_6 which, as stated for dipeptides **33**, **35**, **37** and **39**, competed with the intramolecular hydrogen bonding. For this reason, the tendency to fold decreased and the determination of the conformational bias became difficult.

Secondly, the presence of one Boc protecting group for each γ-amino-L-proline residue present in the β-tetrapeptides gave up to at least four conformers due to its slow rotation, generating a very similar spectrum for each tetrapeptide, nearly superimposable with one another. Therefore, the assignment of each signal for every single residue and conformer is not straightforward. Furthermore, the conformational exchange was found to be in the NMR time scale, making the NOE/ROE analysis even more difficult.

To overcome these problems, the NMR characterization of tetrapeptides **34**, **36**, **38** and **40** was performed heating the samples up to 358 K which, to some extent, averaged the Boc group rotations and facilitated their characterization and signal assignment. Nevertheless, analyzing the N*H* signals for each tetrapeptide, it became evident that their profiles showed higher dispersion for β-*trans*,γ-*cis* **38** and β-*trans*,γ-*trans* **40** than for β-*cis*,γ-*cis* **34**; β-*cis*,γ-*trans* **36** in DMSO-d_6 (Figure 19).

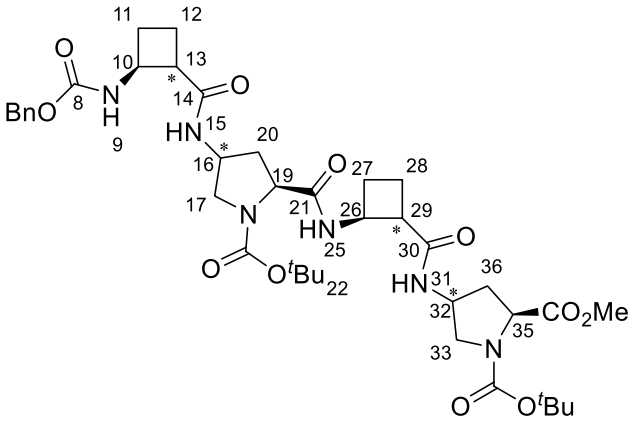

a) N*H* expanded region, 298 K, 600 MHz, DMSO-d_6 b) N*H* expanded region, 358 K, 600 MHz, DMSO-d_6

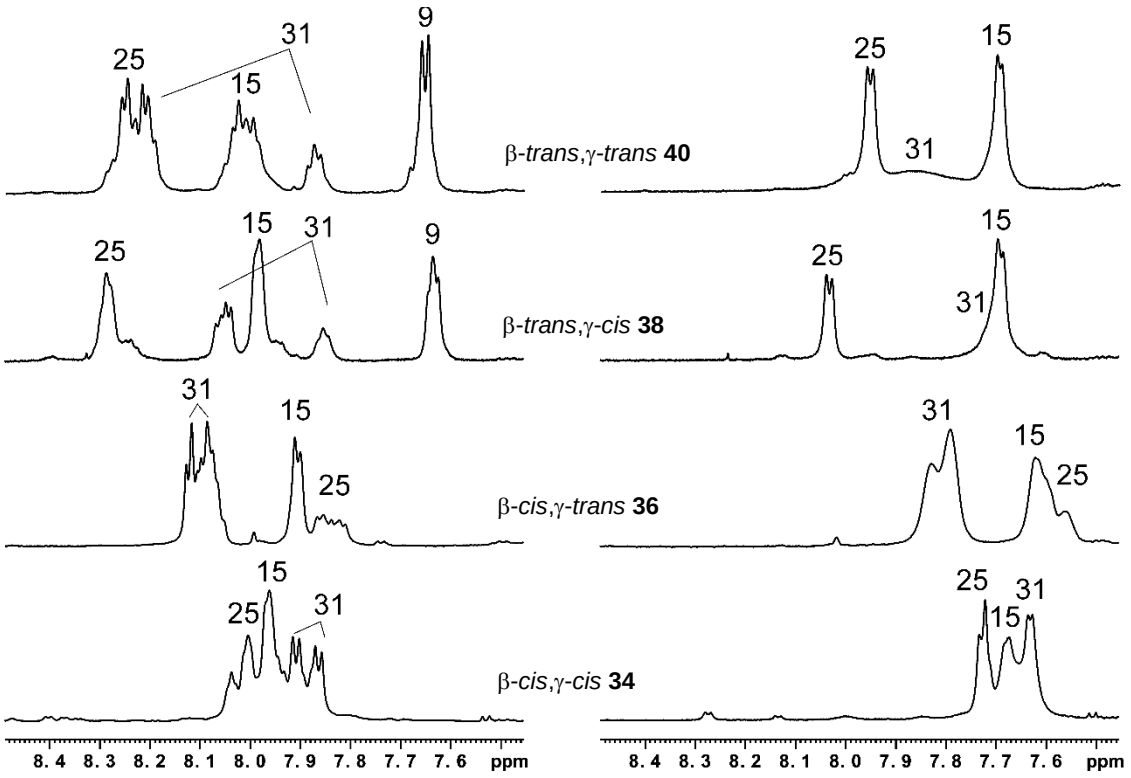

Figure 19. Expansion of the N*H* region of the ^{1}H NMR spectra (600 MHz) of tetrapeptides **34**, **36**, **38** and **40** in DMSO-d_6 at 298 K and 358 K.

This fact suggested the presence of a folded structure when having a β-*trans*-CBAA containing tetrapeptides **38** and **40** and an extended strand conformation when dealing with β-cis-CBAA containing tetrapeptides **34** and **36**. This reinforces the results obtained for their analogous dipeptides **33**, **35**, **37** and **39**. Moreover, focusing in the similar N*H* signal dispersion for tetrapeptides **38** and **40**, it could be concluded that the ordering to generate the secondary structure was driven by the presence of β-*trans*-CBAA residues rather than either *cis*- or *trans*-γ-amino-L-proline. At the same time, comparing tetrapeptides **34** and **36**, it was seen that the presence of a *trans*-γ-amino-L-proline, compared to its *cis* isomer, generates a slightly larger N*H* signal dispersion which is attributable to a slight disruption of the strand conformation suggested for the β-*cis*,γ-*cis* **34** tetrapeptide.

3.3.2.3 Structural study in solution of γ,γ-dipeptides

The NMR characterization of the two diastereomeric γ,γ-dipeptides **41** and **42** was performed using a 600 MHz spectrometer, in $CDCl_3$ at a 35 mM concentration. The existence of rotamers was expected to be observed by using protected peptides with *tert*-butoxycarbonyl groups due to the rotation of these moieties.[57] Again, the conformation studies with the peptides bearing deprotected γ-amino-L-proline residues could not be performed due to their insolubility.

The ^{1}H NMR spectra of both γ,γ-peptides showed the splitting of most of the signals, implying the presence of, at least, two conformers in solution (Figure 20). Regarding γ-*cis*,γ-*cis* **41**, four different conformers could be observed at 298 K with a similar conformational ratio. Interestingly, performing the experiment at 273 K showed the presence of eight different conformers, four of them being minor. The γ-*cis*,γ-*trans* **42** only showed two different conformers at 298 K with a conformational ratio close to 3:2. Lowering the temperature to 273 K promoted the observation of four major conformers and four minor conformers, making very difficult the assignment of a conformational ratio. Apart from the splitting seen for NH_{17}, the most remarkable splitting was observed for protons corresponding to the *tert*-butyl group on the carbamate, the methyl on the ester group and the methyl groups on the cyclobutane moiety.

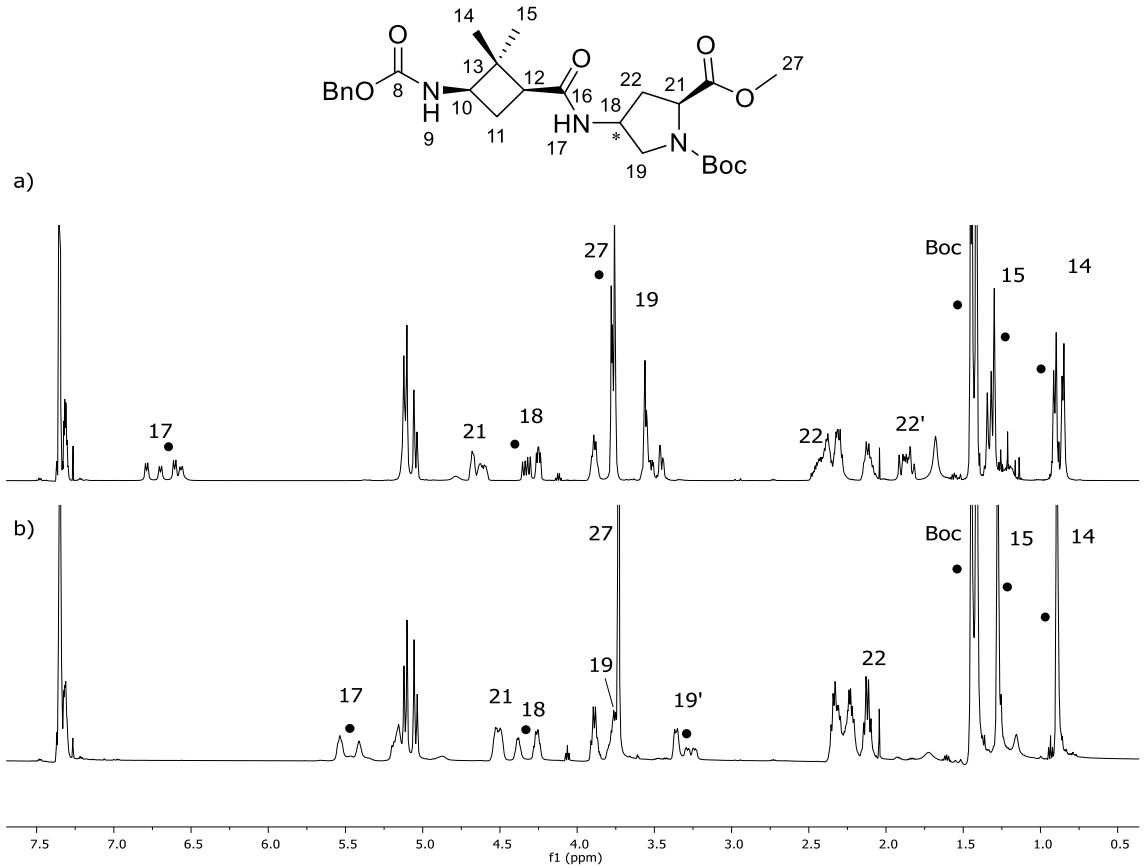

Figure 20. ^{1}H-NMR spectra of dipeptides a) **41** and b) **42** in $CDCl_3$ at 298 K (600 MHz). Numbers show the protons with larger chemical shift difference between dipeptides. Dots correspond to protons that show the different conformers.

To understand the different conformations of γ,γ-dipeptides, sequential TOCs were recorded to see the presence of rotations by only focusing on the proline ring signals. Regarding **41**, the spectrum showed the presence of four major conformations at 273 K where the most different signal was for N*H*$_{17}$ (Figure 21). If examined in detail, H$_{19}$, corresponding to one of the CH_2 of the pyrrolidine ring, turned out to be more anisochronous in conformers 2 and 4 than in conformers 1 and 3. Moreover, H$_{21}$, corresponding to the CH_2 α of the carbonyl group in the pyrrolidine ring, showed a less shielded signal for conformers 2 and 4 than for conformers 1 and 3. Finally, focusing on H$_{18}$, which corresponds to the CH α of the amide group in the pyrrolidine ring, a more shielded signal for conformers 3 and 4 than for conformers 1 and 2 could be observed.

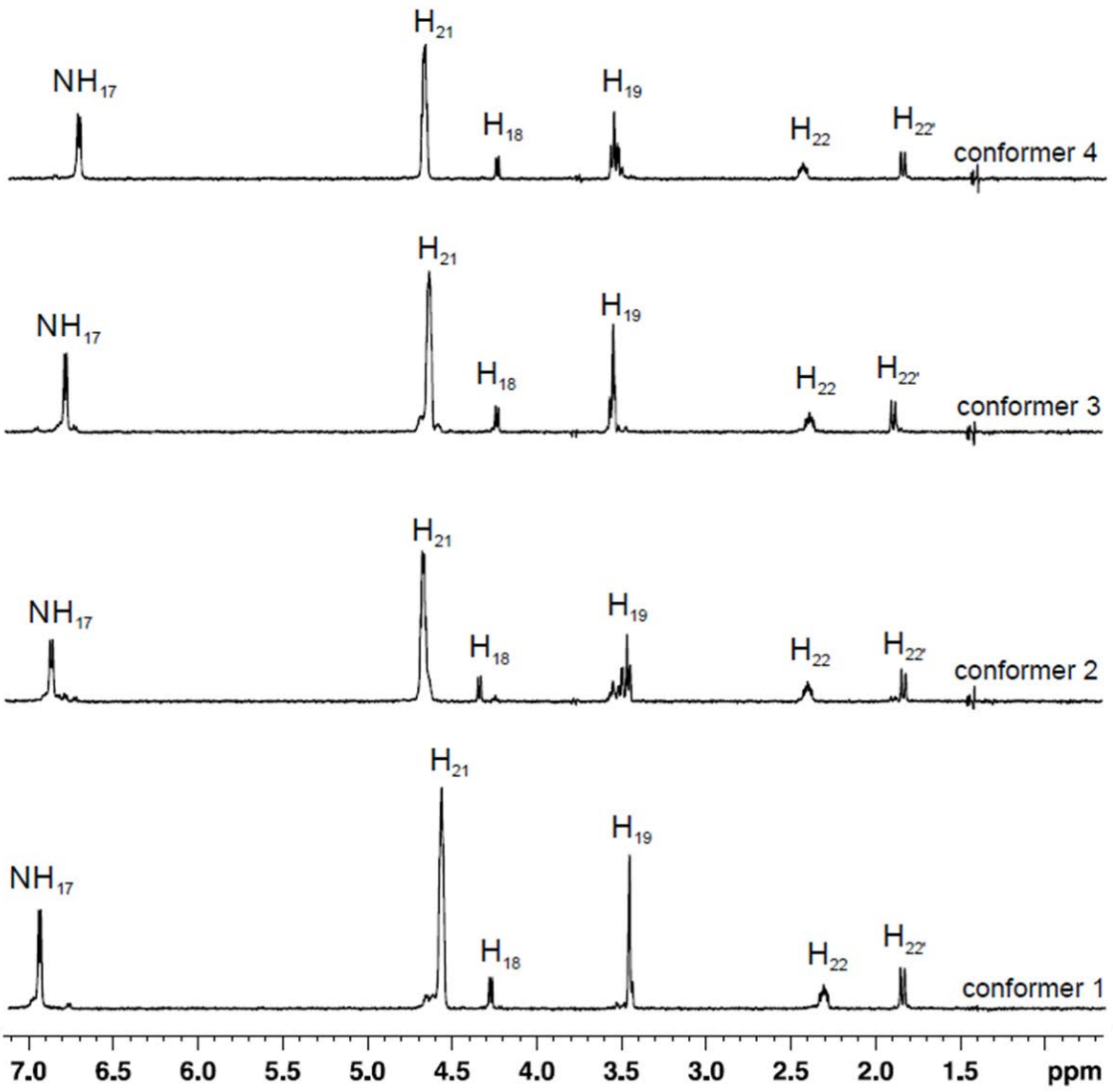

Figure 21. TOC spectra of the different conformers of the γ-*cis*,γ-*cis* **41** performed at 273 K in DMSO-d_6 (600 MHz).

Regarding **42**, the spectrum showed the presence of 4 major conformations at 273 K where the most different signal was for NH_{17} dividing the conformers in two groups: conformer 1 and conformer 2; conformer 3 and conformer 4 (Figure 22). The conformational analysis was very difficult to be performed, with several overlapping signals, probably due to the existence of not very fixed conformations. For example, the most remarkable signal to be observed was H_{18}, corresponding to the CH α of the amide group in the pyrrolidine ring, observing a more deshielded signal for conformers 3 and 4 than for conformers 1 and 2.

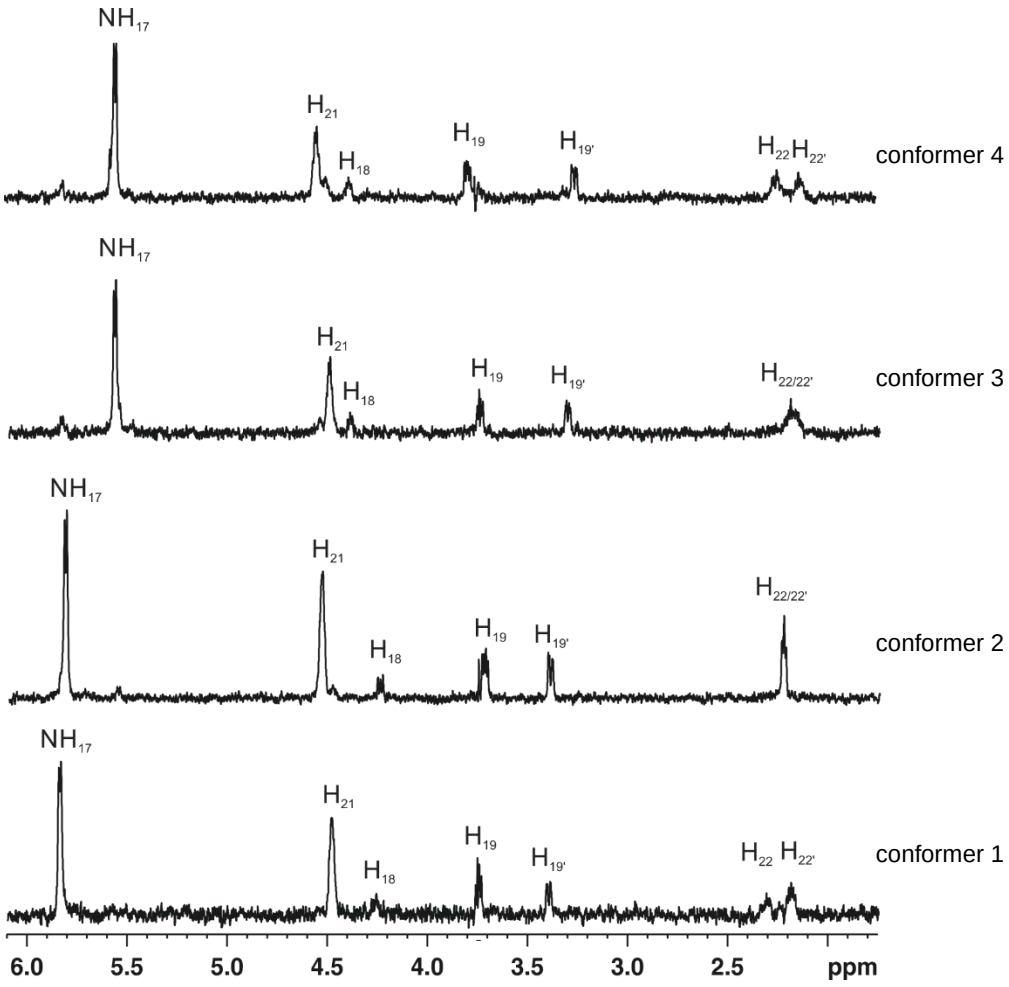

Figure 22. TOC spectra of the different conformers of the **42** performed at 273 K in DMSO-d_6 (600 MHz).

For a more detailed analysis, sequential NOEs were studied in the same conditions as performed for β,γ-dipeptides in section 3.3.2.1. Figure 23 shows 2D NOESY experiments, observing a different NOE pattern depending on whether the proline residue was substituted with a *cis* or *trans* relative configuration.

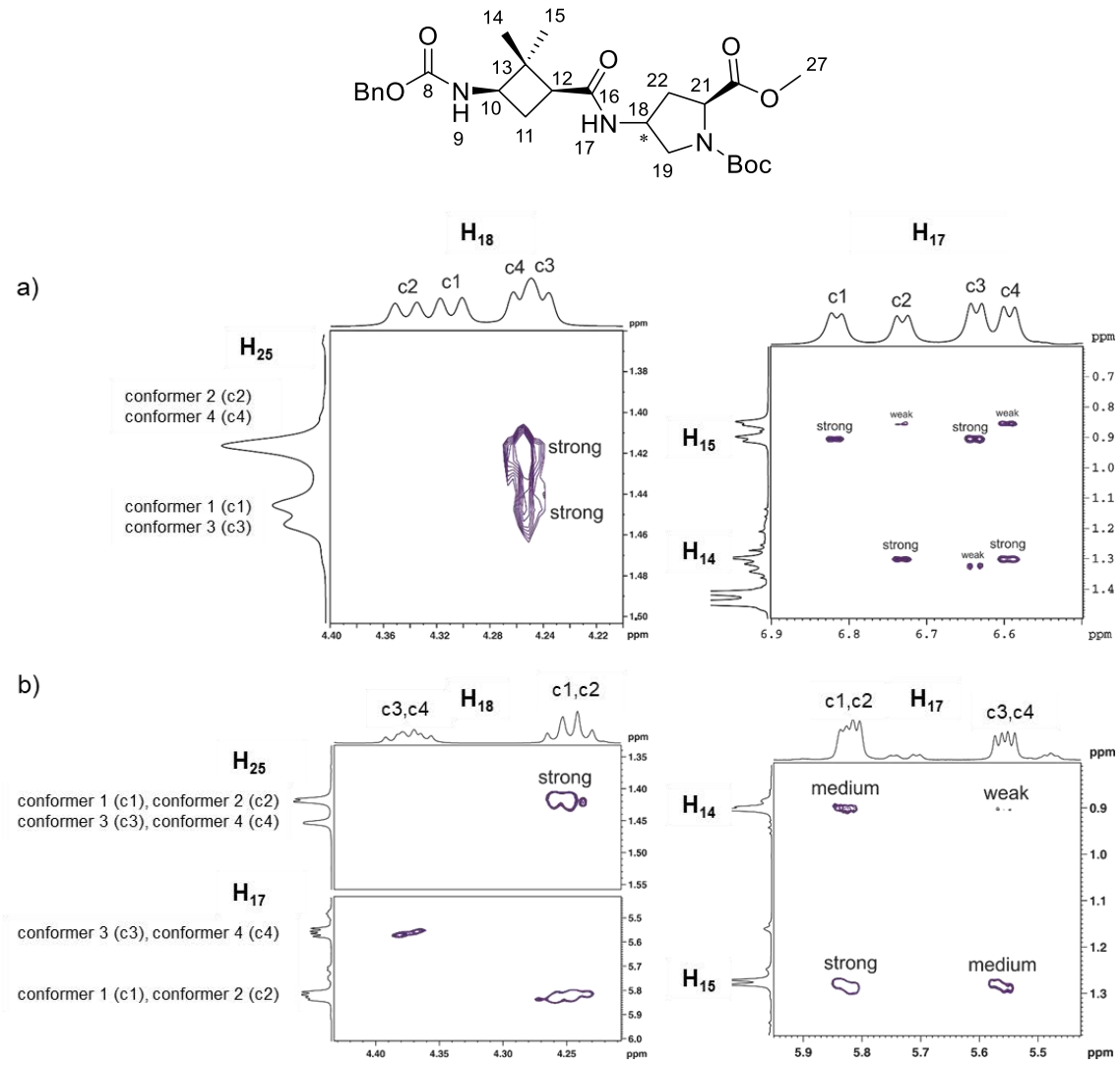

Figure 23. 2D NOESY experiments in DMSO-d_6 at 273 K (600 MHz) focused on H_{17} and H_{18} region. a) **41** and b) **42**.

When having the *cis*-γ-amino-L-proline residue in peptide **41** (Figure 23a), a strong sequential NH_{17}-CH_{14} NOE with a weak NH_{17}-CH_{15} NOE was observed for conformer 1 and conformer 3. On the other hand, conformer 2 and conformer 4 presented a strong NH_{17}-CH_{15} NOE while having a weak NH_{17}-CH_{14} NOE. These results, in combination with TOCs experiments previously described, indicated that an equilibrium of the conformers couples 1/3 and 2/4 is due to a rotation in CH_{12}-NH_{17} dihedral angle, giving different interactions between the methyl groups of the γ-cyclobutane ring and NH_{17}.

Additionally, a strong sequential CH_{18}-^{t}Bu$_{25}$ was observed for conformer 3 and conformer 4, while it was not observed at all for conformer 2 and conformer 1. This observation suggested the rotation of the *tert*-butyl group as expected, previously observed for the β,γ-peptides. Furthermore, the presence of a hydrogen bond NH_{17}-CO$_{26}$ was confirmed (Figure 24a) by observing the chemical shift of NH_{17} (see Figure 20).

On the other hand, when the *trans*-γ-amino-L-proline residue was present in peptide **42** (Figure 23b), a strong sequential NOE CH_{18}-^{t}Bu$_{25}$ and CH_{18}-NH_{17} signals were observed for conformer 1 and conformer 2. However, the first NOE signal was not seen for conformer 3 and conformer 4 and the last one was weaker for these conformers. These NOEs demonstrated the presence of different conformers due to the rotation of the *tert*-butyl group. Secondly, conformer 1 and conformer 2 showed a medium NH_{17}-CH_{14} NOE interaction and a strong sequential NH_{17}-CH_{15} NOE. Moreover, conformer 3 and conformer 4 had a weak NH_{17}-CH_{14} NOE interaction and a strong sequential NH$_{17}$-CH$_{15}$ NOE. These results made it impossible to distinguish the spatial distribution between the couples of conformer 1- conformer 2 and conformer 3- conformer 4, which are mainly formed by the CH_{12}-NH_{17} dihedral angle rotation. Contrary to what was seen for the *cis*-γ-amino-L-proline peptides, no hydrogen bond formation was observed by NMR experiments (Figure 24b) by observing the chemical shift of NH_{17} (see Figure 20).

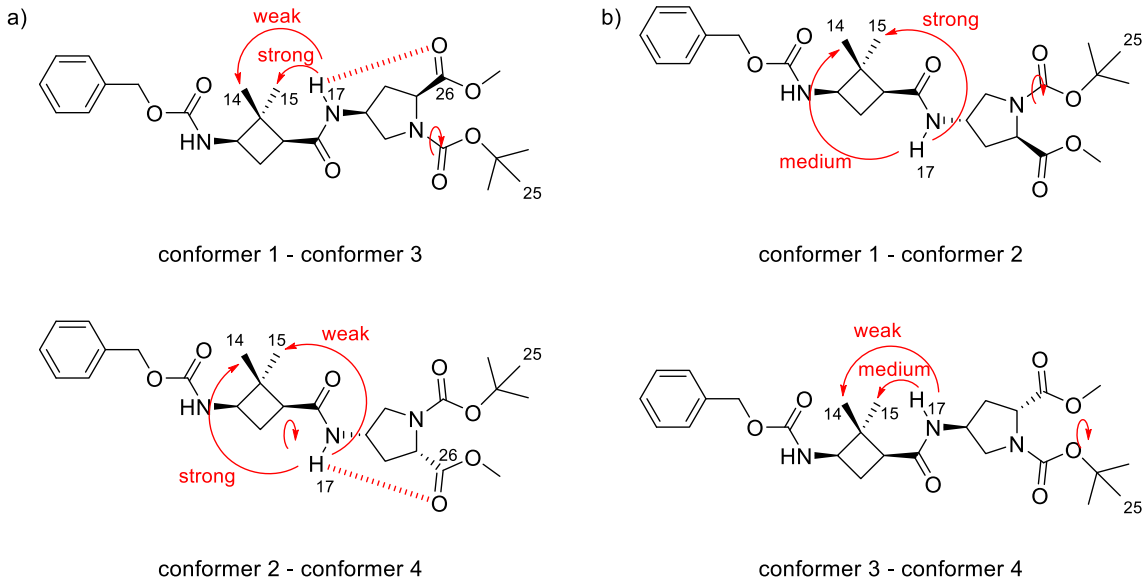

Figure 24. Described secondary interactions and the different conformers seen using high resolution NMR spectrometry. Red arrows represent the observed NOE patterns and red lines represent hydrogen bonds. a) **41** and b) **42**.

3.4 Summary and conclusions

In this part of the thesis, eight β-CBAA,γ-amino-L-proline hybrid peptides and two γ-CBAA,γ-amino-L-proline hybrid peptides were synthesized (Figure 25) in good to moderate yields and their folding patterns were evaluated by means of high resolution NMR spectroscopy.

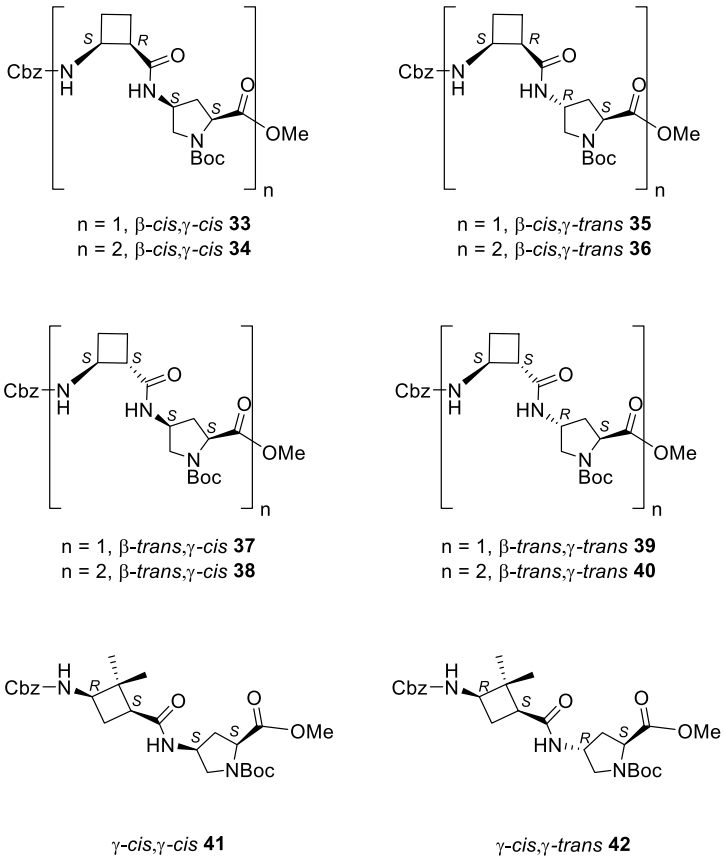

Figure 25. Synthesized and studied hybrid peptides.

Dipeptides containing β-CBAA (Figure 26) showed the formation of defined hydrogen bonds, promoting the formation of a six-membered intra-residue ring for those peptides containing a *cis*-β-CBAA (**33** and **35**) and an eight-membered inter-residue ring for the ones containing a *trans*-β-CBAA (**37** and **39**). This hydrogen bond formation promoted an extended strand-type folding for those peptides containing a *cis*-β-CBAA residue and a more compact twisted folding for the peptides bearing a *trans*-β-CBAA.

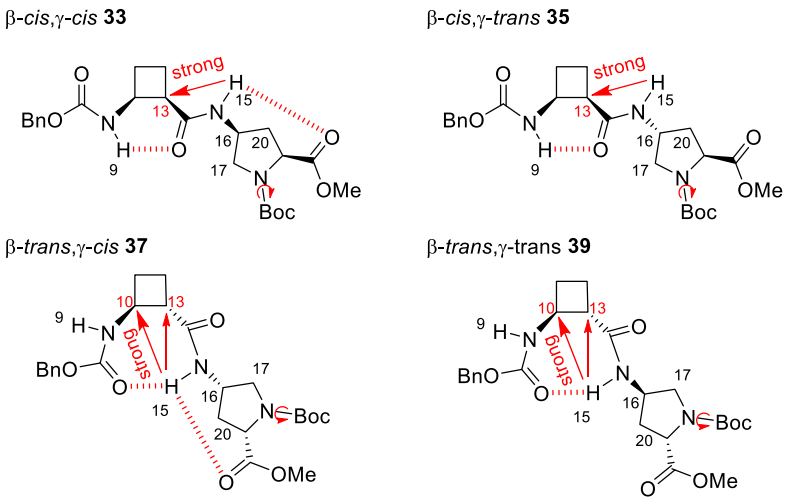

Figure 26. Folding patterns observed for dipeptides **33**, **35**, **37** and **39** by NMR spectroscopy. Red-dashed lines represent hydrogen bonds. Red arrows represent NOE interactions.

The folding patterns in Figure 26 of dipeptides **33**, **35**, **37** and **39** could be extrapolated to their corresponding tetrapeptides **34**, **36**, **38** and **40**, concluding that the ordering to generate the secondary structure was driven by the presence of β-*trans*- or *cis*-CBAA residues rather than either *cis*- or *trans*-γ-amino-L-proline, whose effect is less important than the given by CBAA.

Peptides containing γ-CBAA (Figure 27) showed less defined hydrogen bonds, only present when having a *cis*-γ-amino-L-proline residue with a seven-membered inter-residue hydrogen-bonded ring (**41**). For this reason, more conformers were observed when NOEs and TOCs experiments were performed at low temperature, with four major conformation and four minor ones. On the other hand, the absence of hydrogen bonds when having a *trans*-γ-amino-L-proline residue (**42**) only promoted the formation of four conformers when NOEs and TOCs experiments were performed at low temperature. The different conformers of both γ,γ-dipeptides were assigned to the combination of the "slow" rotation in the CH_{12}-NH_{17} dihedral angle and the "quick" rotation of the *tert*-butyl carbamate.

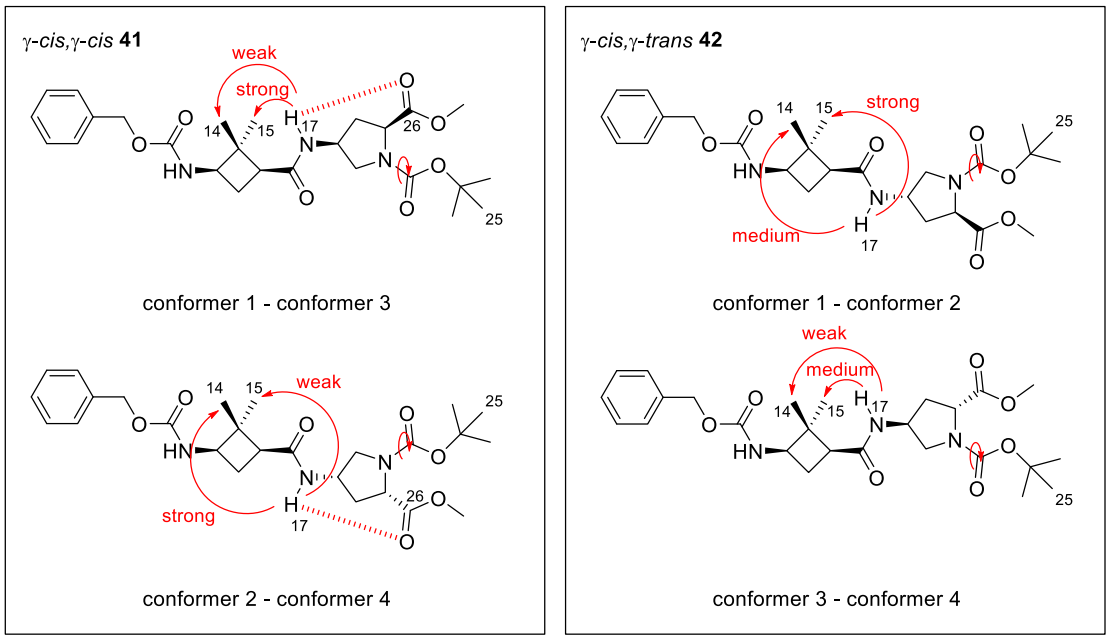

Figure 27. Folding pattern observed for dipeptides **41** and **42** by NMR spectroscopy. Red-dashed lines represent hydrogen bonds. Red arrows represent NOE interactions.

As a main conclusion, the revealed importance of the relative configuration of the parent amino acids on the folding patterns of the resulting hybrid peptides should allow the rational design of new peptides with interesting biological application. Further studies in this field are explained and discussed in Chapter 4 of this thesis.

4. Synthesis of Hybrid CBAA,γ-amino-L-proline Peptides as Cell Penetrating Agents: Studies in *HeLa* Cells and *Leishmania* Parasites

4. Synthesis of Hybrid CBAA,γ-amino-L-proline Peptides as Cell Penetrating Agents: Studies in *HeLa* Cells and *Leishmania* Parasites

4.1 Introduction

Membranes of live cells behave as a selective permeable barrier, which regulates essential biological processes related to the interaction between subcellular compartments, the cell itself and its environment. They are generally formed by a lipid bilayer containing lipids from a chemically diverse set, which are present in various amounts and proportions.[63] The study of molecule transport in living cells through this membrane in order to understand both the entry of external substances, like nutrients or drugs, and the elimination of toxic compounds generated by subcellular organelles is a rising field.[64] The cell membrane is only permeable to low molecular weight hydrophobic compounds, while charged, hydrophilic and low solubility compounds require some help to be translocated inside cells.[65]

The transport control of any compound through the cell membrane is essential due to the necessity to promote or prevent the entrance of bioactive molecules that interact with a high number of therapeutic targets inside the cell. The main issue with biologically active compounds is the low permeability through membranes, which is very difficult for molecules with high molecular weight, high number of hydrogen bond donors and acceptors or with high lipophilicity. The study of the parameters that rule the permeability of biologically active compounds opens a new potential research topic for medical treatment.[66] To overcome the problem, several techniques have been developed to release therapeutic agents in subcellular compartments like microinjection,[67] electroporation[68] and the use of liposomes.[69] However, these methods have some disadvantages such as low efficiency, high toxicity, low bioavailability and low specificity. Thus, methodologies involving the synthesis of cell penetrating peptides (CPPs) have been developed for several years.[70]

In the last decades, a very huge number of synthetic CPPs have been designed using natural peptides and proteins. Peptides have profoundly impacted the development of the modern pharmaceutical industry and have contributed significantly to the advancement of biological and chemical sciences.[71,72]

CPPs have a great internalization capacity and can be easily modified during their building, making them very interesting compounds to be studied in pharmacological applications.[70] Moreover, the great potential of CPPs relies on their ability to carry and release, through the cell membrane, a very wide range of cargo compounds like other peptides, proteins, ribonucleic acids, oligonucleotides, drugs, liposomes, plasmids, quantum dots or another nanoparticles (Figure 28).[73,74]

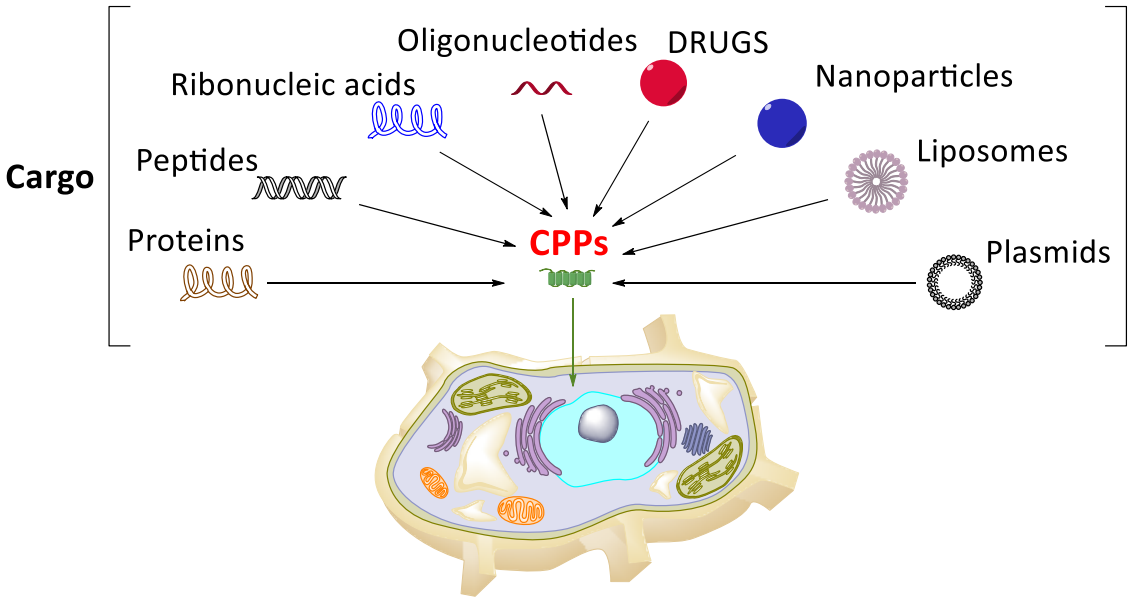

Figure 28. Cargoes that can be attached to CPPs and carried inside cells.

4.1.1 Cell Penetrating Peptides (CPPs)

Generally, CPPs are short (no more than forty residues) positively charged peptides built with basic amino acids, for example, lysine or arginine.[75] These peptides are able to cross the cell membrane and represent one of the most used non-invasive intracellular delivery vectors for cargoes, which can be covalently or non-covalently attached to them,[76] with a high internalization efficiency and low cytotoxicity, both *in vitro* and *in vivo*.[77,78,79] Since the cell membrane penetration activity of trans-acting activator of transcription (TAT) protein from human immunodeficiency virus-1 (HIV-1) was reported,[80,81] different CPPs have been identified from natural sources such as VP22 derived from viral capsid protein in Herpes simplex virus Type 1 (HSV-1);[82] penetratin derived from residues 43-58 of the third helix *Drosophila Antennapedia* homeobox protein;[83,84] and transportan, derived from a neuropeptide galanin and mastoparan.[85]

Moreover, CPPs from synthetic sources have been reported such as poly-arginine,[86] model amphipathic peptides (MAP)[87] and TP2.[88] There are different ways to classify cell penetrating peptides based on origin, sequence, chemical charge, binding type and, the most used classification, physicochemical properties (Figure 29).[89]

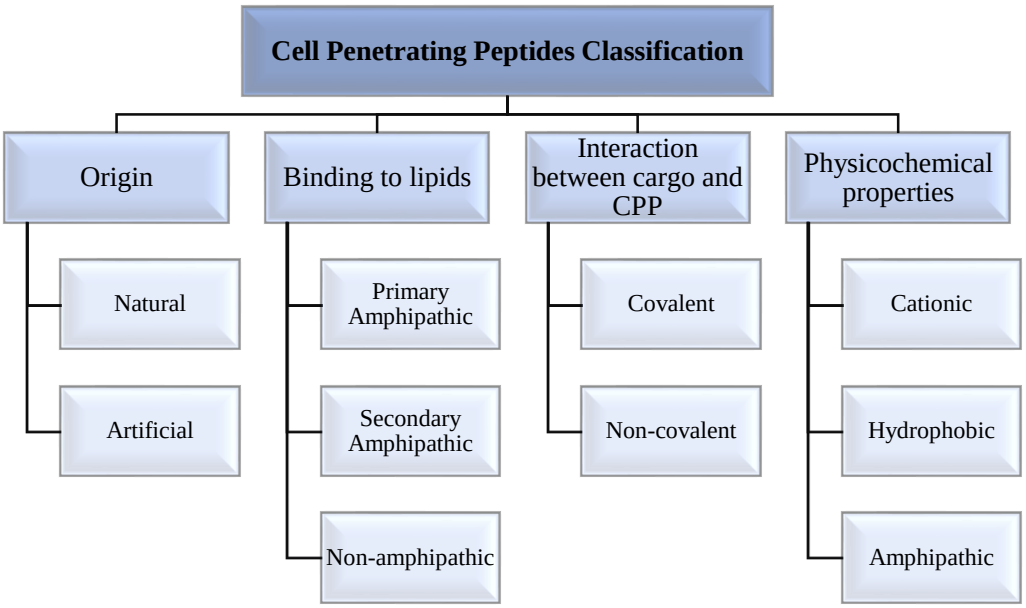

Figure 29. Classification chart of Cell Penetrating Peptides.

Origin classification is used to define the nature of the CPP. Natural CPPs are derived from natural proteins such as DNA- or RNA- binding proteins, viral particle envelope proteins or transactivators of gene transcription. Artificial CPPs are those which are designed based on the structures of natural-derived CPPs.

The binding to lipids classification is used to define the interaction of the CPP with the lipids in the cell membrane. Primary amphipathic are CPPs with a primary structure along with both hydrophobic and hydrophilic residues. Secondary amphipathic CPPs have and α-helix or β-sheet structure upon interaction with a phospholipid membrane. Non-amphipathic have high amount of cationic amino acids such as arginine.

The interaction between cargo and CPP classification define the coupling between the therapeutic agent and the CPP: covalent if it is chemically linked or non-covalent (charge interactions, hydrogen-bonds, etc.) if complexes are formed.

The physicochemical properties classification define the chemical properties of the CPPs. Cationic CPPs are those with high positive net charges, hydrophobic peptides are CPPs with low net charge and amphipathic peptides comprise both cationic and anionic peptides with some hydrophobic residues in their backbone. Some CPPs examples can be seen in Table 1.[73,90]

Table 1. Example of CPPS with their corresponding classification.

Feature	Name	Origin	Sequence
Cationic	TAT_{48-60}	Protein of HIV-1	GRKKRRQRRRPQ
	R8	Synthetic	RRRRRRRR
Amphipathic primary	pVEC	Vascular endothelial cadherin	LLIILRRRIRKQAHAHSK
	Pep-1	Tryptophan-rich cluster/SV40 T antigen NLS	KETWWETWWTEWSQPKKKRKV
Amphipathic alpha helix	MAP	Chemically Synthesized	KLALKLALKALKAALKLA
	Penetratrin	*Drosophila melanogaster*	RQIKIWFQNRRMKWKK
Amphipathic beta sheet	VT5	Synthetic	DPKGDPKDVTVTVTVTVTGKGDPKPD
	AA3H-PLP	Protein of annexin	FITC-MASIWVGHRGRRRQQQQQQRRR
Amphipatic proline rich	Bac 7 (Bac 124)	Bactenecin family of antimicrobial peptides	RRIRPRPPRLPRPRPRPLPFPRPG
Hydrophobic	Pep-7	CHL8 peptide phage clone	SDLWEMMMVSLACQY
	C105Y	α l-Antitrypsin	CSIPPEVKFNKPFVYLI

Cationic peptides present few acid residues and a high positive net charge at physiological pH, which is critical in cellular uptake.[90] The cellular uptake process of cationic CPPs, which appears to be independent of receptors, is initiated by the electrostatic interaction of the cationic groups present in the backbone with the phosphate groups from phospholipids of cell membrane (Figure 30). It has been demonstrated that arginine rich CPPs are more effective in cellular uptake than lysine rich ones, since the guanidine head group of arginine form bidentate hydrogen bonds with the negatively-charged cell membrane components.[91] However, these indiscriminate interactions between cationic CPPs and cell membrane leads to severe toxicity and rapid clearance from blood, restricting their clinical applications.

To solve this, some modifications in the structure of cationic CPPs must be done. For example, the inclusion of hydrophobic amino acids with a low net charge.[92] The hydrophobic motifs can play a critical role in the interaction with hydrophobic domains of cellular membranes and enhance the peptide spontaneous translocations across them in an energy-independent manner.[93] Another important factor to take into account for designing a CPP is the folding they adopt in solution. In Chapter 3 it can be seen how the folding of the peptides depends on the structure and relative configuration of the different amino acids, for example, that of the γ-amino-L-proline derivative. For these reasons and using the knowledge previously obtained in the field, proline-rich peptides (Pro-peptides) have been chosen to be studied in this work.

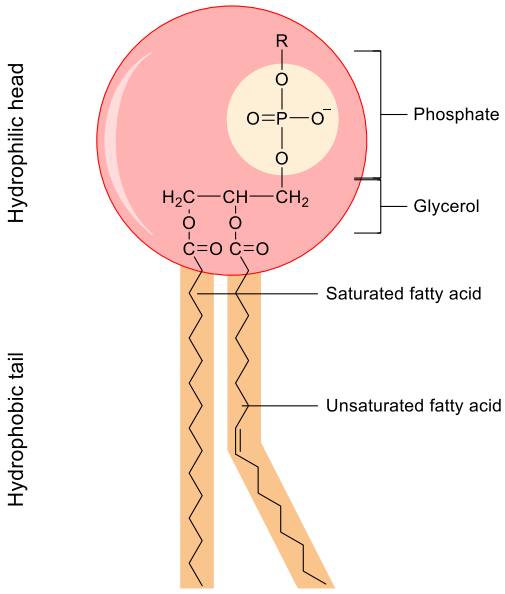

Figure 30. Phospholipid representation composed of a hydrophilic head and two hydrophobic tails. The hydrophilic head group consists of a phosphate-containing group attached to a glycerol molecule. The hydrophobic tails, each containing either a saturated or an unsaturated fatty acid, are long hydrocarbon chains.

4.1.2 Proline-rich cell penetrating peptides

Proline is one of the 20 genetically encoded amino acids but the only one with a secondary amine and a cyclic structure, which constrains its structure. Without modification, the proline-rich CPPs generally retain the excellent water solubility requisite for *in celullo* use. Oligoprolines can adopt two different secondary structures depending on the environment: polyproline I (PPI) and polyproline II (PPII) helix (Figure 31).[94] PPI has, so far, no known biological relevance, while PPII helices are one of the most abundant secondary structures adopted in proteins with α-helices and β-sheets (Figure 31b).[56,95] The right-handed PPI helix is the principal conformation in less polar solvents and consists of all *cis* amide bonds that generate a helical pitch of ≈5.4 Å and 3.3 amino acid residues per turn. The left-handed PPII helix found in aqueous solutions has a less packed helix with ≈9.0 Å and 3.0 amino acid residues per turn, has almost ideal C_3 symmetry along the central screw axis, and contains all *trans* amide bonds (Figure 31a).

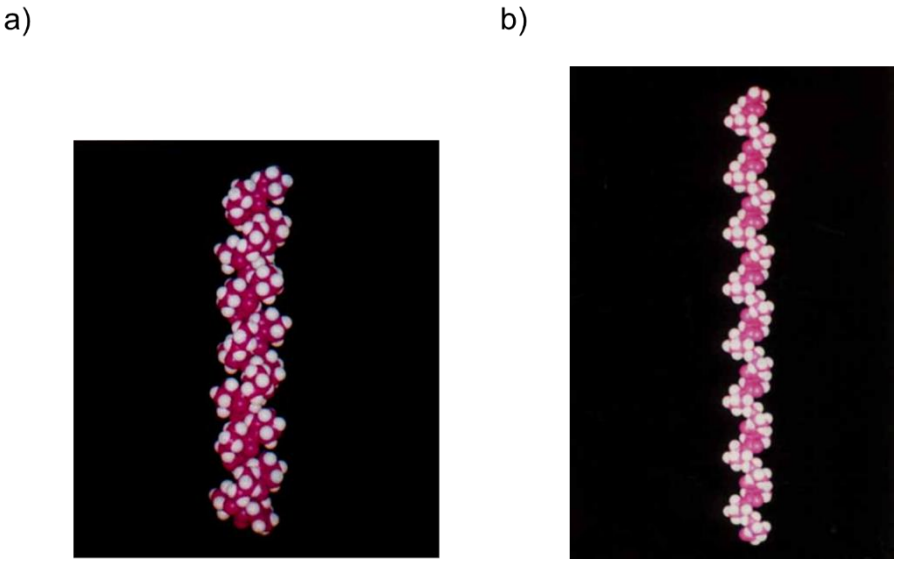

Figure 31. Representation of polyproline helices. a) Righ-handed PPI and b) Left-handed PPII.

Due to the existing equilibrium process between both conformational isomers (*cis*/*trans*), proline-rich peptides can alternate between both structures with a simple change in solvent. Modifications in the pyrrolidine ring, especially at the C^{γ}, can promote one conformation in front of the other.[96]

Moreover, the cellular uptake of oligoprolines can be potentiated with the functionalization at the C^{γ} of the pyrrolidine ring with cationic and hydrophobic functional groups to become a molecular scaffold (Figure 27) enhancing their properties as CPPs.[97,98,99,100] One of the most used modification is the introduction of an amino functional group in the γ-position of the pyrrolidine ring, in order to be used as building block in γ-peptides formation (Figure 27a).[101,102] The peptides built with γ-amino-L-proline present a significant stability towards the presence of proteases, reducing their degradation.[103]

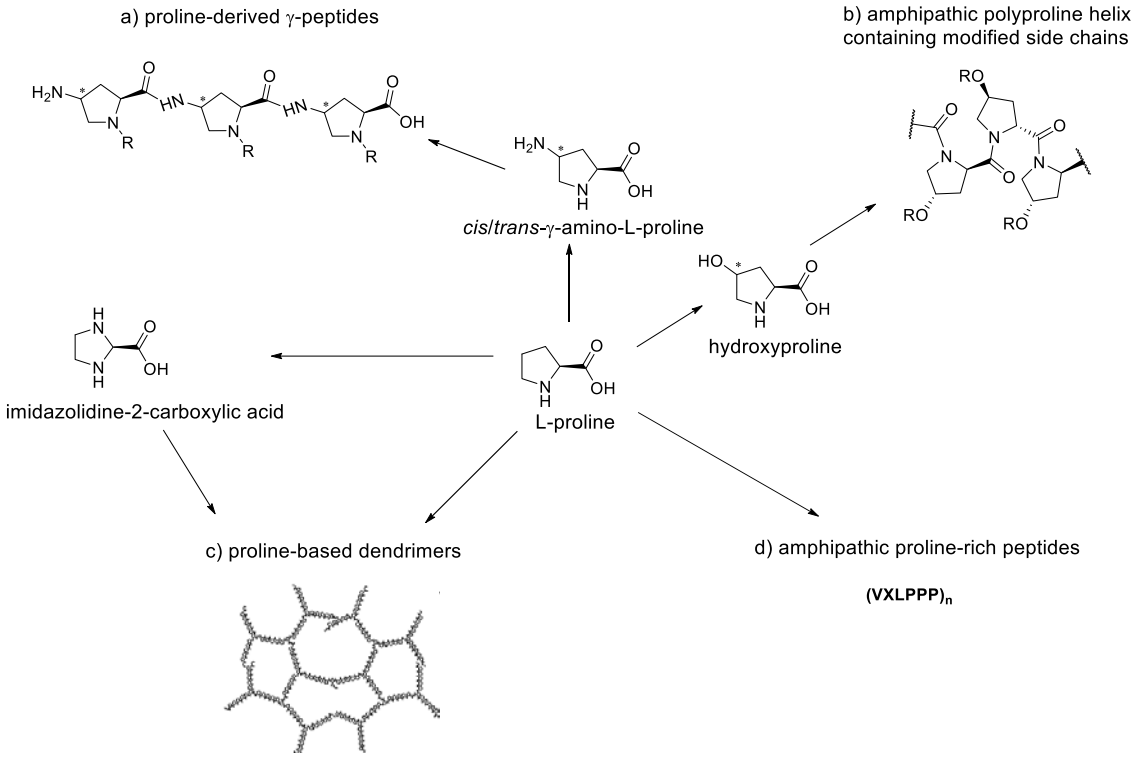

Figure 32. Some families of Pro-based CPP: a) proline derived γ-peptides, synthesized from *cis*-γ-amino-L-proline and functionalized in the N^{α} of the pyrrolidine ring; b) amphipathic polyproline helix containing side chains modified by *O*-alkylation of hydroxyl-L-proline monomer; c) proline-based dendrimers using a proline-like imidazolidine ring as branching unit; d) amphipathic proline rich-peptides, where X=Arg, His, Lys, and n=1 to 3; and e) proline-rich peptides from the anti-microbial peptide Bactenecin 7.

The other big advantage of CPPs containing γ-amino-L-proline residues is the possibility to modify the N^{α} present in the pyrrolidine ring with different groups, modulating the physicochemical properties of the final peptide.[101,102]

Royo, Albericio and co-workers synthesized a family of γ-hexapeptides based on *cis*-γ-amino-L-proline, obtaining good internalization values for *HeLa* cells (cervical cancer cells) and COS-1 (cell line derived from monkey kidney tissue), and presenting both low toxicity and great resistance to proteases. This work was followed by Dr. Carbajo[104] and Dr. Pulido[105] in their PhD thesis, demonstrating that CPPs with guanidinium groups linked to the pyrrolidine ring exhibit a better internalization in *HeLa* cells and *Leshmania donovani* parasites. This is probably due the amphipathic character of proline-rich CPPs (Figure 28 **CF-Gp-4**, **CF-Gp-10** and **CF-Gp-11**). More recently, Wennemers and co-workers have designed oligoproline octamers bearing guanidinium groups directly at the C^{γ} position of the pyrrolidine ring, generating a family of amphiphilic peptides with defined location of positive charge along the backbone, obtaining high efficient cellular uptake.[56,102] Therefore, the combination of proline and a guanidinium group, generates CPPs with a high uptake ability (Figure 33 **Z8** and **X8**). In all these works, the peptides incorporated the 5(6)-carboxyfluoroscein (CF) in order to quantify and locate the peptide inside the cell systems due to the emitted fluorescence in the green region of this moiety.

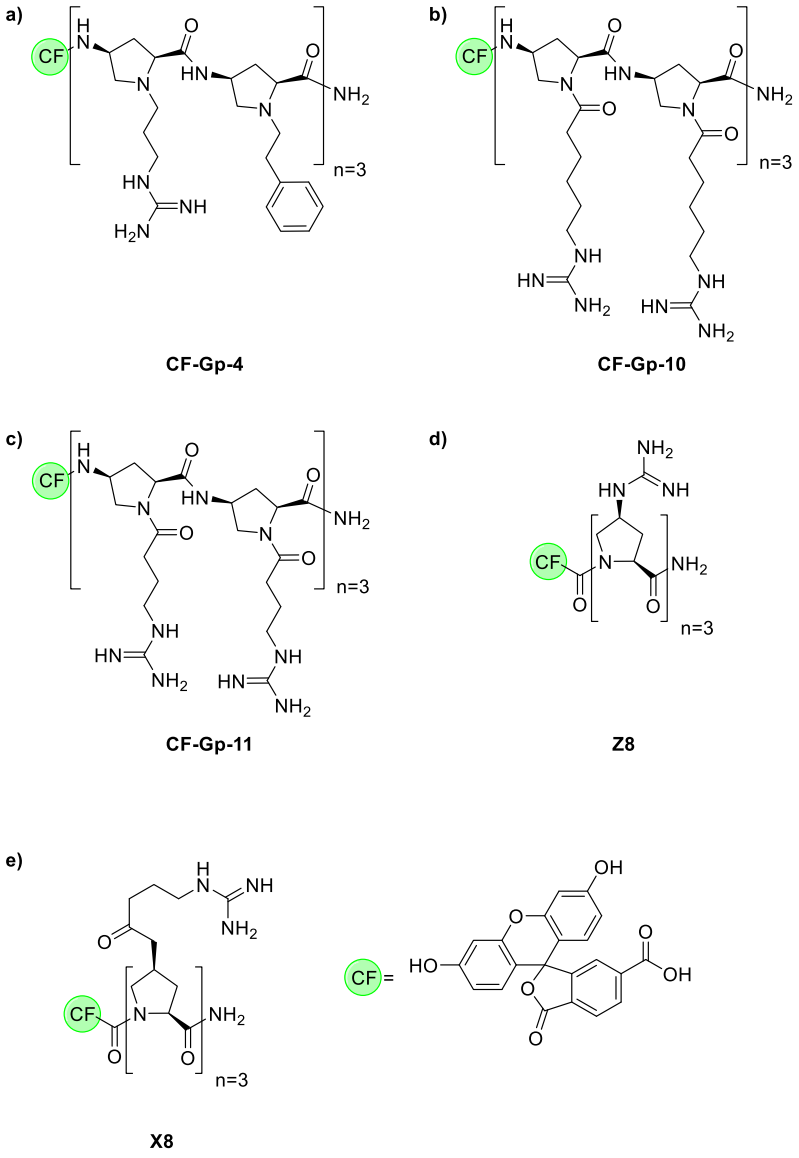

Figure 33. Some guanidylated proline-rich peptides based on *C*$^{\gamma}$-modified proline.

4.1.3 CPPs cellular internalization mechanisms

Despite numerous studies, internalization mechanisms of CPPs remain controversial. It is considered that internalization mechanisms depend on conditions such as CPP type, CPP concentration, cargo type, cell type, experimental methodology, and other factors, similar to some low-molecular compounds.[106,107] Nevertheless, endocytosis and direct translocation through the membrane are generally accepted as internalization mechanisms (Figure 34).[74] Furthermore, it is known that electrostatic interactions between CPPs and negative charges, such as proteoglycans or phospholipids, are essential for initiating CPP internalization.

Proteoglycans constitute a protein heterogeneous group with polysulphate glycosaminoglycans polysaccharides (GAG). For example, arginine residues in CPPs form bidentate binding to negative charged groups, while lysine residues form monodentate binding to them.[108,109]

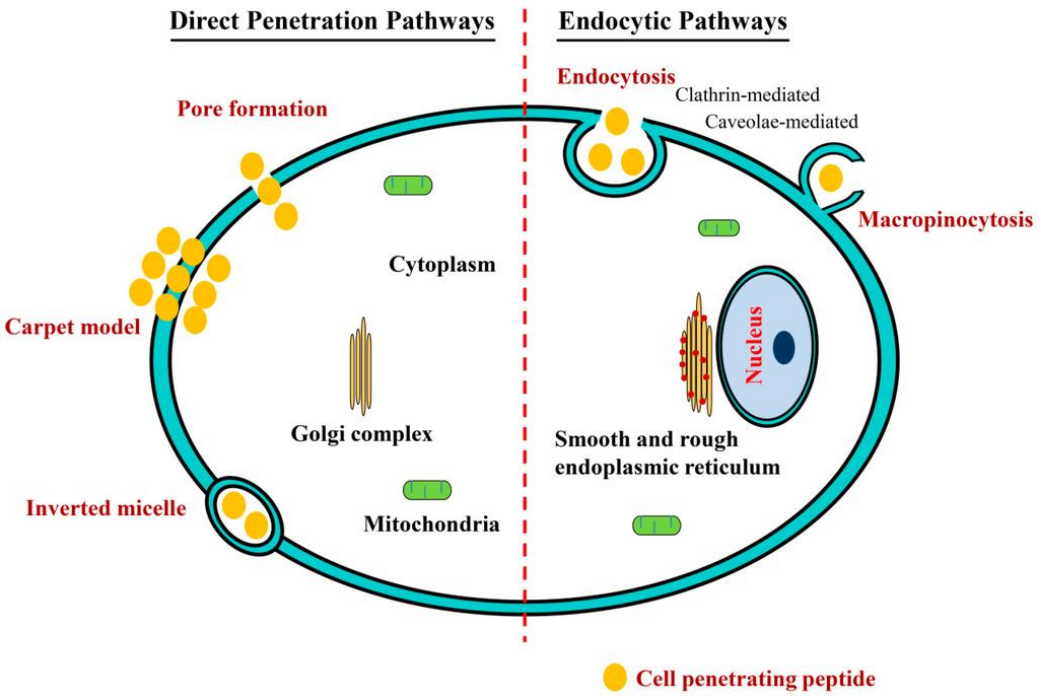

Figure 34. Mechanisms of peptide uptake across the cellular membrane. Extracted from Singh et. al.[110]

For this reason, increasing the number of arginine and lysine residues in CPPs improves the electrostatic interaction between the cell membrane and the peptide, promoting the internalization.[111,112]

Proline-based peptides containing positive charges given by protonated guaninidium groups, present either in the C^{γ} or in the N^{α} of the pyrrolidine ring, can act in the same way as arginine.[56,113] Moreover, work has been done to identify the mechanism by which amphipathic Pro-rich CPPs enter cell, determining that a contribution of both endocytosis and direct translocation through the membrane happens in a determined ratio. This ratio can be changed, as mentioned before, by different factors.[114,115]

4.1.4 *HeLa* Cells

HeLa is a cell type in an immortal cell line used in scientific research. It is the oldest and most commonly used human cell line (Figure 35).[116] The line was derived from cervical cancer cells taken in 1951 from Henrietta Lacks, a patient who died of cancer.[117] The cell line was found to be remarkably durable and prolific, warranting its extensive use in scientific research.[118] In 2009, it was estimated that more than 60 thousand scientific articles were published about research done on *HeLa* cells, with an incredible increasing rate of more than 300 papers each month.[119] Searching for bibliography in Scifinder® one can obtain between 130.000 and 170.000 publications related to this cell line. For all these reasons, *HeLa* cells are the best candidates to perform the initial studies of the penetration ability and toxicity of new drugs, compounds and materials.[120,121]

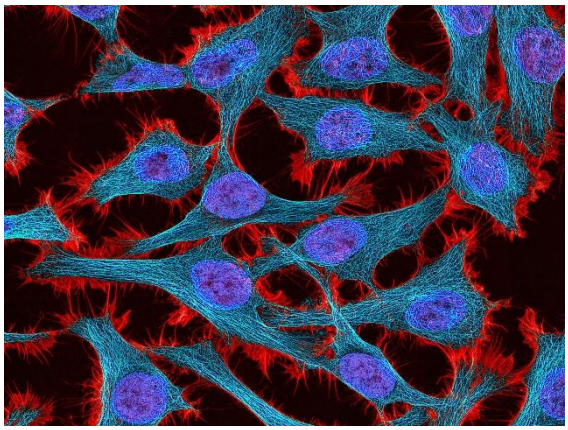

Figure 35. *HeLa* cells observed by using confocal microscopy.

4.1.5 Cell Penetrating Peptides used in *Leishmania donovani* and *Leishmania pifanoi*

4.1.5.1 Leishmaniasis

Infectious diseases such as malaria, tuberculosis, filariasis, visceral leishmaniasis, leprosy and the contagion of the VIH represent a massive problem to worldwide health. The control of these diseases and the eradication of new outbreaks has been a challenging study for the public health. Leishmaniasis has been categorized by the World Health Organization (WHO) as category-I, which includes emerging and not controlled diseases.[122]

In 2010, WHO presented a report describing that more than 350 million people were in risk to come down with leishmaniasis, with approximately 2 million new cases per year.[123] Nowadays, it is estimated that between 700 thousand and 1 million of new cases appear every year with 20 to 30 thousand of deaths annually.[124] The disease is caused by a protozoon kinetoplastid found in *Leishmania* species belonging to Trypanosomatidae family (Table 2).[125] This parasitic infection manifests in several clinical forms including cutaneous leishmaniasis (CL), mucocutaneous leishmaniasis (MCL), diffuse cutaneous leishmaniasis (DCL), visceral leishmaniasis (VL), post-kala-azar dermal leishmaniasis (PKDL) and leishmaniasis recidivans (LR), being the main ones VL, CL and MCL.[126] In 2012, WHO estimated that 500 thousand new cases of visceral leishmaniasis (the most deadly) appear every year, generally caused by the *Leishmania donovani* and *Leishmania infantum* parasites.[127] Moreover, leishmanial infection has become complicated with co-infection of AIDS and it has gained substantial importance in HIV-infected people as an opportunistic infection in regions where both infections are endemic.[128]

Table 2. Principal *Leishmania* species that affect human beings.

	Clinical manifestation	**Species**
Old World, Leishmania subgenre	Visceral Leishmaniasis	***Leishmania donovani***
		Leishmania infantum
	Cutaneous Leishmaniasis	*Leishmania major*
		Leishmania tropica
		Leishmania aethiopica
	Diffuse Cutaneous Leishmaniasis	*Leishmania aethiopica*
New World, Leishmania subgenre	Visceral Leishmaniasis	*Leishmania infantum*
	Cutaneous Leishmaniasis	*Leishmania infantum*
		Leishmania mexicana
		Leishmania pifanoi
		Leishmania amazonensis
	Diffuse Cutaneous Leishmaniasis	*Leishmania mexicana*
		Leishmania amazonensis
New World, Viannia subgenre	Cutaneous Leishmaniasis	*Leishmania braziliensis*
		Leishmania guyanensis
		Leishmania panamensis
		Leishmania peruviana
	Mucocutaneous Leishmaniasis	*Leishmania braziliensis*
		Leishmania panamensis

Leishmania are intracellular parasites that are transmitted to mammalian and infect them by the bites of female sandflies from the Phlebotomus and Lutzomyia genera via anthroponotic or zoonotic cycles.[129,130] The increase in leishmaniasis incidence and prevalence, which is still one of the world's most neglected diseases, is mainly attributed to several risk factors that are clearly man made. Generally, environmental conditions like climatic changes, socio-economic status (malnutrition, poor sanitary conditions), demographic and human behaviors such as great migration, deforestation, urbanization and immunosuppression pose major risks for human leishmaniasis.[131,132,133] The environmental and the population movements probably lead to alteration in the number, range and density of the vector and reservoir and, consequently, may increase human exposure to infected sandflies.[134] In more developed countries *Leishmania* affects exclusively pets, more specifically dogs.[135]

Leishmania parasites are dimorphic organisms: they have two different morphological forms in their life cycle (Figure 36). The amastigote form can be found in the phagocyte of the mammal guest and promastigotes are located in the digestive organs of the vector (sandfly mosquito).[136] These parasites invade, through macrophages, granulocytes or by direct absorption, different tissues located in the liver, the spleen or the bone marrow.[137,138]

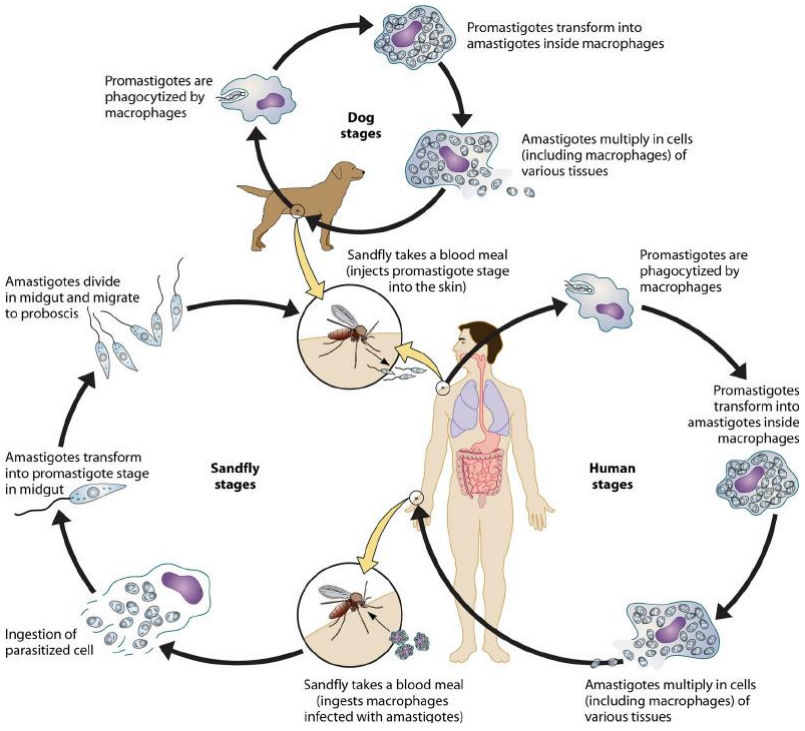

Figure 36. Lyfe cycle of *Leishmania* parasites. Extracted from Petersen et. al.[139]

Treatment of leishmaniasis is still a challenge because there are several problems such as high cost of drugs, high drug-dosage, incidence and prevalence of drug-resistance, side-effects and lack of affordable new antileishmanial drugs.[140] On the other hand, commonly used drugs do not completely eradicate parasites from infected people, making the treatment more difficult by lowering their efficacy and enhancing some of the previous cited problems. [141,142] Moreover, one of the main problems is the high cost of diagnosis, treatment generally paid by patients and loss of household income.[143,144]

Pentavalent antimonial derivatives (Figure 37a and Figure 37b) have been the first line drugs and gold standard in treatment of leishmaniasis disease in humans. Among them, sodium stibogluconate (Pentostam®) and meglumine antimoniate (Glucantime®) are the most used around the world.[145] However, these drugs need long courses of administration (up to 30 days) and are very toxic, with several undesirable adverse side effects.[146] Another resources for leishmaniasis chemotherapy are amphotericin B (Figure 37d), pentamidine (Figure 37c), miltefosine (Figure 37f) and paromomycin (Figure37e).[147]

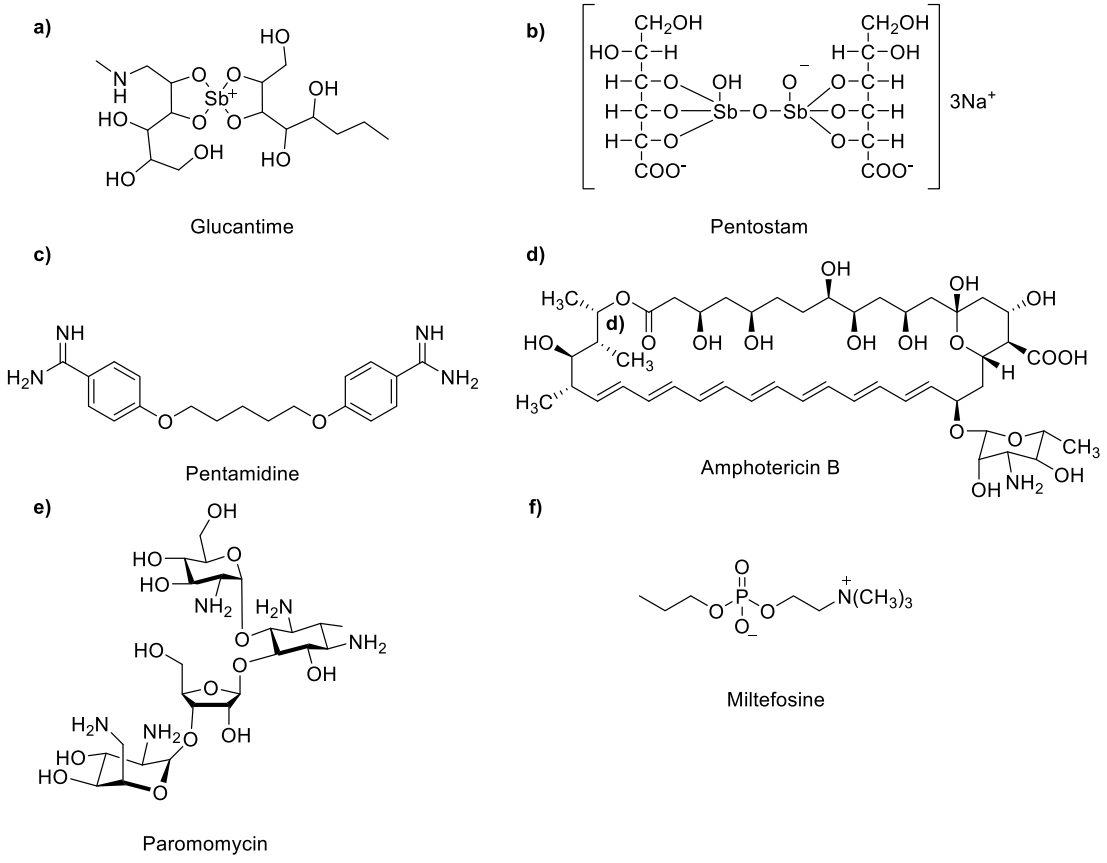

Figure 37. Frequently used antileishmanial drugs.

Amphotericin B (Figure 37d) is an antibiotic and antifungal drug showing effective antileishmanial activity against different species of *Leishmania*, usually administered as the second line treatment. However, adverse side effects are major limiting factors in administration of Amphotericin B.[148,149] To overcome these problems, liposomal Amphotericin B was created, being less toxic, more bioavailable and better tolerated by patients.[150]

Miltefosine (Figure 37f) is an alkyl phosphocholine compound used in treatment of microbial and fungal infection, cutaneous metastases of breast cancer, solid tumors, schistosomiasis and therapy of cutaneous and visceral leishmaniasis.[130] Miltefosine is the first non-parenteral drug and it can be administered orally and locally in treatment of leishmaniasis. However, misuse of the drug, its long half-life of 7 days, inactivation of genes responsible in drug uptake and several adverse side effects are some of its drawbacks.[151,152]

Nowadays, the research is focused in the development of new carriers such as nanoparticles[153] and liposomes,[154] exploring new strategies for the efficient treatment of Leishmaniasis. Nevertheless, Leishmaniasis is a complex disease with different clinical manifestations and which symptoms vary depending on the parasite species. The combination of new drugs, vaccines, delivery systems and better diagnosis tests can be a promising approach to cure the disease.[136]

4.1.5.2 Precedents of conjugated peptides as antileishmanial vectors

As mentioned in the introduction of this Chapter, permeability of the biological membranes is one of the determining factors in the pharmacokinetic process of a drug. For this reason, several bioactive molecules cannot cross the plasmatic membrane, which is a drawback for an efficient treatment. As previously explained, CPPs are reliable candidates for being used as carrier systems due to their ability to conjugate diverse biologically active molecules (covalently or not) and translocate the membrane.[155] Currently CPPs research is mainly focused in drug release treatment in mammal cells but some antimicrobial peptide drug candidates are found in the bibliography.[156] Moreover, peptides with therapeutic approaches against infectious disease are becoming more important during the last years.[157]

The function and structure of the plasmatic membrane for *Leishmania* parasites are different from those described for mammal cells, and this has hindered the study of CPPs for this protozoa. Andreu and co-workers evaluated the use of peptide conjugates (TAT_{48-60} as carrier and miltefosine as antileishmanial drug) on *L. donovani* parasites. Results showed the capacity of internalization and low toxicity of this conjugate both in amastigotes and promastigotes, visualizing the final destination of the antiparasitic drug.[158] More recently, Velázquez and collaborators synthesized a series of amide-bridged cyclic peptides derived from the linear prototype Ac-PKIIQSVGIS-NIe-K-NIe-NH_2 by introduction of the lactam between amino acid side chains that are separated by one helical turn (*i,i+4*). The peptides showed good resistance to proteases and potent *in vitro* activity against *L. Infantum* when conjugated to cationic CPPs.[159]

Proline-rich peptides like γ-peptides **CF-Gp-11**, **CF-Gp-14** and **CF-Gp-15** (Figure 38) showed a high ability to cross the *L. donovani* parasite membrane compared to CF-TAT_{48-57}. However, by the time the quantity of guanidinium groups (with their corresponding positives charge) rose, the toxicity became significantly high against parasites.[105]

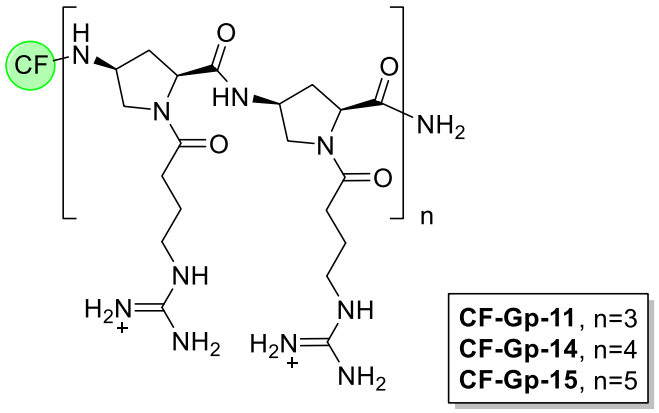

Figure 38. Chemical structure of previously investigated proline-based γ-peptides.

4.1.6 Cyclobutane-derived peptides

As explained in Chapter 2 and 3 of this thesis, our research group has developed the stereo- and enantioselective synthesis of non-natural β-[43,46,160] and γ-amino acids,[3] incorporating the cyclobutane moiety as conformational restricting element. Using this knowledge, a first generation of hybrid peptides built with γ-CBAA and γ-amino-L-proline was prepared by Dr. Raquel Gutiérrez-Abad. In this work, two diastereoisomeric series of γ,γ-peptides were prepared alternating enantiomeric γ-CBAA (1*S*,3*R*)-**71** or (1*R*,3*S*)-**ent-71** and conveniently protected γ-*cis*-amino-L-proline **45**, (Figure 39).[57]

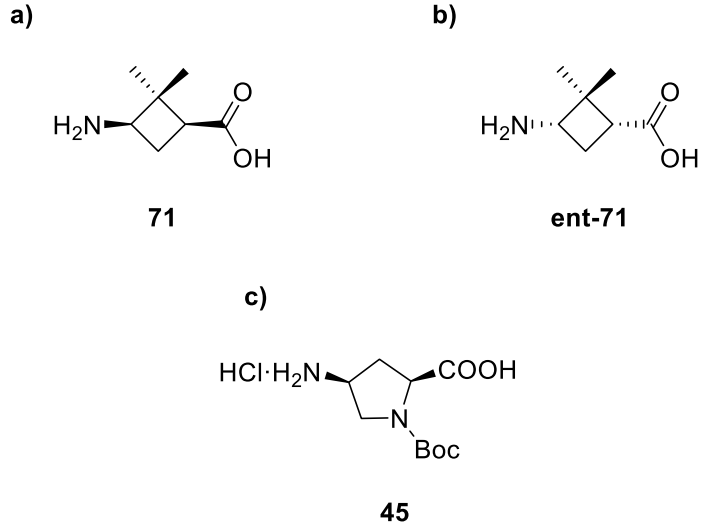

Figure 39. γ-Cyclobutane-based amino acids and γ-*cis*-amino-L-proline used for the synthesis of the first generation of γ,γ-hybrid peptides.

As mentioned in Chapter 3 of this thesis, the presence of the γ-substituted cyclobutane scaffold induces the formation of rigid secondary structures with different conformations in solution. Moreover, the synthesized γ,γ-peptides (Figure 40) showed low toxicity and moderate uptake behavior in *HeLa* cells, demonstrating that the larger the peptide backbone, the better the internalization. Furthermore, the absolute configuration of the cyclobutane moiety was not found to be relevant in the peptide ability to cross the membrane.

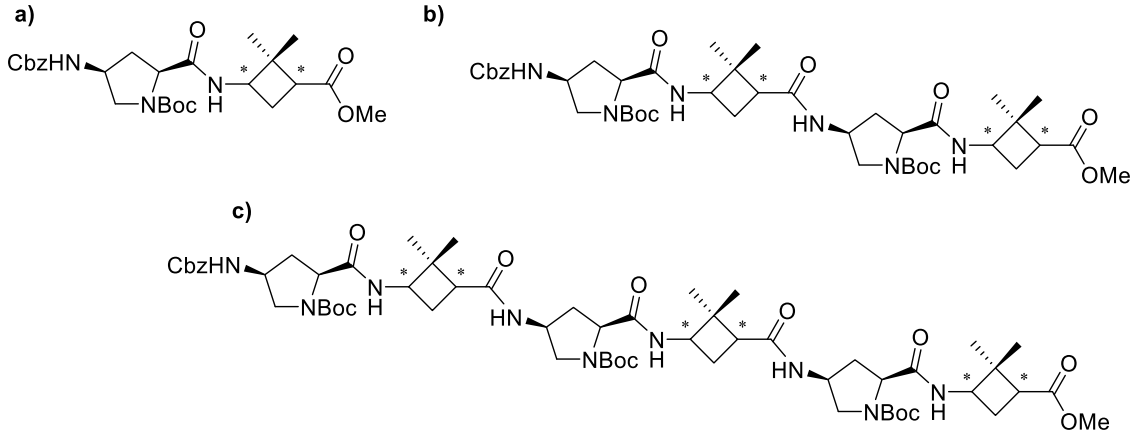

Figure 40. First generation of hybrid peptides synthesized using γ-cis-amino-L-proline **45** and γ-CBAA (1*S*,3*R*)-**71** or (1*R*,3*S*)-**ent-71**, respectively.[57]

Following the previous work, Dr. Esther Gorrea designed and synthesized the second generation of γ,γ-hybrid peptides to study the cell penetrating ability in *HeLa* cells depending on the substituent attached to the N^{α} of the pyrrolidine ring of the *cis*-γ-amino-L-proline residue (Figure 41). None of the synthesized peptides presented toxicity in this cell line. The best internalization result was obtained for the peptide containing a five carbon spacer attached to the N^{α} of the pyrrolidine ring containing a guanidinium group in its end (Figure 42h).[160]

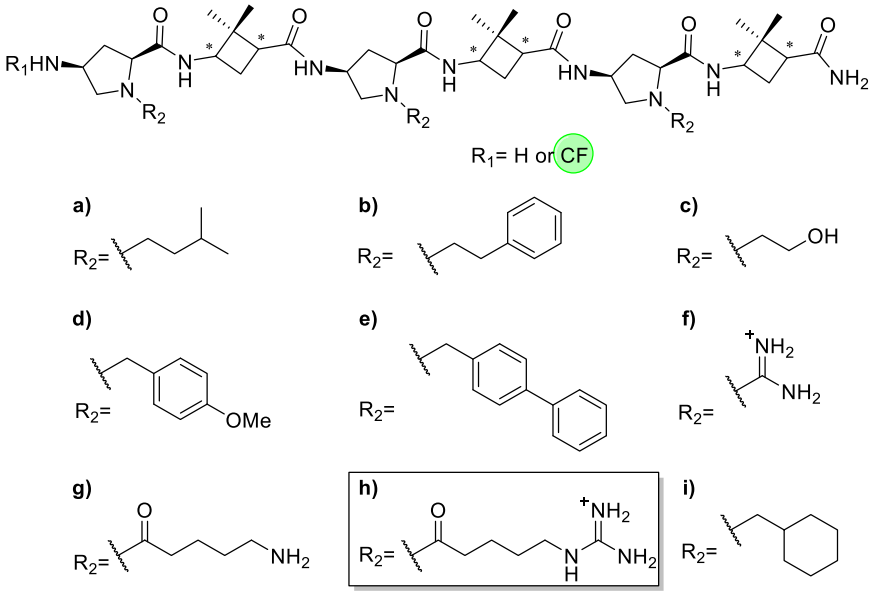

Figure 41. Structures of the second generation hybrid γ-CBAA,γ-*cis*-amino-L-proline peptides.[160]

Thus, the biological study of the hybrid γ-CBAA,γ-amino-L-proline hybrid peptides manifested that the introduction of the cyclobutane moiety in the peptide backbone provided the perfect balance between the positive charges given by the accessible guanidinium group (Figure 42h) and the hydrophobicity contribution of the proline and cyclobutane carbon rings.

With all the previous work in the field, Dr. Jimena Ospina, in her PhD thesis,[161] developed two families of γ-CBAA,γ-amino-L-proline hybrid peptides. The first family was synthesized by combining γ-CBAA **72** and conveniently protected γ-*cis*-amino-L-proline **73**, while the second series was prepared using β-CBAA **74** and γ-*trans*-amino-L-proline **75** joined in alternation (Figure 42).

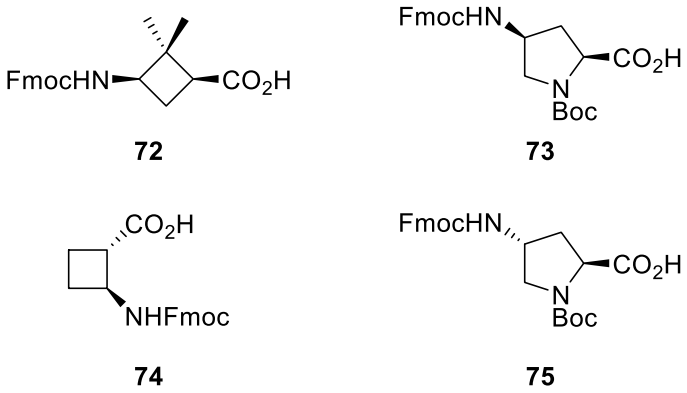

Figure 42. Monomers used as building blocks for the peptide synthesis.

The synthesis of these peptides was performed using solid phase synthesis (SPS) obtaining peptides of different lengths (Figure 43): ones functionalized with CF to follow their uptake in both *Leishmania* parasites and *HeLa* cells and others as free amines in the *N*-terminus. The peptides containing the β-CBAA gave worst results in terms of uptake behavior than those containing γ-CBAA. Furthermore, increasing the length of the peptides did not represent a rise in toxicity for *HeLa* cells and resulted in better uptake abilities for both families. Regarding *Leishmania* parasites, the studies showed encouraging uptake results for both families, especially for γ,γ-hybrid peptides in *L. Donovani* promastigotes.

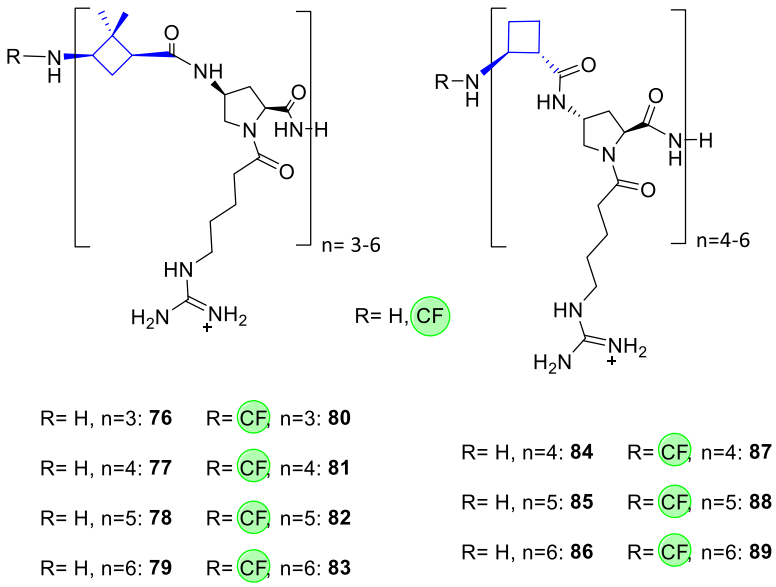

Figure 43. Synthesized hybrid CPPs using γ-/β-CBAA and γ-*cis*-/*trans*-amino-L-proline moieties, respectively. Lengths varied from hexamers to dodecamers.

4.1.7 Solid Phase Synthesis (SPS)

In solid phase synthesis, the peptide is built through continuous cycles of deprotection, coupling and wash (Scheme 10). Due to the necessity of several repetitive steps, the use of solid supports presents interesting synthetic advantages such as the ease to remove the excess of reagents and by-products by filtration and wash processes.

In SPS, the first amino acid, which is *N*-protected, is coupled through its carboxylic acid group to the resin that has a free hydroxyl, chloro or amino group in its surface, producing an ester- or amide-group anchored to the resin, respectively. After fixing the first amino acid, the peptide sequence is generated lineally from the *C*-terminus to the *N*-terminus (C→N strategy). The growth of the peptide skeleton is performed by consecutive cycles of deprotection of the *N*-terminus (X protecting group), which is immediately coupled to the *C*-terminus of the next amino acid. This process (deprotection/coupling) is repeated until the desired sequence is obtained. The functional groups present in the side chains of the peptide must be protected with stable groups (Y) to the deprotection conditions for peptide elongation.

On the other hand, X protecting groups should be labile under mild conditions that preserve the integrity of the peptide and prevent epimerization. However, Y protecting groups can be used to attach functionalized moieties to the peptide backbone, tuning its physicochemical properties. Once the peptide is completely built, the scission of the peptide from the resin is generally performed by using HF or TFA, obtaining peptides with a *C*-terminus carboxylic acid or amide, depending on the chosen resin.

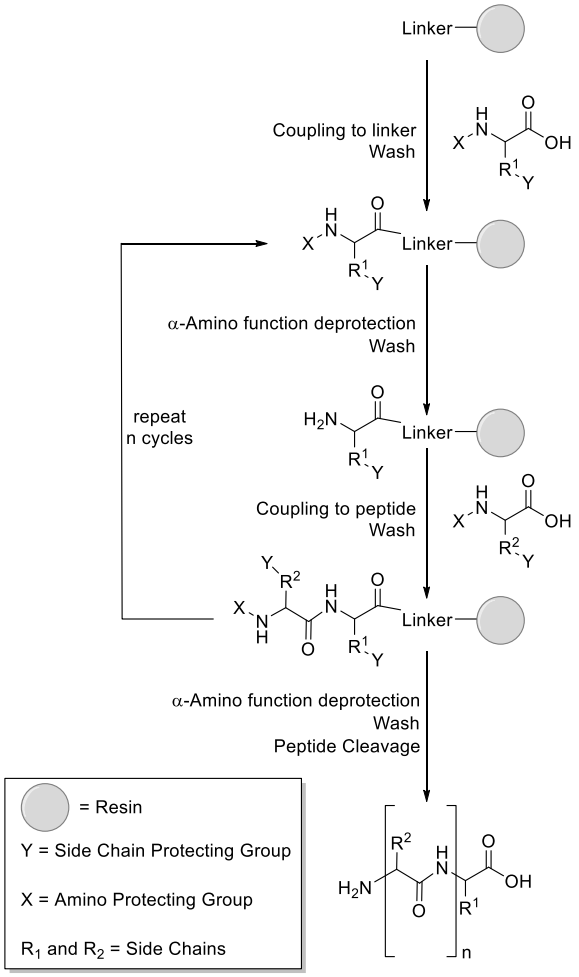

Scheme 10. General protocol for peptide building in SPS.

Coupling and deprotection reactions of the *N*-terminus are followed by means of the ninhydrin test (also known as Kaiser test). Ninhydrin reacts with the presence of primary amines giving a blue color that can be visually detected. Likewise, coupling and deprotection reactions of secondary amines present in the side chains can be monitored using the chloranil test. If the resin remains yellowish, there are no free secondary amines, while if it turns blue, free secondary amines are found (section 7.5). Peptides cleaved from the resin generally require purification and characterization.

4.2 Objectives

Taking into account the results described in Chapter 3 of this thesis and previous results of our group introduced in the present chapter, the stereoselective synthesis of two different γ-*cis*-CBAA and γ-amino-L-proline hybrid peptides was proposed (Figure 44). Once synthesized, they would be evaluated as potential carriers for delivering cargoes across different biological barriers.

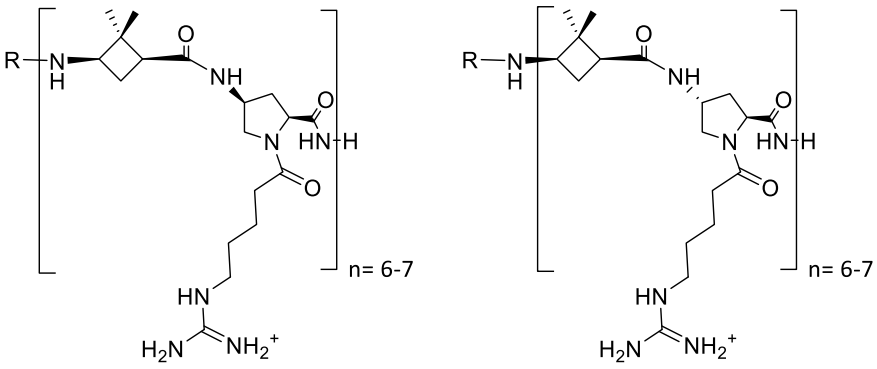

R= H, n=6: **79**

R= H, n=7: **90**

R= CF, n=6: **83**

R= CF, n=7: **91**

R= H, n=6: **92**

R= H, n=7: **93**

R= CF, n=6: **94**

R= CF, n=7: **95**

Figure 44. Proposed structures of hybrid peptides in this work.

The specific objectives of this part were:

- The synthesis of the required monomers with their suitable protections to be used for the synthesis of the peptides by SPS.
- The solid phase synthesis of the γ-*cis*-CBAA,γ-*cis*-amino-L-proline hybrid peptides **79**, **83**, **90**, **91** and the γ-*cis*-CBAA,γ-*trans*-amino-L-proline hybrid peptides **92-95** using the Fmoc/Alloc strategy.
- The solid phase synthesis of TAT_{48-57} reference peptide with and without 5(6)-carboxyfluoroscein (CF), **96** and **97**, respectively (Figure 45).

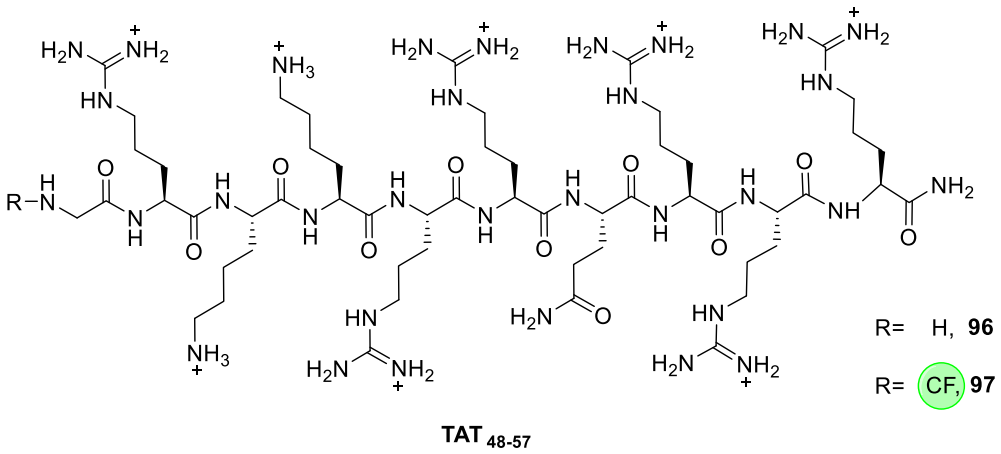

Figure 45. TAT_{48-57} reference peptide structure

- The study of the cytotoxicity and cell penetrating behavior of these hybrid peptides in *HeLa* cells, *Leishmania donovani* and *Leishmania pifanoi* parasites by using MTT assays, flow cytometry and confocal microscopy.
- The conjugation of a drug to the peptides and evaluation of their behavior as potential antileishmanial agents (Figure 47).

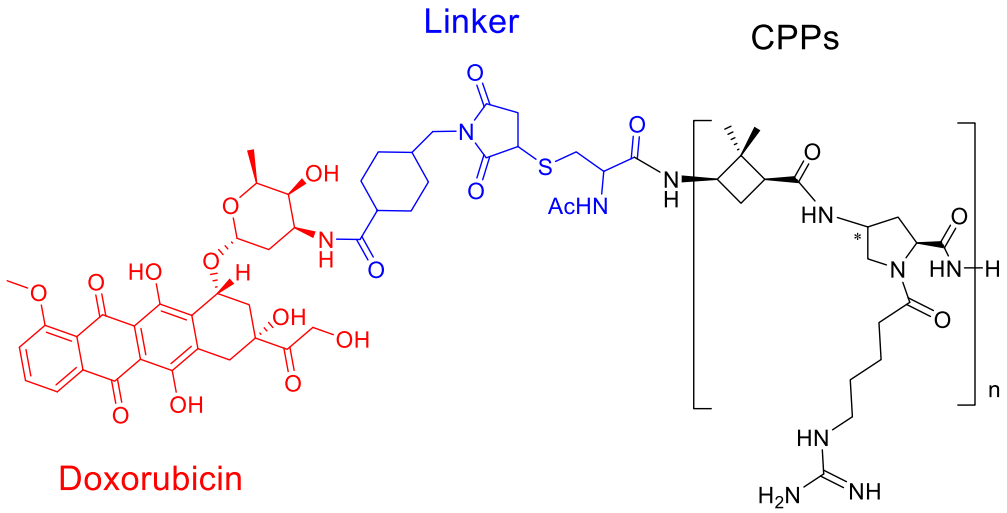

Figure 46. Proposed drug-conjugated peptides.

4.3 Results and discussion

The results of this chapter of this thesis are presented in various sections. First, the synthesis of monomers with the desired protections to be used in SPS is discussed (section 4.3.1). Second, the synthesis of the new hybrid γ-CBAA,γ-amino-L-proline peptides to be studied as CPPs is presented (section 4.3.2). Third, the conjugation of the peptides with doxorubicin is reported (section 4.3.3). Finally, the toxicity and uptake behavior studies of these peptides in *HeLa* cells and *Leishmania* parasites is described (section 4.3.4 to 4.3.6).

4.3.1. Synthesis of monomers with the required protecting groups

Considering that both peptide families were synthesized using the Fmoc/Alloc strategy, it was necessary to have the three amino acids **72**, **98** and **99** N^{γ}-protected with an Fmoc (9-Fluoroenylmethyloxycarbonyl carbamate). Moreover, the protection of the N^{α} of the pyrrolidine ring with an Alloc (1-Allyloxycarbonil) group was required. The side chain (**100**) should be protected with a Boc protecting group to avoid by-products during the synthesis.

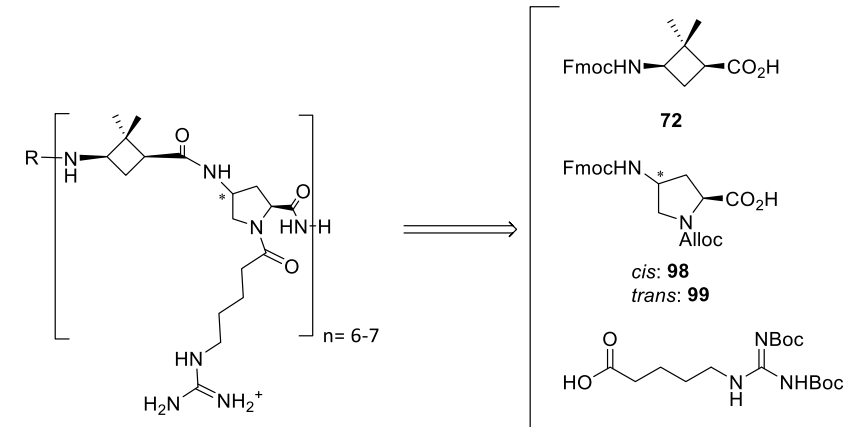

cis-γ-aminoproline	*trans*-γ-aminoproline
R= H, n=6: **79**	R= H, n=6: **92**
R= H, n=7: **90**	R= H, n=7: **93**
R= CF, n=6: **83**	R= CF, n=6: **94**
R= CF, n=7: **91**	R= CF, n=7: **85**

Scheme 11. Retrosynthetic analysis of envisaged peptides and monomers required for their synthesis.

4.3.1.1 Synthesis of γ-cyclobutane monomer 60

γ-Cyclobutane amino acid **72** could be obtained from previously described γ-cyclobutane amino acid **48** (Scheme 12) and following the route developed by the research group.[160]

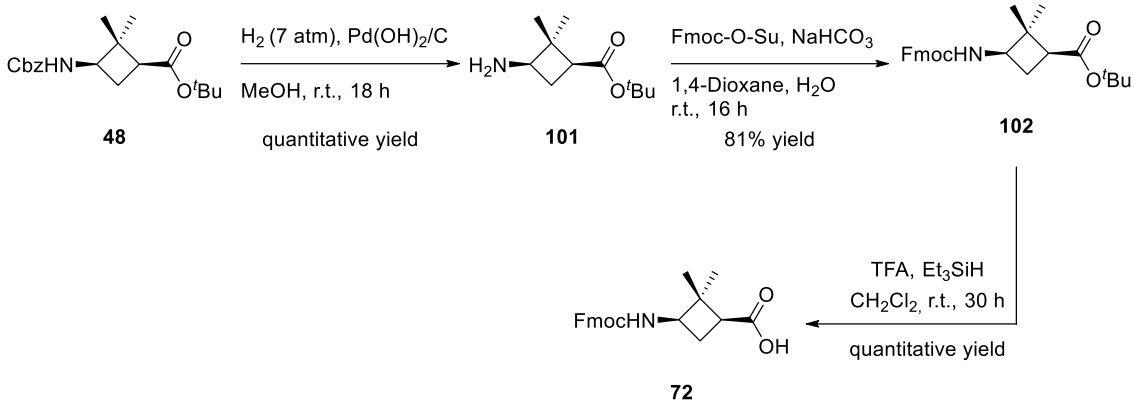

Scheme 12. Synthetic route to afford γ-cyclobutane amino acid **72**.

Starting with orthogonally protected amino acid **48**, a hydrogenation reaction was performed to obtain free amine **101** in quantitative yield. After that, the protection of the amine as Fmoc carbamate **102** was achieved by using Fmoc *N*-hydroxysuccinimide ester (Fmoc-O-Su) in presence of $NaHCO_3$ in 81% yield. Finally, with an acidolysis reaction, the desired γ-cyclobutane amino acid **72** was obtained in quantitative yield.

4.3.1.2 Synthesis of γ-amino-L-proline monomers 98 and 99

γ-Amino-L-proline amino acids **98** and **99** could be obtained from their analogs **73** and **75** with a simple protecting group change in order to adapt the monomer to the chosen resin for SPS of the peptides (Scheme 13).

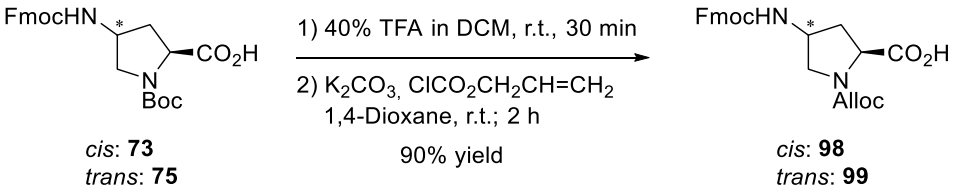

Scheme 13. Synthetic route to obtain the desired γ-amino-L-proline derivatives **98** and **99**.

The synthesis started with the deprotection of the Boc carbamate at the N^{α} of the pyrrolidine ring of any of the commercially available γ-amino-L-proline **73** or **75** by using trifluoroacetic acid (TFA) in dichloromethane. After removal of excess solvents and reagents, allyl chloroformate in the presence of K_2CO_3 was added to obtain compounds **98** and **99** in 90% yield after purification.

4.3.1.3 Synthesis of the side-chain fragment containing the guanidinium group 100

The guanidinium-containing side-chain was synthesized through a reaction involving two commercially available products, **103** and **104** (Scheme 14).

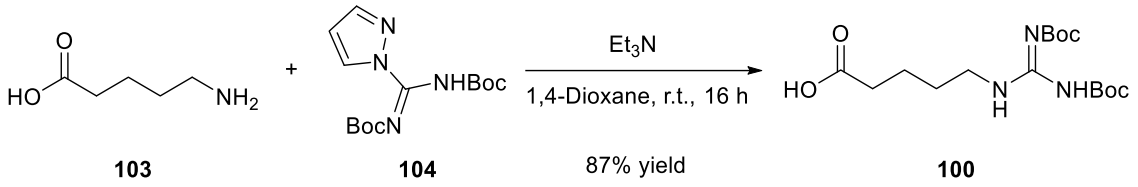

Scheme 14. Synthesis of guanidinium-containing side chain **100**.

The reaction was performed by combining amino acid **103** with the *N*, *N'*-di-Boc-1*H*-pyrazole-1-carboxamidine **104** in the presence of triethylamine. After purification, the desired compound was obtained in 87% yield.

4.3.2 Solid phase synthesis of the peptides

The synthesis of all the peptides included in this thesis was carried out in the Combinatorial Chemistry Unit in Parc Científic of Barcelona (UQC-PCB), directed by Dr. M. Royo. As stated before, the solid phase synthesis (Figure 47) of the peptides was performed by using the Fmoc/Alloc strategy, using the H-rink amide ChemMatrix® resin with 0.47 mmol/g functionalization.

Figure 47. Solid phase synthesis set-up.

4.3.2.1 SPS of γ–CBAA ,γ-amino-L-proline hybrid peptides

Both families containing the *cis*-γ-cyclobutane amino acid and the *cis*-/*trans*-γ-amino-L-proline were synthesized following the same strategy. The first step was the coupling of the chosen γ-amino-L-proline (*cis*-**98** or *trans*-**99**, respectively) to the amino function present in the resin using *N*,*N*'-diisopropylcarbodiimide (DIC) as coupling agent and OxymaPure® as additive. After that, the deprotection of the Fmoc carbamate was performed by using piperidine in DMF (2:8) following with the coupling of the γ-CBAA to the first amino acid using PyBOP as coupling agent, OxymaPure® as additive and DIPEA as base. The sequence was repeated several times to elongate the peptide chain, intercalating the monomers **72** and **98** or **99** (Scheme 15), until reaching the desired length, twelve units (dodecamer) or fourteen units (tetradecamer). The coupling and deprotection reactions were checked by using the colorimetric Kaiser test (ninhydrin test, section 7.5.1).

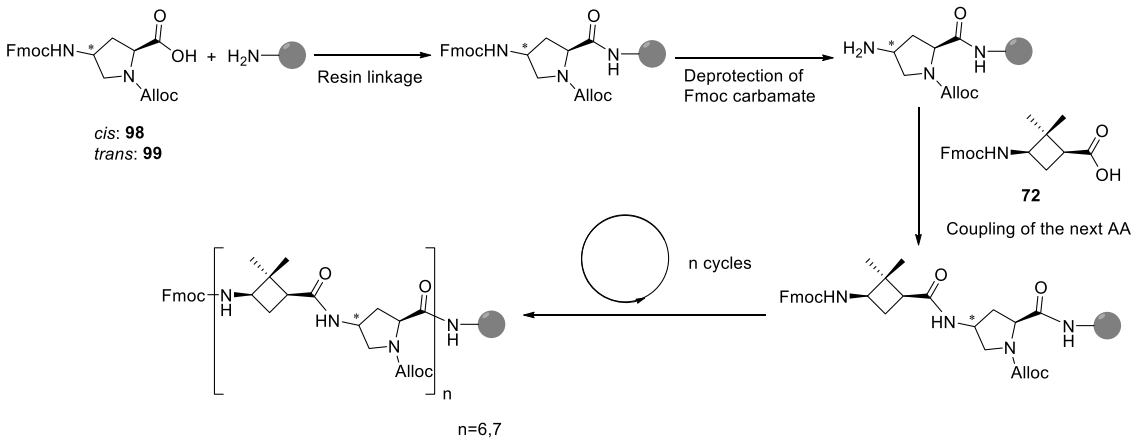

Scheme 15. Peptidic chain elongation of both peptide series.

Once the desired peptide length was obtained, the removal of the Alloc carbamate was achieved by a palladium-catalyzed reduction using $Pd(PPh_3)_4/PhSiH_3$ (12:0.1) in DCM (Scheme 16). By the time the deprotection was checked by using the chloranil test (section 7.5.2), side-chain **100** was coupled using DIC as coupling agent and OxymaPure® as additive.

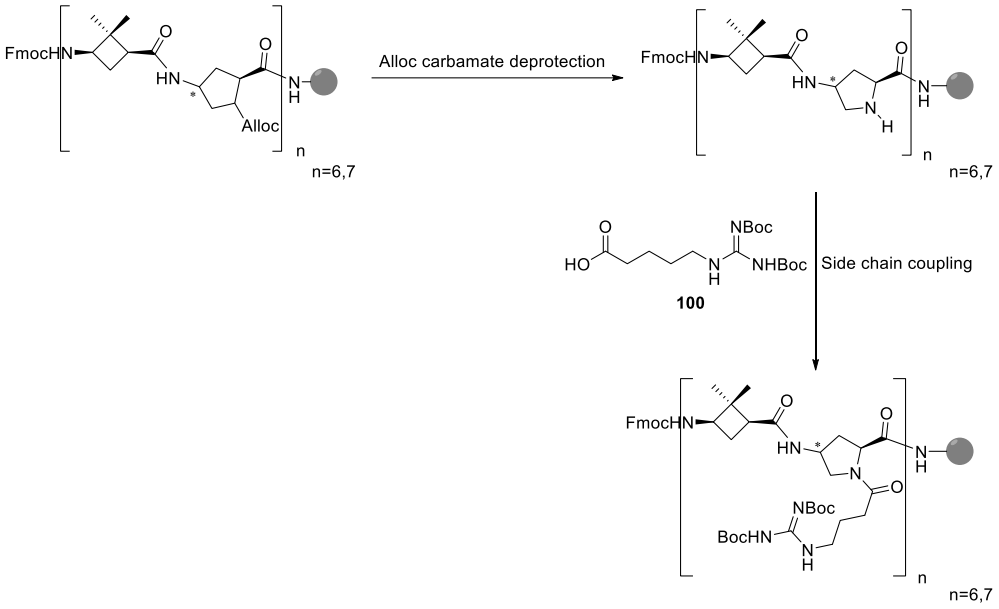

Scheme 16. Side-chain alkylation of the previously synthesized peptidic skeleton.

Each peptidic sequence (dodecamer and tetradecamer) was treated separately. First of all, the last Fmoc protection group was removed and then the resin was divided in two parts. One part of the resin, with the attached peptide, was used to conjugate the peptide to the CF in the *N*-terminal amino group. The other part of the resin was left without performing any modification (Scheme 17).

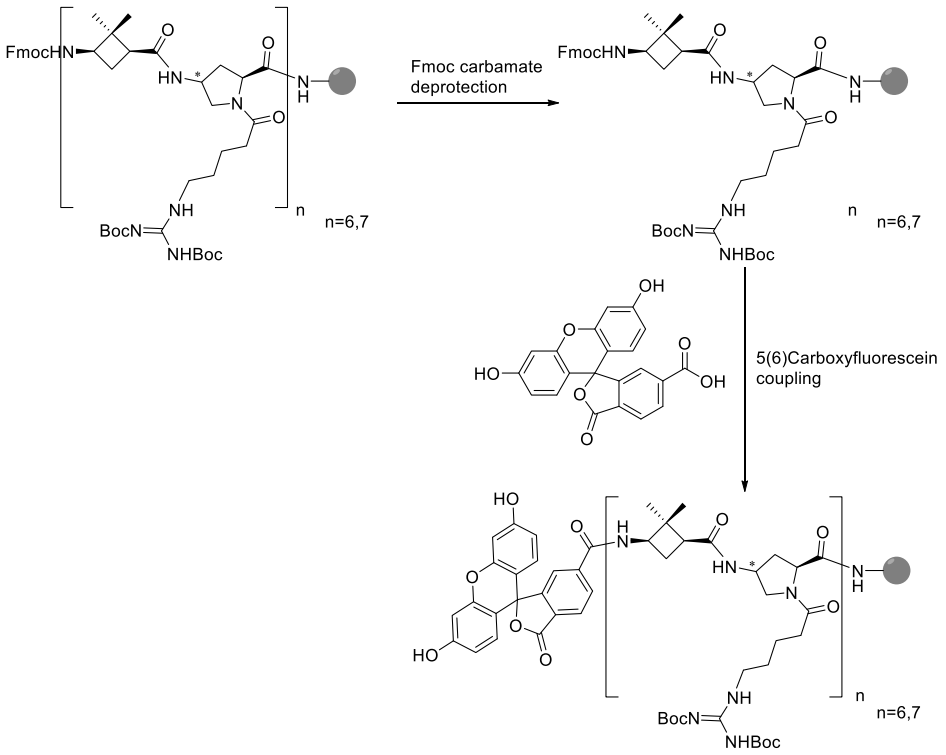

Scheme 17. CF incorporation to the peptide skeleton.

Finally, the cleavage of the peptide from the resin was achieved by acid hydrolysis using a mixture of TFA/TIS/H_2O (95:2.5:2.5). With this methodology, *tert*-butyl carbamates present in the guanidinium group were also removed (Scheme 18). Peptides were then lyophilized, purified by semiprep-RP-HPLC-MS (section 7.4.2.2) and characterized by RP-HPLC-MS and RP-HPLC (sections 7.4.2.1 and 7.4.2.3).

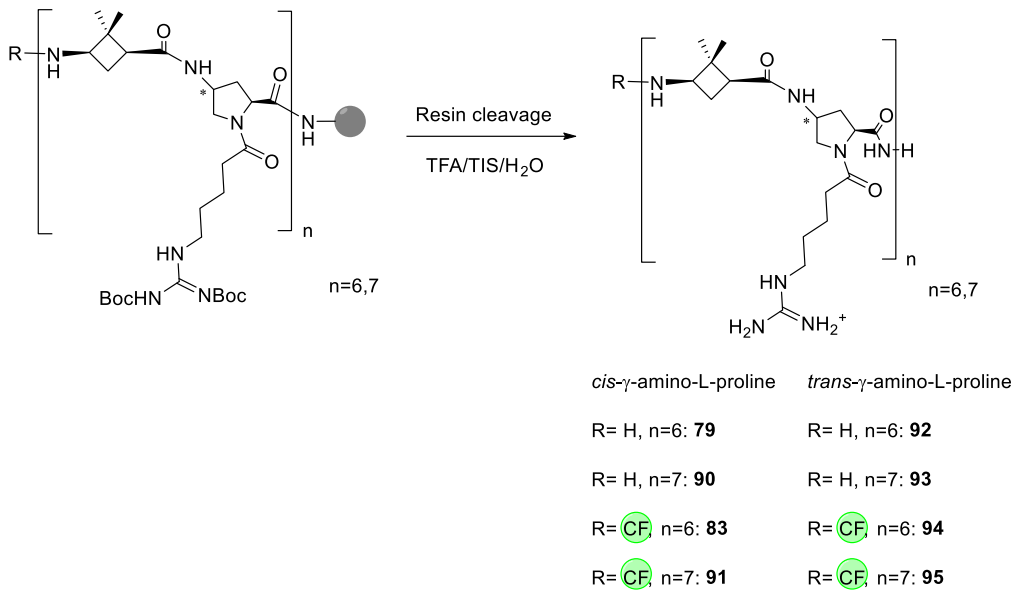

Scheme 18. Peptide cleavage from the resin.

4.3.2.2 SPS of reference peptide TAT_{48-57}

Reference peptide TAT_{48-57} (Figure 45) was synthesized using commercially available conveniently protected amino acids. The peptidic sequence was built by the sequential incorporation of each α-amino acid (R-GRKKRRQRRR-$CONH_2$) from the *C*-terminus to the *N*-terminus using DIC as coupling agent and OxymaPure® as additive. Cleavage and last protecting group removal was performed in the same conditions as described before for γ,γ-peptides. Peptides were then lyophilized, purified by semiprep-RP-HPLC-MS (section 7.4.2.2) and characterized by RP-HPLC-MS and RP-HPLC (sections 7.4.2.1 and 7.4.2.3) obtaining peptides **96** and **97**.

4.3.3 Conjugation of the peptides to doxorubicin

Doxorubicin is an antibiotic from the anthracycline family, generally used in chemotherapy medication for cancer treatment.[162] It works in part by intercalating with the DNA strands. Some evidences as antiparasitic agent were found years ago.[163] Moreover, doxorubicin is known to be fluorescent, which was crucial for studying the peptide uptake in this thesis.

The first step to conjugate the peptides to the doxorubicin started in the point when the peptide skeleton was built and the last Fmoc carbamate was deprotected.

Then, a cysteine residue was attached to the *N*-terminus and, finally an acetylation with Ac_2O and DIPEA was performed to protect the α-amino group followed by the cleavage of the peptide from the resin using the same acidolysis protocol (Scheme 19). These peptides were purified by RP-HPLC-MS.

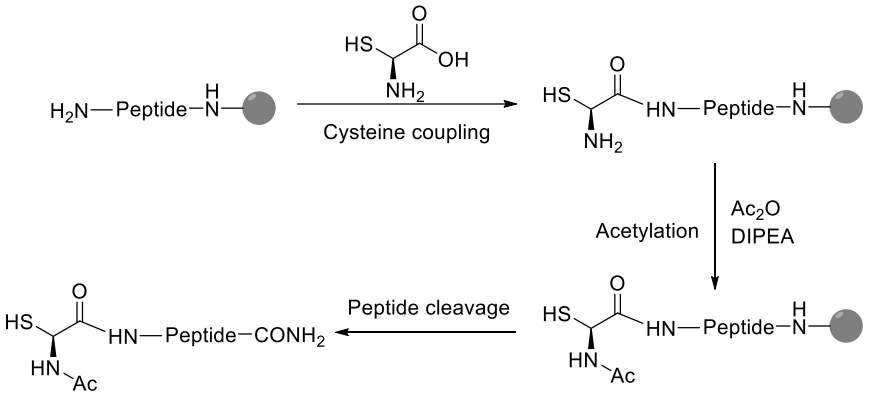

Scheme 19. Peptide preparation for coupling to the doxorubicin.

In order to link the drug to the cysteine residue present in the peptides, a thioeter linkage was required. For this, doxorubicin was previously conjugated to a linker containing a maleimide group (Scheme 20).

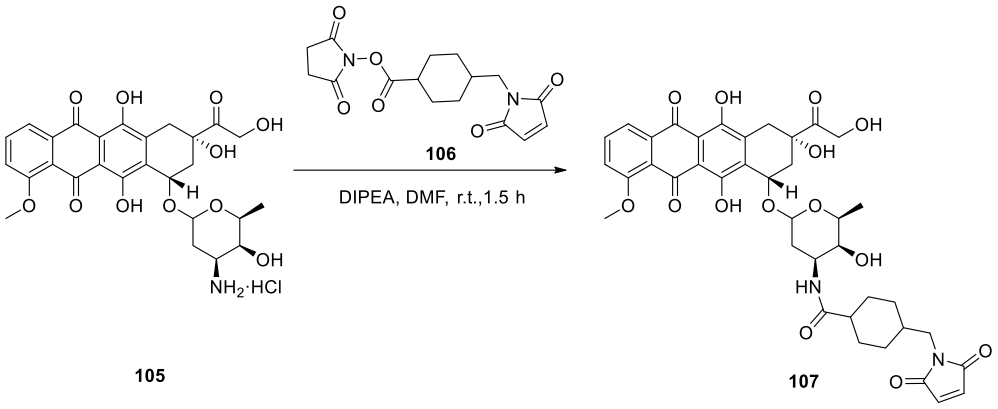

Scheme 20. Doxorubicin conjugation to SMCC.

Doxorubicin (**105**) was dissolved in DMF in presence of DIPEA. Then, succinimidyl 4-(*N*-maleimidomethyl)-cyclohexane-1-carboxylate (SMCC-**106**) was added. The reaction was performed in darkness and followed by HPLC-MS. Generally, after 1.5 h the reaction was over. The final product **107** was used directly in the next step.

To the solution containing compound **107** obtained in the previous step, phosphate-buffered saline (PBS) was added and the pH was adjusted to 6-7 with 1 M HCl. Then, the chosen cysteine-containing peptide was added and the mixture was left stirring at room temperature, following the reaction by HPLC-MS. The obtained peptides **108**-**110** were purified and characterized by HPLC and HPLC-MS (Figure 48).

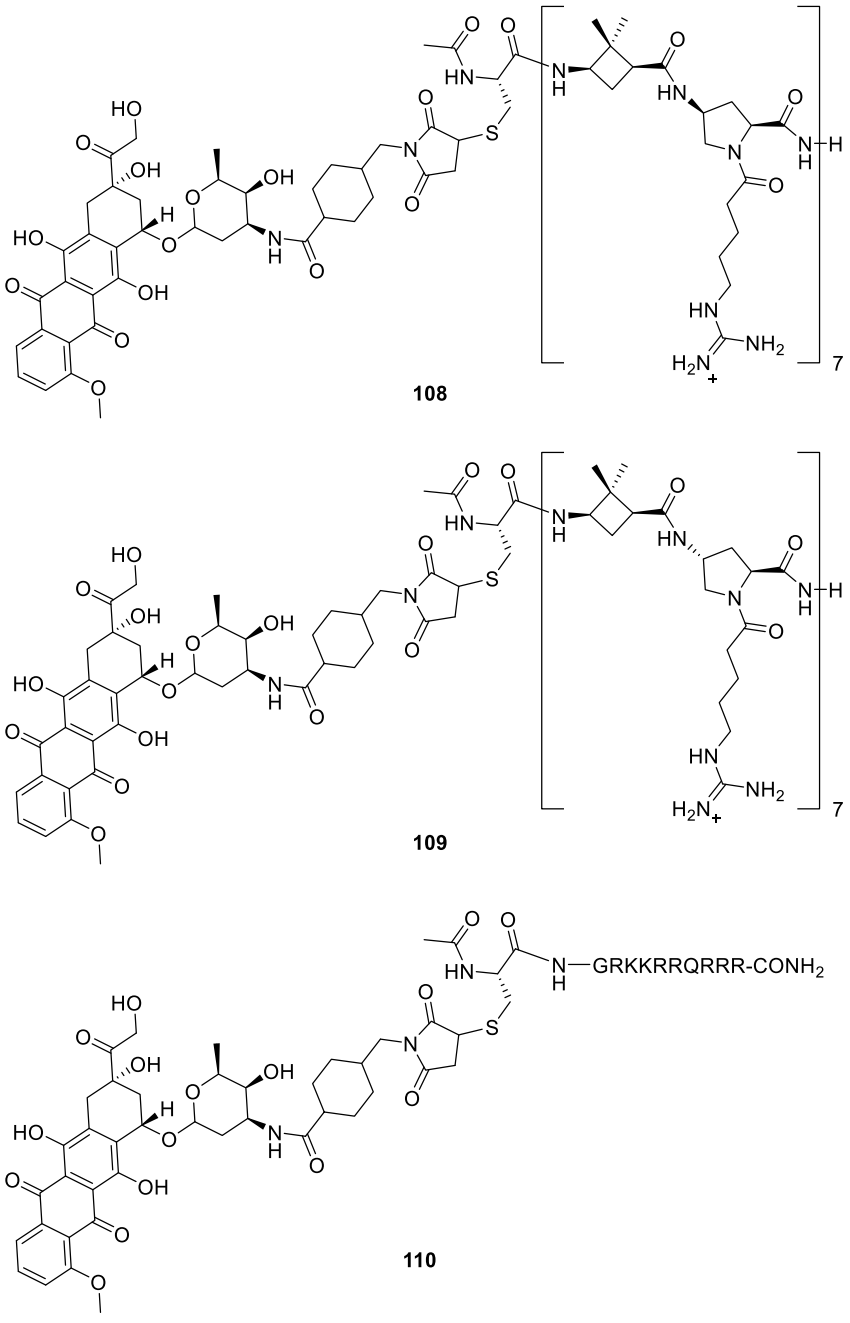

Figure 48. Synthesized peptides conjugated to doxorubicin, **108**-**110**.

4.3.4 Biological studies in *HeLa* cells of the γ-CBAA,γ-amino-L-proline peptides

Once all the peptides were obtained, biological studies of cell viability (toxicity of peptides) and cellular internalization (uptake behavior) were performed. In these studies, the length of the peptides, the stereochemistry of the γ-amino-L-proline residue and the inclusion of more positive charges were evaluated. The work performed in *HeLa* cells was done in collaboration with Prof. Carme Nogués and Dr. Nerea Gaztelumendi in the Departament de Biologia Cel·lular, de Fisiologia i d'Immunologia at the Universitat Autònoma of Barcelona. The eight synthesized peptides in this thesis and TAT_{48-57} were studied at different concentrations.

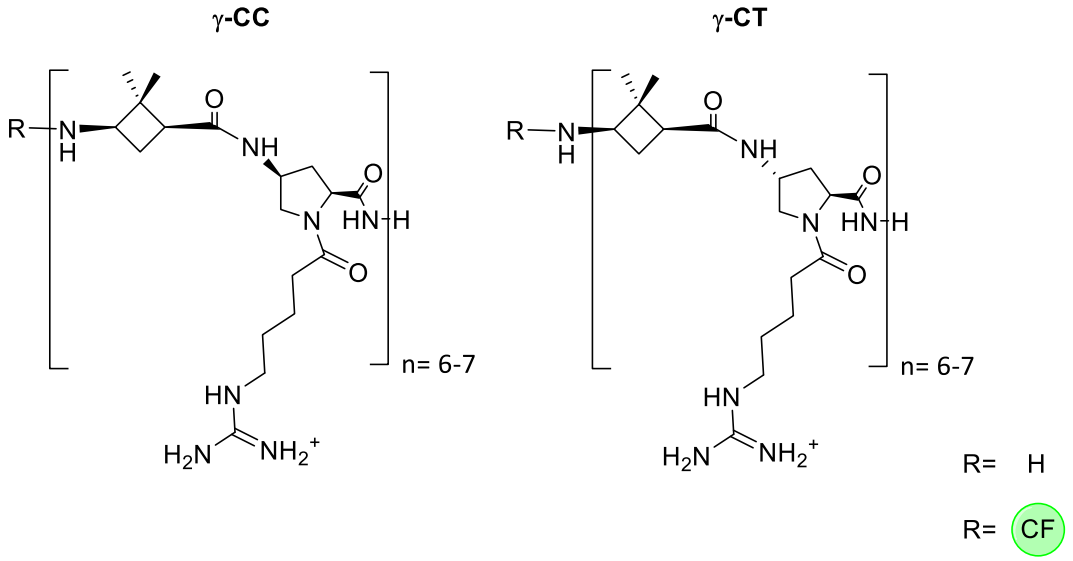

Figure 49. Structures of studied peptides in this part of the thesis.

4.3.4.1 Toxicity studies in *HeLa* cells of the γ-CBAA,γ-amino-L-proline peptides

Cytotoxicity in *HeLa* cells of the γ-CBAA, γ-amino-L-proline peptides was evaluated after 24 hours of incubation of the cells in the presence of the peptides. The reading was carried out using the MTT (3-(4,5-dimethylthiazol-2-yl)-2,5-diphenyltetrazolium bromide) assay as described in section 7.6.2.

After the cell treatment with peptides of different length of the two families: γ-*cis*-CBAA,γ-*cis*-amino-L-proline (γ-CC), γ-*cis*-CBAA,γ-*trans*-amino-L-proline (γ-CT); the viability in all cases was over 90% in concentrations of 10, 25 and 50 μM (Figure 50). As can be observed, rising the number of positive charges, directly related to the number of guanidinium groups in the peptide skeleton, did not show an increase in the toxicity of the peptides.

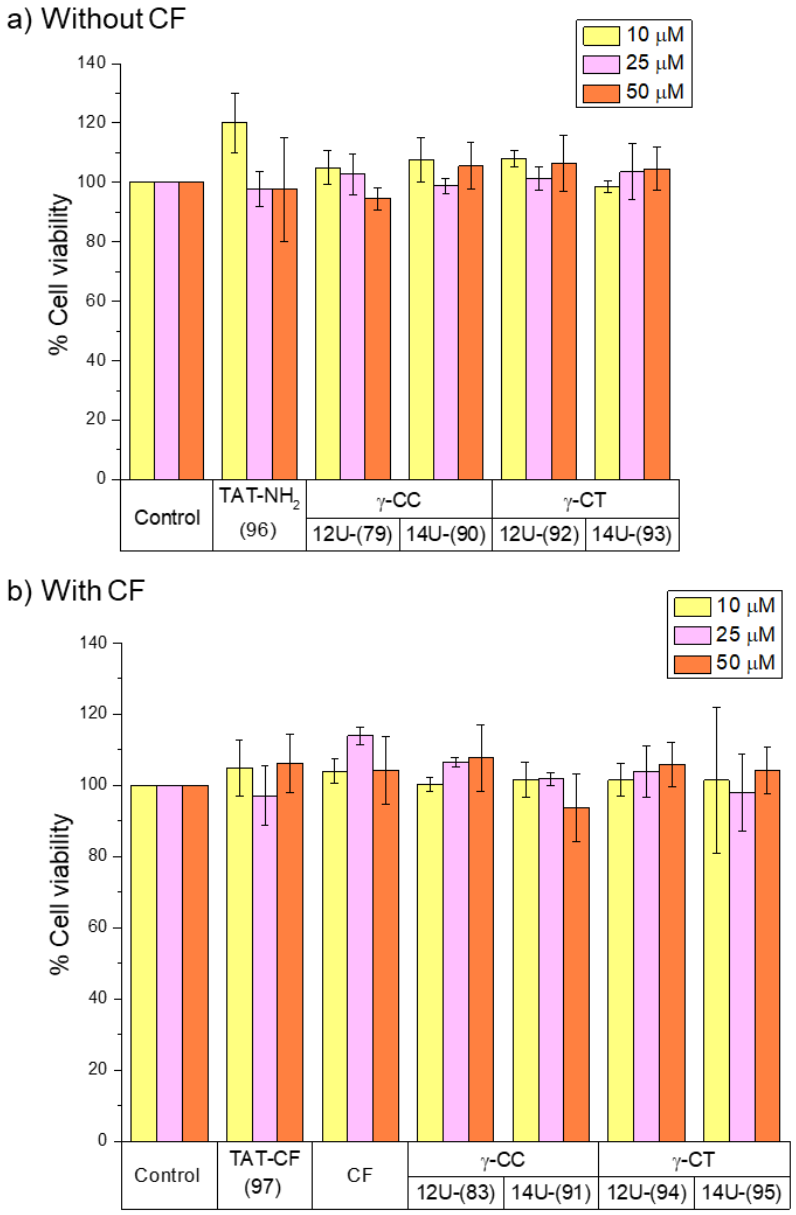

Figure 50. Cell toxicity of the prepared γ,γ-hybrid peptides and TAT_{48-57}. a) Peptides with terminal free amine. b) Peptides conjugated with CF at the *N*-terminus. The cell viability was calculated using the MTT assay with 24 h incubation at three different concentrations. Error bars represent the standard deviation (SD) of three independent experiments.

Additionally, it could be observed that the presence of the CF did not interfere with the viability in *HeLa* cells, obtaining the same values than for the peptides with the free terminal amino group. The results observed were in concordance with the toxicity determined in polyarginine peptides, which presented low toxicity for compounds with less than 10 guanidinium residues.[164]

Therefore, it can be concluded that using different stereochemistry in the peptide skeleton, rising the number of charges (with more guanidinium groups) and proportionally making larger peptides, did not affect the cell membrane integrity and did not inhibit the cell proliferation.

4.3.4.2 Uptake behavior in *HeLa* cells of the γ-CBAA,γ-amino-L-proline peptides

The ability to cross the cell membrane was determined by flow cytometry, using CF as fluorophore group in all of the peptides and TAT_{48-57}. Peptides were incubated in presence of *HeLa* cells for 2 hours, following the procedure described in section 7.6.3. After this time, the cells were evaluated before and after adding propidium iodide (PI), which is a DNA intercalating agent that was used to discard false positives. In order to avoid the reading of possible peptides present outside the cell membrane, the pH was adjusted to 6 using 1 M HCl.

Analyzing the positive cell population after the incubation with the peptides, it could be observed that more than 98% cells presented fluorescence for the different peptide families. This result implied that the peptides could internalize in almost all of the cells. However, when analyzing the fluorescence of the peptides in front of the fluorescence of TAT_{48-57} (positive control) or CF (negative control) two different scenarios were observed (Figure 51).

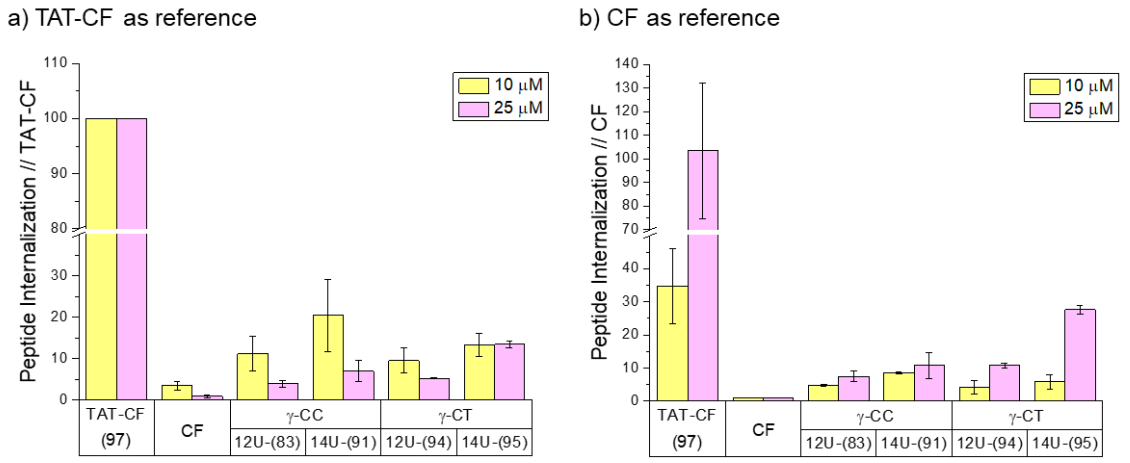

Figure 51. Peptide internalization of the γ,γ-hybrid peptides and TAT_{48-57} conjugated with CF in *HeLa* cells. Cells were incubated at two different peptide concentration for 2 h at 37 ºC. Error bars represent SD of three independent experiments. a) Internalization evaluated using **97** as reference (100% signal). b) Internalization evaluated using CF as reference (CF=1).

Focusing on Figure 51a, it was observed that at 10 μM concentration higher values of relative peptide internalization were obtained if compared with 25 μM concentration. This is probably explained due to the fact that TAT_{48-57} internalized at higher rates at 25 μM concentration (TAT is extremely concentration-dependent in cell uptake)[165] and, when performing the calculations to obtain the relative internalization of each peptide, they showed lower values than for 10 μM. This fact could be corrected using the negative control CF as can be seen in Figure 51b. Another possible explanation was the difference in the internalization pathways depending on the peptide concentration. At low concentration endocytosis is the most probable mechanism of absorption of hydrophobic and amphipathic peptides, while at higher concentrations direct translocation is the general procedure. The rates to calculate the predominant mechanism can vary depending on the CPPs structure and the cell lines.[166] Moreover, γ-CT peptide family showed better uptake behavior if compared with the peptides of the same number of amino acids of the γ-CC family. Additionally, looking at values using CF as reference, the uptake of γ-CT peptides turned to be more concentration dependent than γ-CC ones.

Additionally, images taken by confocal microscopy were used to localize the peptides inside the cells using CF as fluorophore group. Incubation of the cells in the presence of peptides at 10 μM concentration was done for 2 hours, following the procedure described in section 7.6.4. CellMask™ was used in order to dye the cell membrane in red and Hoechts was used to dye the DNA in blue, generating reference points which helped to localize the peptides. In these conditions, the peptide internalization was clearly observed (Figure 52).

a) 14U-CF **91**

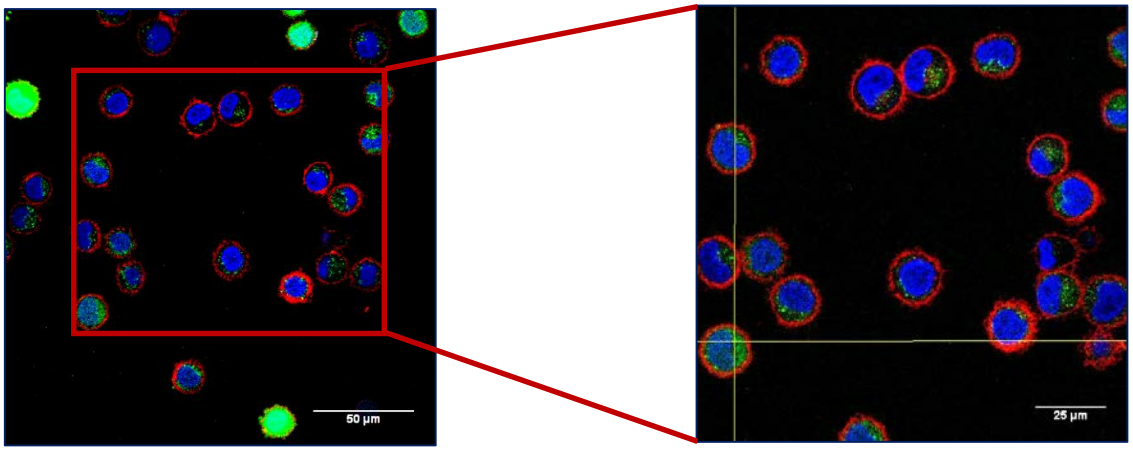

b) 14U-CF **95**

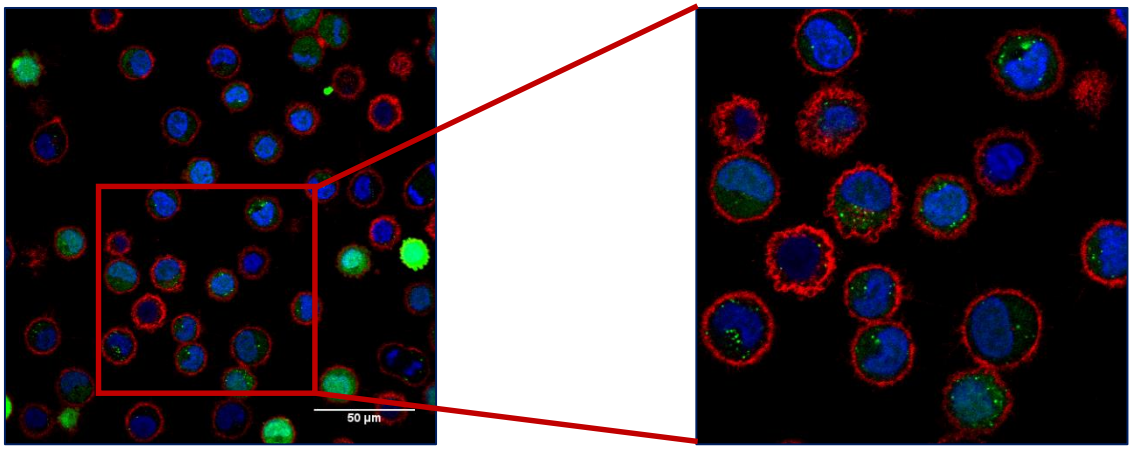

Figure 52. Confocal microscopy images of *HeLa* cells incubated with the tetradecamer peptides during 2 h at 10 μM peptide concentration at 37 ºC after treatment with 1 M HCl. CellMask™ colors the plasmatic membrane in red and Hoechst colors the DNA in blue, generating reference intracellular areas to facilitate the localization of the peptides. a) γ-*cis*-CBAA,γ-*cis*-amino-L-proline tetradecamer conjugated with CF, **91** b) γ-*cis*-CBAA,γ-*cis*-amino-L-proline tetradecamer conjugated with CF, **95**.

Obtained images were useful to observe dotted quantities of both γ,γ-hybrid peptides **91** and **95** inside the living cells, which suggested endocytosis as mechanism of internalization. It has been previously shown that amphipathic CPPs bind with high affinity to lipid membranes, because of their hydrophobic nature,[167,168] which tends to be associated with vesicle formation.[169,170] However, charge interaction is important for membrane binding of secondary amphipathic CPPs, which are CPPs with random conformation in aqueous solution but exhibit defined conformations after binding to polyanionic molecules. Therefore, the insertion of this kind of CPPs into the lipid bilayer on the cell surface is dependent on the charge interaction.[171] The next step in the internalization mechanism is mainly dependent on different factors such as peptide concentration, peptidic sequence, composition of the lipids in the cell membrane, temperature, incubating time, etc.[172]

On the other hand, confocal images of TAT_{48-57} conjugated with CF suggested that both direct translocation and endocytosis were present due the diffuse and punctuated quantities of the peptide present inside cells (Figure 53). However, an experimental design to explore uptake mechanisms of all of the peptides studies in this work must be performed.

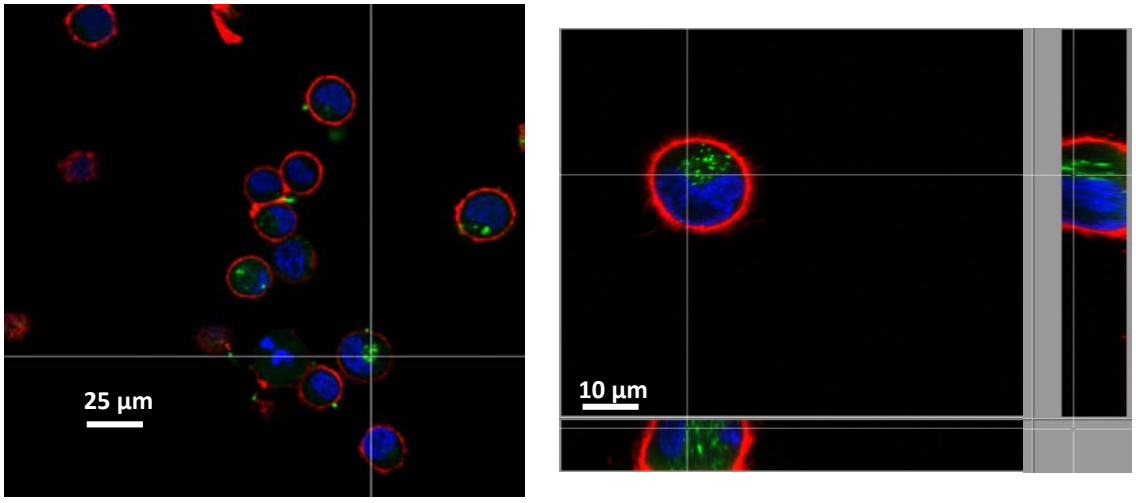

Figure 53. Confocal microscopy images of *HeLa* cells incubated with TAT_{48-57} conjugated to CF during 2 h at 10 µM peptide concentration at 37 ºC after treatment with 1 M HCl. CellMask™ colors the plasmatic membrane in red and Hoechst colors the DNA in blue, generating reference intracellular areas to facilitate the localization of the peptides.

4.3.5 Biological studies in *Leishmania Donovani* promastigotes and *Leishmania Pifanoi* amastigotes of the γ-CBAA,γ-amino-L-proline peptides

Following the previous work, biological studies of parasite viability (toxicity of peptides) and parasite internalization (uptake behavior) were performed. In these studies, the length of the peptides, the stereochemistry of the γ-amino-L-proline residue and the inclusion of more positive charges were evaluated. The work performed in *Leishmania* parasites was done in collaboration with Dr. Luis Rivas and Dr. Mª Angeles Abengozar of Centro de Investigaciones Biológicas-CSIC (CIB-CSIC) in Madrid. Only the peptides containing the CF conjugation (**83**, **91**, **94**, **95**) and the TAT_{48-57}-CF (**97**) were studied at different concentrations.

4.3.5.1 Toxicity studies in *Leishmania Donovani* promastigotes and *Leishmania Pifanoi* amastigotes parasites of the γ-CBAA,γ-amino-L-proline peptides

Cytotoxicity in *Leishmania Donovani* promastigotes and *Leishmania Pifanoi* Amastigotes of the γ-CBAA,γ-amino-L-proline peptides was evaluated after 4 hours of incubation of the parasites in presence of the peptides. The reading was done using the MTT assay as described in section 7.7.2.

After incubation, results showed a decrease in the viability when the concentration of the peptide was increased compared to non-treated parasites, in both *Leishmania Pifanoi* amastigotes (Figure 54a) and *Leishmania Donovani* promastigotes (Figure 54b). Also, larger peptides (**91** and **93**) showed more toxicity than shorter ones (**83** and **95**) due to the rise in the number of guanidinium groups and, proportionally, the number of positive charges. This fact was in concordance with previous results in the field.[105] Moreover, the γ-CT family appeared to be more toxic than γ-CC one. Furthermore, peptides demonstrated to be more toxic in *Leishmania Donovani* promastigotes (Figure 54b) than in *Leishmania Pifanoi* amastigotes (Figure 54a).

At the highest concentration (50 μM) the viability was calculated to be more than 50% in all cases for *Leishmania Pifanoi* amastigotes, while it was less than 50% for all cases in *Leishmania Donovani* promastigotes. More specifically, tetradecameric peptide **95** of the γ-CT family was the most toxic peptide compared in this work in both *Leishmania* parasites. The lowest survival value of 24% was obtained for *Leishmania Donovani* promastigotes in 50 μM concentration (Figure 54b).

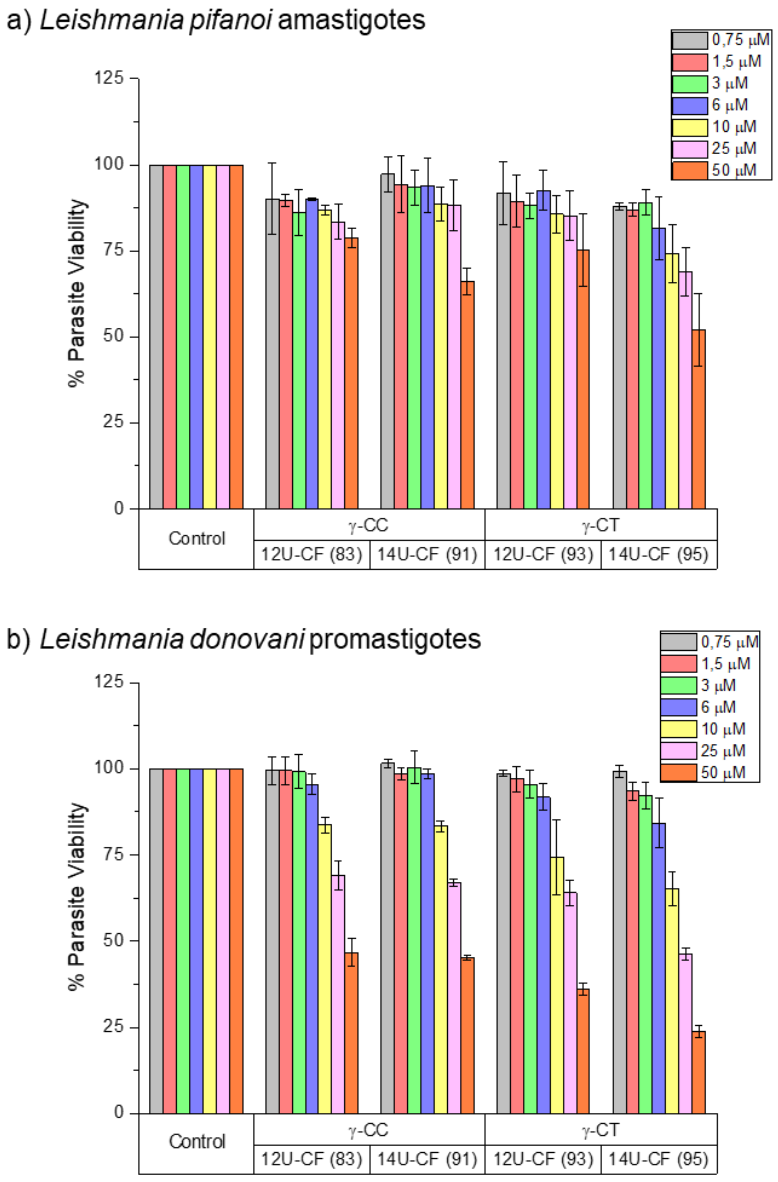

Figure 54. Parasite toxicity of the prepared γ,γ-hybrid peptides and TAT_{48-57} conjugated with CF. The parasite viability was calculated using the MTT assay with 4 h incubation at different concentrations using non treated parasites as 100% lecture. Error bars represent the standard deviation (SD) of three replicates. a) *Leishmania Pifanoi* amastigotes b**)** *Leishmania Donovani* Promastigotes.

4.3.5.2 Uptake behavior and cell localization in *Leishmania Donovani* promastigotes and *Leishmania Pifanoi* amastigotes parasites of the γ-CBAA,γ-amino-L-proline peptides

The ability to cross the cell membrane was determined by flow cytometry, using CF as fluorophore group in all of the peptides and TAT_{48-57}. *Leishmania Donovani* and *Leishmania Pifanoi* parasites were incubated in presence of peptides at 10 μM concentration for 4 hours, following the procedure described in section 7.7.3. TAT_{48-57} was used as positive control for all the experiments.

As observed in Figure 55, similar results were obtained for both parasites systems. Docecamers **83** and **93** had similar fluorescence values than reference peptide TAT_{48-57}-CF **97**. Moreover, tetradecamers **91** and **95** had higher fluorescence values than the reference peptide. However, intensity of fluorescence was too low in *Leishmania Pifanoi* amastigotes (Figure 55a) using the same settings as for *Leishmania Donovani* promastigotes (Figure 55c), making it difficult to evaluate the differences between both biological systems (relative internalization, selectivity of the peptide, etc).

On *Leishmania Donovani* promastigotes both tetradecamers **91** and **95** presented a higher fluorescence value, which is proportional to the internalization of the peptide (236% and 140%, respectively), than the one observed for TAT_{48-57}-CF.

This meant that peptides **91** and **95** had a better internalization ability than the reference peptide and could be proposed as potential carriers due to their low cytotoxicity, as explained in section 4.3.5.1.

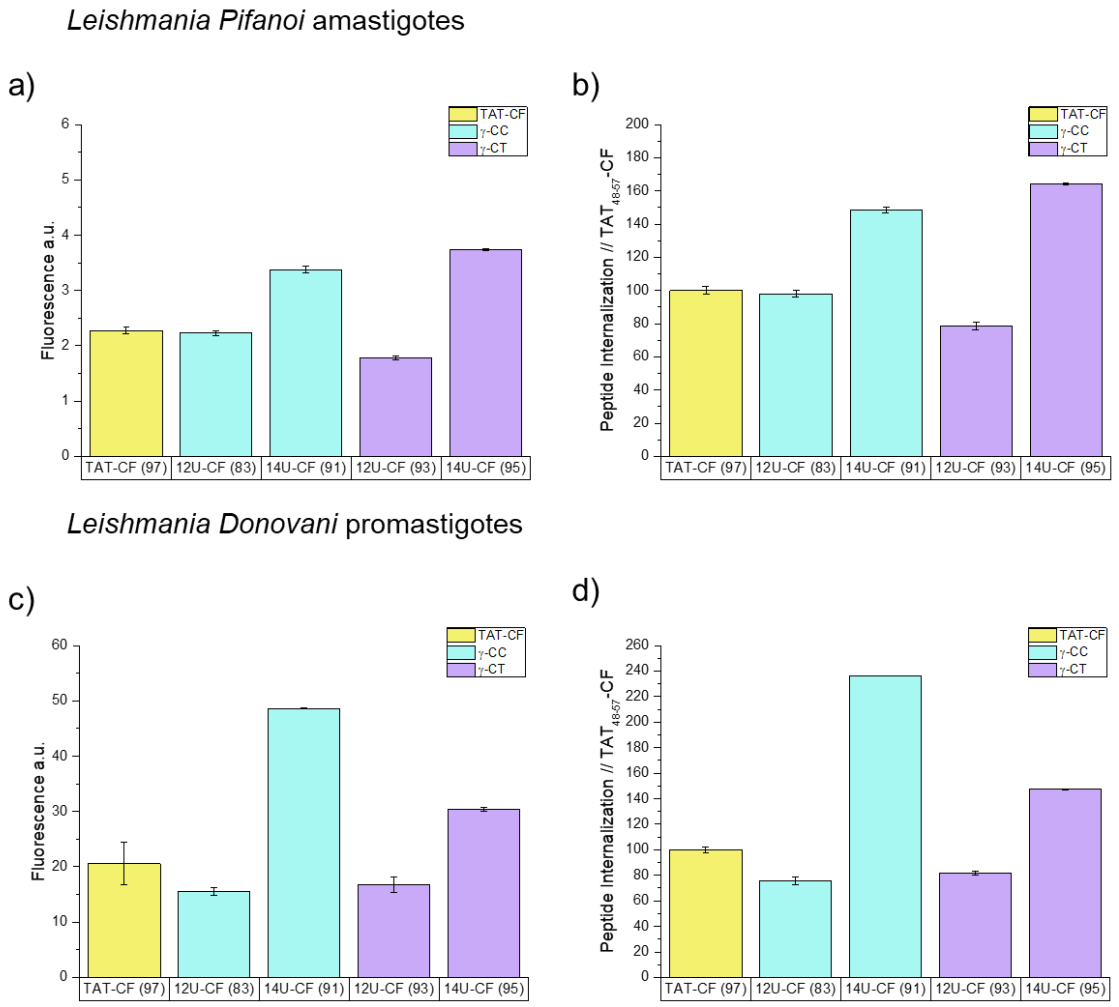

Figure 55. Fluorescence reading of the γ,γ-hybrid peptides and TAT_{48-57} conjugated with CF. Parasites were incubated for 4 h with a peptide concentration of 10 μM at 26 ºC. Error bars represent standard deviations (SD) of three independent experiments. a) Raw fluorescence value for peptides in *Leishmania Pifanoi* amastigotes, b) Internalization evaluated using TAT_{48-57} as reference (100% signal) in *Leishmania Pifanoi* amastigotes, c) Raw fluorescence value for peptides in *Leishmania Donovani* promastigotes, d) Internalization evaluated using TAT_{48-57} as reference (100% signal) in *Leishmania Donovani* promastigotes.

Additionally, images taken by confocal microscopy were used to localize the peptides inside the parasites using CF as fluorophore group. Incubation of the parasites in presence of peptides at 10 μM concentration was done for 4 hours, following the procedure described in section 7.7.4. 2-(4-Amidinophenyl)-1*H*-indole-6-carboxamidine (DAPI) was used to dye the DNA in blue, generating a reference point which helped to localize the peptides.

However, the low fluorescence obtained for *Leishmania Pifanoi* amastigotes in flow cytometry made impossible to take images by confocal microscopy of the peptides incubated on these systems. Only peptides incubated in *Leishmania Donovani* promastigotes were evaluated in this thesis (Figures 56 and 57).

a) 12U-CF **83**

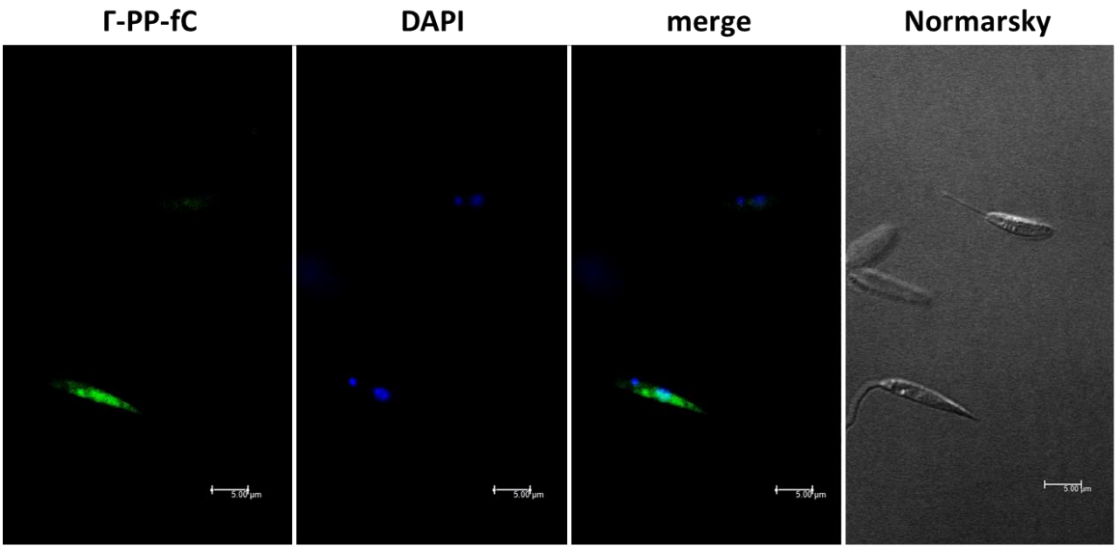

b) 14U-CF **91**

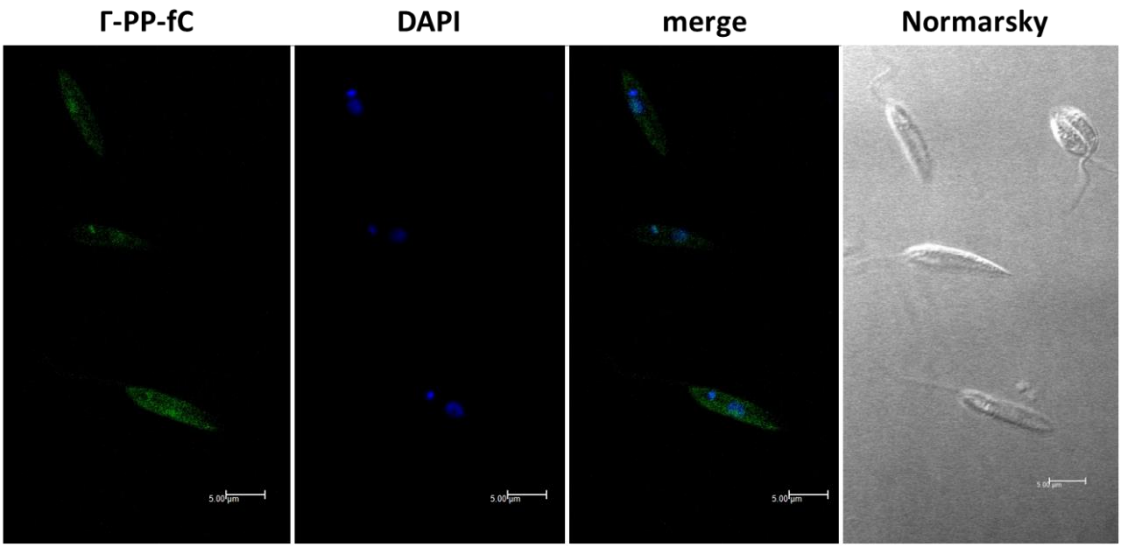

Figure 56. Confocal microscopy images of *Leishmania Donovani* promastigotes incubated with the peptides during 2 h at 10 μM peptide concentration at 26 ºC DAPI colors the DNA in blue, generating reference intracellular areas to facilitate the localization of the peptides. a) γ-*cis*-CBAA,γ-*cis*-amino-L-proline dodecamer conjugated with CF, **83** b) γ-*cis*-CBAA,γ-*cis*-amino-L-proline tetradecamer conjugated with CF, **91**.

a) 12U-CF **93**

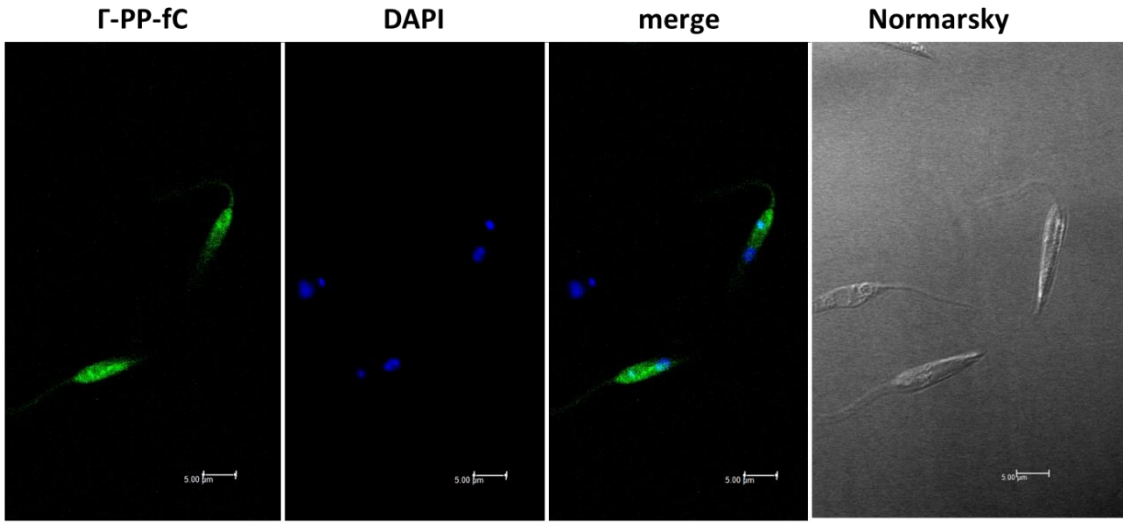

b) 14U-CF **95**

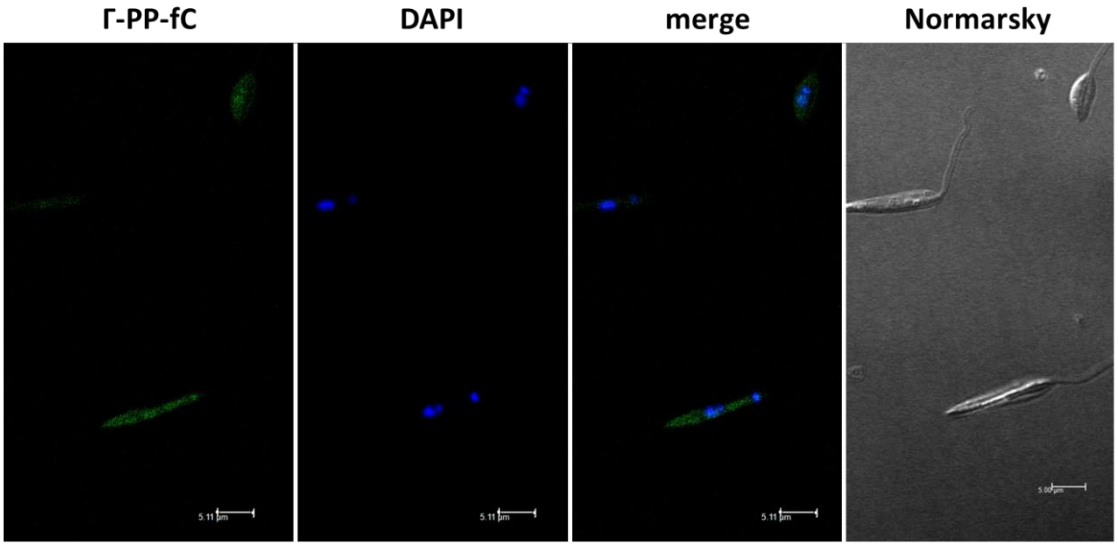

Figure 57. Confocal microscopy images of *Leishmania Donovani* promastigotes incubated with the peptides during 2 h at 10 μM peptide concentration at 26 ºC DAPI colors the DNA in blue, generating reference intracellular areas to facilitate the localization of the peptides. a) γ-*cis*-CBAA,γ-*trans*-amino-L-proline dodecamer conjugated with CF, **93** b) γ-*cis*-CBAA,γ-*trans*-amino-L-proline tetradecamer conjugated with CF, **95**.

Figure 56 and Figure 57 corroborated the results obtained by flow cytometry. For dodecameric peptides **83** and **93** a dotted uniform distribution in some of the parasites was observed, while for tetradecameric peptides **91** and **95** a dotted uniform distribution was homogeneously observed.

When compared with TAT_{48-57}-CF **97** (Figure 58), it was clearly observed that the synthesized peptides penetrated better in the case of the tetradecamers and similarly to TAT in the case of the dodecamers.

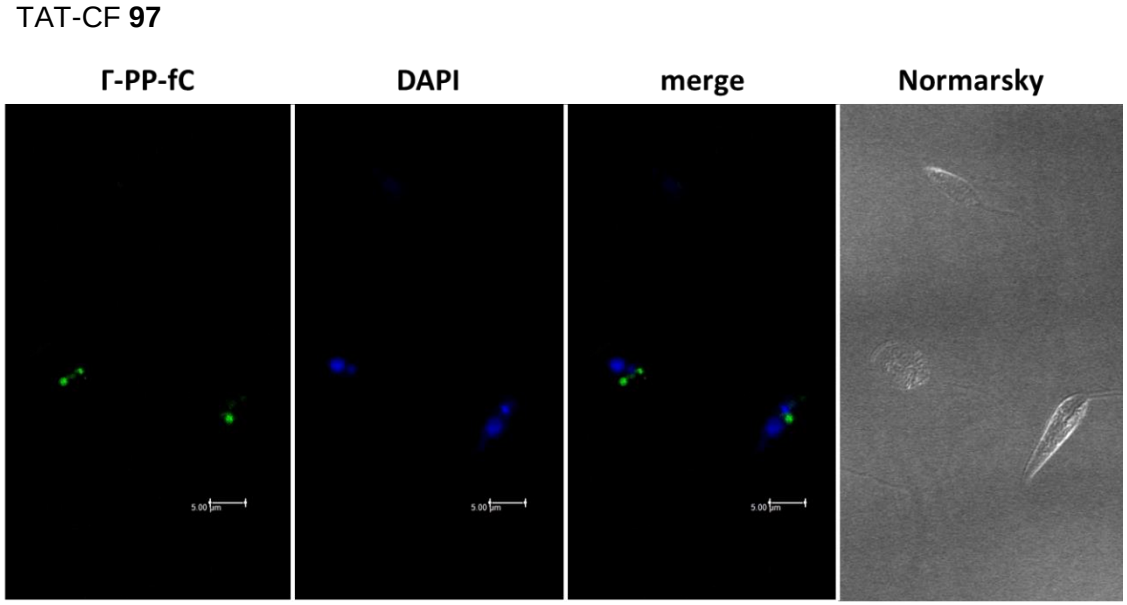

Figure 58. Confocal microscopy images of *Leishmania Donovani* promastigotes parasites incubated with the TAT_{48-57}-CF (**97**) during 2 h at 10 μM peptide concentration at 26 ºC DAPI colors the DNA in blue, generating reference intracellular areas to facilitate the localization of the peptides.

Looking at these encouraging results, it was decided to conjugate a drug to the best peptides (**91** and **95**). The chosen drug was doxorubicin, which could act both as antileishmanial agent and fluorophore. More details are explained in section 4.3.6 of this thesis.

4.3.6 Evaluation as drug delivery agents of the synthesized peptides conjugated to doxorubicin in *Leishmania Donovani* promastigotes

Using the knowledge obtained in previous studies in this thesis, peptides were conjugated to doxorubicin and biological studies were performed to check the parasite viability (toxicity of peptides conjugated to drug) and parasite internalization (uptake behavior) in *Leishmania Donovani* promastigotes. In these studies the stereochemistry of the γ-amino-L-proline residue and the effect of the conjugated drug were evaluated. Peptides evaluated in this part were those conjugated with doxorubicin (section 4.3.3) **108**, **109** and reference peptide **110**.

Preliminary studies regarding the parasites viability were performed at different concentrations and with different incubation times.

Generally, it was observed that synthesized hybrid peptides **108** and **109** had a more toxic effect towards parasites than reference peptides **110** at both 4 and 72 hours incubation (Figure 59). Moreover, at 4 hours incubation, parasites incubated with doxorubicin showed higher proliferation activity when more quantity of the drug was present. However, at 72 hours incubation, the doxorubicin started to inhibit the proliferation of the parasites.

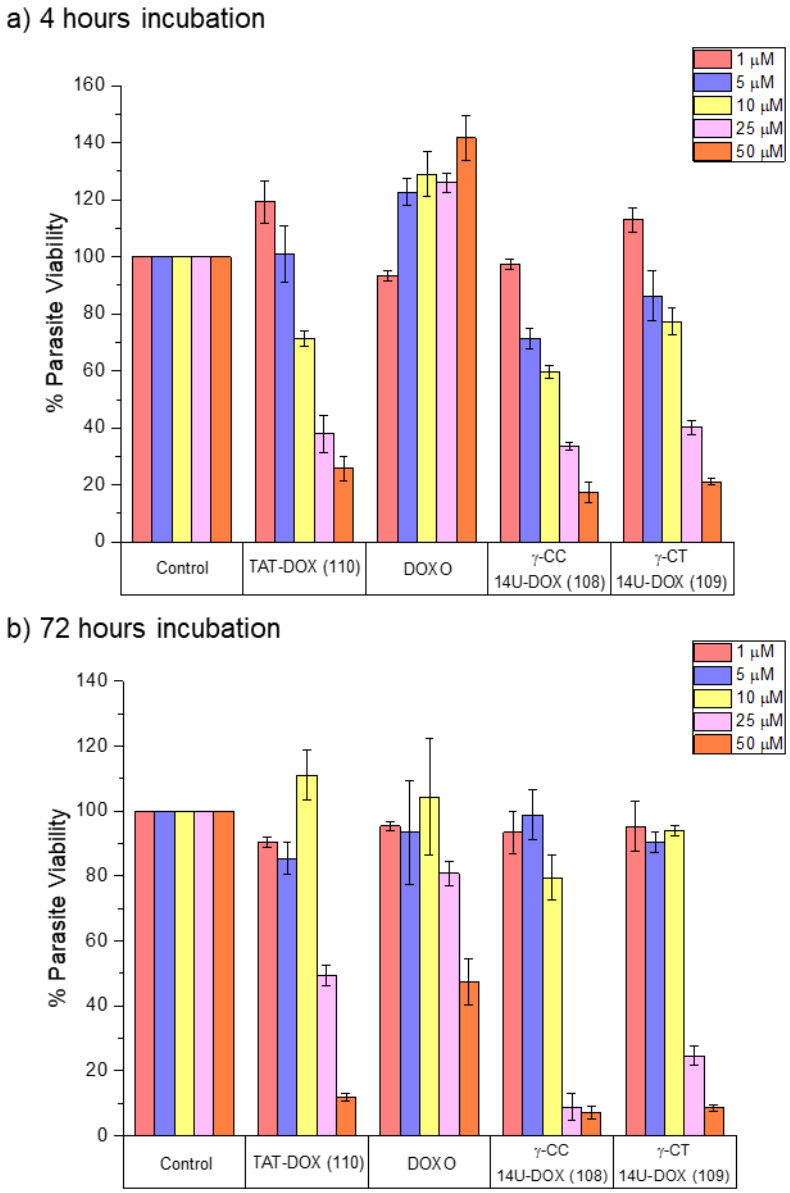

Figure 59. Parasite toxicity of the prepared γ,γ-hybrid peptides and TAT_{48-57} conjugated with CF. The parasite viability was calculated using the MTT assay at different concentrations using non treated parasites as 100% lecture. Error bars represent the standard deviation (SD) of three replicates. a) 4 hours parasite incubation, b) 72 hours parasite incubation.

Looking at Figure 59b, it could be observed that peptides **108** and **109** inhibit the proliferation of the parasites after the first hours of incubation at high concentrations (25 and 50 μM) but did not paralyze the replication of the parasites in the rest of the concentrations.

With the previous results in hand, a preliminary flow cytometry experiment was performed at 5 and 10 μM concentrations during 2 and 4 hours (Figure 60).

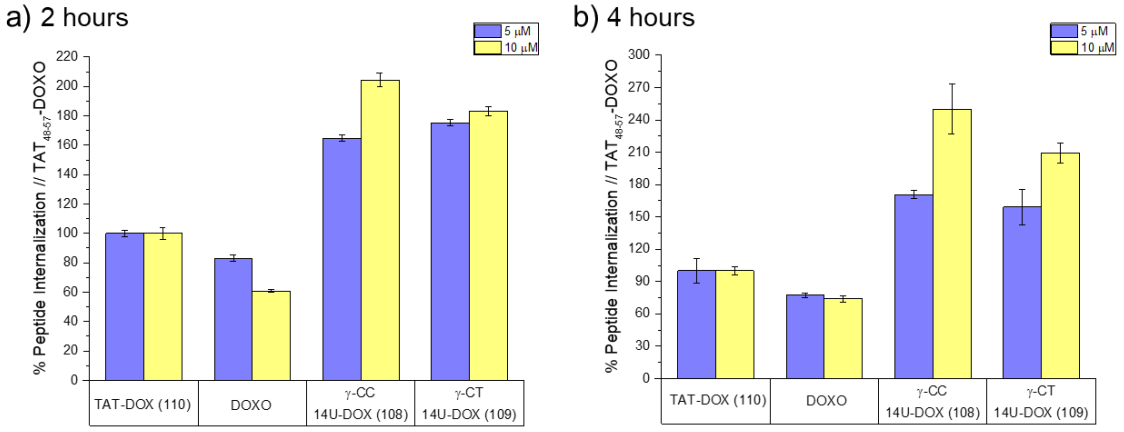

Figure 60. Fluorescence percentage of the γ,γ-hybrid peptides in relation with TAT_{48-57} (100% of signal) conjugated with doxorubicin. Parasites were incubated for different times with a peptide concentration of 5 and 10 μM at 26 ºC. Error bars represent standard deviations (SD) of three replicates. a) 2 h of parasite incubation, b) 4 h of parasite incubation.

As seen in Figure 60, peptides **108** and **109** had a better internalization value than reference peptide **110**, with similar tendencies to those seen in section 4.3.5.2. This meant that the uptake ability of the peptides was not changed by the addition of the cysteine residue, the linker and the conjugation to the doxorubicin. Moreover, it could be seen that doxorubicin alone could not enter the cells with the same efficacy than conjugated with a peptide. Furthermore, it was seen that rising the time of incubation also rose the internalization of the peptides. Overall, the best CPP was **108** with a 250% of internalization respective to TAT_{48-57}-Doxo **110** with a 10 μM concentration incubated for 4 h.

Additionally, an experiment was designed to try to explain and understand the internalization pathway. In order to do this, *Leishmania Donovani* promastigotes parasites were incubated with peptides conjugated to doxorubicin for 4 h at 26 ºC. After that, the fluorescence emitted by doxorubicin was checked and registered. Then, SYTOX (a DNA stain marker) was added to the parasites and the fluorescence was registered again in order to check the permeability of the parasites membrane.

Finally, Triton X-100 (a nonionic surfactant used to lyse cells and permeabilize the membranes of living cells) was added and the maximum fluorescence value for all the parasites was registered.

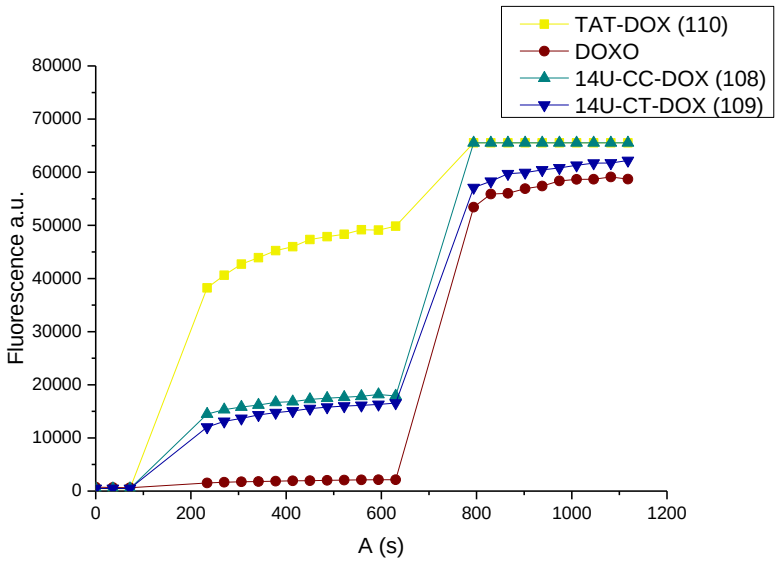

Figure 61. Fluorescence values of parasites incubated with hybrid peptides and TAT_{48-57} conjugated to doxorubicin and doxorubicin alone. Parasites were incubated for 4 h with a peptide concentration of 10 μM at 26 ºC. Times from 0 to 72 seconds: parasites incubated alone with peptides and doxorubicin. Times from 234 to 634 seconds: parasites treated with SYTOX. Times from 794 to 1118 seconds: parasites treated with SYTOX and Triton X-100.

Figure 61 shows the different fluorescence values for all of the studied peptides and doxorubicin incubated with parasites. Analysis were made at several times and conditions. Looking at doxorubicin, it was seen that both non-treated parasites and SYTOX-treated ones gave similar values of fluorescence, which was clearly increased when the parasites were lysed using Triton X-100. This suggested that doxorubicin did not permeabilize or damage the parasite membrane. Regarding hybrid peptides **108** and **109**, non-treated parasites showed low fluorescence, but SYTOX-treated ones gave higher values, meaning that some permeabilization or damage was present in the membrane. However, the greatest increment in fluorescence when adding SYTOX was observed in TAT_{48-57} (**110**). This connoted that the reference peptide seemed to damage the parasite membrane more than the hybrid peptides **108** and **109**, as the observed maximum fluorescence was closer for TAT_{48-57}.

4.4 Summary and conclusions

In this chapter, two families of hybrid γ-CBAA,γ-amino-L-proline peptides were synthesized and evaluated as potential drug delivery agents in two biological systems: *HeLa* cells and *Leishmania* parasites. TAT_{48-57} was used as reference peptide.

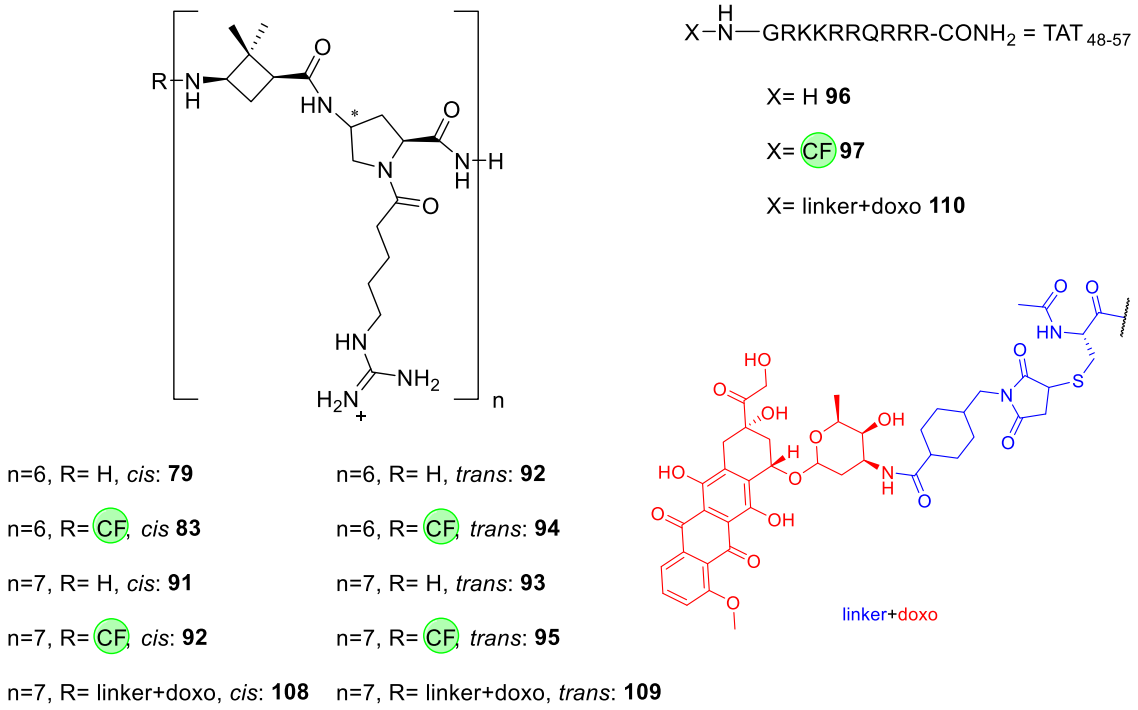

Figure 62. All synthesized and evaluated peptides in this part of the thesis.

Peptides did not show toxicity for *HeLa* cells at any concentration when evaluated using the MTT assay, but were only not toxic at low concentration (≤10 mM) for *Leishmania Donovani* promastigotes and *Leishmania Pifanoi* amastigotes parasites.

Moreover, the uptake of the peptides was evaluated by flow cytometry obtaining a similar reading. In *HeLa* cells a moderate penetration of the peptides was observed when compared to the reference TAT_{48-57}, while in *Leishmania Pifanoi* and *Leishmania Donovani* promastigotes the synthesized hybrid peptides resulted to be twice as efficient as the reference peptide, obtaining suitable candidates to be used as delivery systems.

For this reason, experiments with the peptides coupled to doxorubicin were started and some encouraging results were obtained. The toxicity of doxorubicin was enhanced when coupled to the hybrid γ-CBAA,γ-amino-L-proline peptides and the penetration ability was determined to be similar between peptides conjugated with doxorubicin and peptides containing the carboxyfluorescein moiety. Moreover, some preliminary studies point out that hybrid peptides did not damage the parasite membrane as TAT_{48-57} did.

In general, the results encourage to follow with further studies in the field. Experiments in different biological systems could be performed to check the preference of the peptides for *Leishmania* parasites in front of *HeLa* cells and other cellular lines. Furthermore, trying to elucidate the penetration mechanism could be of interest to get more insight on how these peptides work. Moreover, the toxicity of the peptides in non-cancer cell should be evaluated.

5. Synthesis and Properties of a new Gd^{3+} Complex with an Open-chain Ligand as Potential New MRI Contrast Agent

5. Synthesis and Properties of a new Gd^{3+} Complex with an Open-chain Ligand as Potential New MRI Contrast Agent

5.1 Introduction

Medical imaging technologies allow to produce visual representations of the internal aspect of the body for clinical analysis and medical intervention while remaining as non-invasive techniques. Among these one can find, for instance, radiography, ultrasonography, echocardiography and magnetic resonance imaging (MRI). The latter has become one of the most important and efficient tools in medical diagnosis and biomedical research in the last years.[173] MRI has been continuously growing since the original application and has been combined with drug targeting systems becoming useful for monitoring biodistribution, target site accumulation and drug release. In the clinic, image guided drug delivery can be used to substantially improve pharmacokinetics, and therefore the safety and the therapeutic potential of a drug treatment.[174]

MRI-related techniques were developed in 1970s by physicist Peter Mansfield and chemist Paul Lauterbur, who were awarded with the Nobel Prize in Physiology or Medicine in 2003. The techniques are based on the Nuclear Magnetic Resonance phenomenon, but the word "nuclear" was dropped to avoid negative associations with radioactivity and prevent alarm of the patients.[175,176,177] MRI is a non-invasive technique which does not expose the body to radiation, while providing real-time monitoring of molecular events occurring even at the cellular level. In clinical and research MRI, hydrogen atoms are most often used to generate a detectable radio-frequency signal that is received by antennas in close proximity to the anatomy being examined.

Protons are one of the most abundant nuclides in the human body since 60-70% of the body weight is made of water and fat. For this reason, MRI is based on the measurement of water proton relaxation rates in tissues, providing three-dimensional high resolution images (Figure 63).[178]

Figure 63. MRI Image of a human body.

Considering ^{1}H as charged rotating spheres which generate a magnetic dipole, as consequence of having their own electrical charge and spin, they can precess around the axis of a strong and external applied magnetic field, B_0. The precession frequency (ν_0), which is described by the nature of the atom and the strength of the magnetic field, is called Larmor frequency. Two possible precessions may occur, the one with the magnetic moment aligned parallel to the applied field and the one with an anti-parallel orientation along the longitudinal axis of B_0 (z axis for definition). The predominant orientation determines the energy level of the spin, while the resulting net magnetization (M_0) is originated by the energy difference between these two levels. Taking into account that the parallel level is less energetic, more protons are present in this level, making the total magnetization vector parallel to B_0 (Figure 64).

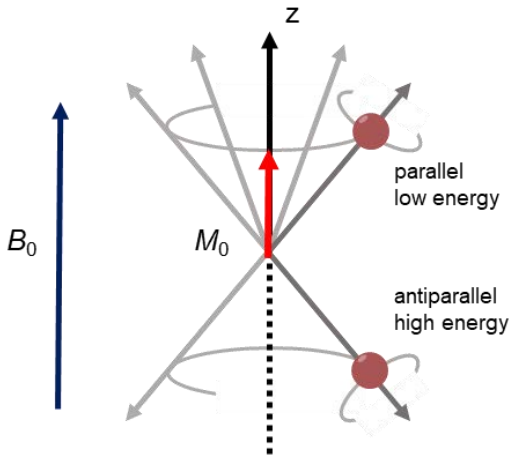

Figure 64. Proton spin in the presence of a constant magnetic field. Net M_0 remains parallel to B_0 due to the lower state is more populated.

The basic NMR experiment consists in applying a radio frequency (RF) pulse, induced by a perpendicular magnetic field created by a RF coil, which flips the magnetization into the xy plane (Figure 65). By the time the pulse is finished, the system returns to the equilibrium, precessing around the z axis and the signal decreases in the xy plane.

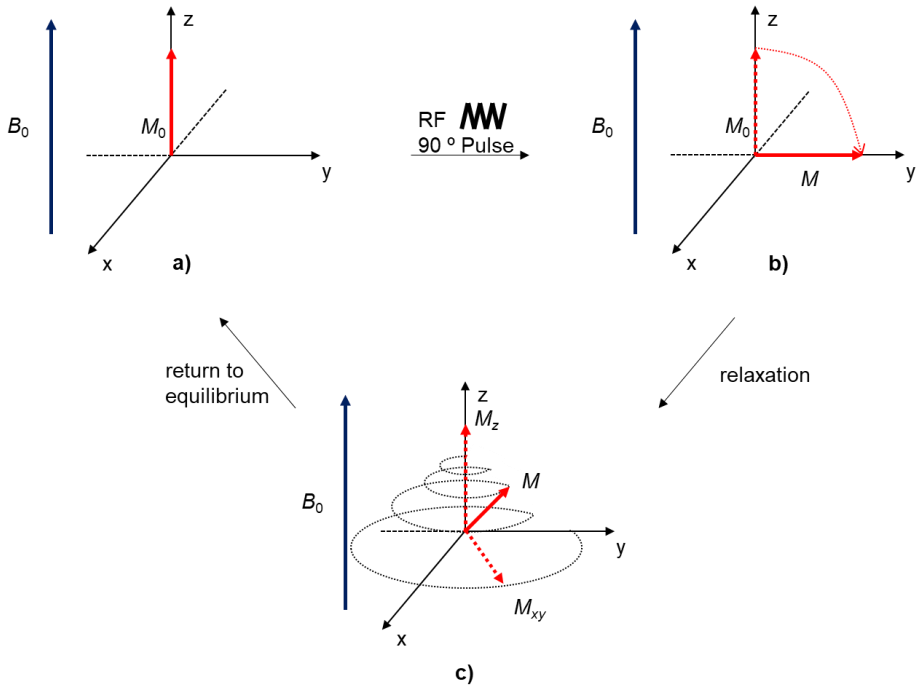

Figure 65. **a)** Net magnetization (M_0) at equilibrium when the spins are placed in a permanent magnetic field B_0. **b)** RF pulse applied, flipping the magnetization (M) to the xy plane. **c)** M precesses around the z axis returning to the equilibrium.

Moreover, at the end of the RF pulse, when the system is returning to the equilibrium, the magnetization in the xy plane decreases exponentially with a time constant T_2 (transverse relaxation time), and the magnetization rises exponentially on axis z a time constant T_1 (longitudinal relaxation time) (Figure 66).[173]

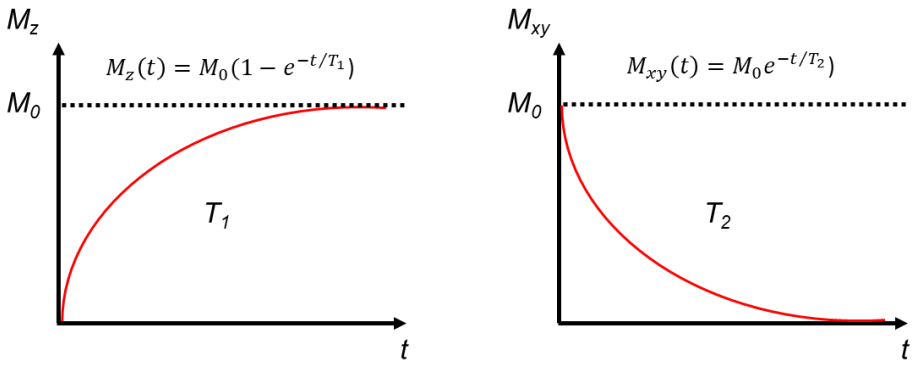

Figure 66. Representation of the different relaxation processes. On the z axis (left) and on the xy plane (right).

MRI signal intensity is expressed in gray levels: a high intensity signal appears in white and a weak intensity signal turns black or dark gray in T_1-weighted images, being the opposite in T_2-weighted ones (Figure 67). An MR image is obtained by contrast between different biological tissues by modifying their intrinsic physical parameters such as water proton density (ρ), T_1 and T_2. Tissues with high longitudinal relaxation rates, $1/T_1$, produce higher signal intensity and therefore brighter regions in the image, on the other hand the increase in the transversal relaxation times, $1/T_2$, produce darker regions. Diagnostic information can be obtained due to the different relaxation rates and proton density present in healthy and damaged tissues. However, these rates are not different enough to obtain high resolution images and some external contrast agents are required to enhance the contrast of the images, and more important, to reduce the time of clinic experiments.

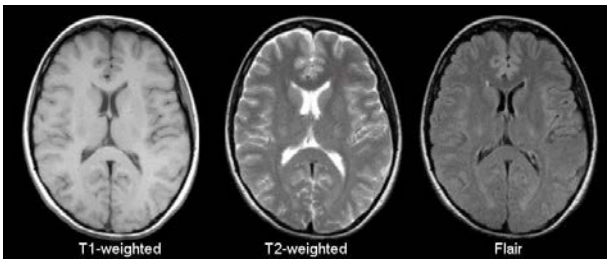

Figure 67. T_1- and T_2-weighted images of a brain.

5.1.1 Contrast agents for MRI

Contrast agents (CA) are chemical substances that improve the sensitivity and the specificity of MRI experiments.[179] The most used compounds are based on paramagnetic species containing unpaired electrons such as Gd^{3+}, Mn^{+2} and Fe^{3+}, but CAs without a coordinated metal in the structure can also be found. Contrast agents are divided depending on the metal or chemical group that interact with protons present in water molecules by exchanging their own protons or the coordinated solvent ones (Figure 68).[180]

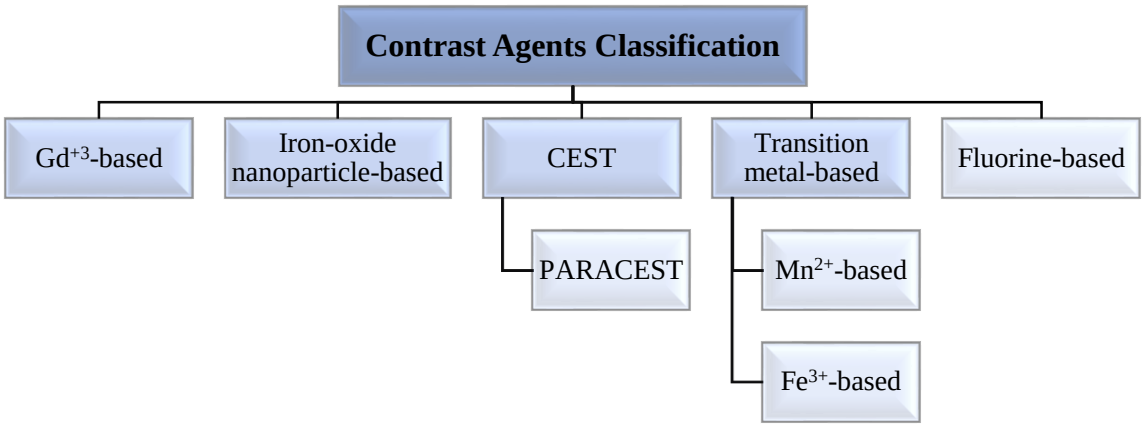

Figure 68. Classification of contrast agents.

Gd^{3+}-based CAs are those that have a coordinated Gd^{3+} ion in their structures. Iron-oxide nanoparticle-based are contrast agents that contain a nucleus made of iron-oxide nanoparticles, which are generally coated with another metal. Transition metal-based CAs are those with a coordinated paramagnetic metal (different of Gd^{3+}) in their skeleton. These three families have water directly coordinated to the metals, which is exchanged with other water molecules of the medium. Chemical Exchange Saturation Transfer (CEST) and Paramagnetic Chemical Exchange Saturation Transfer (PARACEST) contrast agents are molecules that exchange their own protons (generally attached to NH functions) with the solvent in the medium to relax the protons. PARACEST CAs also incorporate a paramagnetic metal in their structure to enhance their properties. Finally, fluorine-based contain ^{19}F atoms, which are active in the NMR and are currently used for cell tracking and lung imaging.

The function of CAs containing paramagnetic species is to reduce relaxation times, T_1 and/or T_2 of the solvent protons that are directly coordinated to the metal and then spread this relaxation to the water molecules present in the tissues, enhancing the image contrast. On the other hand, if no metal is present in the CA structure, exchangeable protons directly bonded to the structure are the ones that performe the function of the coordinated solvent.

Among all the paramagnetic metal ions, Gd^{3+} is the most used in contrast agents and has been selected for the work described in this chapter.

5.1.2 Gd^{3+}-based contrast agents for MRI

Gd^{3+}-based contrast agents present the best effect on T_1 due to the seven unpaired electrons of Gd, which makes it the most paramagnetic stable metal ion.[181] However, Gd^{3+} ion is highly toxic for living organisms (LD_{50} 0.1 mmol/kg), which is contradictory to the high doses that are required to inject. This toxicity comes from the possibility of Gd^{3+} ions to interact with different endogenous metabolites and exchange with Ca^{2+} regulated transmissions due to their similar ionic radius.[182,183] In order to avoid the toxicity and enhance the effect of Gd^{3+} as contrast agent, the metal is chelated forming thermodynamically stable complexes. The best ligands to coordinate gadolinium are the ones with O- and N-donor atoms, due to the metal ion preference to form ionic bonds in its complexes.[184] In order to leave at least one coordination site for the binding of a water molecule, the polyamino carboxylate-based ligands used in Gd^{3+} complexes are usually octadentate.

The first open-chain complex **$[Gd(DTPA(H_2O)]^{2-}$** (commercially known as Magnevist®) was approved for clinic MRI application in 1988 by the US Food and Drug Administration (FDA).[185,186] A year later, the macrocyclic complex **$[Gd(DOTA)(H_2O)]^{-}$** was discovered, presenting a higher kinetic inertness (Figure 69).

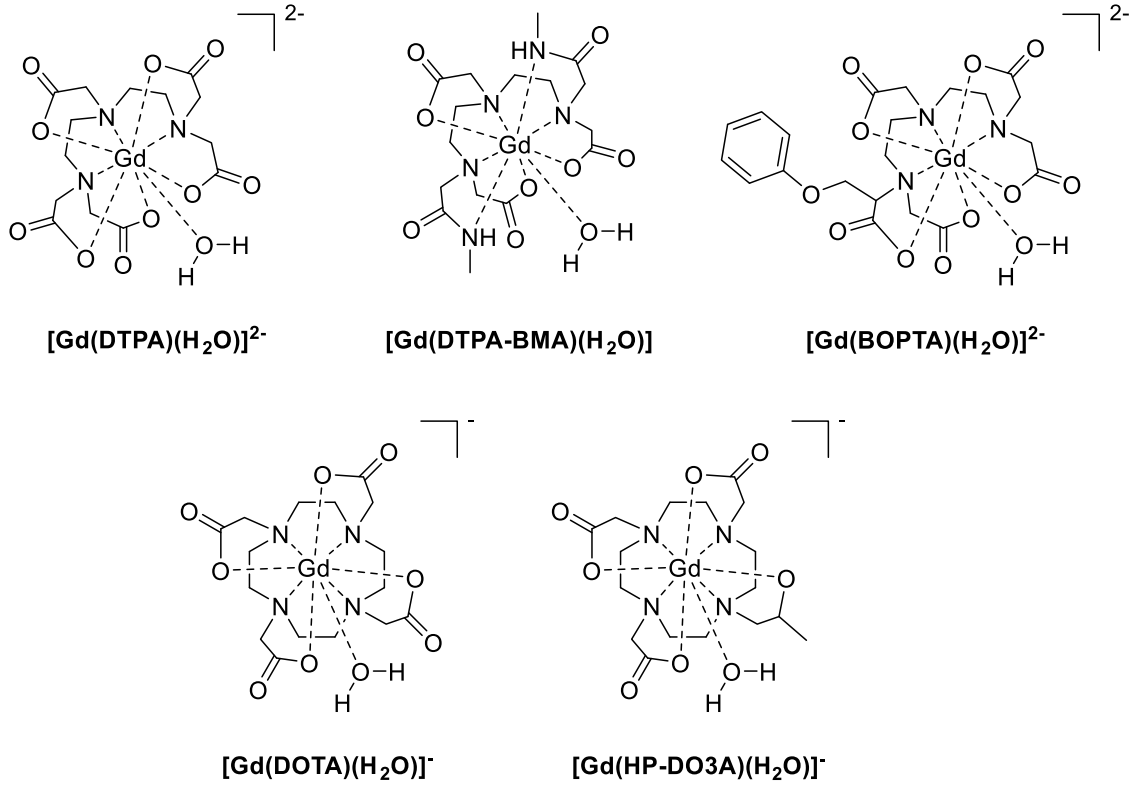

Figure 69. Gd^{3+} complexes used as MRI contrast agents approved by the US FDA.

As shown in Figure 69, most of the approved MRI contrast agents are compounds generated using the first two complexes. Moreover, the only uncharged compound is **[Gd(DTPA-BMA)(H_2O)]**, which was designed to palliate the pain side effect related to the negative charges. However, recent studies have showed that negatively charged contrast agents prevent the possible binding of anions present in the body (carbonates, sulfates, …).[187] The majority of CAs shown in Figure 69 rapidly equilibrate in the intravascular and interstitial fluid compartments, called collectively extracellular compartment, which demonstrate that they are not specific for any tissue.[188] The terminal half-life for blood elimination of these agents is around 2 h when administered to subjects with normal renal functions.[189] The only exception in the list is **[Gd(BOPTA)(H_2O)]$^{2-}$**, which is a CA that is differently biodistributed, improving the image contrast of the brain and the liver.[190]

In the last years, Gd^{3+} toxicity has been studied in more depth due to an upraise in the number of patients with nephrogenic systemic fibrosis (NFS), caused by the administration of contrast agents containing Gd^{3+} ions to subjects with renal insufficiency.[191,192]

Moreover, some cases of gadolinium deposition in the brain structures and bones are reported in bibliography, in which Gd^{3+} can be observed in bone tissue for more than 8 years after administration.[193] The leaching of Gd^{3+} and the deposition in the different tissues, provoking the disease, seems to have relation with the type of contrast agent used, specifically with those with less thermodynamic stability and kinetically labile.[194,195] In order to prevent the release of the free metal, strong kinetic inertness and high thermodynamic stabilities are required to ensure the complete complexation at physiological pH.[196,197,198,199]

This inertness is strongly related to the structure of the ligand. Generally, linear ligands present faster dissociation kinetics than macrocyclic ligands. Nevertheless, in the last years some highly inert linear ligands have been designed, studying the relationship between structure and related efficiency-stability.

The new designed ligands were based in the incorporation of rigid functions to the structure, improving the stability and inertness of the final lanthanide complexes (Figure 70). For example, **Cddadpa** ligand, showed high thermodynamic stability and unprecedented kinetic inertness for a linear ligand, obtaining comparable results with those of some macrocyclic complexes.[200]

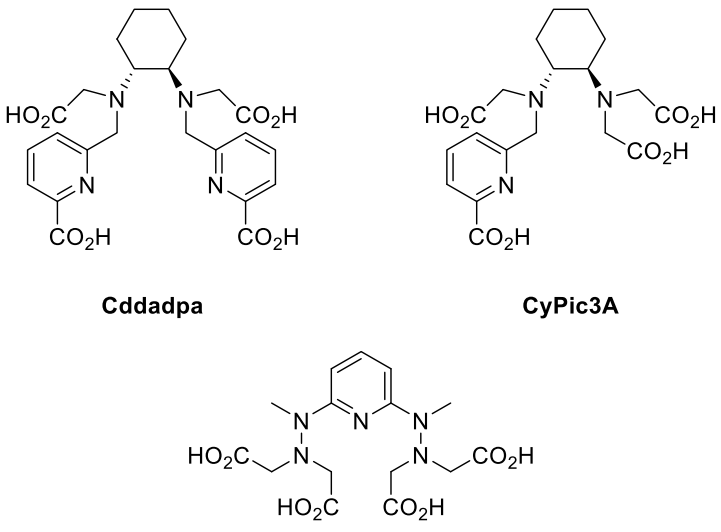

Figure 70. Structures of new and rigid ligands used for complexing Gd^{3+} that afforded good stabilities and inertness.

The incorporation of the picolinate moiety in combination with the use of a cyclic structure like the cyclohexane improved the kinetic inertness, showing similar values to **[Gd(DTPA(H$_2$O)]$^{2-}$**, despite the presence of more than one water molecule in case of **[Gd(CyPic3A)(H$_2$O)$_2$]$^-$**.[201, 202] Furthermore, lowering the ligand basicity, for example in **[Gd(HYD)(H$_2$O)]$^-$** with hydrazine functions, was identified as an important factor to improve the kinetic inertness.[203]

Taking this into account, new linear open chain-ligands can be developed to improve the ones in the market.

5.1.3 Design of contrast agents

As stated in this thesis, the understanding of the mechanism of water proton relaxation is the most important step when designing more efficient contrast agents. This solvent relaxation, when dilute paramagnetic species are present, is described by the Solomon, Bloembergen and Morgan theory.[204,205,206] In Gd^{3+} contrast agents, the relaxivity (r_1) of a contrast agent is the parameter used to measure its efficiency. It is defined as the enhancement of the longitudinal relaxation rate of the water protons per millimol per liter of paramagnetic compound (Equation 1)

$$\frac{1}{T_{1,obs}} = \frac{1}{T_{1,d}} + r_1[CA]$$

Equation 1

Where $1/T_{1,obs}$ is the observed solvent relaxation rate and $1/T_{1,d}$ is the relaxation rate in the absence of paramagnetic compound and [*CA*] is the concentration of paramagnetic compound in mmol/L.

Contrast agents containing Gd^{3+} rise the relaxation rates of the water protons through two different contribution: the inner sphere relaxivity (r_1^{IS}) and the outer sphere relaxivity (r_1^{OS}) (Equation 2). The first one, is altered due to the direct bonding of water molecules to the metal ion.

The second one, is increased by exchange between water molecules of the inner sphere and the water molecules of the solvent that diffuse in the environment of the complex, propagating the paramagnetic influence.

$$r_1 = r_1^{IS} + r_1^{OS}$$

Equation 2

The outer sphere contribution is not as important as the inner sphere one. The difficulty to modulate the random translational diffusion makes harder to control the outer sphere relaxivity. Some researchers also consider another contribution, which is called second sphere, due to water molecules that are not directly bonded to the metal ion but are in the proximity of the complex for a long time.[207,208] The presence of carboxylate or phosphonate groups forming hydrogen bonds with water molecules present in the environment, increases the lifetime of these water molecules in the second sphere thereby increasing the probability that they will be relaxed.[209,210] However, this contribution is usually taken into account in the outer-sphere parameter.

The inner sphere relaxivity is calculated with Equation 3.

$$r_1^{IS} = \frac{1}{1000}\frac{q}{55.5}\frac{1}{T_{1m} + \tau_m}$$

Equation 3

q is referred to the number of water molecules directly coordinated to the paramagnetic ion. τ_m is the lifetime of the water molecules in the inner sphere (equal to the reciprocal water exchange rate, $1/k_{ex}$). T_{1m} refers to the longitudinal relaxation rate of inner sphere protons and is dependent on the rotational correlation time (τ_R), the electron spin relaxation times (T_{1e} and T_{2e}) and the exchange rate of the inner sphere water molecules (k_{ex}).

These parameters can be modified in order to enhance the relaxivity:

- *The number of water molecules in the inner sphere,* $\boldsymbol{q}$. The more coordinated water molecules to the ion, the higher the relaxivity. However, complexes with high hydration levels tend to be less thermodynamically stable, increasing the probabilities of having metal leaching. Despite contrast agents with three water molecules have been designed, only molecules with one water molecule coordinated to the metal are approved for clinical applications.[211,212,213] Furthermore, endogenous anion can replace the water molecules coordinated to the metal, decreasing the efficiency of the contrast agent.[214]
- *The exchange rate between the bound water molecules and the solvent,* $\boldsymbol{k_{ex}}$. The exchange must not be neither slow nor fast. When having a slow water exchange the paramagnetic effect is not transmitted to the solution, while if it is too fast, the bound water molecules do not stay the enough time to feel the paramagnetic effect of the metal ion. An optimal balance of this parameter is required to maximize its effects. [197,215,216]
- *The rotational correlation time,* $\boldsymbol{\tau_R}$. This parameter describes the molecular tumbling of the Gd-water proton vector. The most important parameter and the limiting factor of the relaxivity of low molecular and not supramolecular-based contrast agents. For small chelates, the higher their molecular weight, the bigger is the increase in relaxivity. However, this relation is not maintained for big complexes. Some possibilities to optimize this parameter without making bigger complexes is the use of macromolecules or large aggregates.[217,218]
- *Electronic relaxation times,* $\boldsymbol{T_{1e}}$ *and* $\boldsymbol{T_{2e}}$, and the *distance between water protons and the metal ion,* $\boldsymbol{r_{GdH}}$. These parameters influence the relaxivity, however, it is difficult to modulate them with the structure of the ligand and small success has been achieved.

These important parameters are schematically represented in a Gd^{3+} complex in Figure 71.

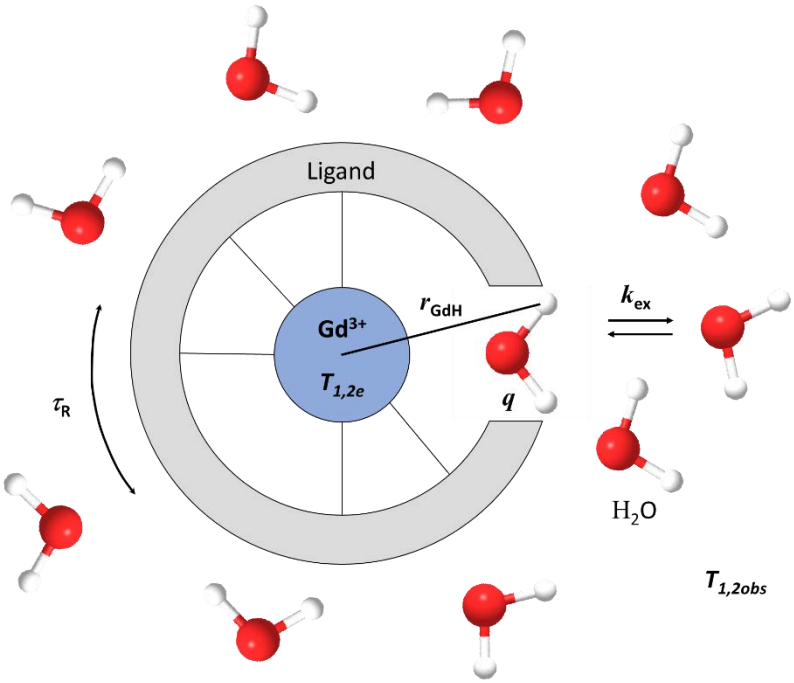

Figure 71. Schematic representation of the parameters that influence the relaxivity.

These parameters should be taken into account when designing new chelate ligands for the study of high efficient contrast agents. Using the Solomon, Bloembergen and Morgan equations, the full optimization of all parameters should lead to relaxivity values up to 100 $mM^{-1}s^{-1}$ at 20 MHz field in complexes with one water molecule in their inner sphere. Nowadays, commercially available contrast agents are in the range of 4 to 6 $mM^{-1}s^{-1}$. This evidence encourages the development and study of ligands and contrast agents that can fulfill the needs in the field.

5.1.4 Cyclobutane-containing ligands in contrast agents for MRI

In our research group, cyclobutane-cored triamines conjugated to **[Gd(DOTA)(H$_2$O)]$^-$** were studied few years ago. The different substitution of the complex was found to be an important factor for high relaxivities (Figure 72).[161]

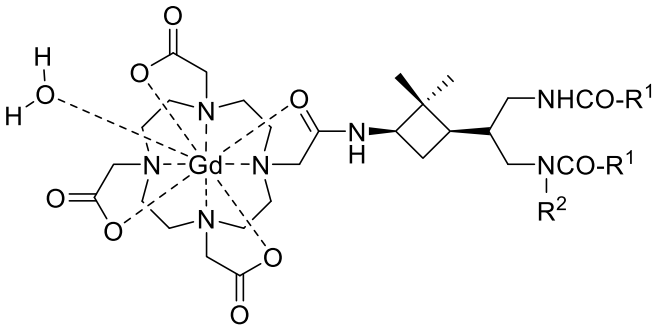

111 **a:** R^1 = OBn, R^2 = H
b: R^1 = *p*-NO_2-C_6H_4, R^2 = H
c: R^1 = Me, R^2 = H
d: R^1 = OBn, R^2 = Me

Figure 72. Previously studied structures of Gd^{3+} complexes based on cyclobutane-cored triamines conjugated with **[Gd(DOTA)(H$_2$O)$^-$]**.

Both carbamate **111a** and *p*-nitrobenzamide **111b** showed lower relaxivity values than reference contrast agent **[Gd(DOTA)(H$_2$O)]$^-$**, whereas *N*-methylcarbamate **111d** had an r_1 value similar to it. However, the acetamide-based complex **111c** exhibited better behavior than the reference contrast agent, showing stronger positive contrast enhancement on T_1-weighted images and higher r_1 (Figure 73).

Computational studies showed that the different substitutions in the amine protecting groups in the cyclobutane side-chains promoted different behavior regarding the water exchange rate. The presence of a strong hydrogen bond within the side-chains in the structure of **111c** induced the formation of an extended conformation, favoring water dissociation. On the other hand, molecules containing an aromatic protecting group **111a**, **111b** and **111d** showed a slow water exchange rate due the hindrance of the coordinated water.

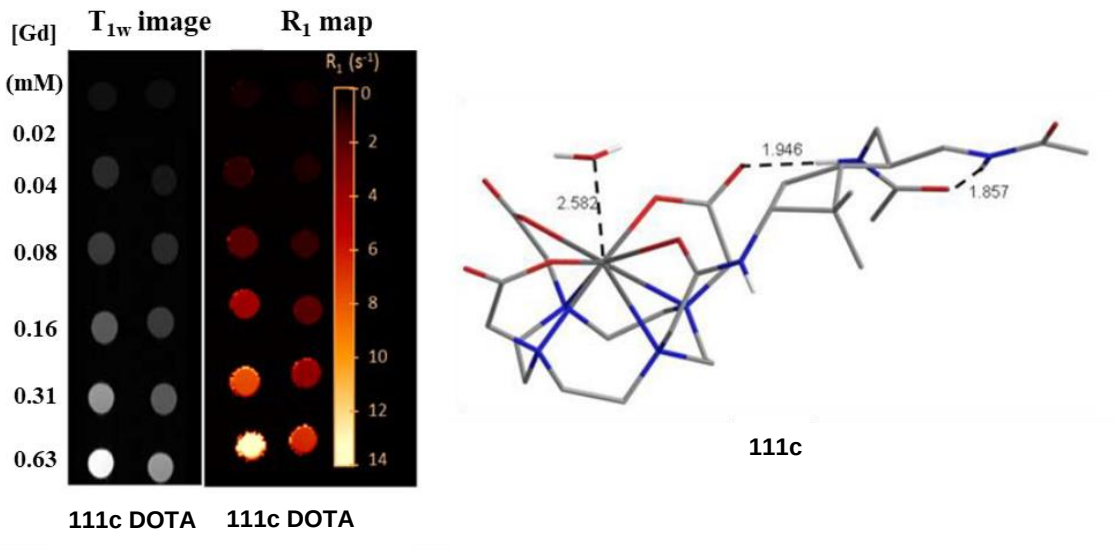

Figure 73. T_1-weighted images and r_1 map of phantoms of solutions of **111c** and **[Gd(DOTA)(H₂O)]⁻** at various concentrations (left) and calculated structure of **111c** presenting an extended conformation (right).

More recently, Dr. Oriol Porcar designed, synthesized and studied two different ligands containing the cyclobutane scaffold to conjugate both with Gd^{3+} and Mn^{2+} for the development of new contrast agents (Figure 74).[219]

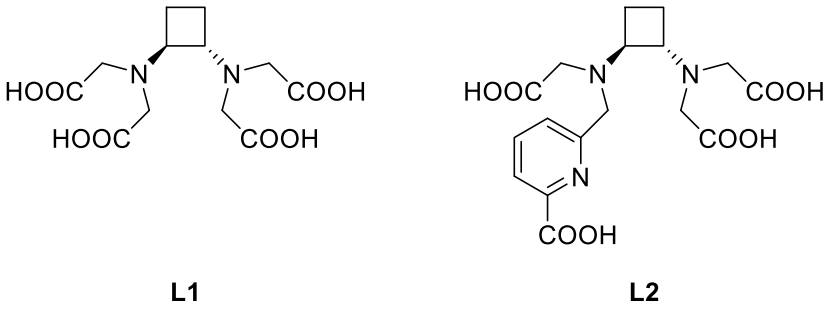

Figure 74. Structure of designed, synthesized and studied ligands by Dr. Porcar.

Results for **[Mn(L1)(H₂O)]²⁻** showed a relatively good thermodynamic stability, but NMRD revealed the presence of free Mn^{2+}, making the complex not suitable for clinical applications. Moreover, for **[Gd(L1)(H₂O)₃]⁻** the stability decreased considerably due to the presence of free labile water in the inner coordination sphere.

However, **[Gd(L2)(H_2O)$_2$]$^-$** showed interesting results in both thermodynamic stability (K_i = 17.4) and relaxivity (r_1 = 7.86 $mM^{-1}s^{-1}$ at 20 MHz and 25 ºC), comparable to other bishydrated Gd^{3+} complexes. Thus, the incorporation of the picolinate function played an important role in the properties of these complexes.

These results encouraged the group to continue using the rigid cyclobutane scaffold for the preparation and further study of new ligands to be used as potential contrast agents.

5.2 Objectives

In this part of the thesis and following the previous results, the synthesis of a new chiral cyclobutane-based ligand, **L3** was proposed to be complexed with Gd^{3+} and studied as potential MRI contrast agent (Figure 75).

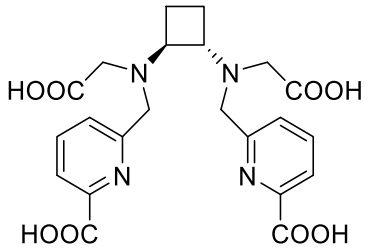

L3

Figure 75. Structure of the new target ligand.

Observing the number of coordinating centers for **L3** (8 sites), it was expected to have a theoretical hydration number of 1. Furthermore, the effect of the incorporation of a second picolinate moiety with respect to **L2** would be rationalized by means of the effect of the different hydration number in the stability, the inertness and the efficiency. Moreover, the obtained results would be compared with the studies of related contrast agents from the bibliography and from our research group.

The objectives of this part were:

- The synthesis of the ligand **L3** to prepare the corresponding metal complexes.
- The potentiometric study of the ligand and its metal complexes to understand its basicity and thermodynamic stability
- The study of the exact number of water molecules in the inner sphere, *q*, under different conditions.
- The study of the relaxivity under different conditions and the physicochemical parameters that influence it.

5.3 Results and discussion

The results of this chapter of the thesis are presented in four parts. First, the synthesis of the ligand is described in section 5.3.1. Later, the potentiometric studies are explained (section 5.3.2) followed by the luminescence studies (section 5.3.3). Finally, relaxometric measurements are discussed (section 5.3.4). All the parameters studies were carried out in collaboration with Dr. Éva Jakab Toth from Centre de Biophysique Moléculaire in Orléans (France).

5.3.1 Overview of the synthesis of ligand L3

Taking into account the experience in our research group preparing cyclobutane-based diamines and the reactions shown previously in this thesis, the target ligand could be obtained following the retrosynthetic pathway shown in Scheme 21.

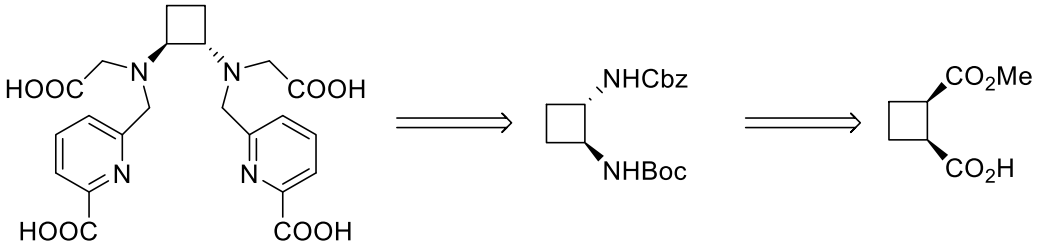

Scheme 21. General retrosynthetic pathway for ligand **L3**.

The retrosynthetic pathway for **L3** had a key intermediate **112**. *trans*-Diamine **112** was prepared according to the synthesis previously described by our research group.[9]

The synthetic route to obtain **L3** was stereoselective and led to the enantiopure compound. However it was not as straightforward as one would expect. The synthesis of key intermediate **112** and the process to obtain **L3** are described in the following pages.

5.3.1.1 Synthesis of orthogonally protected *trans*-diamine 112

The synthesis to obtain orthogonally protected *trans*-diamine **112** could be achieved in one step from protected amino acid **56**, which synthesis is explained in chapter 3 of the present thesis.

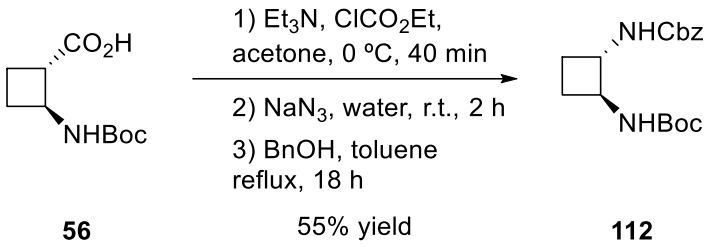

Scheme 22. Synthesis of key *trans*-diamine **112**.

The orthogonally protected *trans*-diamine **112** was prepared stepwise by treatment of amino acid **56** with ethyl chloroformate and triethylamine, followed by reaction with sodium azide. The resultant acyl azide was heated to reflux in the presence of benzyl alcohol. The in situ formation of an isocyanide through a Curtius rearrangement and subsequent reaction with the alcohol led to the desired *trans*-diamine **112** in 55% yield.

5.3.1.2 Synthesis of ligand L3

Several strategies were tried to synthesize **L3**, but most of them resulted in the generation of undesired byproducts or in the degradation of the reactants. The first thought was to insert the picolinate groups by two consecutive reductive aminations (Scheme 23).

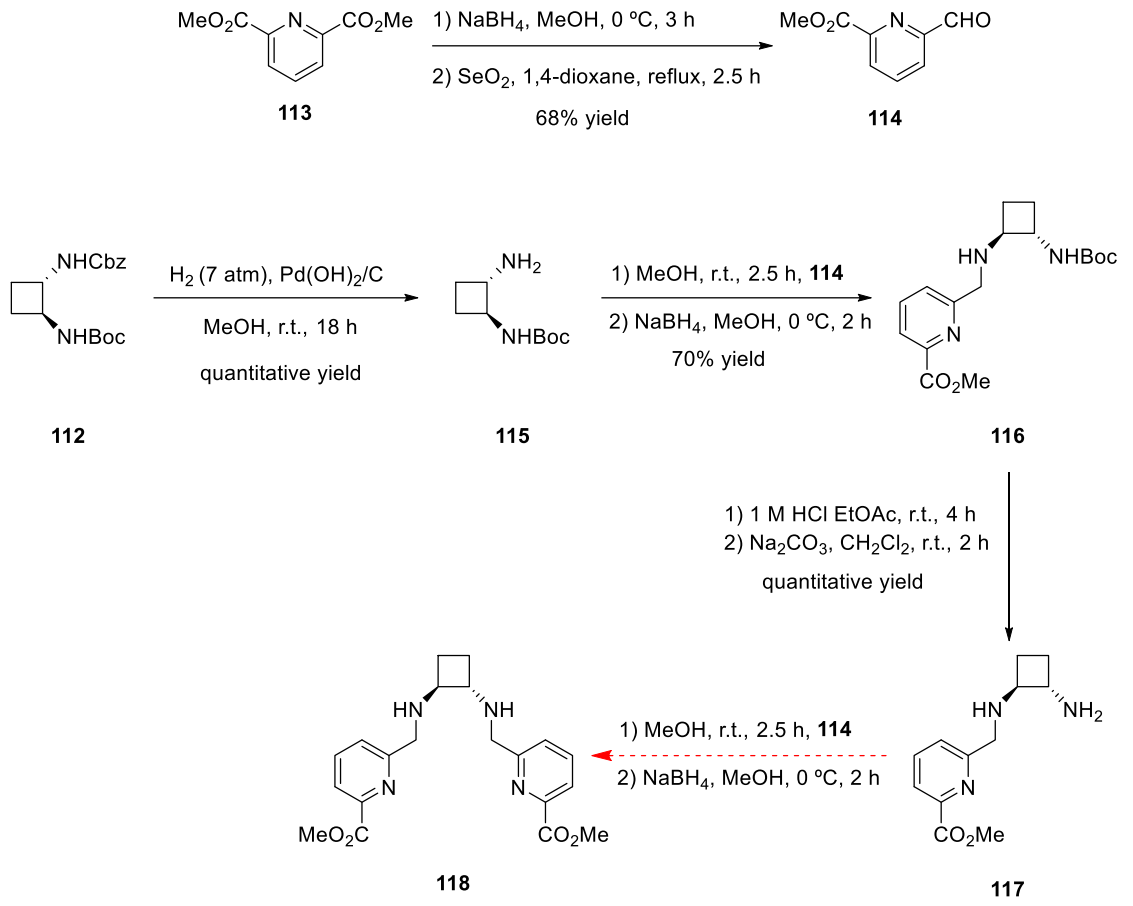

Scheme 23. Attempt to synthesize **118** by a reductive amination.

Starting from *trans*-diamine **112**, a catalytic hydrogenation was performed to obtain free amine **115** in quantitative yield. Then, a reductive amination was performed by using aldehyde **114**, previously synthesized by a partial reduction of **113**, and $NaBH_4$ as reductive agent to obtain **116** with a 70% yield. After that, an acidolysis reaction was carried out, followed by a neutralization using Na_2CO_3, obtaining amine **117** in quantitative yield. Finally a second reductive amination was tried to obtain functionalized *trans*-diamine **118**. Unluckily, the product was not obtain and starting material was recovered. This reaction was also tried by starting with the deprotection of the amine with the Boc protecting group and by the double deprotection of the amines, followed by a double reductive amination. The results of the reactions were the same.

Expecting that the problem could come from the reaction mechanism of the reduction amination, a second strategy was envisaged, in where the first picolinate group was introduced by a reductive amination, and the next one could be added by alkylation, expecting a high steric hindrance due to the presence of the first picolinate (Scheme 24).

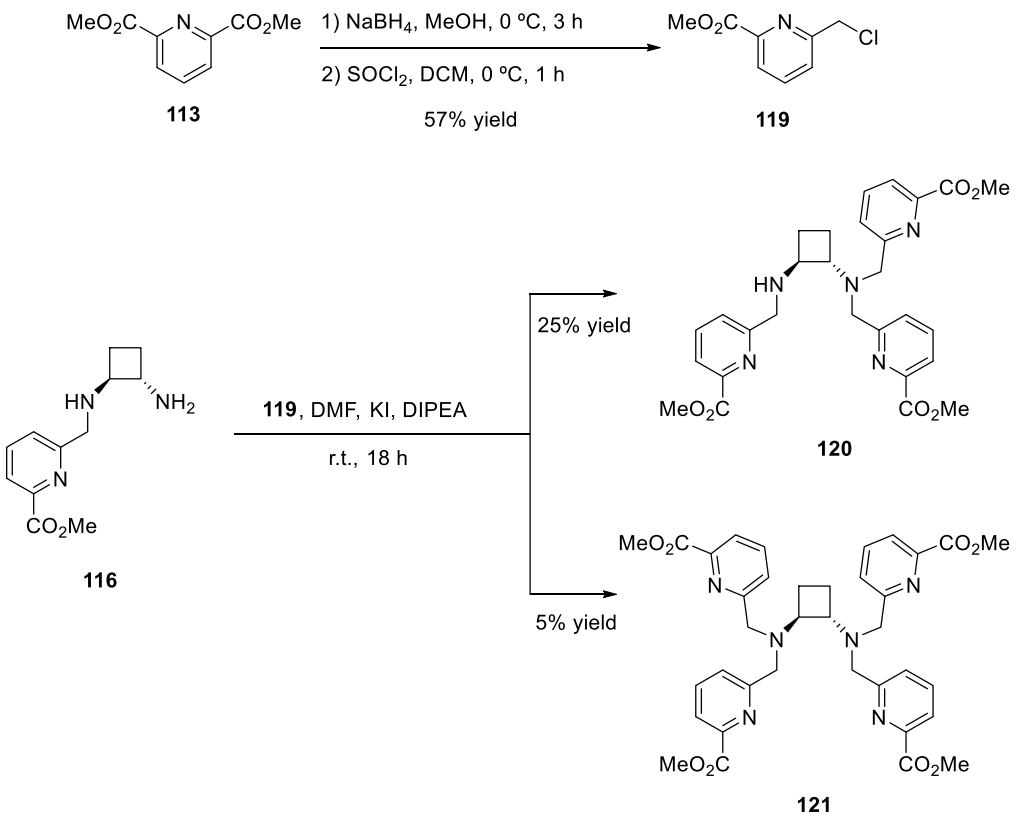

Scheme 24. Second synthetic route to obtain product **118**. Using this procedure only products **120** and **121** were obtained.

Starting from previously described amine **116**, an alkylation reaction was carried out using chloride **119**, prepared through the mono reduction of **113** followed by a chlorination, in the presence of KI and DIPEA. Unfortunately, product **118** was not obtained, but tri- and tetrasubstituted, **120** and **121** respectively, were achieved.

Confirming that the alkylation of the amines was not a valid option, a third strategy was attempted from a different point of view: the direct alkylation of the carbamates. The nitrogen of a carbamate is not unreactive at all and there are some precedents in the bibliography where this reaction is performed.[220] First of all both amines should be protected in the same way and benzyl carbamate was chosen for this. After that, an alkylation was tried (Scheme 25).

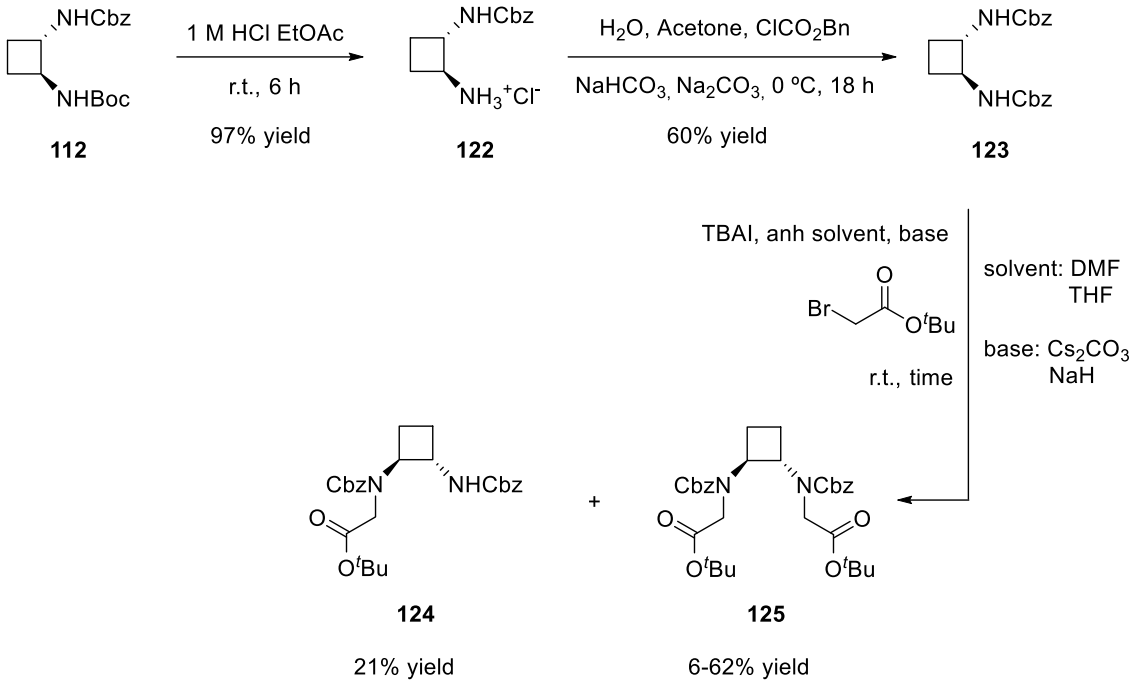

Scheme 25. Synthetic pathway to obtain alkylated carbamate **125**. Yields vary depending on the used base.

Double benzyl carbamate **123** was obtained, in 58% overall yield, using benzyl chloroformate at 0 ºC after the synthesis of the free amine **122** by means of an acidolysis reaction of **112**. Then, the direct alkylation of the carbamates was performed using *tert*-butyl bromoacetate, TBAI and a base. A first attempt was performed using DMF and Cs_2CO_3 as base, but after a week only 6% of the desired double alkylated product **125** was obtained. Then, a stronger base (NaH) was used in THF, obtaining **125** in 62% after 72 h of reaction. In both processes a 21% of monoalkylated carbamate **124** was obtained. Starting material **123** was also recovered in different quantities.

After achieving **125** in good yield, the synthesis was followed as seen in Scheme 26.

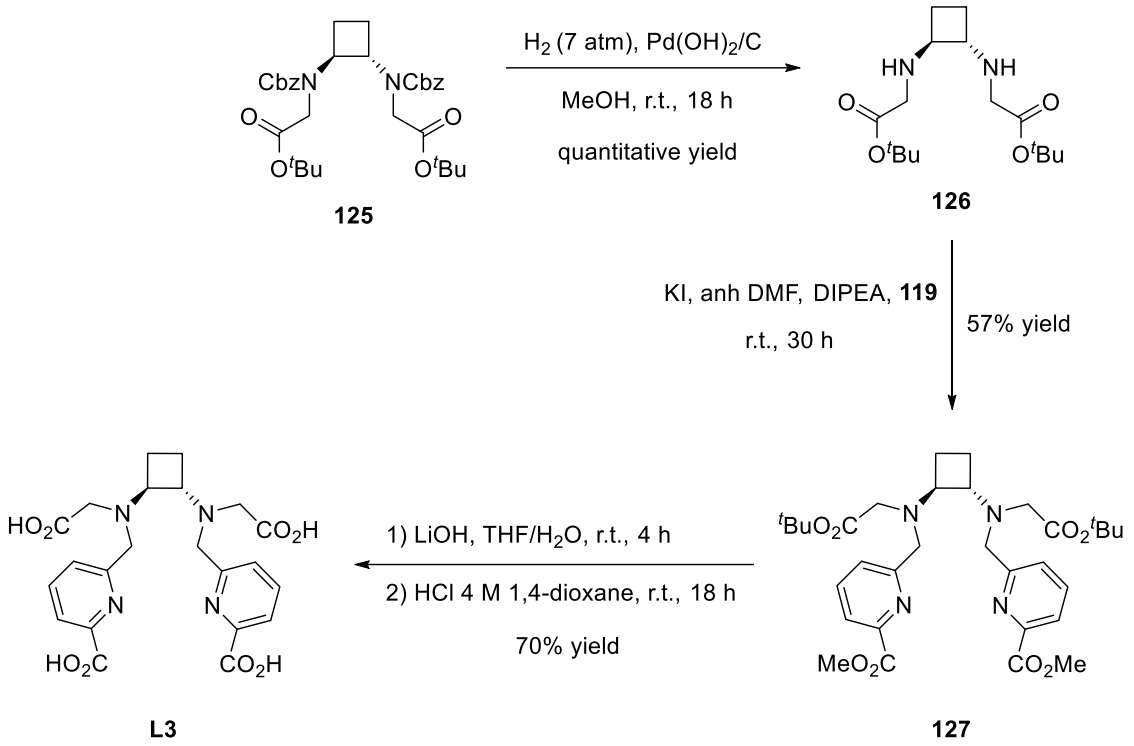

Scheme 26. Synthetic route to obtain ligand **L3**.

Starting from **125**, a catalytic hydrogenation was performed to obtain alkylated *trans*-diamine **126** in quantitative yield. Then, an alkylation reaction was performed in order to attach the picolinate unit to both branches by using **119**, KI and DIPEA in 57% yield. After that, removal of the methyl ester by saponification using lithium hydroxide followed by acidolysis of *tert*-butyl esters produced **L3** in 70% yield.

5.3.2 Potentiometric studies

pH-Potentiometric titrations were carried out to study both the protonation constants of **L3** and the stability constants of the formed metal complexes with different metal ions (Gd^{3+}, Mn^{2+} and Zn^{2+}). This method is widely used to describe the equilibrium processes metal complexes of polyaminopolycarboxylate ligands in solution. It can only be used if the equilibrium is quickly reached, which is a feature that is generally attributed to linear ligands, but not to macrocyclic ones.

In order to understand and discuss the results obtained during the experiments, **L3** was compared with both **L1** and **L2** and with different linear ligands from the bibliography (Figure 76).[199,200,221]

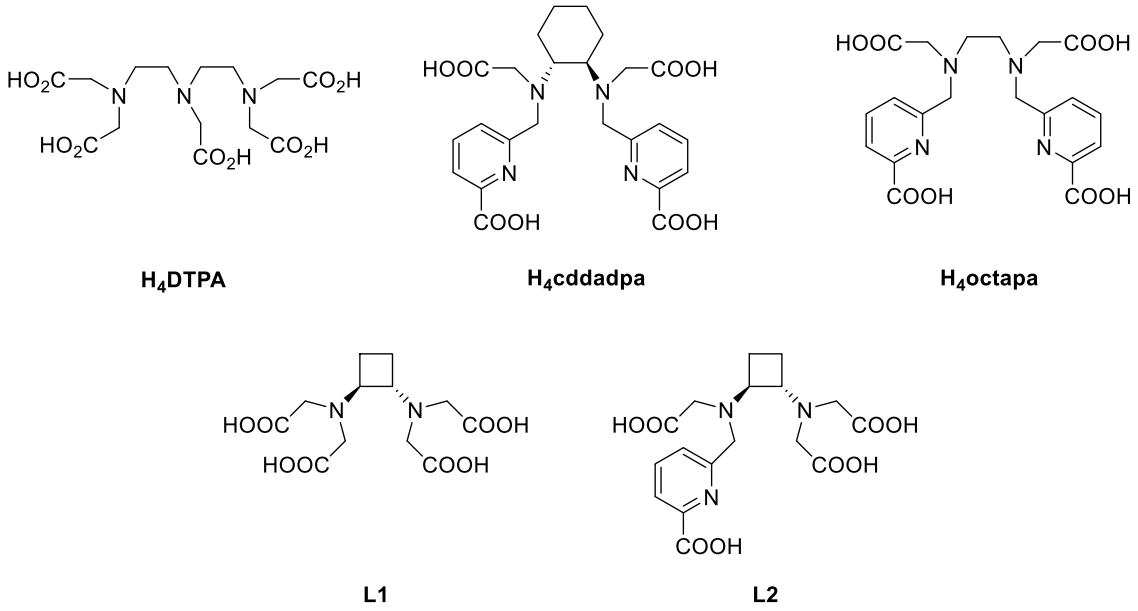

Figure 76. Structure of ligands described in the bibliography and synthesized in our research group as part of RMI contrast agents.

Two different factors influence the proton concentration of an aqueous solution containing a metal complex: the protonation constants of the ligand and the interaction between the metal ion and the different protonated species of the ligand. For this reason, comprehension of the ligand protonation constants is fundamental for determining the stability constants of the metal complexes.

Protonation constants of ligands, K_i, stability constants of complexes, K_{ML} and protonation constants of complexes, K_{MHiL} are described and defined in Equations 4-6.

$$K_i = \frac{[H_iL]}{[H_{i-1}L][H^+]}$$

Equation 4

$$K_{ML} = \frac{[ML]}{[M][L]}$$

Equation 5

$$K_{MH_iL} = \frac{[M(H_iL)]}{[M(H_{i-1}L)][H^+]}$$

Equation 6

Where [M], [L] and [ML] are the equilibrium concentrations of free metal ion, deprotonated ligand and deprotonated complex, respectively.

First of all, it was taken into account that the equilibrium should be reached rapidly to study protonation and stability constants by pH-potentiometry. Then, to avoid dilution effects, only the first base-based titration was considered to calculate the protonation constants of the ligand, which were calculated using computer software Hyperquad 2008 considering equations 4-6.[222] Once the ligand was studied, the stability constants of the metal complexes of **L3** were also determined from direct potentiometric titrations, as the complex formation was fast (Figure 77).

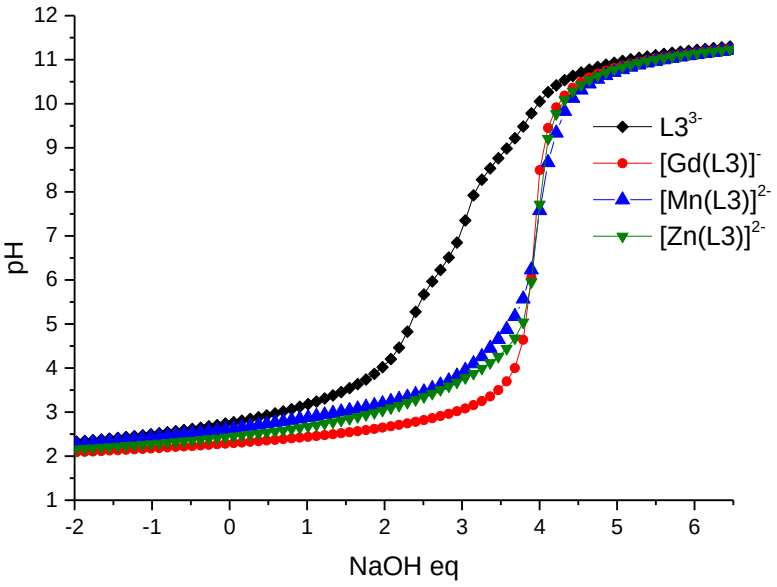

Figure 77. Potentiometric pH titrations curves for ligand **L3** in the absence (black) and in the presence of some metal ions at 1:1 metal/ligand ratio: Gd^{3+} (red), Mn^{2+} (blue) and Zn^{2+} (green). [M] = [L] = 2 mM + 0.1 M KCl, 25 ºC in N_2 (1 atm).

These experiments were carried out using the same conditions as with the free ligand, but containing 1 equivalent of metal cation (Gd^{3+}, Mn^{2+} or Zn^{2+}). At least 2 or 3 independent experiments were carried out to determine these values. The results are shown in (Table 3).

Observing Figure 77 it is clear that in the presence of a metal, the equivalence point of the curves was shifted to higher concentrations of NaOH, which indicates the formation of the metal-ligand complexes. This shift was also used to corroborate the concentration of the ligand stock solution, which was equal to the calculated before the experiments. The titration curve was cut before reaching pH 10 due to the precipitation of a solid, which could be attributed to the formation of an insoluble hydroxo complex. To calculate the stability constants and the protonation of the complexes, titration curves were refined using the same computer software Hyperquad 2008 used before.[222] All the collected data is shown in table 3.

Experiments showed five protonation constants for **L3**, the same as for **L1** and **L2**. Dr. Porcar determined that the two first logK_i values for **L1** could be attributed to the protonation of the two amines, followed by the protonation of the carboxylate functions.

However, the same correlation of protonation constants for **L2** could only be hypothesized to be the same as **L1**, due to the addition of the picolinate function. The same can be applied in the case of **L3**. For example, in the studies of a ligand containing a pyridine ring, the protonation of the pyridine function was not observed in the typically studied pH-range (2-12).[201] In fact, the incorporation of a second pyridine in **L3** lowered even more the first protonation constant if compared with **L1** (0.77 units of log$K$), but its global basicity was 3.17 units of log$K$ higher.

Looking at related ligand constants, it can be observed that **L3** has a lower first protonation constant than **Cddadpa**, but higher than **octapa**. **L3** and **Cddadpa** showed equivalent values when comparing the total basicity, 3 units of log$K$ higher than **octapa**. This effect could be attributed to the rigidity given by both the cyclohexyl and cyclobutyl units compared to the ethylene bridging unit, which is more flexible. Comparing the results obtained for **L3** those for **DTPA** it can be seen that both the first protonation constant and the total basicity were lower for the studied ligand.

Table 3. Protonation constants and standard deviations of **L3** and stability constants of its metal complexes (25 ºC, I = 0.1 M KCl). Results of ligands found in the bibliography and previously studied complexes are also shown. Numbers between parentheses represent the error of the measurements.

	L1	**L2**	**L3**	**octapa**[199]	**Cddadpa**[200]	**DTPA**[221]
log K_1^H	9.66 (0.01)	9.58 (0.02)	8.89 (0.03)	8.52	9.35	9.93
log K_2^H	5.84 (0.01)	6.00 (0.04)	6.61 (0.05)	5.40	5.66	8.37
log K_3^H	3.06 (0.02)	3.78 (0.04)	4.26 (0.06)	3.65	4.20	4.18
log K_4^H	2.08 (0.03)	2.32 (0.05)	2.97 (0.06)	2.97	3.72	2.71
log K_5^H	1.71 (0.08)	2.07 (0.05)	2.79 (0.06)	1.66	2.62	2.00
Σ log K_i^H	22.35	23.75	25.52	22.20	25.55	27.19
log K_{GdL}	14.73 (0.01)	17.41 (0.01)	18.00 (0.02)	20.23	20.68	22.03
log K_{GdHL}	2.36 (0.03)	2.35 (0.02)	3.28 (0.03)	-	2.38	1.96
log K_{MnL}	10.26 (0.01)	14.71 (0.01)	15.81 (0.07)	14.32	-	14.54
log K_{MnHL}	4.07 (0.02)	3.25 (0.01)	3.60 (0.05)	2.90	-	4.37
log K_{MnH2L}	-	-	3.35 (0.05)	-	-	-
log K_{ZnL}	12.26 (0.01)	15.22 (0.01)	16.28 (0.05)	19.32	15.85	17.45
log K_{ZnHL}	4.10 (0.01)	3.78 (0.01)	4.00 (0.04)	-	3.81	5.08
log K_{ZnH2L}	-	-	3.41 (0.04)	-	-	-

The complex formed by Gd^{3+} ion and **L3** presented a nonprotonated and a monoprotonated mononuclear complex species. However, the complexes formed by Mn^{2+} and Zn^{2+} and **L3** presented the same species as the Gd^{3+} with the addition of a diprotonated mononuclear complex specie. This behavior was not only completely different from that observed for **L1** and **L2**, but also from the bibliography ligands. These mono- and diprotonated complexes were observed at low pH and could be attributed to the protonation of a non-coordinating carboxylate function.

All the stability constants ($\log K_i$) obtained during the experiments of **Gd(L3)**, **Mn(L3)** and **Zn(L3)** were higher than those for both **L1** and **L2** ligands, which can be easily explained looking at the structure and the one or two extra coordinating sites, respectively, which **L3** has. Comparing **Gd(L3)** stability constant with other ligands values showed differences of 2.23 units lower than **Gd(octapa)**, 2.68 units lower than **Gd(Cddadpa)** and 4.03 units lower than **Gd(DTPA)**, which may point that the distribution of the coordinating sites, mainly ruled by the rigidity given by the cyclobutane scaffold, could not be appropriate to fit the metal. However, this behavior was not observed on the **Mn(L3)**, which had the highest stability for all the ligands, indicating that there is not a correlation between different metals and ligands. Unfortunately, the **Mn(L3)** complex is not interesting for MRI applications, because it should not have any water molecule directly coordinating the metal, but it was helpful to gain some insight about structure and stability.

Results in the bibliography have demonstrated that *in vivo* toxicity of Gd complexes is caused by the release of Gd^{3+} ions, which can be promoted by the transmetallation with endogenous cations, such as Zn^{2+}, Cu^{2+} or Ca^{2+}.[173,223,224] Fortunately, **Gd(L3)** stability constant was higher than **Zn(L3)**, preventing the transmetallation with Zn cations, which is a crucial parameter for clinical applications.

Studies of the species distribution in function of the pH were also carried out to rationalize in which range of pH the complexes were thermodynamically stable. Species distribution plots were calculated using the experimental protonation and stability constants using the computing software HySS (Figure 78).[225]

In Figure 77, the representation of the molar fraction of the species of different systems in function of the pH was done. For example, **L3** in water at pH = 7.3 (close to the physiological pH) is in 81% in its monoprotonated specie (**$L3H^{3-}$**) and 17% in its diprotonated form (**$L3H_2^{2-}$**). Although it is not represented, the fully deprotonated form (**$L3^{4-}$**) was observed in a 99.5% distribution at a pH above 11.3.

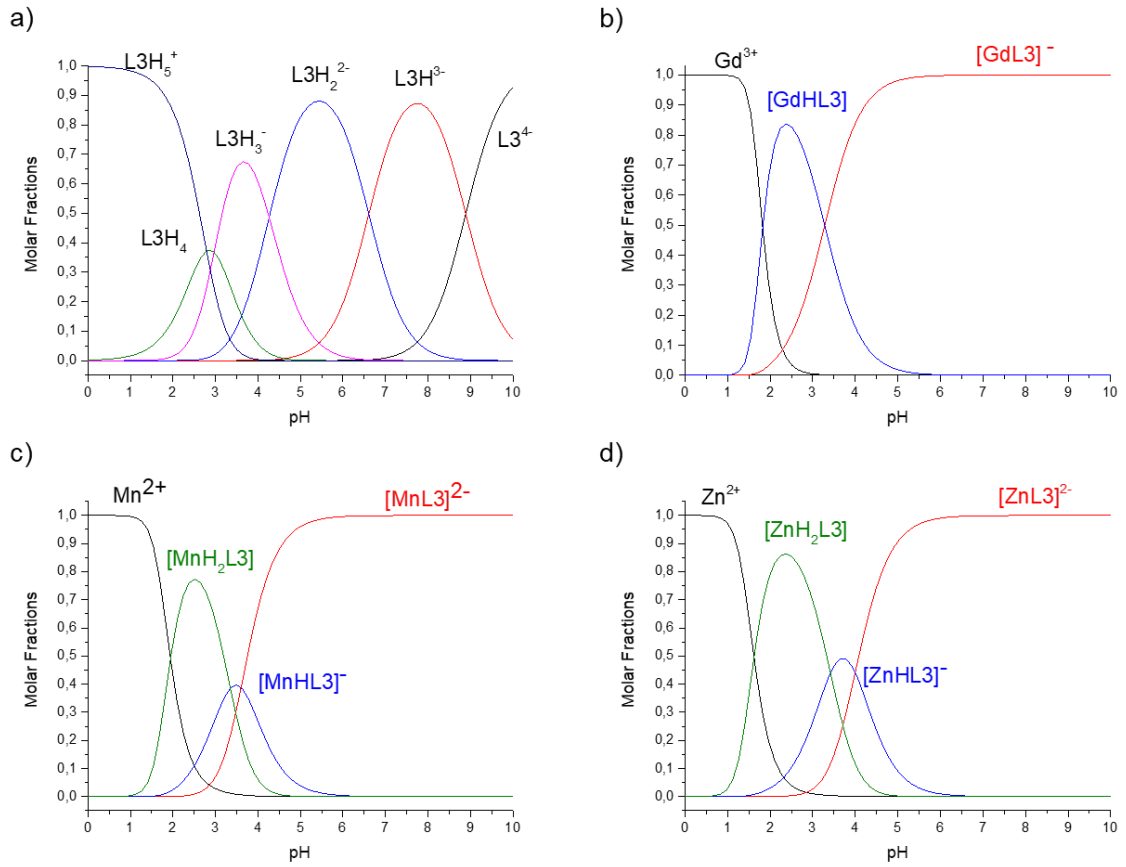

Figure 78. Species distribution curves of the ligand. a) in absence of metal, b) with Gd^{3+}, c) with Mn^{2+}, d) with Zn^{2+}.

Using the species distribution curves, the pH range in which these complexes could be stable enough to be used can be determined. This is a key factor to ensure that no free metal species are found during structural and relaxometric studies, which may lead to erroneous values during the experiments. These curves were calculated considering one equivalent of ligand and metal, but it should be mentioned that the addition of more ligand equivalents could be a good solution in the case a complex was not stable for its study at the desired pH. Quantitative results are shown in Table 4.

Table 4. pH ranges where complexes were thermodynamically stable and molar fractions in percentage of the complexes at pH = 3, 5 and 7.

Complex	**Stability ML** pH range[a]	**Complex ML** (pH = 3) (%)	**Complex ML** (pH = 5) (%)	**Complex ML** (pH = 7) (%)
Gd(L3)	5.3-10	38.5	98.3	100
Mn(L3)	5.6-10	9.3	96.4	99.9
Zn(L3)	6.0-10	3.6	91.5	99.9

[a] pH values at which molar fraction of complexes were higher than 99%. Beyond pH = 10 it was not determined.

As seen in Table 4, the Gd complex had a wider usable pH range, followed by Mn and Zn complexes. None of the complexes were completely stable at pH = 5, but **Gd(L3)** was the most stable at this pH. As mentioned in the previous page, these pH ranges were taken into account to perform the structural and relaxometric studies.

5.3.3 Luminescence studies for determining *q*

Luminescence spectroscopy was used in order to analyze the number of water molecules directly coordinated to the metal ion, *q*. Since this parameter is linearly proportional to the relaxivity of the inner sphere, determining *q* in aqueous solution was crucial to explain the aspects that control the relaxivity.[173] This parameter can be determined using different methodologies specific to lanthanide complexes, but none of them can be directly applied to Gd^{3+} complexes with accuracy.

The most used alternative method consists on measuring the luminescence lifetime of solution of Eu^{3+} and Tb^{3+} chelates by luminescence spectroscopy, in order to determine the hydration number of lanthanide complexes.[226] Although most of lanthanides ions present luminescence, some of them have higher emission due to differences between the excited and the ground state of each one. Among all lanthanides, Eu^{3+} and Tb^{3+} are the most used, because their emission is in the visible range and their luminescence lifetimes are long, in contrast to Gd^{3+}.[181,227] Moreover, Eu^{3+} and Tb^{3+} are near Gd^{3+} in the periodic table, so similar physicochemical properties are expected (especially comparable ionic radius). For this reason, applying these methodologies to their chelates was expected to give a good estimation for the hydration number of the corresponding Gd^{3+} complex.

Horrocks and Sudnick proposed a method that consists in the measureament of luminescence lifetimes of excited states of Eu^{3+} and Tb^{3+} in separated solutions of H_2O and D_2O.[228,229] The decay of the excited state of the lanthanide ion is promoted by an efficient non-radiative pathway provided by the OH oscillators of coordinated water molecules. The pathway is less efficient in the case of OD oscillators of coordinated D_2O molecules, making more difficult to reach the ground state. The difference between the efficiency of both oscillators is directly related to the number of water molecules coordinate to the lanthanide ion. The following empiric equation (Equation 7) is used to calculate q from the differences of luminescence decay lifetime in H_2O and D_2O, τ_{H2O} and τ_{D2O}.

$$q = A\left(\frac{1}{\tau_{H_2O}} - \frac{1}{\tau_{D_2O}} - B\right)$$

Equation 7

Where A is a specific constant for each lanthanide ion related to the efficiency of this ion to decay and B is a correction factor when polyaminopolycarboxylate-based ligands are present. These empirical constant take values of $A = 1.2$ and $B = 0.25$[230] or $A = 1.11$ and $B = 0.31$,[231] both for Eu^{3+}.

In this thesis, the luminescence decay lifetime of **Eu(L3)** was recorded to study the number of water molecules directly coordinated to the metal, *q*. The results would be extrapolated to **Gd(L3)**. In order to perform this study, the absorption, emission and excitation spectra of **Eu(L3)** were recorded to check the maximum wavelength at which the decay lifetime would be registered.

The absorption spectrum showned a single band due to the combination of a π-π^* and n- π^* transitions of the picolinate functions. The maximum in the excitation spectrum was at 268 nm. The addition of the picolinate functions produced a more efficient excitation, obtaining a higher emission of Eu^{3+}. The emission spectrum of **Eu(L3)** showed $^5D_0 \rightarrow {}^7F_J$ (J = 0 – 4) transitions with maxima at 616 nm expected for this metal ion. Then, the decay of the emission intensity was recorded at 616 nm, following an excitation at 268 nm. Luminescence lifetimes and *q* values of **Eu(L3)** compared to those obtained for **Eu(L1)** and **Eu(L2)** are shown in Table 5. These experiments were carried out in 0.2 mM concentration of complex in 0.1 M Hepes buffer with pH and pD = 7.

Table 5. Luminescence lifetimes (τ) of **Eu(L1)**, **Eu(L2)** and **Eu(L3)** complexes and number of water molecules coordinates (*q*) to Eu^{3+} ion.

Complex	τ_{H2O} (ms)	τ_{D2O} (ms)	q^a	q^b
[Eu(L1)]$^-$	0.241	0.760	3.1	2.8
[Eu(L2)]$^-$	0.405	2.16	2.1	1.9
[Eu(L3)]$^-$	0.544	1.984	1.3	1.1

q^a obtained from Equation 7 with A= 1.2 and B = 0.25. q^b obtained from Equation 7 with A= 1.11 and B = 0.31.

As shown in Table 5, the luminescence lifetime value for **Eu(L3)** in D_2O was much higher than that in H_2O, following the same pattern than the previously studied ligands.

It has to be remarked that, in general, the hydration values (*q*) obtained with Beeby's constants[230] were slightly higher than expected, while using Horrock empirical constants showed lower values than the theoretical ones.[231229] Nevertheless, the values obtained were around the expected value of *q* for all the ligands. Thus, for **Eu(L1)** and **Eu(L2)** the calculated number of water molecules (*q*) was considered to be 3 and 2, respectively. For **Eu(L3)** both hydration values were above the theoretical number of coordinated water molecules, 1. The method employed to measure these values is not exact and its error is inside the decimal deviations, which may point to 1 coordinated water for **Eu(L3)**. Another possibility is the spontaneous loss of a coordination site with the metal ion, which promotes the coordination of a second water molecule in some of the formed complexes. This phenomenon was observed in the analogous **Eu(cddadpa)** and the hydration value was considered to be 1.[200] Further experiments must be performed to confirm the hydration value (*q*).

In conclusion, and assuming that *q* = 1 for **Eu(L3)**, the Gd^{3+} ion in this complex has 9 coordinating sites, 8 of them occupied by **L3** and 1 water molecule (Figure 79).

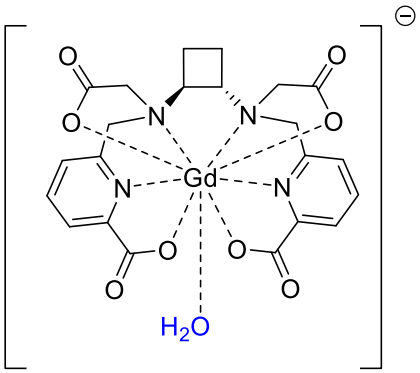

[Gd(L3)(H$_2$O)]$^-$

***q* = 1**

Figure 79. Structure and *q* value of [**Gd(L3)(H$_2$O)]$^-$**. Charges are omitted for clarity of the drawing.

5.3.3.1 Anion binding studies

Studying the possibility that endogenous anions replace water molecules coordinated to the metals is crucial to investigate the potential of a ligand in *in vivo* applications. Although this experiment is generally performed with unsaturated lanthanide complexes that contain more than one inner-sphere water molecules, the possibility that more than one water is coordinated in **Gd(L3)**, explained in the previous page, could be checked by this technique. The complexes are able to bind relevant anions, such as carbonate, phosphate or citrate to form ternary complexes, which require the replacement of one or more water molecules coordinated to the Gd^{3+} ion.[232,233] In fact, the relaxivity of the molecule is drastically decreased if one or more water molecules are displaced by an ion, which is not desirable in a biological environment.[234] For example, the relaxivity of the macrocyclic **Gd(DO3A)** complex, which contains 2 water molecules, decreases to the half in the presence of different anions.[235] However, there are examples in the bibliography where Gd^{3+} linear complexes with two water molecules do not bind anions or the binding is very weak.[236] This could be possible due to two different factors. The first one is explained by the electrostatic repulsion between the negatively charged complex and the anions.[202] The second is related to the non-adjacent positions that water molecules occupy in the inner sphere around the metal.[237]

There are different methodologies to study the anion binding, like measuring the relaxivity or the luminescence decay lifetimes in the presence of different equivalents of anions. In this thesis, the luminescence lifetime of the **Eu(L3)** complexes in H_2O and D_2O was measured in the presence of carbonate and phosphate, in order to check the formation of ternary complexes. These two anions are generally responsible for the relaxivity decrease in biological media. Moreover, the interaction with the metal is different from each other: phosphate has been demonstrated to interact in a monodentate way, while carbonate binds in a bidentate manner. The decays of the emission intensity of **Eu(L3)** in the presence of 10 and 50 equivalents of carbonate and phosphate were independently recorded in H_2O and D_2O. 50 equivalents are above the physiological concentrations of this anion in human plasma. The same conditions used in section 5.3.3 for determining q in the absence of anions were applied, but in this case, the pH was shifted to 7.4. The q^a values in the absence and presence of anions are shown in Table 6.

Table 6. q^a Values of Eu(L3) in the absence and presence of 10 and 50 equivalents of phosphate and carbonate, respectively.

	q **[a] values**				
Complex	**Anion free**	**phosphate**		**carbonate**	
		10 eq	50 eq	10 eq	50 eq
[Eu(L3)]$^-$	1.3	1.3	1.2	1.3	1.3

q^a obtained from Equation 7 with A = 1.2 and B = 0.25. 0.20 mM EuL, 0.1 M Hepes buffer, pH and pD = 7.4, 25 ºC.

As can be appreciated in Table 6, the resulting *q* values of **Eu(L3)** did not show any decrease with the addition of 10 or 50 equivalents of phosphate or carbonate. With these results, the formation of ternary Eu^{3+} complexes with these anions was excluded and the same behavior for **Gd(L3)** complex should be expected. Moreover, the possibility that a second water could be coordinated to the metal in a near position, which would have led to the binding of the anions was discarded. Nevertheless, the scenario where two water molecules are coordinated in a far position from the other one, is not totally dismissed. To check this possibility X-ray diffraction analyses would be required to get more insight of the presence of several water molecules in the complex. Unfortunately, unsuitable crystals were obtained.

In summary, the experiment concluded that **Gd(L3)** is stable in front of the action of endogenous anions and thus, suitable for biological experiments without suffering any relaxivity decrease.

5.3.4 Relaxivity studies

As stated in the introduction of this chapter, relaxivity (r_1) defines the efficiency of a contrast agent (CA) used in MRI. This parameter can be defined as the enhancement of the longitudinal relaxation rate of the water protons per millimol per liter of paramagnetic compound (see Equation 1).

Different physico-chemical parameters regulate the relaxivity, including electron relaxation parameters, rotational correlation times and water exchange rate. In order to obtain realistic and contrasted results, the studies and determination of these parameters should be done independently. In this part of the thesis, the relaxivity and the parameters that govern it for **Gd(L3)** were studied by proton nuclear magnetic relaxation dispersion (^{1}H NMRD) profiles and temperature-dependent ^{17}O NMR. Simultaneously using both techniques, the parameters were calculated. In the following pages, the results of both techniques are discussed.

5.3.4.1 NMRD Profiles

The representation of the relaxation rates or relaxivity in function of the applied magnetic field (B_0) or the Larmor frequency in a logarithmic scales shown in ^{1}H NMRD profiles. Several parameters affect the relaxivity of a proton such as temperature, sample composition, pressure and magnetic field. NMRD profiles are useful tools to separate the interaction mechanisms and dynamics that influence the relaxation. All the equations and parameters that describe the relaxivity are explained in detail in section 7.11.

NMRD profiles of **Gd(L3)** were recorded in aqueous solution at 25 ºC, 37 ºC and 50 ºC in the frequency range of 0.04 to 80 MHz, which correspond to magnetic fields of $9.4 \cdot 10^{-4}$ T to 1.9 T, respectively. To ensure the complete complexation and avoid the presence of free Gd^{3+}, which would have affected the results, an extra amount of ligand (more than 1:1 metal-ligand ratio) was added. The ^{1}H NMRD profile of **Gd(L3)** is shown in Figure 80.

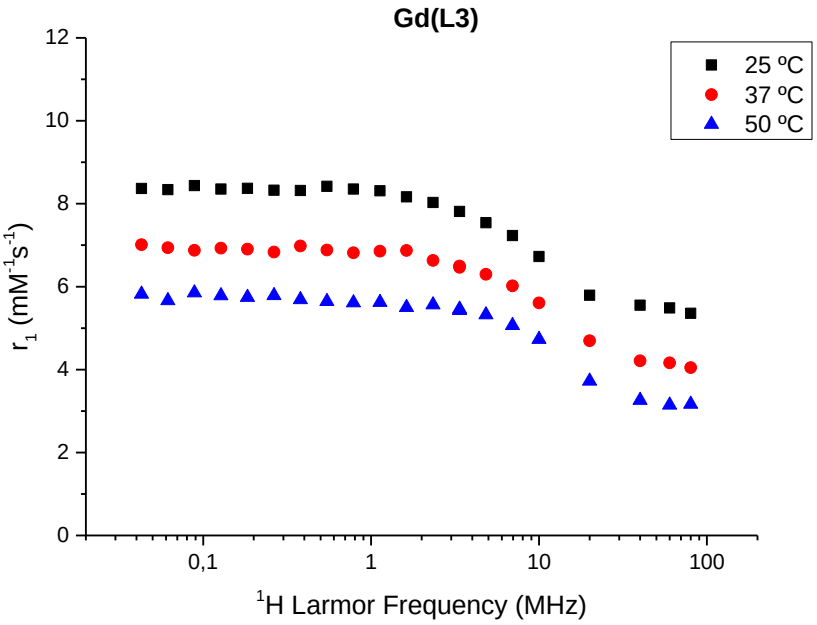

Figure 80. NMRD profiles of 2.13 mM **Gd(L3)** + 5% L3 at 25 ºC (black), 37 ºC (red) and 50 ºC (blue) at pH = 7.

It was observed that an increase of the temperature lowered the relaxivity values, which was consistent with a faster rotation of the complex at higher temperature being the limiting factor of the relaxivity. The shapes of the NMRD profiles were typical for non-macromolecular Gd^{3+}chelates. At low Larmor frequencies (below 1 MHz) relaxivity values were constant. The same phenomena was observed at high Larmor frequencies (above 60 MHz), where the values were constant again. The NMRD profiles and the value of relaxivity at 20 MHz was coherent with a complex with one water molecule in their inner sphere. These values were compared with the values of some relevant and related ligands from the bibliography and from previous work in the group (Table 7).

Table 7. Relaxivity values (r_1) and number of coordinated water molecules (q) at 20 MHz of **Gd(L1)**, **Gd(L2)**, **Gd(L3)** and Gd complexes from the bibliography.

	Gd(L1)	**Gd(L2)**	**Gd(L3)**	**Gd(octapa)**[199]	**Gd(cddadpa)**[200]	**Gd(DTPA)**[185]
r_1	8.8	7.9	5.8	5.6	5.0	4.3
q	3	2	1.2	1	1	1

r_1 values in $mM^{-1}s^{-1}$ at 25 ºC. [a] 0.47 T.

Coherently, the relaxivity of **Gd(L3)** was lower than both **Gd(L1)** and **Gd(L2)** at 20 MHz, because it was the compound with less water molecules coordinating in the inner sphere. The addition of more water molecules generally means the increasing in the relaxivity of the Gd^{3+} complexes but it is achieved by lowering its thermodynamic stability and inertness. In conclusion, designing complexes with the minimum water molecules in the inner sphere is the way to go, suggesting that the maximum of hydration number for a small complex could be two, due to the less stability of compounds containing more.

The relaxivity of **Gd(L3)** at 20 Mhz and 25 ºC is 0.2 units higher than **Gd(octapa)** and 0.8 units higher than **Gd(cddadpa)**. In this case, the cyclobutane unit favors the relaxivity compared to both the cyclohexane and ethylene bridges. Nevertheless, the theory that more more than one water molecule was present in the coordinating inner sphere (in Table 7 was represented as 1.2 waters) could also explain this increase in the relaxivity value. Unfortunately, there is no information about the rotational correlation times or electron-spin relaxation times of either **Gd(octapa)** or **Gd(cddadpa)** in the bibliography, so the rationalization of the difference between relaxivity of the complexes could not be done.

5.3.4.2 ^{17}O NMR studies

The evaluation of the parameters that describe the water exchange rate and rotational dynamics of paramagnetic complexes were performed using ^{17}O NMR variable temperature measurements. Equations and parameters that describe ^{17}O NMR are explained in detail in section 7.12.

In ^{17}O NMR experiments, the transverse and longitudinal ^{17}O relaxation rates, $1/T_1$, $1/T_2$ and the ^{17}O chemical shifts, ω, are measured from samples containing the paramagnetic compound and from a reference, such as acidic water or another diamagnetic compound, in an independent way. The difference in the parameters obtained from both the sample and the reference are named reduced transverse or longitudinal ^{17}O relaxation rate, $1/T_{1r}$, $1/T_{2r}$ and ^{17}O reduced chemical shift, $\Delta\omega_r$.

The different water exchange kinetics at different temperature ranges is the main reason why ^{17}O NMR experiments are performed at different temperatures. For example, in the slow exchange region, the reduced transverse relaxation rates increase with temperature. In this region, the water exchange rate, k_{ex}, is determined by $1/T_{2r}$. On the other hand, in the fast exchange rate region at high temperatures, T_{2r} decreases with temperature and it is determined by $1/T_{2m}$, which is the transverse relaxation rate of the coordinated water. Sometimes, the inflection point of these two different kinetic regions can be observed in the working temperature range of this method (273-373 K).

The longitudinal and transverse ^{17}O relaxation rates ($1/T_1$, $1/T_2$) and the chemical shifts were measured at 9.36 T in aqueous solution of **Gd(L3)** in a temperature range of 276 to 348 K. Unfortunately, differences between the paramagnetic solution and the reference were not high enough to get reproducible results for the longitudinal ^{17}O relaxation rate ($1/T_1$) However, data from the transverse ^{17}O relaxation rates ($1/T_2$) and chemical shifts were robust and were plotted in function of temperature in Figure 81.

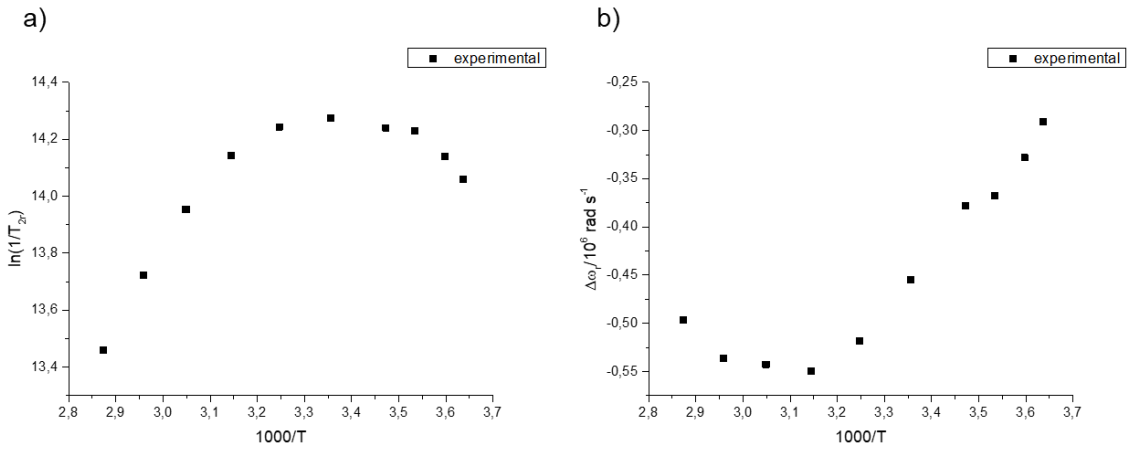

Figure 81. a) Reduced transverse ^{17}O NMR relaxation rates. b) ^{17}O NMR chemical shifts. Concentration was 6.45 mM at pH = 6.5.

In Figure 81 can be observed a change over the function associate with the two different exchange regions in both the $1/T_{2r}$ and $\Delta\omega_r$ plots. The fitting of these curves at the slow kinetic region allowed to determine the water exchange rate more accurately than in the cases where this region is not observed.

5.4 Summary and conclusions

In this part of the thesis, a ligand containing the 1,2-cyclobutane diamine structure bearing two picolinate units and two acetate ones was synthesized and complexed with Gd^{3+} (Figure 82). Potentiometric studies showed that **Gd(L3)** has a high stability constant, K_i (18.0), comparable with other ligands with one coordinating water molecules. Moreover, this constant was higher than those for Mn^{2+} and Zn^{2+}, which is crucial for biological applications.

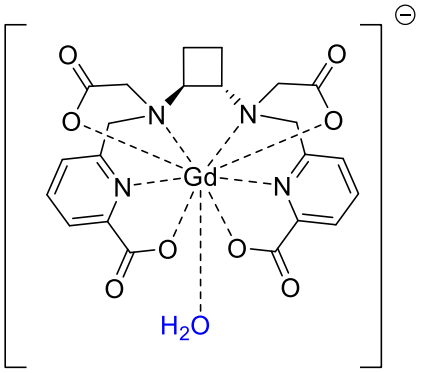

[Gd(L3)(H$_2$O)]$^-$

***q* = 1**

Figure 82. Structure and *q* value of [**Gd(L3)(H$_2$O)]$^-$**. Charges are omitted for clarity of the drawing.

Luminescence experiments of analogous Eu^{3+} complexes pointed that q = 1.2, which could be an error of the method or mean that some coordination points are lost and some ligands coordinate more than one water molecule at the same time. In the presence of phosphate or carbonate anions, the hydration number of **Eu(L3)** kept constant. These results should be the same for **Gd(L3)**, making the relaxivity stable in *in vivo* experiments.

The relaxivity value (r_1) of **Gd(L3)** was 5.8 $mM^{-1}s^{-1}$ at 20 MHz and 25 ºC, which is the highest value for a monohydrate ligand of the ones compared in this thesis.

In summary, taking into account the suitable properties described in this thesis, the **Gd(L3)** complex could become a useful candidate for a clinical use.

Further studies of the physicochemical parameters obtained by ^{17}O NMR are under investigation.

6. General Conclusions

6. General Conclusions

In this thesis, cyclobutane has been used as a scaffold for the development of different systems with various applications. These compounds have been prepared using the previously acquired experience in the research group on stereoselective synthesis strategies. During the elaboration of this thesis, many different techniques have been used to synthesized, characterize and study the designed compounds.

Short Hybrid CBAA, γ-amino-L-Proline Peptides: six families of peptides based on the alternated combination of β- or γ-CBAA and *cis*- or *trans*-γ-amino-L-proline were synthesized. High resolution NMR experiments were performed in different solvents and temperatures to check their folding ability and patterns. The presence of *cis*-γ-amino-L-proline originated the formation of an intra-residue hydrogen bond, which was not detected when a *trans*-γ-amino-L-proline was part of the structure. Moreover, having a β-CBAA promoted the formation of more intra-residue hydrogen bonds, originating different secondary structures depending on the stereochemistry of the unit. When γ-CBAA containing peptides were studied only inter-residue hydrogen bonds were observed. This study helped to rationalize the design of new cell penetrating peptides.

Peptides as cell penetrating agents: two families of hybrid peptides based on the γ-CBAA and *cis*- or *trans*-γ-amino-L-proline were synthesized using solid phase methodologies. Toxicity and uptake behavior was evaluated in two biological systems: *HeLa* cells and *Leishmania* parasites, obtaining very good results in *HeLa* cell viability and in uptake behavior for *Leishmania Donovani* promastigotes when compared with the reference peptide. Doxorubicin was coupled to the best candidates and preliminary studies were carried out, which were encouraging as peptides with the conjugated drug showed more activity against the parasites than the drug itself or the reference peptide. These results confirm that the synthesized CPPs are suitable carriers for drug delivery.

6. General Conclusions

MRI contrast agent: one new cyclobutane diamine-based ligand was complexed with Gd^{3+} and studied, **Gd(L3)**, showing suitable features as contrast agent for MRI, due to its high stability and relaxivity. Results were rationalized and compared with two other related ligands synthesized previously in our research group and also with some clinically approved agents, indicating that the studied complex could be better in some aspects than them. The **Gd(L3)** could be a potential candidate for medical applications. Further experiments are being carried out to describe the physicochemical parameters that rule the relaxivity of the compound.

7. Experimental Methodologies

7. Experimental Methodologies

7.1 ^{1}H NMR and ^{13}C NMR spectroscopy

^{1}H NMR and ^{13}C NMR spectra were recorded at *Servei de Ressonància Magnètica Nuclear* from the Universitat Autònoma de Barcelona (UAB) in Bellaterra, Spain and at *Centre de Biophysique Moléculaire* (CBM) from *CNRS* in Orléans, France.

The spectrometers used in the UAB were:

- AC 250 Bruker for ^{1}H at 250 MHz and ^{13}C at 62.5 MHz.
- AVANCE 360 Bruker for ^{1}H at 360 MHz and ^{13}C at 90 MHz.
- ARX 400 Bruker for ^{1}H at 400 MHz and ^{13}C at 100 MHz.
- AV 600 Bruker for ^{1}H at 600 MHz and ^{13}C at 150 MHz.

The spectrometers used in the CBM was:

- Avance III HD 600 equipped with a BBFP probe for ^{1}H at 600 MHz and ^{13}C at 150 MHz.

Chemical shifts of signals are given in ppm, using as reference the following values:

- $CDCl_3$: δ 7.28 for ^{1}H and 77.16 for ^{13}C.
- CD_3OD: δ 3.31 for ^{1}H and 49.00 for ^{13}C.
- DMSO-d_6: δ 7.28 for ^{1}H and 77.16 for ^{13}C.
- D_2O: δ 4.79 for ^{1}H.

The abbreviations used to describe multiplicity of signals are: s (singlet), d (doublet), dd (doublet of doublets), t (triplet), dt (doublet of triplets), q (quartet), p (pentet), broad s (broad singlet), broad d (broad doublet), m (multiplet, denotes complex pattern).

NMR signals were assigned with the help of DEPT, NOESY, ROESY, COSY, TOCSY, HMBC and HSQC experiments, when convenient.

7.2 Infrared spectroscopy (IR)

IR spectra were recorded on a Sapphire-ATR spectrophotometer, being the signal an average of 16 scans. Peaks are reported in cm^{-1}.

7.3 High resolution mass spectrometry (HRMS)

HRMS spectra were recorded at *Servei d'Ànalisi Química* from the Universitat Autónoma de Barcelona in a Bruker Squire 3000 micoTOFTQ spectrometer using ESI-MS (QTOF).

7.4 Chromatography

7.4.1 Flash chromatography

Column chromatography was performed with Scharlau™ silica gel for flash chromatography (mean pore: 60 Å; particle size: 0.04-0.06 mm, 230-400 mesh (ASTM)), using nitrogen as driving gas.

Some reactions were monitored by thin-layer chromatography (TLC) using ALUGRAM™ SIL/UV_{254} pre-coated aluminum sheets. Layer of 0.20 mm of thickness covered with silica gel 60 with fluorescent indicator UV_{254}. Different methods were used to visualize the spots:

- Irradiation under a LED UV-light (UV_{254}) using a VILBER LOURMAT™ lamp, VL-4LC model.
- Staining thin-layers under acidic solutions of vanillin in ethanol and heating them with a heat gun.
- Staining thin-layers under solutions of $KMnO_4$ in water and heating them with a heat gun.

7.4.2 High-performance liquid chromatography (HPLC)

All the HPLC related techniques were carried out at *Unitat de Química Combinatoria* (UQC) in the Parc Científic of Barcelona (PCB).

7.4.2.1 Reverse-phase HPLC coupled to a mass spectrometer (RP-HPLC-MS)

RP-HPLC-MS spectra for monitoring coupling reactions on solid phase synthesis and for determining the final mass of the peptides were carried out in two system equipment consisting on a Watters Alliace 2695 with a multichannel UV-vis detector Photodiode Array Detector 2996 and a Water 2795 Separation Module coupled to a mass spectrometer Micromass ZQ with an electrospray (ES) probe.

The column used was the XBridge® BEH 130 C18 (4.6 x 100 mm, 3.5 μm). Used flux was 1.6 mL/min and the eluents were A: H_2O/HCOOH (99.9:0.10, v/v) and B: CH_3CN/HCOOH (99.93:0.07, v/v). Spectra were recorded at λ = 220 nm.

7.4.2.2 Semipreparative reverse-phase HPLC coupled to a mass spectrometer (Semiprep-RP-HPLC-MS)

Semiprep-RP-HPLC-MS was used to purify the peptides. This equipment was built using a binary gradient Waters 2545 integrated with two pumps, a high pressure mixer, a Waters Alliance 2767 sample manager module and an automatic fraction collector coupled to a dual UV-vis λ Absorbance Detector 2487 and a mass spectrometer Micromass ZQ.

The column used was the XBridge® BEH C18 (19 x 100 mm, 5 μm). Used flow was 16 mL/min for 10 minutes and the eluents were A: CH_3CN/HCOOH (99.93:0.07, v/v) and B: H_2O/HCOOH (99.9:0.10, v/v). The gradient used for each peptide is described in section 7.16.

7.4.2.3 Reverse-phase HPLC (RP-HPLC)

RP-HPLC was used to measure the purity of the compounds and to make a repurification in some cases where the Semiprep-RP-HPLC-MS was not enough. This equipment consisted in a Watter Alliace 2695 with a multichannel UV-vis detector Photodiode Array Detector 2998.

The column used was the XBridge® BEH 130 C18 (4.6 x 100 mm, 3.5 μm). The used flow was 1 mL/min and the eluents were A: H_2O/TFA (99.9:0.10, v/v) and B: CH_3CN/TFA (99.9:0.10, v/v). Spectra were recorded at λ = 220 nm. The gradient used for each peptides is described in section 7.16.

7.5 Qualitative tests performed in SPS

7.5.1 Kaiser Qualitative Test (ninhydrin test)

The test is used to determine the presence/absence of primary amines. It was performed by adding a small portion of peptide-resin (0.5-2.0 mg) in a glass tube to which 6 drops of reagent A and 2 drops of reagent B were added. After 3 minutes inside an oven at 110 ºC the color of the mixture is checked. A yellow coloration indicates the absence of primary amines in the resin (negative test) and a blue-green coloration indicates the presence of primary amines in the resin (positive test).

Reagent A: A hot solution of phenol (40 g) in absolute ethanol (10 mL) was prepared. On the other hand, 2 mL of a solution of potassium cyanide (55 mg) in water (100 mL) was added over 100 mL of pyridine. 4 g of Amberlite® resin MB-3 were added to both mixtures and stirred for 45 minutes. After that, the solutions were filtered and mixed.

Reagent B: A solution of ninhydrin (2.5 g) in ethanol (50 mL) was prepared. This solution was put in a closed vessel avoiding exposition to light.

7.5.1 Chloranil Test

The test is used to determine the presence/absence of secondary amines. The reagent used was a saturated solution of 2,3,5,6-tetrachloro-1,4-benzoquinone (chloranil, 0.75 mg) in toluene (25 mL). It was prepared by adding a small portion of peptide-resin (0.5-2.0 mg) in a glass tube to which 6 drops of chloranil solution and 20 drops of acetone were added. The mixture is stirred and left for 5 minutes at room temperature. A yellowish coloration of the resin indicates the absence of secondary amines in the resin (negative test) and a blue or green coloration indicates the presence of secondary amines in the resin (positive test).

7.6 Toxicity and uptake experiments in *HeLa* cells

HeLa cell line was used to evaluate both the toxicity and uptake behavior of the synthesized peptides. Toxicity was checked using MTT assay, the uptake was evaluated by flow cytometry and the intracellular localization was observed by confocal microscopy.

7.6.1 *HeLa* cells culture

The preservation and proliferation *in vitro* of the *HeLa* cell line was performed in falcon tubes with a 25 cm^2 area two times a week in subcultures with a 1:10 proportion using MEM culture media supplemented with 10% of Fetal Bovine Serum (FBS) and 1% of 200 mM L-Glutamine (Biowest). Trypsin was used to release the cells, which are generally attached to the surface of the falcon, during the subculture procedure. Once the process was finished, supplemented MEM was added to neutralize the effect of the trypsin.

During the preservation, proliferation and development of the experiments the cells where in incubators with a humid atmosphere, a 5% of CO_2 and at 37 ºC of temperature.

7.6.2 *HeLa* cells cytotoxicity assays (MTT assays)

The MTT (3-(4,5-dimethylthiazol-2-yl)-2,5-diphenyltetrazolium bromide) assay described by Mosmann in 1983,[238] was used to analyze the cell viability, and proportionally the peptides toxicity. This colorimetric assay allows to rate the cell proliferation using the metabolic activity of living cells. MTT (yellow color) is reduced by the mitochondrial enzymes to formazan, an insoluble purple crystal which absorbance can be read with a spectrophotometer after its solubilization by an organic solvent. The higher the absorbance value, the higher the enzymatic activity, and therefore the more number of living cells are present.

To carry out this assay, *HeLa* cells were seeded in plates with 24 wells (Nunc) with a concentration of $6 \cdot 10^4$ cells/mL (around 30.000 cells per well). After 24 h of incubation, the culture medium was removed and the cells were incubated for an extra 24 h in the presence of different peptides concentrations (10, 25 and 50 μM) diluted with non-supplemented MEM. After this time, the culture media was removed and the wells were washed with 500 μL of HBSS (Biowest) before adding 500 μL of MTT (Sigma-Aldrich) with a 0.1 mg/mL concentration. After 3 h (minimum) of incubation at 37 ºC in darkness, the MTT was removed and the plates were kept safely until the reading with the spectrophotometer. By that time, the formazan crystals were dissolved using DMSO and the absorbance was recorded at 540 nm in an X3 Multilabel Plate Reader coupled to a PerkinElmer 2030 Manager control software.

At least 3 independent experiments with TAT as reference peptide and non-treated cells as control were performed. Moreover, the experiments were replicated 4 times for each peptide and concentration. The normalization of the results was performed considering the average of the absorbance value of the control population as 100% of cellular proliferation (Equation 8).

$$\%\, Cell\ viability = \frac{Average\ Absorbance\ of\ treated\ cells}{Average\ Absorbance\ of\ non-treated\ cells} 100$$

Equation 8

7.6.3 Uptake in *HeLa* cells

The ability of the peptides to cross the cell membrane in *HeLa* cells was performed using flow cytometry. This technique allows to detect and quantify the fluorescence in a cellular suspension through the individual analysis of the emitted signal of each cell. In order to have fluorescence from the peptides, CF was coupled to them. This fluorophore is excited with a laser and then it emitts light in the green region of the spectra. If the peptide is able to cross the cell membrane, the CF is excited inside the cell and then it emits a signal, which is detected by a sensor in the equipment.

To carry out this assay, *HeLa* cells were seeded in plates of 35 mm (Nunc) in a concentration of $1 \cdot 10^5$ cells/mL (around 200.000 cells per well). After 24 h of incubation, the culture medium was removed and the cells were incubated for an extra 2 h in the presence of different peptides concentrations (10 and 25 μM) diluted with non-supplemented MEM. After that time, the culture medium was removed and washed twice with HBSS and the cells were trypsinized with 0.5 mL of 0.25% trypsin-EDTA for 5 min at 37 ºC. After that, 2 mL of supplemented MEM were added to neutralize the trypsin effect, and the cellular suspension was transferred to a conical tube to be centrifuged for 5 min at 300 G. The supernatant was discarded and the cells were resuspended in 2 mL of HBSS and centrifuged in the same conditions. After removing the supernatant, the pellet was resuspended in 200 μL of PBS at pH = 6. The fluorescence was recorded in a BD FACSCanto cytometer coupled to FACSDiva v 7.0 software.

Additionally, a second fluorescence measurement was performed. In this case the emission came exclusively by living cells. In order to do that, to the cellular suspension in PBS was added 1 μL of propidium iodide (IP). This agent can intercalate the DNA and emit light in the red range. Furthermore it is not a permeable agent, so it can only enter the nucleus if the cell membrane is not present, which results in the death of the cell. With this experiment we could discard false positives from cells that were dead or damaged.

At least 3 independent experiments with TAT as positive reference peptide, CF as negative reference, and non-treated cells as control were performed. Moreover, the experiments were carried out twice for each peptide and concentration. The normalization of the results was performed considering the average of the emitted fluorescence value of the cells treated with CF = 1 (Equation 9).

$$Peptide\ internalization = \frac{Average\ Fluorescence\ from\ treated\ living\ cells}{Average\ Fluorescence\ from\ CF\ treated\ living\ cells}$$

Equation 9

7.6.4 *Hela* Cells intracellular localization

In order to check the peptide distribution inside the cells, confocal microscopy was used. This technique allows visualizing the emitted signal from a fluorophore in a specific focal level avoiding the signal coming from upper and lower levels. Furthermore, the observed different focal levels can be superposed after the readings to generate a tridimensional image of the cell. This methodology is widely used to determine the localization of molecules inside the cell or in subcellular organelles.

To carry out this assay, *HeLa* cells were seeded in plates of 35 mm (Nunc) in a concentration of $1 \cdot 10^5$ cells/mL (around 200.000 cells per well). After 24 h of incubation, the culture medium was removed and the cells were incubated for an extra 2 h in the presence of peptides at 25 μM concentration diluted with non-supplemented MEM. After that time, the culture medium was removed and washed three times with HBSS, and CellMask™ Deep Red Plasma Membrane Stain (Molecular Probes) and Hoechst vital, 33342, Trihydrichloride Trihydrate (Molecular Probes) were added. CellMask™ stain the cell membrane in red, while Hoechst stain the DNA in blue, generating reference points. After 10 min of incubation at 37 ºC, the culture medium was removed and cells were washed twice with HBSS. Then PBS with pH = 6 was added and the cells were incubated for 20 min. The measurements were performed using an Olympus Fluoview FV1000 confocal laser scanning microscopy using uplsapo 60x / 1.35 immersion oil and Olympus Fluoview as control software. Orthogonal projections were generated using Imaris.

7.7 Toxicity and uptake experiments in *Leishmania* parasites

Leishamnia Donovani promastigotes and *Leishmania Pifanoi* amastigotes cell line were used to evaluate both the toxicity and uptake behavior of the synthesized peptides. Toxicity was checked using MTT assay, the uptake was evaluated by flow cytometry and the intracellular localization was observed by confocal microscopy.

7.7.1 *Leishmania* parasites culture

The parasites were cultured at 26 ºC in Roswell Park Memorial Institute (RPMI) media supplemented with 10% of non-activated fetal bovine serum, 2 mM L-glutamine, unicilin at 20 U/mL and Gentamicine at 48 mg/mL.

7.7.2 *Leishmania* parasites viability assays

The peptide toxicity in *Leishmania* parasites was evaluated with the MTT assay explained in section 7.6.2, but with some differences. Parasites were incubated in plates with 96 wells at a final concentration of 2 x 10^6 cells/mL in 1% glucose-Hank's media. Parasites were incubated at different peptide concentrations for 4 h at 26 ºC. After this time, the MTT was added and the parasites were left for 1 h. Then, DMSO was added to dissolve the formazan crystals. The plates measure was performed in a Bio-Rad 640 plate at 595 nm. Equation 8 was used to calculate the parasites viability.

7.7.3 Uptake in *Leishmania* parasites

The peptide uptake in *Leishmania* parasites was evaluated by flow cytometry explained in section 7.6.3, but with some differences. Parasites were incubated in plates with 96 wells at a final concentration of 2 x 10^6 cells/mL in 1% glucose-Hank's media. Parasites were incubated at different peptide concentrations for 2 or 4 h at 4 ºC or 26 ºC. After this time, 200 μL of suspension were centrifuged at 1200 rpm for 5 min at 4 ºC and washed twice with HBBS-Glc. They were resuspended with HBBS-Glc with a final concentration of 1 x 10^6 cells/mL and propidium iodide was added to eliminate false positives from dead parasites. Samples were analyzed in a FC500 flow cytometer.

At least two experiments where carried out. The normalization of the results was performed considering the average of the emitted fluorescence value of the cells treated with TAT = 100 (Equation 10).

$$Peptide\ internalization = \frac{Average\ Fluorescence\ treated\ living\ cells}{Average\ Fluorescence\ TAT\ treated\ living\ cells} 100$$

Equation 10

7.7.4 *Leishmania* parasites intracellular localization

The peptide localization inside *Leishmania* parasites was evaluated by confocal microscopy explained in section 7.6.4, but with some differences. Parasites were incubated in plates with 96 wells at a final concentration of 2 x 10^6 cells/mL in 1% glucose-Hank's media. Parasites were incubated at different peptide concentrations for 2 or 4 h at 4 ºC or 26 ºC, in presence of Rhodamine-Dextran as stain of flow phase endocytosis (red) and DAPI as nucleic acid stain present in the nucleus and in the kinetoplast.

7.8 Sample preparation for metal complexes

The ligand concentrations were determined by calculating the difference between two observed equilibrium points in the pH-potentiometric titration of the ligands alone. Also, calculating the difference between equilibrium points of the ligand alone and the ligands with the metals (1 eq) gave the same results. Gd and Eu (for luminescence lifetimes) concentrations were determined by titrating the metal solutions with standardized Na_2H_2EDTA in urotropine buffer (pH 5.6-5.8) in the presence of xylenol orange as an indicator

Moreover, at the end of the ^{17}O NMR experiments, Gd complex concentrations was rechecked by bulk magnetic susceptibility (BMS) shift.

The BMS shifts of ^{1}H NMR signals for an inert reference caused by the addition of paramagnetic compounds were studied in order to determine the concentration of paramagnetic metal in solution (Equation 11).[239]

$$\Delta_x = \frac{4\pi cs}{T}\left(\frac{\mu_{eff}}{2.84}\right)10^3$$

Equation 11

Where the concentration of paramagnetic solute is given by *c* in mol l^{-1}, *s* is dependent on the shape of the sample and its position in the magnetic field. *S* = 1/3, -1/6 and 0 for cylinder parallel to the main field, a cylinder perpendicular to the main field, and a sphere, respectively. *T* is the absolute temperature and μ_{eff} is the effective magnetic moment for a particular lanthanide ion. D_x is measured for a reference compound, in this case, *tert*-butanol.

7.9 Potentiometric studies

Carbonate-free 0.1 KOH and 0.1 M HCl were prepared from Fisher chemical concentrates. Potentiometric titrations were performed in 0.1 M aqueous KCl under nitrogen atmosphere, and the temperature was controlled to 25±0.1 ºC. The pH was measured in each titration with a combined micro pH glass electrode (Metrohm 6.0224.100) filled with 3 M KCl, and the titrant addition was automated by use of a 785 DMP titrino system (Metrohm). The electrode was calibrated in hydrogen ion concentration by titration of HCl with KOH in 0.1 M electrolyte solution.[240] The electrode stander potential (E^0) and the slope factor (*f*) were determined before titrations using the Glee software.[241] Continuous potentiometric titration with 0.1 M HCL and KOH were conducted in aqueous solution containing 5 mL of 2 mM in 0.1 M KCl **L3**, with 2 min waiting between successive points. The titrations of the metal complexes were performed with the same ligand solutions containing 1 equivalent of metal cation, also with 2 min waiting time between two points.

Protonation constants of ligands, stability constants of complexes and protonation constants of complex are described and defined in Equation 4-6.

$$K_i = \frac{[H_iL]}{[H_{i-1}L][H^+]}$$

Equation 4

$$K_{ML} = \frac{[ML]}{[M][L]}$$

Equation 5

$$K_{MH_iL} = \frac{[M(H_iL)]}{[M(H_{i-1}L)][H^+]}$$

Equation 6

Where [M], [L] and [ML] are the equilibrium of free metal ion, deprotonated ligand, and deprotonated complex, respectively. Experimental data were refined using the computer software Hyperquad 2008.[222] Species distribution plots were calculated taking the experimental constants using the computed software HySS.[225] The ionic product of water used at 25 ºC was $pK_w = 13.77$, while the ionic strength was kept at 0.1 M.[242] Fixed values were used for pK_w, ligand acidity constants and total concentration of metal, ligand and acid.

7.10 Lifetime measurements

Europium luminescence lifetimes were recorded on an Agilent Cary Eclipse fluorescence spectrophotometer by recording the decay of the emission intensity at 616 nm, following an excitation at 268 for **L3**. Direct excitation of the metal at 396 nm gave similar results.

Concentrations of **EuL3** of 0.20 mM in 0.1 M Hepes buffer in H_2O and D_2O solutions at pH, pD = 7. Same experiments but adding 10 and 50 equivalents of phosphate and carbonate were performed. The settings are shown in Table 8. Different decay curves were collected for each sample and the lifetimes were analyzed as monoexponential decays and fitted using the spectrophotometer software.

Table 8. Experimental conditions to record luminescence decay lifetimes.

Parameter	**Value**
Gate time	0.05 ms
Delay time	0.1 ms
Flash count	1
Total decay time (H_2O)	5 ms
Total decay time (D_2O)	15 ms
Cycles	100
PMT detector	800 mV

Equation 7 was used to calculate the number of water molecules coordinated to the europium chelates.

$$q = A\left(\frac{1}{\tau_{H_2O}} - \frac{1}{\tau_{D_2O}} - B\right)$$

Equation 7

Where τ_{H2O} and τ_{D2O} are the luminescence decay lifetimes recorded in water and deuterium oxide, respectively. These empirical constant take values of A = 1.2 and B = 0.25[243] or A = 1.11 and B = 0.31,[244] both for Eu^{3+}.

7.11 Relaxometric measurements

^{1}H NMRD profiles were recorded on a Stelar SMARTracer Fast Field Cycling relaxometer (0.01-10 mHz) and a Bruker WP80 NMR electromagnet adapted to variable field measurements (20-80 MHz) and controlled by a VTC91 temperature control unit and maintained by a gas flow at CBM in Orléans.

The concentration of the solution used were 2.13 mM **GdL3** + 5% **L3** at pH = 7. The temperature was determined by previous calibration with a Pt resistance temperature probe.

The least-squares fit of the ^{1}H NMRD data was performed using Visualiseur/Optimiseur in MATLAB 8.3 software.[245,246]

7.11.1 Equations used for the analysis of the NMRD profiles

The observed longitudinal proton relaxation rate, $1/T_{1,obs}$ is the sum of the diamagnetic and paramagnetic contributions as shown in Equation 1.

$$\frac{1}{T_{1,obs}} = \frac{1}{T_{1,d}} + \frac{1}{T_{1,p}} = \frac{1}{T_{1,d}} + r_1[Gd]$$

Equation 1

Where r_1 is the proton relaxivity, and the concentration of the paramagnetic species (in this case Gd) is usually given in millimol per liter (mmol L^{-1}) for dilute systems.[173] The relaxivity can be separated into two terms; the inner and outer sphere, as showed in Equation 2.

$$r_1 = r_1^{IS} + r_1^{OS}$$

Equation 2

The inner sphere term is obtained in Equation 3, where q is the number of water molecules in the inner sphere, τ_m is the lifetime of a water molecule in the inner sphere (equal to $1/k_{ex}$, k_{ex} is the water exchange rate) and T_{1m} is the longitudinal relaxation rate of inner sphere protons.[204,247,248,249,250]

$$r_1^{IS} = \frac{1}{1000}\frac{q}{55.5}\frac{1}{T_{1m} + \tau_m}$$

Equation 3

The longitudinal relaxation rate of inner sphere protons, T_{1m} is expressed by Equation 12, where r_{GdH} is the electron spin-proton distance, γ_I is the nuclear gyromagnetic ratio, ω_I is the proton resonance frequency and ω_S is the Larmor frequency of the Gd^{3+} electron spin.

$$\frac{1}{T_{1m}} = \frac{2}{15}\left(\frac{\mu_0}{4\pi}\right)^2 \frac{\hbar^2\gamma_I^2\gamma_S^2}{r_{GdH}^6} S(S+1)[3J(\omega_I;\tau_{d1}) + 7J(\omega_S;\tau_{d2})]$$

Equation 11

$$\frac{1}{\tau_{di}} = \frac{1}{\tau_m} + \frac{1}{\tau_{RH}} + \frac{1}{T_{ie}} \qquad i = 1,2$$

Equation 12

Where τ_{RH} is the overall rotational correlation time, and its assumed to have a simple exponential temperature dependence as showed in Equation 13. E_R is the corresponding activation energy.

$$\tau_{RH} = \tau_{RH}^{298} exp\left\{\frac{E_R}{R}\left(\frac{1}{T} - \frac{1}{298.15}\right)\right\}$$

Equation 13

The longitudinal and transverse electronic relaxation rates, $1/T_{1e}$ and $1/T_{2e}$ are expressed in Equation 14 and 15, where τ_v is the electronic correlation time for the modulation of the zero-field-splitting interaction, *Ev* is the corresponding activation enerdy and Δ_2 is the mean square zero-field-splitting energy. We assumed a single exponential dependence of t_v versus temperature (Equation 14).[251,252]

$$\left(\frac{1}{T_{1e}}\right)^{ZFS} = \frac{1}{25}\Delta^2\tau_v\{4S(S+1)-3\}\left(\frac{1}{1+\omega_S^2\tau_v^2}+\frac{4}{1+4\omega_S^2\tau_v^2}\right)$$

Equation 14

$$\left(\frac{1}{T_{2e}}\right)^{ZFS} = \Delta^2\tau_v\left(\frac{5.26}{1+0.372\omega_S^2\tau_v^2}+\frac{7.18}{1+1.24\omega_S^2\tau_v^2}\right)$$

Equation 15

$$\tau_v = \tau_v^{298} exp\left\{\frac{E_v}{R}\left(\frac{1}{T}-\frac{1}{298.15}\right)\right\}$$

Equation 16

The outer sphere contribution can be described by Equation 17, where J^{OS} is associated spectral density function (Equation 18) and j = 1, 2.[253,254]

$$r_1^{OS} = \frac{32N_A\pi}{405}\left(\frac{\mu_0}{4\pi}\right)^2\frac{\hbar^2\gamma_I^2\gamma_S^2}{a_{GdH}D_{GdH}}S(S+1)[3J^{OS}(\omega_I,T_{1e})+7J^{OS}(\omega_S,T_{2e})]$$

Equation 17

$$J^{OS}(\omega, T_{je}) = \left[\frac{1 + \frac{1}{4}\left(i\omega\tau_{GdH} + \frac{\tau_{GdH}}{T_{je}}\right)^{1/2}}{1 + \left(i\omega\tau_{GdH} + \frac{\tau_{GdH}}{T_{je}}\right)^{1/2} + \frac{4}{9}\left(i\omega\tau_{GdH} + \frac{\tau_{GdH}}{T_{je}}\right) + \frac{1}{9}\left(i\omega\tau_{GdH} + \frac{\tau_{GdH}}{T_{je}}\right)^{3/2}} \right]$$

Equation 18

The diffusion coefficient for the diffusion of a water proton from the bulk of solvent to the Gd^{3+}, D_{GdH} is assumed to follow an exponential function versus the inverse of the temperature (Equation 19), where E_{GdH} is the activation energy and D_{GdH}^{298} is the diffusion coefficient at 298.15 K.

$$D_{GdH} = D_{GdH}^{298} exp\left\{\frac{E_{GdH}}{R}\left(\frac{1}{298.15} - \frac{1}{T}\right)\right\}$$

Equation 19

7.12 Temperature-dependent ^{17}O NMR spectroscopy

^{17}O NMR spectroscopy was recorded at Centre de Biophysique Moléculaire (CBM) from CNRS in Orléans, France. The spectrometer used was Bruker Avance 400 (9.36 T, 54.2 MHz). The longitudinal and transverse ^{17}O relaxation rates ($1/T_1$, $1/T_2$) and the chemical shifts were measured in aqueous solutions of 6.45 mM **GdL3** in a temperature range of 275-348 K. The temperature was calculated according to previous calibration with ethylene glycol and methanol.[255] An acidified water solution ($HClO_4$, pH = 3.3) was used as external reference for the Gd complex. Longitudinal relaxation time (T_1) was obtained by the inversion-recovery method. The transverse relaxation time (T_2) was obtained by the Carr-Purcell-Meiboom-Gill spin-echo technique.[256] The samples were sealed in glass spheres fitter into 10 mm NMR tubes to avoid susceptibility corrections of chemical shifts.[257] To improve sensitivity, ^{17}O-enriched water (10% $H_2{}^{17}O$) was added to the solutions to reach around 1% enrichment. The ^{17}O NMR data have been treated according to the Solomon-Bloembergen-Morgan theory of paramagnetic relaxation (equations in the next page). The least-squares fit of the ^{17}O NMR data was performed using Visualiseour/Optimiseur in MATLAB 8.3 software.[245,246]

7.12.1 Equations used for the analysis of the ^{17}O NMR

From the measured ^{17}O NMR relaxation rates and angular frequencies of the paramagnetic solution, $1/T_1$, $1/T_2$, ω, and from the reference, $1/T_{2A}$, $1/T_{1A}$ and ω_A, it is possible to calculate the reduced relaxation rates and chemical shifts, $1/T_{2r}$, $1/T_{1r}$ and $\Delta\omega_r$ (Equations 18-20), where $1/T_{2m}$, $1/T_{1m}$ are the relaxation rate of the bound water and $\Delta\omega_m$ is the chemical shift difference between bound and bulk water, τ_m is the mean residence time or the inverse of water exchange rate k_{ex} and P_m is the mole fraction of the bound water.[205,257]

$$\frac{1}{T_{1r}} = \frac{1}{P_m}\left[\frac{1}{T_1} - \frac{1}{T_{1A}}\right] = \frac{1}{T_{1m}+\tau_m} + \frac{1}{T_{1OS}}$$

Equation 18

$$\frac{1}{T_{2r}} = \frac{1}{P_m}\left[\frac{1}{T_2} - \frac{1}{T_{2A}}\right] = \frac{1}{\tau_m}\frac{T_{2m}^{-2} + \tau_m^{-1}T_{2m}^{-1} + \Delta\omega_m^2}{(\tau_m^{-1} + T_{2m}^{-1})^2 + \Delta\omega_m^2} + \frac{1}{T_{2OS}}$$

Equation 19

$$\Delta\omega_r = \frac{1}{P_m}(\omega - \omega_A) = \frac{\Delta\omega_m}{(1 + \tau_m T_{2m}^{-1})^2 + \tau_m^2\Delta\omega_m^2} + \Delta\omega_{OS}$$

Equation 20

The outer sphere contributions to the ^{17}O relaxation rates $1/T_{1OS}$ and $1/T_{2OS}$ can be neglected according to previous studies. Then Equations 18-20, can be further simplified into Equations 21 and 22.

$$\frac{1}{T_{1r}} = \frac{1}{T_{1m} + \tau_m}$$

Equation 21

The exchange rate is assumed to be described by the Eyring equation (Equation 22), where $\Delta S^{\ddagger}$ and $\Delta H^{\ddagger}$ are the entropy and enthalpy of activation for the water exchange, and k_{ex}^{298} is the exchange rate at 298.15 K. R is the usual gas constant whereas, h and k_B are the Plank and Boltzmann constant, respectively.

$$\frac{1}{\tau_m} = K_{ex} = \frac{k_B T}{h} \exp\left\{\frac{\Delta S^{\ddagger}}{R} - \frac{\Delta H^{\ddagger}}{RT}\right\} = \frac{k_{ex}^{298} T}{298.15} exp\left\{\frac{\Delta H^{\ddagger}}{R}\left(\frac{1}{298.15} - \frac{1}{T}\right)\right\}$$

Equation 22

In the transverse relaxation, the scalar contribution, $1/T_{2sc}$ is the most important. In Equation 23, $1/\tau_{s1}$ is the sum of exchange rate and the electron spin relaxation rate constant.

$$\frac{1}{T_{2m}} \cong \frac{1}{T_{2sc}} = \frac{S(S+1)}{3}\left(\frac{A}{\hbar}\right)^2 \left(\tau_{s1} + \frac{\tau_{s2}}{1 + \omega_S^2 \tau_{s2}^2}\right)$$

Equation 23

$$\frac{1}{T_{s1}} = \frac{1}{\tau_m} + \frac{1}{T_{1e}}$$

Equation 24

The ^{17}O longitudinal relaxation rates in Gd^{3+} solutions are the sum of the contributions of the dipole-dipole (*dd*) and quadrupolar (*q*) mechanism as expressed by Equations 25-27 for non-extreme narrowing conditions, where γ_s is the electron and g_I is the nuclear gyromagnetic radio ($\gamma_s = 1.76 \cdot 10^{11}$ rad s^{-1} T^{-1}, $\gamma_I = -3.626 \cdot 10^{7}$ rad s^{-1} T^{-1}), r_{GdO} is the effective distance between the electron charge and the ^{17}O nucleus, l is the nuclear spin (5/2 for ^{17}O), χ is the quadrupolar coupling constant and η is and asymmetry parameter.

$$\frac{1}{T_{1m}} = \frac{1}{T_{1dd}} + \frac{1}{T_{1q}}$$

Equation 25

$$\frac{1}{T_{1dd}} = \frac{2}{15}\left(\frac{\mu_0}{4\pi}\right)\frac{\hbar\gamma_I^2\gamma_S^2}{r_{GdO}^6}S(S+1)[3J(\omega_I,\tau_{d1}) + 7J(\omega_S,\tau_{d2})]$$

Equation 26

$$\frac{1}{T_{1q}} = \frac{3\pi^2}{10}\frac{2I+3}{I^2(2I-1)}\chi^2(1+\eta^2/3)[0.2J_1(\omega_I) + 0.8J_2(\omega_I)]$$

Equation 27

In equation 20 the chemical shift of the bound water molecule, Dw_m, depends on the hyperfine interaction between Gd^{3+} electron spin and the ^{17}O nucleus and is directly proportional to the scalar constant $A/\hbar$, as expressed in Equation 28.

$$\Delta\varpi_m = \frac{g_L\mu_B S(S+1)B}{3k_BT}\frac{A}{\hbar}$$

Equation 28

The isotropic Landé g factor is equal to 2.0 for Gd^{3+}, B represents the magnetic field, and k_B is the Boltzmann constant.

7.13 Details on other techniques

- **Optical rotation, $[\alpha]_D$**, were measured using a RUDOLPH RESEARCH ANALYTICAL Autopol I Automatic polarimeter using a 1 dm path. Some measurements were done using a PERKIN ELMER Polarimeter 341 using a 1 dm path in *IQAC-CSIC* in Barcelona.
- **Melting points** were determined on a hot stage using a Kofler apparatus, REICHERT AUSTRIA model.
- **Micro-distillations** were carried out in a BÜCHI™ distiller, Glass Oven B-585 model.
- **Lyophilization** of samples were done using a TELSTAR™ lyophilizer, LyoQuest-85 model.
- **Hydrogenations** were carried out in an autoclave hydrogenation T-reactor Swagelok™, with a pressure capacity from 1 to 20 atm (kg/cm^2).
- **Photochemical reactions** were performed in a Pyrex T-shaped photochemical reactor from TRALLERO&SCHLEE™. Irradiation is emitted from a mercury lamp of 400 W medium pressure ELECTRO DH™. Refrigeration of the inside of the reactor and an external bath are kept at -30 ºC by a C40P TERMO SCIENTIFIC™ refrigerator, Phoenix II model.
- **Reagents** were used directly from commercial sources and solvents were anhydrized when needed using standard procedures.[258]
- **Deuterated solvents** were used directly from commercial source Eurisotop™.

7.14 Synthetic procedures

For a better and easier understanding for the reader there are some clarifications about the nomenclature, molecule numeration and the atom numeration that need to be made:

- The numeration of the molecules has been stablished in order of appearance during the text.
- IUPAC nomenclature has been used to name the majority of the compounds.
- For the most complex molecules a nomenclature based on the composition of the compound has been used in order to avoid large names.
- The numeration of each atom is arbitrary and does not correspond to the number that defines its name in IUPAC nomenclature.

3-Oxabicyclo[3.2.0]heptane-2,4-dione, 50

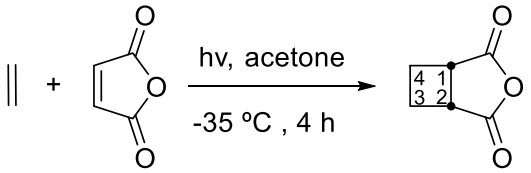

1 **2** **50**

A solution of maleic anhydride (2.52 g, 25.7 mmol) in acetone (500 mL) was cooled to -30 ºC. The solution was saturated with ethylene and the system was irradiated through a Pyrex filter for 4 h. The solvent was removed under vacuum to afford pure compound **50** as a pale solid (3.25 g, 25.7 mmol, quantitative yield).

Spectroscopic data for compound 50:

^{1}H NMR (250 MHz, $CDCl_3$): δ 2.35 (m, 2H, H_{4S}, H_{3R}), 2.74 (m, 2H, H_{4R}, H_{3S}), 3.52 (m, 2H, H_1, H_2)

Spectroscopic data are consistent with those reported in reference:

Tufariello, J. J.; Milowsky, A.S.; Al-Nuri, M.; Goldstein, S. *Tetrahedron Lett.* **1987**, *28*, 267-270.

Dimethyl (1*R*,2*S*)-cyclobutane-1,2-dicarboxylate, 51

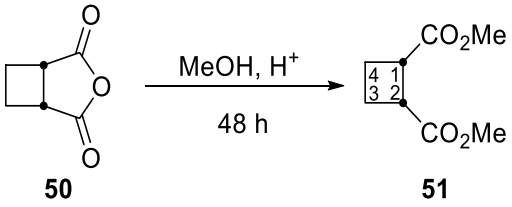

50 **51**

A solution of **50** (3.20 g, 25.4 mmol) and concentrated H_2SO_4 (3.00 mL) in methanol (60 mL) were stirred at room temperature for 48 h. Dichloromethane (120 mL) was added to the organic phase and it was successively washed with water (2 x 50 mL) and brine (1 x 50 mL).

The organic layer was then dried over $MgSO_4$, filtered off and concentrated in order to provide the corresponding crude as yellowish oil. For a better purification, it was distilled under vacuum at 150 ºC (3.50 g, 20.3 mmol, 80% yield).

Spectroscopic data for compound 51:

^{1}H NMR (250 MHz, $CDCl_3$): δ 2.10 (m, 2H, H_{3S}, H_{4R}), 2.29 (m., 2H, H_{3R}, H_{4S}), 3.31 (m, 2H, H_1, H_2), 3.58 (s, 6H, Me)

Spectroscopic data are consistent with those reported in reference:

Sabbioni, G.; Jones, J.B. *J. Org. Chem.* **1987**, *52*, 4565-4570.

(1*S*,2*R*)-2-(Methoxycarbonyl)cyclobutanecarboxylic acid, 47

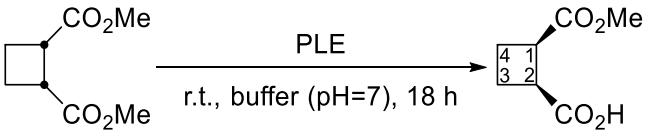

51 **47**

Diester **51** (1.00 g 5.81 mmol) was dissolved in 60 mL of a buffer solution previously prepared from 0.1 M KH_2PO_4 at pH = 7. Pig liver esterase (PLE) (28 mg) was added to the solution and the mixture was stirred at room temperature for 18 h. The reaction was maintained at pH 7 by adding a solution of 1 M NaOH. Then, 10% HCl was added to reach pH 2. The acidic solution was extracted with ethyl acetate (4x100 mL), using brine to break the generated interface.

The organic extracts were dried over magnesium sulfate and the solvent was evaporated under vacuum to dryness obtaining the half-ester **47** as a colorless oil (0.870 g, 5.50 mmol, 95% yield, 97% ee).

Spectroscopic data for compound 47:

^{1}H NMR (250 MHz, $CDCl_3$): δ 2.23 (m, 2H, H_{3S}, H_{4R}), 2.41 (m, 2H, H_{3R}, H_{4S}), 3.43 (m, 2H, H_1, H_2), 3.69 (s, 3H, Me)

Spectroscopic data are consistent with those reported in reference:

Sabbioni, G.; Jones, J.B. *J. Org. Chem.* **1987**, *52*, 4565-4570.

Methyl (1*R*,2*S*)-2-(benzyloxycarbonylamino) cyclobutane-1-carboxylate, 43

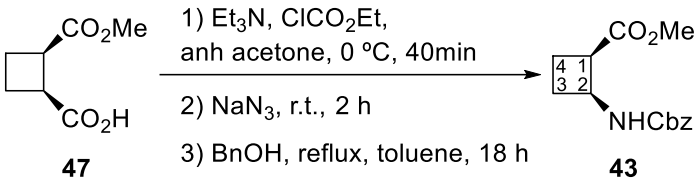

47 **43**

To an ice-cooled solution of half-ester **47** (1.70 g, 10.7 mmol) in anhydrous acetone (40 mL), triethylamine (2.00 mL, 14.3 mmol, 1.3 eq) and ethyl chloroformate (1.3 mL, 14.2 mmol, 1.3 eq) were subsequently added. The mixture was stirred at 0 ºC for 40 minutes. Then, sodium azide (1.80 g, 26.9 mmol, 2.5 eq) in 10 mL of water was added and the resultant solution was stirred at room temperature for 1.5 h. The reaction mixture was extracted with dichloromethane (4x50 mL), and the organic extracts were dried over magnesium sulfate. Solvents were removed under reduced pressure to give the corresponding acyl azide as a yellow oil, which was used in the next step without further purification. WARNING: Acyl azides are instable reagents: it is very important not to heat the final product while it is being dried, and the solvent must not be removed until full dryness. To the obtained acyl zaide, benzyl alcohol (2.90 mL, 27.9 mmol, 2.6 eq) in toluene (50 mL) was added and then the mixture was heated to reflux for 18 h. Toluene was removed under reduced pressure and then the excess of benzyl alcohol was evaporated under vacuum at 150 ºC. The residue was chromatrographed on silica gel (3:1 hexane-EtOAc) obtaining carbamate **43** as an oil (1.76 g, 6.68 mmol, 62% yield).

Spectroscopic data for compound 43:

^{1}H NMR (250 MHz, $CDCl_3$): δ 2.01 (m, 2H, H_{3R}, H_{4S}), 2.19-2.47 (m, 2H, H_{3S}, H_{4R}), 3.42 (m, 1H, H_1), 3.70 (s, 3H, Me), 4.58 (m, 1H, H_1), 5.13 (s, 2H, CH_2-Ph), 5.69 (br. s., 1H, NH) 7.39 (m, 5H, H_{Ar}).

Spectroscopic data are consistent with those reported in reference:

Martín-Vilà.; Muray, E; P. Aguado, G.; Alvarez-Larena, A.; Branchadell, V.; Minguillón, C.; Giralt, E.; and Ortuño, R.M. *Tetrahedron Asymmetry* **2000**, *11*, 3569-3584.

Methyl (1*R*,2*S*)-2-(*tert*-butoxycarbonylamino) cyclobutane-1-carboxylate, 53

METHOD A:

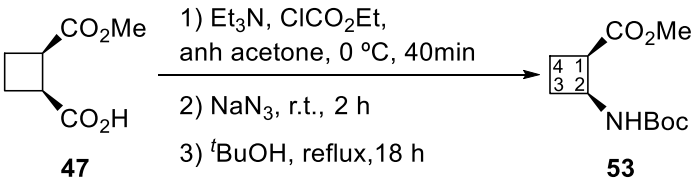

47 **53**

To an ice-cooled solution of half-ester **47** (1.70 g, 10.7 mmol) in anhydrous acetone (40 mL), triethylamine (2.00 mL, 14.3 mmol, 1.3 eq) and ethyl chloroformate (1.3 mL, 14.2 mmol, 1.3 eq) were subsequently added. The mixture was stirred at 0 ºC for 40 minutes. Then, sodium azide (1.80 g, 26.9 mmol, 2.5 eq) in 10 mL of water was added and the resultant solution was stirred at room temperature for 1.5 h. The reaction mixture was extracted with dichloromethane (4x50 mL), and the organic extracts were dried over magnesium sulfate. Solvents were removed under reduced pressure to give the corresponding acyl azide as a yellow oil, which was used in the next step without further purification. WARNING: Acyl azides are instable reagents: it is very important not to heat the final product while it is being dried, and the solvent must not be removed until full dryness. To the obtained acyl azide, *tert*-butanol was added as the solvent and the reagent. The mixture was heated to reflux and stirred for 18 h. Then, the solvent was evaporated under vacuum, and the residue was purified by column chromatography (9:1 hexane-EtOAc as eluent) affording the diprotected amino acid **53** as a white solid (1.10 g, 4.36 mmol, 41% yield).

METHOD B:

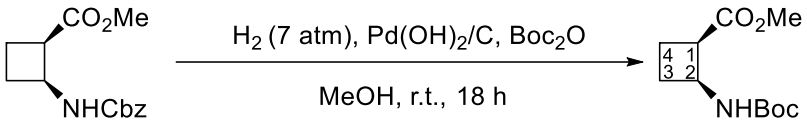

43 **53**

Diprotected amino acid **43** (1.36 g, 5.16 mmol) in MeOH (15 mL) was hydrogenated under 7 atmospheres of pressure in the presence of and Boc_2O (1.39 mL, 6.75 mmol, 1.3 eq) 30% $Pd(OH)_2/C$ (0.41 g, 30% weight) at r.t. overnight. The reaction mixture was filtered through Celite® and solvent was removed under vacuum and the residue was purified by column chromatography (3:1 hexane-EtOAc) affording the desired carbamate **53** as a white solid (0.970 g, 4.24 mmol, 82% yield).

Spectroscopic data for compound 53:

^{1}H NMR (250 MHz, $CDCl_3$): δ 1.41 (s, 9H, *t*-Bu), 1.85-2.03 (m, 2H, H_{3R}, H_{4S}), 2.10-2.42 (m, 2H, H_{3S}, H_{4R}), 3.38 (m, 1H, H_1), 3.70 (s, 3H, Me), 4.45 (m, 1H, H_2), 5.36 (br. s., 1H, N*H*).

Spectroscopic data are consistent with those reported in reference:

Izquierdo, S.; Rúa, F. Sbai, A.; Parella, T.; Álvarez-Larena, A.; Branchadell, V.; and Ortuño, R.M. *J. Org. Chem.* ***2005***, *70*, 7963-7971.

(1*R*,2*S*)-2-(*tert*-Butoxycarbonylamino)cyclobutane-1-carboxylic acid, 54

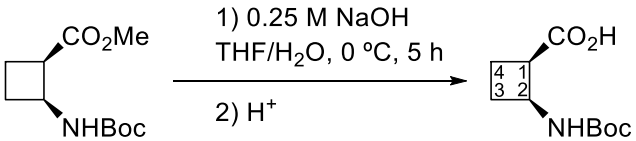

53 **54**

To an ice-cooled solution of amino acid **53** (0.900 g, 3.93 mmol) in a 1:10 mixture of THF-water (44 mL), 0.25 M NaOH aqueous solution (40 mL, 10.0 mmol, 2.5 eq) was added and the resultant mixture was stirred for 5 h. (Reaction progress was monitored by TLC). The reaction mixture was washed with dichloromethane (20 mL), and 5% HCl aqueous solution was added to the aqueous phase to reach pH 2.

The acid solution was extracted with ethyl acetate (4x50 mL) and dried over magnesium sulfate. Solvent was removed at reduced pressure to afford acid **54** as a white crystalline solid (0.750 g, 3.53 mmol, 89% yield) without need of further purification.

Spectroscopic data for compound 54:

^{1}H NMR (250 MHz, $CDCl_3$): δ 1.45 (s, 9H, *t*-Bu), 1.70-2.35 (m, 4H, H_{3R}, H_{3S}, H_{4R} H_{4S}), 3.36 (m, 1H, H_1), 4.35 (m, 1H, H_2), 5.57 (br. s., 1H, N*H*).

Spectroscopic data are consistent with those reported in reference:

Izquierdo, S.; Rúa, F. Sbai, A.; Parella, T.; Álvarez-Larena, A.; Branchadell, V.; and Ortuño, R.M. *J. Org. Chem.* ***2005***, *70*, 7963-7971.

tert-Butyl (1*S*,2*R*)-2-(carbamoyl)cyclobutylcarbamate, 55

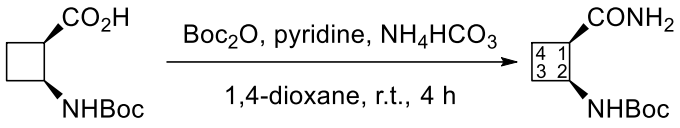

54 **55**

A mixture containing carboxylic acid **54** (0.30 g, 1.39 mmol), Boc_2O (0.43 g, 2.19 mmol, 1.5 eq), ammonium bicarbonate (0.330 g, 4.17 mmol, 3.0 eq) and pyridine (0.29 mL, 3.52 mmol, 2.5 eq) in 1,4-dioxane (5 mL) was stirred at room temperature for 5 h. Water (10 mL) was added, then the mixture was evaporated to dryness under reduced pressure. Ethyl acetate was added and the solution was washed with water (4x20 mL) then dried over magnesium sulfate and evaporated under vacuum to give the desired product **55** as a white powder without further purification (0.280 g, 1.30 mmol, 94% yield).

Spectroscopic data for compound 55:

^{1}H NMR (250 MHz, $CDCl_3$): δ 1.44 (s, 9H, *t*-Bu), 1.84-2.44 (m, 4H, H_{3R}, H_{3S}, H_{4R} H_{4S}), 3.33 (m, 1H, H_1), 4.44 (m, 1H, H_2), 5.36 (br. s.; 2H, NH_{amide}), 5.58 (br. s., 1H, N*H*).

Spectroscopic data are consistent with those reported in reference:

Fernandes, C.; Pereira, E.; Faure, S.; Aitken. D.J., *J. Org. Chem.* **2009**, *74*, 3217-3220.

(1*S*,2*S*)-2-(*tert*-Butoxycarbonylamino)cyclobutane-1-carboxylic acid, 56

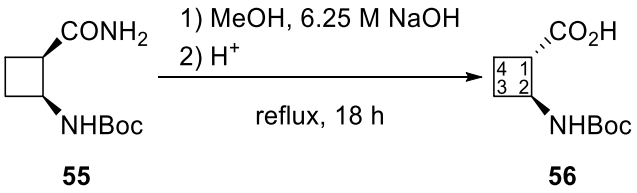

55 **56**

A solution of **55** (0.280 g, 1.31 mmol) in MeOH (15 mL) was treated with 6.25 M aqueous NaOH solution (7 mL) and the mixture was heated to reflux overnight. The methanol was then removed by careful evaporation under reduced pressure and the residual aqueous phase was washed with ethyl acetate (3x20 mL). The aqueous phase was then cooled to 0 ºC and then 5% HCl was added slowly until pH=2. The aqueous phase was then extracted with ethyl acetate (4x50 mL) and the combined organic extracts were dried over magnesium sulfate and concentrated under vacuum. The free acid **56** was obtained in a 5:1 ratio (*trans*:*cis*) as a white powder (0.180 g, 0.836 mmol, 64% yield). The *cis* and *trans* monomers were separated once methylated.

Spectroscopic data for compound 56:

^{1}H NMR (250 MHz, $CDCl_3$): δ 1.48 (s, 9H, *t*-Bu), 1.75-2.32 (m, 4H, H_{3R}, H_{3S}, H_{4R} H_{4S}), 3.13 (m, 1H, H_1), 4.14 (m, 1H, H_2), 5.08 (br. s., 1H, N*H*).

Spectroscopic data are consistent with those reported in reference:

Fernandes, C.; Pereira, E.; Faure, S.; Aitken. D.J., *J. Org. Chem.* **2009**, *74*, 3217-3220.

Methyl (1*S*,2*S*)-2-(*tert*-butoxycarbonylamino) cyclobutane-1-carboxylate, 57

METHOD A:

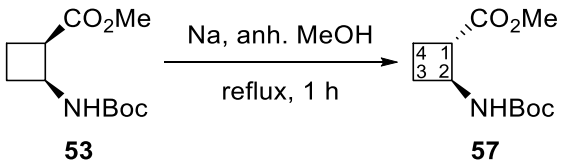

53 **57**

To ester **53** (0.30 g, 1.31 mmol), anhydrous MeOH (60 mL) was added under N_2 atmosphere. Then, sodium (0.14 g, 6.09 mmol, 4.6 eq) was added and the mixture was stirred until its total dissolution. The mixture was heated to reflux and stirred for 1 h. Then, the solution was cooled at 0 ºC with water and ice and 1 M HCl (8.6 mL, 8.6 mmol, 6.6 eq) was added. The solvent was then evaporated under vacuum. The remaining water was extracted with ethyl acetate (4x50 mL) and the organic extracts were dried over magnesium sulphate and the solvent was evaporated under vacuum. Flash chromatography (3:1 Hexane-EtOAc) provided *trans* amino acid **57** as a white solid (0.20 g, 0.872 mmol, 66% yield) as well as some starting amino acid **53** (0.03 g, 0.131 mmol 10% yield).

METHOD B:

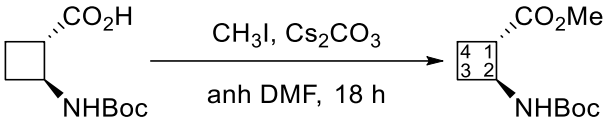

56 **57**

A *trans*:*cis* mixture of acid monomer with 5:1 ratio (0.100 g, 0.460 mmol) was methylated by the action of an excess of methyl iodide (0.1 mL,1.61 mmol, 3.5 eq) in the presence of Cs_2CO_3 (0.17 g, 0.55 mmol, 1.2 eq) in a DMF solution (10 mL) overnight. Flash chromatography (3:1 hexane-EtOAc) provided pure orthogonally protected amino acid **57** as a white solid (0.076 g, 0.332 mmol, 71% yield). Ester **53** was also obtained from the purification process (0.0100 g, 0.0436 mmol, 9% yield).

Spectroscopic data for compound 57:

^{1}H NMR (250 MHz, $CDCl_3$): δ 1.45 (s, 9H, *t*-Bu), 1.95 (m, 3H, H_{3R}, H_{4R} H_{4S}) 2.28 (m, 1H, H_{3S}), 3.00 (m, 1H, H_1), 3.70 (s, 3H, Me), 4.23 (m, 1H, H_2), 4.78 (br., s, 1H, N*H*).

Spectroscopic data are consistent with those reported in reference:

Fernandes, C.; Gauzy, C.; Yang, Y.; Roy, O.; Pereira, E.; Faure, S.; Aitken. D.J. *Synthesis* **2007**, *14*, 2222-2232.

(1*S*,2*S*)-2-(Methoxycarbonyl)cyclobutan-amine hydrochloride, 58

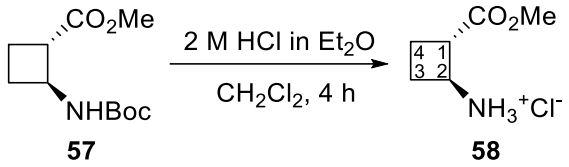

57 **58**

To a solution of **57** (0.100 g, 0. 44 mmols) in CH_2Cl_2 (8 mL), was added 2 M HCl in Et_2O (3.7 mL, 74 mmols, 16.8 eq). After 4 h (the reaction was monitored by TLC), a white precipitate was observed. The solvent was removed under vacuum obtaining **58** (0.072 g, quantitative yield) as a white solid, without further purification.

Spectroscopic data for compound 58:

^{1}H NMR (250 MHz, $CDCl_3$): (250 MHz, $CDCl_3$): δ 2.02 (m, 1H, H_{3S}), 2.14-2.64 (m, 4H, H_{3R}, H_{4R} H_{4S}, H_1), 3.73 (s, 3H, Me), 4.16 (m, 1H, H_2), 8.56 (br. s., 3H, NH_3^+).

Spectroscopic data are consistent with those reported in reference:

Torres, E.; Gorrea, E.; Da Silva, E.; Nolis, P.; Branchadell, V.; Ortuño, R.M. *Org. Lett.* **2009**, *11*, 2301-2304.

Methyl (1*S*,2*S*)-2-(benzyloxycarbonylamino)cyclobutane-1-carboxylate, 44

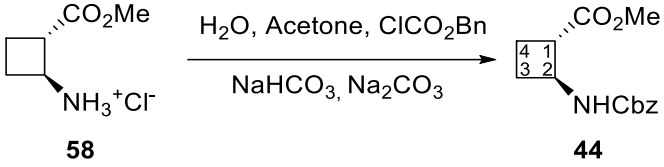

58 **44**

To an ice cooled solution of **58** (0.210 g, 1.27 mmol) in water (40 mL) and acetone (5.5 mL), $NaHCO_3$ (0.220 g, 2.62 mmol, 2 eq) and Na_2CO_3 (0.420 g, 3.96 mmol, 3 eq) were added. The mixture was stirred until the complete dissolution of the carbonates. Then, benzyl chloroformate (0.3 mL, 2.10 mmol, 1.6 eq) was added and the mixture was stirred at 0 ºC (reaction was monitored by TLC). After 5 h, the reaction was extracted with EtOAc (4x50 mL) and the organic layer was dried over magnesium sulfate.

The solvent was removed under vacuum, and the excess of benzyl chloroformate was lyophilized. The residue was purified by column chromatography (2:1 hexane-EtOAc) to afford monomer **44** (0.240 g, 70% yield) as a white solid.

Spectroscopic data for compound 44:

^{1}H NMR (250 MHz, $CDCl_3$): δ 1.84–2.07 (m, 3H, H_{3R}, H_{4R} H_{4S}) 2.19-2.41 (m, 1H, H_{3S}), 3.08 (m, 1H, H_1), 3.72 (s, 3H, Me), 4.32 (m, 1H, H_2), 5.00-5.19 (m,, 3H, N*H*$_2$, CH_2-Ph), 7.37 (s. 5H, Arom).

Spectroscopic data are consistent with those reported in reference:

Illa, O., Olivares, J.A., Nolis, P., Ortuño, R.M. *Tetrahedron* **2017**, *73*(44), 6286-6295.

(1*S*,2*S*)-2-(Benzyloxycarbonylamino)cyclobutane-1-carboxylic acid, 59

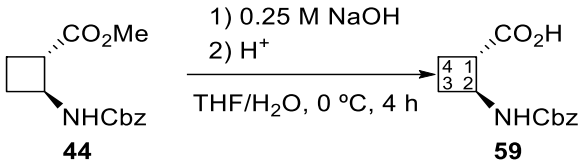

To an ice-cooled solution of amino acid **44** (0.170 g, 0.650 mmol) in a 1:10 mixture of THF-water (22 mL), 0.25 M NaOH aqueous solution (6.50 mL, 1.63 mmol, 2.5 eq) was added and the resultant mixture was stirred for 4 h. (Reaction progress was monitored by TLC). The reaction mixture was washed with dichloromethane (15 mL), and 5% HCl aqueous solution was added to the aqueous phase to reach pH 2. The acid solution was extracted with ethyl acetate (4x30 mL) and dried over magnesium sulfate. Solvent was removed at reduced pressure to afford acid **59** as a white crystalline solid (0.75 g, 89% yield) without need of further purification.

Spectroscopic data for compound 59:

^{1}H NMR (250 MHz, $CDCl_3$): *δ* 1.82-2.30 (m, 4H, H_3, H_4), 3.14 (m, 1H, H_1), 4.23 (m, 1H, H_2), 5.15 (s, 2H, C*H*$_2$Ph), (broad s, 1H, NH), 7.37 (m, 5H, H_{Ar}).

Spectroscopic data are consistent with those reported in reference:

Illa, O., Olivares, J.A., Nolis, P., Ortuño, R.M. *Tetrahedron*, **2017**, *73*(44), 6286-6295.

(1*R*,2*S*)-2-(Benzyloxycarbonylamino)cyclobutane-1-carboxylic acid, 52

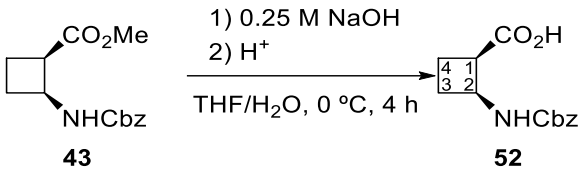

43 **52**

To an ice-cooled solution of amino acid **43** (0.300 g, 1.20 mmol) in a 1:10 mixture of THF-water (25 mL), 0.25 M NaOH aqueous solution (12.0 mL, 3.00 mmol, 2.5 eq) was added and the resultant mixture was stirred for 4 h. (Reaction progress was monitored by TLC). The reaction mixture was washed with dichloromethane (30 mL), and 5% HCl aqueous solution was added to the aqueous phase to reach pH 2. The acid solution was extracted with ethyl acetate (4x40 mL) and dried over magnesium sulfate. Solvent was removed at reduced pressure to afford acid **52** as a white crystalline solid (0.250 g, 88% yield) without need of further purification.

Spectroscopic data for compound 52:

^{1}H NMR (250 MHz, $CDCl_3$): δ 2.07-2.15 (m, 2H, H_{3R}, H_{4R}) 2.32-2.41 (m, 2H, H_{3S}, H_{4s}), 3.08 (m, 1H, H_1), 3.42 (m, 1H, H_1), 4.56 (m, 1H, H_2), 5.10 (s, 2H, CH_{2CBz}), 5.67 (s.a.,1H, NH), 7.41 (s. 5H, H_{Ar}).

Spectroscopic data are consistent with those reported in reference:

Martín-Vilà.; Muray, E; P. Aguado, G.; Alvarez-Larena, A.; Branchadell, V.; Minguillón, C.; Giralt, E.; and Ortuño, R.M. *Tetrahedron Asymmetry* **2000**, *11*, 3569-3584.

Dipeptide 33

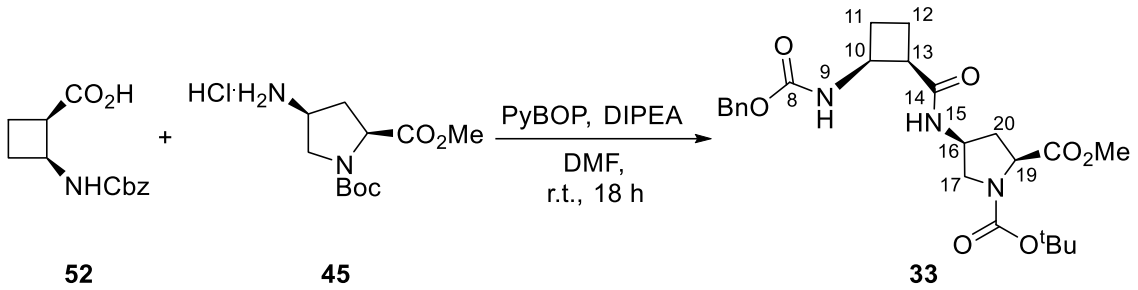

Carboxylic acid cyclobutane **52** (0.340 g, 1.36 mmol) and PyBOP (0.780 g, 1.50 mmol, 1.1 eq) were dissolved in anhydrous DMF (5 mL) in a round bottom flask under nitrogen. Then, freshly distilled DIPEA (0.940 mL, 5.40 mmol, 4 eq) was added. The solution was stirred at room temperature for 10 minutes. In another round bottom flask under nitrogen, *cis*-γ-amino- N^{α}-Boc-L-proline methyl ester hydrochloride **45** (0.420 g, 1.5 mmol, 1.1 eq) was dissolved in the minimum amount of anhydrous DMF. This solution was transferred to the flask containing the carboxylic acid derivative and was stirred at room temperature for 18 h. After this, EtOAc was added and the resulting solution was washed with a saturated aqueous solution of $NaHCO_3$ (x4). The organic layer was dried over $MgSO_4$ and the solvent was evaporated under vacuum. The reaction crude was purified by column chromatography over silica gel (EtOAc-Hexane 3:2) obtaining dipeptide **33** as a white solid (0.547 g, 1.15 mmol, 85% yield).

Spectroscopic data for compound 33:

[α]$_D$ = -60.8 (c=1.0 in MeOH).

M.p: 46-50 ºC (from EtOAc).

IR (ATR): 3396, 2950, 1741, 1696, 1654, 1533 cm^{-1}.

^{1}H NMR (600 MHz, DMSO-d_6): major conformation: δ 1.39 (s, 9H, *t*-Bu), 1.63 (m, 1H, H_{20}), 1.77 (m, 1H, H_{12}), 1.95 (m, 1H, $H_{12'}$), 2.17 (m, 2H, H_{11}), 2.44 (m, 1H, $H_{20'}$), 3.09 (m, 1H, H_{17}), 3.64 (s, 3H, Me), 3.67 (m, 1H, $H_{17'}$), 4.18 (m, 1H, H_{19}), 4.27 (m, 2H, H_{16}, H_{10}), 4.95 (m, 2H, H_7), 7.32 (m, 6H, NH_9, H_{Ar}), 7.80 (m, 1H, NH_{15}). minor conformation: δ all signals coincide with the major conformer except for: 1.58 (s, 9H, *t*-Bu), 3.62 (s, 3H, Me).

^{13}C NMR (150 MHz, DMSO-d_6): major conformer δ 17.9 (C_{12}), 27.6 (C_{11}), 28.3 (C_{Boc}), 36.3 (C_{20}), 45.7 (C_{13}), 47.1 (C_{16}), 47.3 (C_{10}), 50.4 (C_{17}), 52.4 (Me), 58.0 (C_{19}), 65.6 (C_7), 79.7 ($C_{q\ tBu}$), 128.0 (C_{Ar}), 128.2 (C_{Ar}), 128.8 (C_{Ar}), 137.5 (C_{Ar}), 153.0 (CO_{Boc}), 155.6 (C_8), 171.9 (C_{14}), 173.5 (C_{21}); minor confomer: δ 17.9 (C_{12}), 27.4 (C_{11}), 28.5 (C_{Boc}), 35.3 (C_{20}), 45.6 (C_{13}), 47.3 (C_{10}), 47.8 (C_{16}), 50.9 (C_{17}), 52.4 (Me), 58.0 (C_{19}), 65.6 (C_7), 79.7 ($C_{q\ Boc}$), 127.9 (C_{Ar}), 128.2 (C_{Ar}), 128.8 (C_{Ar}), 137.5 (C_{Ar}), 153.8 (CO_{Boc}), 155.6 (C_8), 171.8 (C_{14}), 173.1 (C_{21}).

HRMS: calculated for $C_{24}H_{33}N_3O_7Na$ (M+Na): 498.2211, Found: 498.2221.

Dipeptide 35

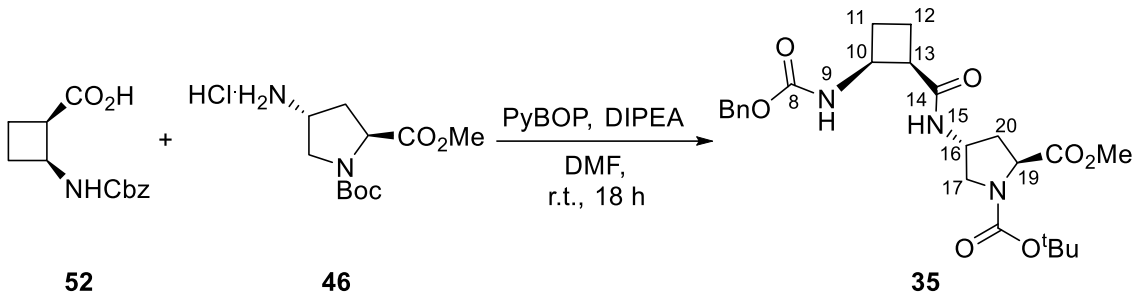

Carboxylic acid cyclobutane **52** (0.200 g, 0.80 mmol) and PyBOP (0.460 g, 0.88 mmol, 1.1 eq) were dissolved in anhydrous DMF (4 mL) in a round bottom flask under nitrogen. Then, freshly distilled DIPEA (0.560 mL, 3.20 mmol, 4 eq) was added.

The solution was stirred at room temperature for 10 minutes. In another round bottom flask under nitrogen, *trans*-γ-amino- N^{α}-Boc-L-proline methyl ester hydrochloride **46** (0.250 g, 0.88 mmol, 1.1 eq) was dissolved in the minimum amount of anhydrous DMF. This solution was transferred to the flask containing the carboxylic acid derivative and was stirred at room temperature for 18 h. After this, EtOAc was added and the resulting solution was washed with a saturated aqueous solution of $NaHCO_3$ (x4). The organic layer was dried over $MgSO_4$ and the solvent was evaporated under vacuum. The reaction crude was purified by column chromatography over silica gel (EtOAc-Hexane 3:2) obtaining dipeptide **35** as a white solid (0.320 g, 0.67 mmol, 84% yield).

Spectroscopic data for compound 35:

[α]D = -67.4 (c=1.0 in MeOH).

M.p: 49-50 ºC (from MeOH).

IR (ATR): 3304, 1745, 1693, 1650, 1534 cm^{-1}.

^{1}H NMR (600 MHz, DMSO-d_6): major conformation: δ 1.35 (s, 9H, *t*-Bu), 1.79 (m, 1H, H_{12}), 1.95 (m, 2H, $H_{12'}$), 2.06 (m, 2H, H_{20}), 2.18 (m, 1H, H_{11}), 3.03 (m, 1H, H_{17}), 3.18 (m, 1H, H_{13}), 3.59 (m, 1H, $H_{17'}$), 3.68 (s, 3H, Me), 4.27 (m, 2H, H_{19}, H_{10}), 4.99 (m, 2H, H_7), 7.35 (m, 6H, NH_9, H_{Ar}), 8.02 (d, *J*= 6 Hz, 1H, N*H*$_{15}$). minor conformation: δ all signals coincide with the major conformer except for: 2.97 (m, 1H, H_{17}), 3.65 (s, 3H, Me), 5.02 (m, 2H, H_7), 7.95 (d, *J*= 6 Hz, 1H, NH_{15}).

^{13}C NMR (150 MHz, DMSO-d_6): major conformer δ 17.9 (C_{12}), 27.5 (C_{11}), 28.5 (C_{Boc}), 36.0 (C_{20}), 45.6 (C_{13}), 47.0 (C_{16}), 47.2 (C_{10}), 52.0 (C_{17}), 52.4 (Me), 58.0 (C_{19}), 65.7 (C_7), 79.6 ($C_{q\ tBu}$), 127.9 (C_{Ar}), 128.2 (C_{Ar}), 128.8 (C_{Ar}), 137.5 (C_{Ar}), 153.2 (CO_{Boc}), 155.6 (C_8), 171.8 (C_{14}), 173.5 (C_{21}); minor confomer: δ 17.9 (C_{12}), 27.4 (C_{11}), 28.3 (C_{Boc}), 34.9 (C_{20}), 45.5 (C_{13}), 47.3 (C_{13}), 47.5 (C_{16}), 51.6 (C_{17}), 52.4 (Me), 57.7 (C_{19}), 65.6 (C_7), 79.7 ($C_{q\ Boc}$), 127.9 (C_{Ar}), 128.2 (C_{Ar}), 128.8 (C_{Ar}), 137.5 (C_{Ar}), 153.9 (CO_{Boc}), 155.6 (C_8), 171.8 (C_{14}), 173.0 (C_{21}).

HRMS: calculated for $C_{24}H_{33}N_3O_7Na$ (M+Na): 498.2211, Found: 498.2212.

Dipeptide 37

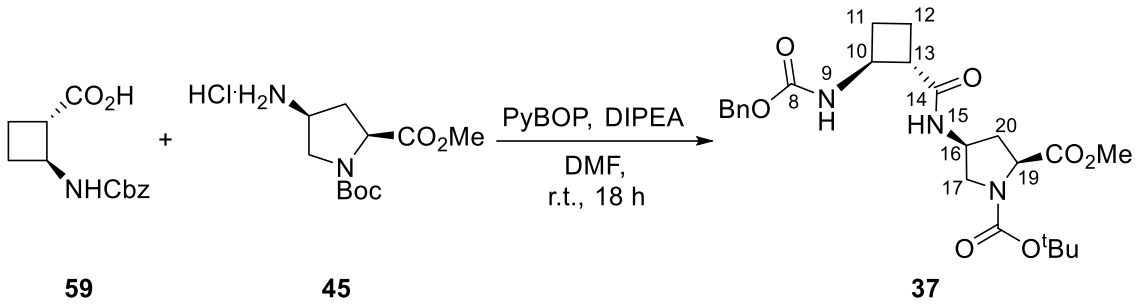

59 **45** **37**

Carboxylic acid cyclobutane **59** (0.250 g, 0.98 mmol) and PyBOP (0.560 g, 1.08 mmol, 1.1 eq) were dissolved in anhydrous DMF (5 mL) in a round bottom flask under nitrogen. Then, freshly distilled DIPEA (0.680 mL, 3.92 mmol, 4 eq) was added. The solution was stirred at room temperature for 10 minutes. In another round bottom flask under nitrogen, *cis*-γ-amino- N^{α}-Boc-L-proline methyl ester hydrochloride **45** (0.300 g, 1.08 mmol, 1.1 eq) was dissolved in the minimum amount of anhydrous DMF. This solution was transferred to the flask containing the carboxylic acid derivative and was stirred at room temperature for 18 h. After this, EtOAc was added and the resulting solution was washed with a saturated aqueous solution of $NaHCO_3$ (x4). The organic layer was dried over $MgSO_4$ and the solvent was evaporated under vacuum. The reaction crude was purified by column chromatography over silica gel (EtOAc-Hexane 3:2) obtaining dipeptide **37** as a white solid (0.357 g, 0.75 mmol, 77% yield).

Spectroscopic data for compound 37:

[α]$_D$ = +3 (c=1.0 in MeOH).

M.p: 65-68 ºC (from EtOAc).

IR (ATR): 3293, 2954, 1684 cm^{-1}.

^{1}H NMR (600 MHz, DMSO-d_6): major conformation: δ 1.33 (s, 9H, *t*-Bu), 1.64 (m, 1H, H_{12}), 1.77 (m, 2H, $H_{12'}$, H_{20}), 1.84 (m, 1H, H_{11}), 2.01 (m, 1H, $H_{11'}$), 2.45 (m, 1H, $H_{20'}$), 2.86 (m, 1H, H_{13}), 3.06 (m, 1H, H_{17}), 3.66 (s, 3H, Me), 3.67 (m, 1H, $H_{17'}$), 4.06 (m, 1H, H_{10}), 4.21 (m, 2H, H_{16}, H_{19}), 5.00 (s, 2H, H_7), 7.35 (m, 5H, H_{Ar}), 7.65 (d, *J*= 8.5 Hz, 1H, NH_9), 7.92 (m, 1H, NH_{15}).minor conformation: δ all signals coincide with the major conformer except for: δ 1.60 (s, 9H, *t*-Bu) and 3.64 (s, 3H, Me).

^{13}C NMR (150 MHz, DMSO-d_6): major conformer δ 18.2 (C_{12}), 26.2 (C_{11}), 28.3 (C_{Boc}), 35.7 (C_{20}), 47.4 (C_{16}), 47.8 (C_{13}), 48.2 (C_{10}), 50.8 (C_{17}), 52.4 (Me), 57.9 (C_{19}), 65.8 (C_7), 79.6 ($C_{q\ tBu}$), 128.3 (C_{Ar}), 128.4 (C_{Ar}), 128.8 (C_{Ar}), 137.5 (C_{Ar}), 153.1 (CO_{Boc}), 155.7 (C_8), 172.4 (C_{14}), 173.5 (C_{21}); minor confomer: δ 18.2 (C_{12}), 26.2 (C_{11}), 28.5 (C_{Boc}), 34.8 (C_{20}), 47.9 (C_{13}), 48.2 (C_{16}), 48.3 (C_{10}), 51.4 (C_{17}), 52.3 (Me), 57.5 (C_{19}), 65.8 (C_7), 79.8 ($C_{q\ Boc}$), 128.3 (C_{Ar}), 128.4 (C_{Ar}), 128.8 (C_{Ar}), 137.5 (C_{Ar}), 153.8 (CO_{Boc}), 155.6 (C_8), 172.4 (C_{14}), 173.1 (C_{21}).

HRMS: calculated for $C_{24}H_{33}N_3O_7Na$ (M+Na): 498.2211, Found: 498.2223.

Dipeptide 39

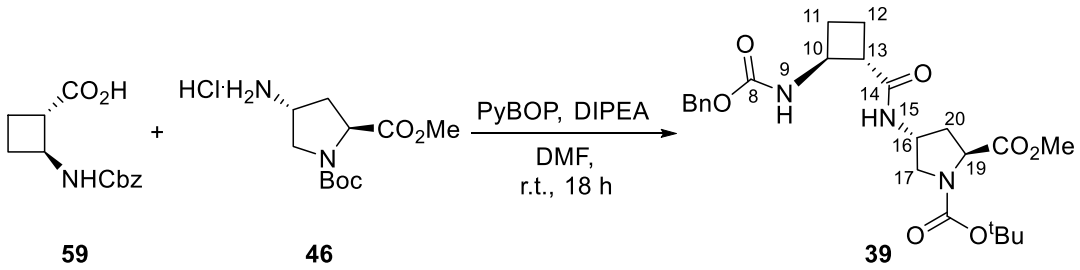

Carboxylic acid cyclobutane **59** (0.150 g, 0.60 mmol) and PyBOP (0.340 g, 0.66 mmol, 1.1 eq) were dissolved in anhydrous DMF (4 mL) in a round bottom flask under

nitrogen. Then, freshly distilled DIPEA (0.420 mL, 2.40 mmol, 4 eq) was added. The solution was stirred at room temperature for 10 minutes.

In another round bottom flask under nitrogen, *trans*-γ-amino- N^{α}-Boc-L-proline methyl ester hydrochloride **46** (0.190 g, 0.66 mmol, 1.1 eq) was dissolved in the minimum amount of anhydrous DMF. This solution was transferred to the flask containing the carboxylic acid derivative and was stirred at room temperature for 18 h. After this, EtOAc was added and the resulting solution was washed with a saturated aqueous solution of $NaHCO_3$ (x4). The organic layer was dried over $MgSO_4$ and the solvent was evaporated under vacuum. The reaction crude was purified by column chromatography over silica

Spectroscopic data for compound 39:

[α]D = -62 (c=0.8 in MeOH).

M.p: 50-54 ºC (from EtOAc).

IR (ATR): 3271, 1746, 1689, 1647 cm^{-1}.

^{1}H NMR (600 MHz, DMSO-*d*$_6$): major conformation: δ 1.33 (s, 9H, *t*-Bu), 1.71 (m, 2H, H_{12}, $H_{12'}$), 1.88 (m, 1H, H_{11}), 2.02 (m, 2H, $H_{11'}$, H_{20}), 2.16 (m, 1H, $H_{20'}$), 2.86 (ddd, *J*= *J'*= *J''*= 9.0 Hz, 1H, H_{13}), 3.17 (dd, *J*= 10.5 Hz, *J'*= 4.0 Hz, 1H, H_{17}), 3.52 (dd, *J*= 10.9 Hz, *J'*= 6.1 Hz, 1H, $H_{17'}$), 3.68 (s, 3H, Me) 4.04 (m, 1H, H_{10}), 4.24 (m, 1H, H_{16}), 4.30 (m, 1H, H_{19}), 5.00 (m, 2H, H_7), 7.36 (m, 5H, H_{Ar}), 7.65 (d, *J*= 8.5 Hz, 1H, NH_9), 8.10 (d, *J*= 6.4 Hz, 1H, NH_{15}). minor conformation: δ all signals coincide with the major conformer except for: δ 1.39 (s, 9H, *t*-Bu), 2.11 (m, 1H, $H_{20'}$), 2.86 (ddd, *J*= *J'*= *J''*= 9.0 Hz, 1H, H_{13}), 3.12 (dd, *J*= 10.6 Hz, *J'*= 5.2 Hz, 1H, H_{17}), 3.56 (dd, *J*= 10.7 Hz, *J'*= 6.5 Hz, 1H, $H_{17'}$), 3.65 (s, 3H, Me), 8.07 (d, *J*= 6.6 Hz, 1H, NH_{15}).

^{13}C NMR (150 MHz, DMSO-*d*$_6$): major conformer δ 17.8 (C_{12}), 25.9 (C_{11}), 28.3 (C_{Boc}), 36.2 (C_{20}), 47.6 (C_{16}), 48.2 (C_{13}), 48.6 (C_{10}), 51.6 (C_{17}), 52.4 (Me), 58.0 (C_{19}), 65.8 (C_7), 79.6 ($C_{q\ tBu}$), 128.3 (C_{Ar}), 128.4 (C_{Ar}), 128.8(C_{Ar}), 137.4 (C_{Ar}), 153.2 (CO_{Boc}), 155.6 (C_8), 172.3 (C_{14}), 173.5 (C_{21}); minor confomer: δ 18.1 (C_{12}), 26.0 (C_{11}), 28.5 (C_{Boc}), 35.0 (C_{20}), 48.1 (C_{16}), 48.1 (C_{13}), 48.4 (C_{10}), 51.9 (C_{17}), 52.4 (Me), 57.7 (C_{19}), 65.8 (C_7), 79.7 ($C_{q\ Boc}$), 128.3 (C_{Ar}), 128.4 (C_{Ar}), 128.8 (C_{Ar}), 137.4 (C_{Ar}), 153.9 (CO_{Boc}), 155.6 (C_8), 172.3 (C_{14}), 173.0 (C_{21}).

HRMS: calculated for $C_{24}H_{33}N_3O_7Na$ (M+Na): 498.2211, Found: 498.2221.

gel (EtOAc-Hexane 3:2) obtaining dipeptide **39** as a white solid (0.320 g, 0.40 mmol, 66% yield).

Dipeptide 60

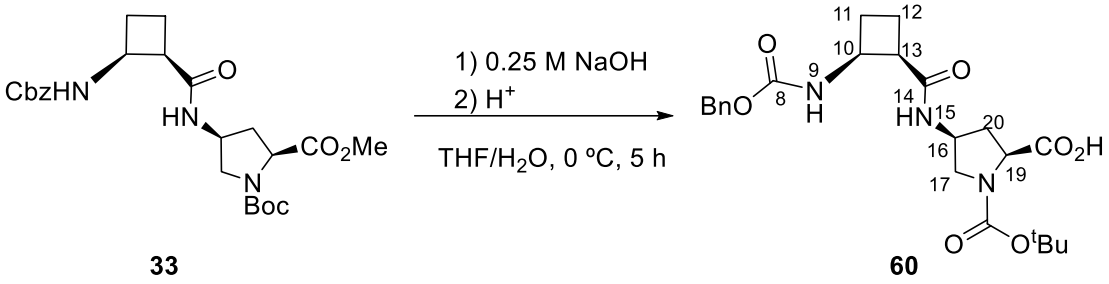

33 **60**

Dipeptide **33** (0.240 g, 0.50 mmol) was dissolved in a 1:10 mixture of THF-H_2O (15 mL). The round bottom flask was placed in an ice-water bath. Then a 0.25 M NaOH aqueous solution was added (5 mL, 1.26 mmol, 2.5 eq) and the reaction was monitored by TLC (generally after 5 h it was completed). After, the reaction mixture was acidified to pH 3 with a 5% HCl solution. Then the product was extracted with EtOAc (4 x 30 mL). The organic layers were combined, dried over $MgSO_4$ and the solvent was evaporated under vacuum obtaining acid dipeptide **60** (0.220 g, 0.48 mmol, 94% yield). The crude was used without any further purification.

Spectroscopic data for compound 60:

[α]D = -59.4 (c=1.00 in MeOH).

M.p: 80-82 ºC (from EtOAc).

IR (ATR): 3349, 3302, 2975, 1683, 1648 cm^{-1}

^{1}H NMR (250 MHz, $CDCl_3$): δ 1.46 (s, 9H, ^{t}Bu), 1.81-2.34 (m, 6H, H_{11}, H_{12}, H_{20}), 3.16 (s, 1 H, H_{13}), 3.28-3.78 (m, 2H, H_{17}), 4.37 (m, 2H, H_{16}, H_{19}), 5.10 (m, 2H, H_7, H_{10}), 5.93 (1H, *N*H), 6.82 (1H, *N*H), 7.33 (s, 5H, H_{Ar}).

HRMS: calculated for $C_{23}H_{31}N_3O_7Na$ (M+Na): 484.2054, Found: 484.2044.

Dipeptide 61

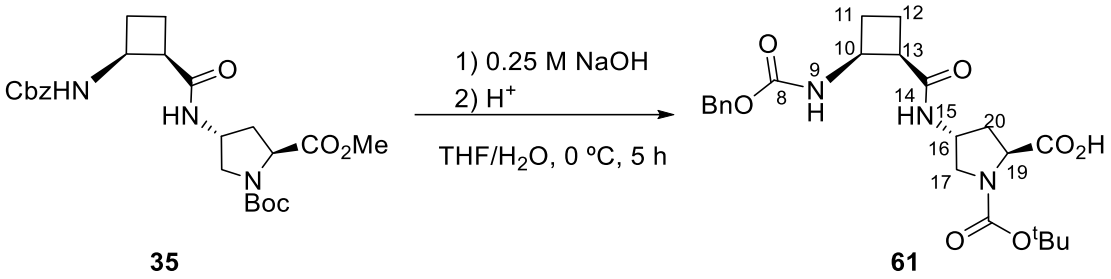

35 **61**

Dipeptide **35** (0.240 g, 0.50 mmol) was dissolved in a 1:10 mixture of THF-H_2O (15 mL). The round bottom flask was placed in an ice-water bath. Then a 0.25 M NaOH aqueous solution was added (5 mL, 1.26 mmol, 2.5 eq) and the reaction was monitored by TLC (generally after 5 h it was completed). After, the reaction mixture was acidified to pH 3 with a 5% HCl solution. Then the product was extracted with EtOAc (4 x 30 mL). The organic layers were combined, dried over $MgSO_4$ and the solvent was evaporated under vacuum obtaining acid dipeptide **61** (0.220 g, 0.48 mmol, 94% yield). The crude was used without any further purification.

Spectroscopic data for compound 61:

[α]$_D$ = -61.7 (c=1.05 in MeOH).

M.p: 82-84 ºC (from MeOH).

IR (ATR): 3328, 2948, 2360, 1685, 1540 cm^{-1}

^{1}H NMR (250 MHz, CD_3OD): (250 MHz, $CDCl_3$): δ 1.46 (s, 9H, ^{t}Bu), 1.81-2.34 (m, 6H, H_{11}, H_{12}, H_{20}), 3.09 (s, 1 H, H_{13}), 3.76 (m, 1H, H_{17}), 4.27 (m, 1H, $H_{17'}$), 4.33-4.49 (H_{19}, H_{10}), 5.07 (m, 2H, H_7), 7.34 (s, 5H, H_{Ar}).

^{13}C NMR (62.5 MHz, $CDCl_3$): δ 17.7 (CH_2), 27.7 (CH_3-^{t}Bu), 35.12 (CH_2), 36.0 (CH_2), 66.6 (C_7), 80.7 (C-^{t}Bu), 127.8 (C_{Ar}), 128.5 (C_{Ar}), 137.2 (C_{Ar}), 154.6 (CO), 155.0 (CO), 156.9 (CO), 173.7 (CO).

HRMS: calculated for $C_{23}H_{31}N_3O_7Na$ (M+Na): 484.2054, Found: 484.2058.

Dipeptide 62

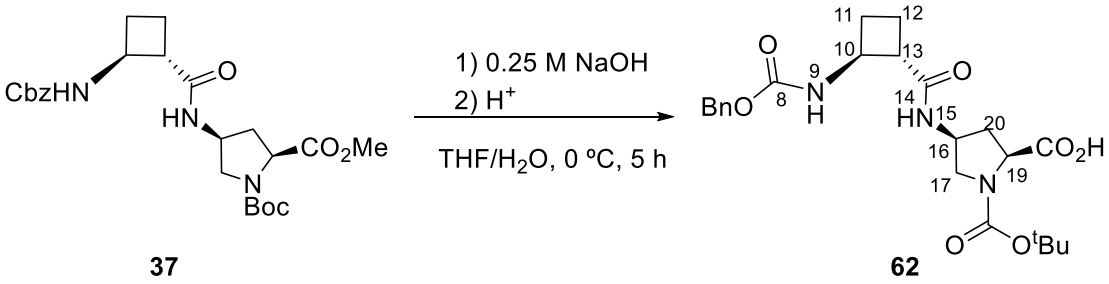

37 **62**

Dipeptide **37** (0.200 g, 0.42 mmol) was dissolved in a 1:10 mixture of THF-H_2O (15 mL). The round bottom flask was placed in an ice-water bath. Then a 0.25 M NaOH aqueous solution was added (4.2 mL, 1.10 mmol, 2.5 eq) and the reaction was monitored by TLC (generally after 5 h it was completed). After, the reaction mixture was acidified to pH 3 with a 5% HCl solution. Then the product was extracted with EtOAc (4 x 30 mL). The organic layers were combined, dried over $MgSO_4$ and the solvent was evaporated under vacuum obtaining acid dipeptide **62** (0.180 g, 0.39 mmol, 90% yield). The crude was used without any further purification.

Spectroscopic data for compound 62:

[α]D = 10.7 (c=1.00 in MeOH).

M.p: 142-145 ºC (from CH_2Cl_2).

IR (ATR): 3292, 2940, 1746, 1698, 1648 cm^{-1}

^{1}H NMR (250 MHz, CD_3OD): (250 MHz, $CDCl_3$): δ 1.45 (s, 9H, ^{t}Bu), 1.80-2.03 (m, 4H, H_{11}, H_{12}, H_{20}), 2.11-2.20 (m, 1H, $H_{11'}$), 2.55 (m, 1H, H_{20}), 2.89 (s, 1 H, H_{13}), 3.32 (m, 1H, H_{17}), 3.79 (m, 1H, $H_{17'}$), 4.08-4.36 (m, 3H, H_{10}, $H_{16,}$ H_{19}), 5.08 (m, 2H, H_7), 7.36 (s, 5H, H_{Ar}).

^{13}C NMR (62.5 MHz, $CDCl_3$): δ 18.0 (C_{12}), 25.2 (C_{11}), 27.5 (CH_3-^{t}Bu), 35.9 (C_{20}), 51.0 (C_{17}), 51.7 (C_{10}), 58.3 (C_{19}), 66.6 (C_7), 80.8 (C-^{t}Bu), 127.8 (C_{Ar}), 128.0 (C_{Ar}), 128.5 (C_{Ar}), 137.2 (C_{Ar}), 154.6 (CO), 157.1 (CO), 174.2 (CO), 175.4 (CO).

HRMS: calculated for $C_{23}H_{31}N_3O_7Na$ (M+Na): 484.2054, Found: 484.2065.

Dipeptide 63

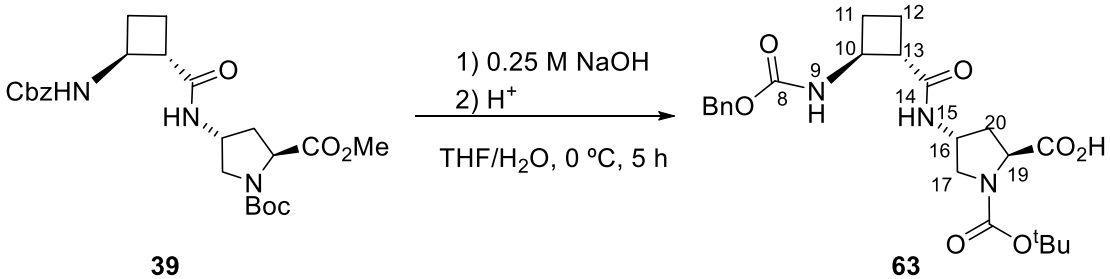

39 **63**

Dipeptide **39** (0.240 g, 0.50 mmol) was dissolved in a 1:10 mixture of THF-H_2O (15 mL). The round bottom flask was placed in an ice-water bath. Then a 0.25 M NaOH aqueous solution was added (5 mL, 1.26 mmol, 2.5 eq) and the reaction was monitored by TLC (generally after 5 h it was completed). After, the reaction mixture was acidified to pH 3 with a 5% HCl solution. Then the product was extracted with EtOAc (4 x 30 mL). The organic layers were combined, dried over $MgSO_4$ and the solvent was evaporated under vacuum obtaining acid dipeptide **63** (0.220 g, 0.48 mmol, 94% yield). The crude was used without any further purification.

Spectroscopic data for compound 63:

[α]D = -9.9 (c=1.05 in MeOH).

M.p: 86-89 ºC (from CH_2Cl_2).

IR (ATR): 3270.37, 2974.17, 1678.05, 1648.67, 1530.44 cm^{-1}

^{1}H NMR (250 MHz, CD_3OD): (250 MHz, $CDCl_3$): δ 1.45 (s, 9H, ^{t}Bu), 1.80-2.05 (m, 4H, H_{11}, H_{12}, H_{20}), 1.87-1.92 (m, 1H, H_{11}), 2.12 (m, 1H, $H_{20'}$), 2.89 (s, 1 H, H_{13}), 3.24 (m, 1H, H_{17}), 3.67 (m, 1H, $H_{17'}$), 4.10-4.40 (m, 3H, H_{10}, $H_{16,}$ H_{19}), 5.06 (m, 2H, H_7), 7.36 (s, 5H, H_{Ar}).

HRMS: calculated for $C_{23}H_{31}N_3O_7Na$ (M+Na): 484.2054, Found: 484.2072.

Dipeptide 64

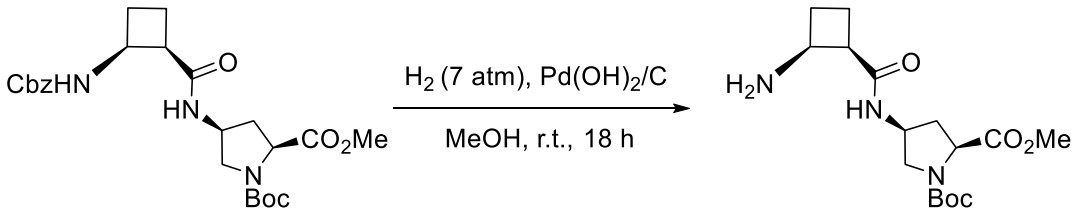

33 **64**

Dipeptide **33** (0.250 g, 0.53 mmol) was dissolved in the minimum amount of methanol in a hydrogenation reactor. $Pd(OH)_2$ 20% on carbon (50 mg) was added and the mixture was hydrogenated during 15 h under 7 atmospheres of pressure. Then, the solution was filtered over Celite. The Celite was washed with methanol and the filtrate was evaporated under reduced pressure. The crude containing amine **64** was used immediately without any further purification.

Dipeptide 65

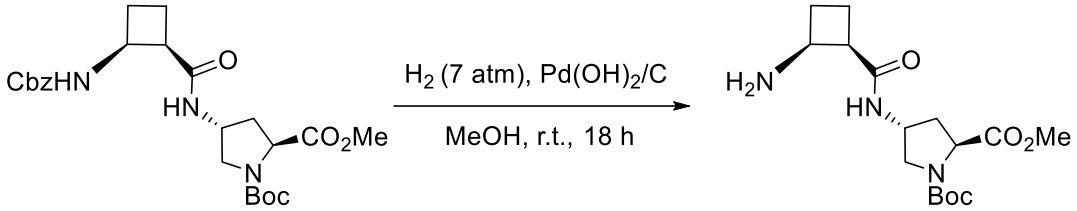

35 **65**

Dipeptide **35** (0.100 g, 0.22 mmol) was dissolved in the minimum amount of methanol in a hydrogenation reactor. $Pd(OH)_2$ 20% on carbon (20 mg) was added and the mixture was hydrogenated during 15 h under 7 atmospheres of pressure. Then, the solution was filtered over Celite. The Celite was washed with methanol and the filtrate was evaporated under reduced pressure. The crude containing amine **65** was used immediately without any further purification.

Dipeptide 66

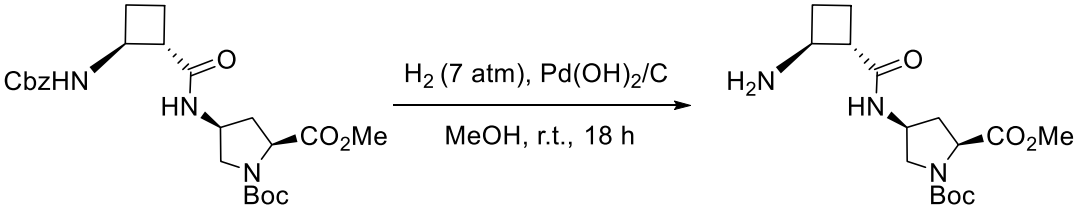

37 **66**

Dipeptide **37** (0.120 g, 0.25 mmol) was dissolved in the minimum amount of methanol in a hydrogenation reactor. $Pd(OH)_2$ 20% on carbon (24 mg) was added and the mixture was hydrogenated during 15 h under 7 atmospheres of pressure. Then, the solution was filtered over Celite. The Celite was washed with methanol and the filtrate was evaporated under reduced pressure. The crude containing amine **66** was used immediately without any further purification.

Dipeptide 67

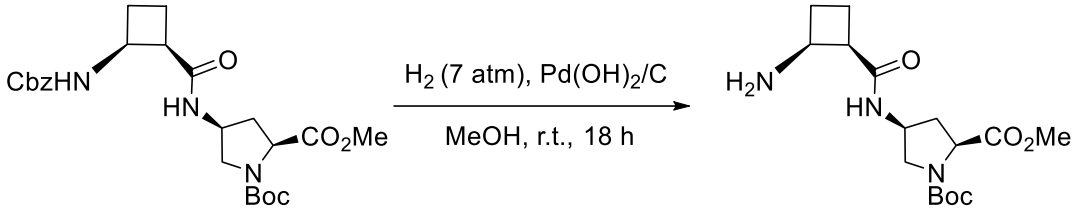

39 **67**

Dipeptide **39** (0.230 g, 0.48 mmol) was dissolved in the minimum amount of methanol in a hydrogenation reactor. $Pd(OH)_2$ 20% on carbon (46 mg) was added and the mixture was hydrogenated during 15 h under 7 atmospheres of pressure. Then, the solution was filtered over Celite. The Celite was washed with methanol and the filtrate was evaporated under reduced pressure. The crude containing amine **67** was used immediately without any further purification.

Tetrapeptide 34

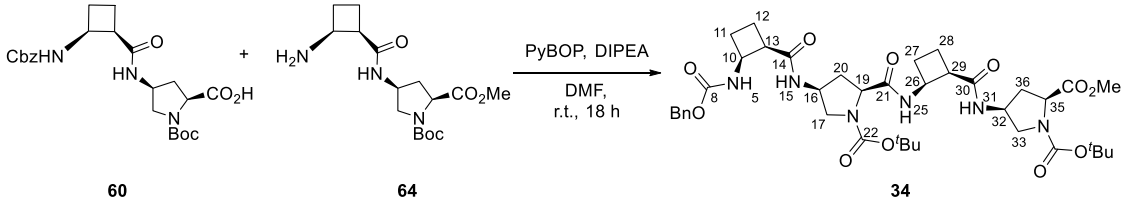

The free carboxylic acid dipeptide derivative **60** (0.184 g, 0.400 mmol, 1 eq) and PyBOP (0.230 mg, 0.440 mmol, 1.1 eq) is dissolved in anhydrous DMF (4 mL) in a round bottom flask under nitrogen. Then, freshly distilled DIPEA (0.280 ml, 1.60 mmol, 4 eq) is added. The solution is stirred at room temperature for 10 minutes. In another round bottom flask under nitrogen, the *N*-terminus-deprotected dipeptide **64** (0.140 g, 0.400 mmol, 1 eq) is dissolved in the minimum amount of anhydrous DMF. This solution is transferred to the flask containing the *C*-terminus-deprotected dipeptide and is stirred at room temperature for 18 h. After this, EtOAc is added and the resulting solution is washed with a saturated aqueous solution of $NaHCO_3$ (x4). The organic layer is dried over $MgSO_4$ and the solvent is evaporated under vacuum. The reaction crude was purified by column chromatography over silica gel (EtOAc) obtaining tetrapeptide **34** as a white solid (0.133 g, 0.17 mmol, 42% yield).

Spectroscopic data for compound 34:

[α]$_D$ = -92 (c=1.0 in MeOH).

M.p: 102-105 ºC (from EtOAc).

IR (ATR): 3294, 2948, 2464, 1695, 1647, 1533 cm^{-1}.

^{1}H NMR (600 MHz, DMSO-d_6,358 K): major conformation: δ 1.40 (s, 18H, *t*-Bu), 1.55 (m, 2H, H_{28}), 1.65 (m, 1H, H_{20}), 1.80 (m, 2H, H_{12}, H_{36}), 2.00 (m, 1H, $H_{12'}$), 2.10 (m, 2H, H_{27}), 2.15 (m, 1H, H_{11}), 2.20 (m, 1H, $H_{11'}$), 2.40 (m, 1H, $H_{20'}$), 2.50 (m, 1H, $H_{36'}$), 3.15 (m, 4H, H_{17}, H_{29}, H_{33}, H_{13}), 3.25 (m, 2H, H_{13}, H_{33}), 3.70 (m, 5H, $H_{17'}$, $H_{33'}$, Me), 4.10 (m, 1H, H_{19}), 4.20 (m, 4H, H_{16}, H_{26}, H_{32}, H_{35}), 4.30 (m, 1H, H_{10}), 5.00 (m, 2H, CH_2Ph), 6.80 (m, 1H, NH_9), 7.35 (m, 5H, H_{Ar}), 7.60 (m, 1H, NH_{31}), 7.70 (m, 2H, NH_{15}, NH_{25}).

^{13}C NMR (150 MHz, DMSO-d_6, 358 K): major conformation: δ 18.9 (C_{12}), 23.0 (C_{28}), 28.3 (C_{11}), 28.5 (C_{Boc}), 28.7 (C_{23} and C_{39}), 35.4 (C_{27} and C_{36}), 36.0 (broad, C_{20}), 45.4 (C_{13}, C_{29}), 47.0-48.00 (C_{10}, C_{16}, C_{26}, C_{32}), 51.2 (C_{33}), 52.2 (Me), 52.4 (C_{17}), 55.4 (C_{19}), 58.0 (C_{35}), 59.2 (C_{19}), 65.9 (C_7), 79.7 ($C_{q\ tBu}$), 128.0 (C_{Ar}), 128.7 (C_{Ar}), 137.6 (C_{Ar}), 153.5 (broad C_{21}, C_{37}), 155.5 (C_8), 172.0 (C_{14}), 172.5 (C_{24}, C_{30}), 173.3 (C_{40}).

HRMS: calculated for $C_{39}H_{56}N_6O_{11}Na$ $(M+Na)^+$: 807.3899, Found: 807.3898.

Tetrapeptide 36

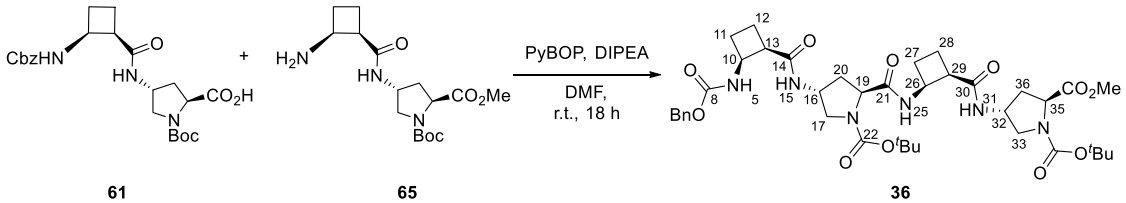

61 **65** **36**

The free carboxylic acid dipeptide derivative **61** (0.100 g, 0.220 mmol, 1 eq) and PyBOP (0.125 mg, 0.242 mmol, 1.1 eq) is dissolved in anhydrous DMF (3 mL) in a round bottom flask under nitrogen. Then, freshly distilled DIPEA (0.150 ml, 0.88 mmol, 4 eq) is added. The solution is stirred at room temperature for 10 minutes. In another round bottom flask under nitrogen, the *N*-terminus-deprotected dipeptide **65** (0.048 g, 0.220 mmol, 1 eq) is dissolved in the minimum amount of anhydrous DMF.

This solution is transferred to the flask containing the *C*-terminus-deprotected dipeptide and is stirred at room temperature for 18 h. After this, EtOAc is added and the resulting solution is washed with a saturated aqueous solution of $NaHCO_3$ (x4). The organic layer is dried over $MgSO_4$ and the solvent is evaporated under vacuum. The reaction crude was purified by column chromatography over silica gel (EtOAc) obtaining tetrapeptide **36** as a white solid (0.086 g, 0.11 mmol, 53% yield

Spectroscopic data for compound 36:

$[\alpha]_D$ = -81 (c=1.0 in MeOH).

M.p: 92-93 ºC (from EtOAc).

IR (ATR): 3294, 1744, 1649, 1536 cm^{-1}.

^{1}H NMR (600 MHz, DMSO-*d_6*,358 K): major conformation: δ 1.40 (s, 18H, *t*-Bu), 1.55 (m, 2H, H_{28}), 1.85 (m, 1H, H_{12}), 1.95 (m, 1H, H_{20}), 2.00 (m, 2H, $H_{12'}$, H_{27}), 2.15 (m, 5H, H_{11}, $H_{20'}$, H_{36}), 3.10 (m, 2H, H_{17}, H_{29}), 3.25 (m, 2H, H_{13}, H_{33}), 3.60 (m, 1H, $H_{33'}$), 3.70 (m, 4H, $H_{17'}$, Me), 4.15 (m, 1H, H_{19}), 4.30 (m, 5H, H_{10}, H_{16}, H_{26}, H_{32}, H_{35}), 5.05 (m, 2H, CH_2Ph), 6.80 (m, 1H, NH_9), 7.35 (m, 5H, H_{Ar}), 7.60 (m, 2H, NH_{15}, NH_{25}), 7.80 (m, 1H, NH_{31}).

^{13}C NMR (150 MHz, DMSO-*d_6*, 358 K): major conformation: δ 18.6 (C_{12}), 23.0 (C_{28}), 28.2 (C_{11}), 28.5 (C_{Boc}), 28.7 (C_{23} and C_{39}), 35.4 (C_{27}), 37.0 (broad, C_{20} and C_{36}), 45.3 (C_{13}, C_{29}), 47.4 (C_{10}, C_{26}), 47.8 (C_{16}, C_{32}), 51.9 (C_{33}), 52.2 (Me), 52.4 (C_{17}), 58.1 (C_{35}), 59.4 (C_{19}), 65.9 (C_7), 79.7 ($C_{q\ tBu}$), 128.0 (C_{Ar}), 128.7 (C_{Ar}), 137.6 (C_{Ar}), 154.0 (broad C_{21}, C_{37}), 155.5 (C_8), 172.0 and 172.5 (C_{14}, C_{24}, C_{30}), 173.0 (C_{40}).

HRMS: calculated for $C_{39}H_{56}N_6O_{11}Na$ $(M+Na)^+$: 807.3899, Found: 807.3893.

Tetrapeptide 38

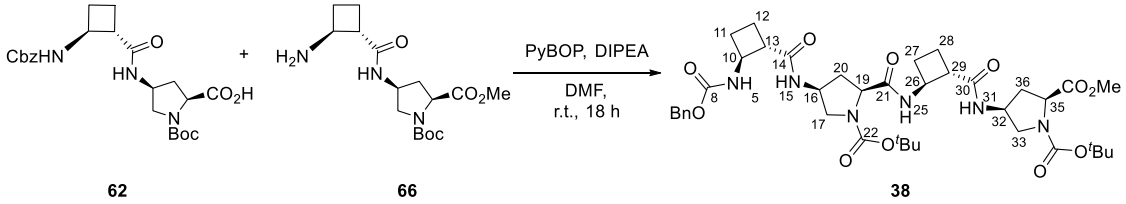

The free carboxylic acid dipeptide derivative **62** (0.160 g, 0.350 mmol, 1 eq) and PyBOP (0.200 mg, 0.385 mmol, 1.1 eq) is dissolved in anhydrous DMF (4 mL) in a round bottom flask under nitrogen. Then, freshly distilled DIPEA (0.250 ml, 1.40 mmol, 4 eq) is added. The solution is stirred at room temperature for 10 minutes. In another round bottom flask under nitrogen, the *N*-terminus-deprotected dipeptide **66** (0.120 g, 0.350 mmol, 1 eq) is dissolved in the minimum amount of anhydrous DMF. This solution is transferred to the flask containing the *C*-terminus-deprotected dipeptide and is stirred at room temperature for 18 h. After this, EtOAc is added and the resulting solution is washed with a saturated aqueous solution of $NaHCO_3$ (x4). The organic layer is dried over $MgSO_4$ and the solvent is evaporated under vacuum. The reaction crude was purified by column chromatography over silica gel (EtOAc) obtaining tetrapeptide **38** as a white solid (0.180 g, 0.23 mmol, 65% yield).

Spectroscopic data for compound 38:

[α]$_D$ = -2 (c=1.0 in MeOH).

M.p: 107-110 ºC (from EtOAc).

IR (ATR): 3303, 2977, 1746, 1678, 1650 cm^{-1}.

^{1}H NMR (600 MHz, DMSO-*d*$_6$,358 K): major conformation: δ 1.38 (s,18H, *t*-Bu), 1.71 (m, 3H, H_{12}, $H_{20,}$ H_{28}), 1.85 (m, 2H, $H_{12'}$, H_{36}), 1.90 (m, 3H, H_{11}, H_{27}, $H_{28'}$), 2.08 (m, 2H, $H_{11'}$, $H_{27'}$), 2.40 (m, 1H, $H_{20'}$), 2.50 (m, 1H, $H_{36'}$), 2.88 (m,1H, H_{13}), 2.92 (m, 1H, H_{29}), 3.20 (m, 2H, H_{17}, H_{33}), 3.68 (s, 4H, Me, $H_{17'}$), 3.70 (m, 1H, $H_{33'}$), 4.60 (m, 2H, H_{10}, H_{19}), 4.25 (m, 4H, H_{16}, H_{26}, H_{32}, H_{35}), 5.04 (m, 2H, H_7), 7.38 (m, 5H, H_{Ar}), 7.70 (m, 2H, $NH_{15,}$ NH_{31}), 8.05 (m, 1H, NH_{25}).

^{13}C NMR (150 MHz, DMSO-*d*$_6$, 358 K): major conformation: δ 18.2 (C_{12}), 18.9 (C_{28}), 25.7 (C_{27}), 26.4 (C_{11}), 28.5 (C_{Boc}), 28.6 (C_{Boc}), 36.0 (broad, C_{36}), 37.0 (broad, C_{20}), 47.2 (C_{26}), 47.6 ($C_{16,}$ C_{29}, C_{32}), 48.1 (C_{13}), 48.8 (C_{10}), 51.4 (C_{33}), 52.1 (Me), 52.4 (C_{17}), 58.0 (C_{35}), 58.2 (C_{19}), 65.8 (C_7), 79.8 ($C_{q\ tBu}$), 128.2 (C_{Ar}), 128.8 (C_{Ar}), 137.6 (C_{Ar}), 155.5 (C_8), 172.0 and 172.5 (C_{14}, C_{24}, C_{30}), 173.0 (C_{40})

HRMS: calculated for $C_{39}H_{57}N_6O_{11}Na$ $(M+H)^+$: 785.4080, Found: 785.4110.

Tetrapeptide 40

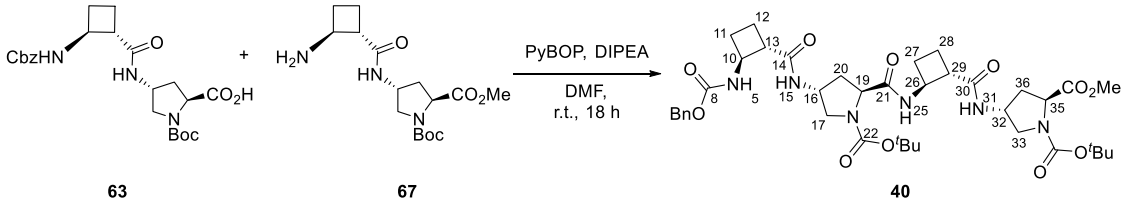

63 67 40

The free carboxylic acid dipeptide derivative **63** (0.050 g, 0.100 mmol, 1 eq) and PyBOP (0.060 mg, 0.110 mmol, 1.1 eq) is dissolved in anhydrous DMF (2 mL) in a round bottom flask under nitrogen. Then, freshly distilled DIPEA (0.070 ml, 0.4 mmol, 4 eq) is added. The solution is stirred at room temperature for 10 minutes. In another round bottom flask under nitrogen, the *N*-terminus-deprotected dipeptide **67** (0.034 g, 0.100 mmol, 1 eq) is dissolved in the minimum amount of anhydrous DMF.

This solution is transferred to the flask containing the *C*-terminus-deprotected dipeptide and is stirred at room temperature for 18 h. After this, EtOAc is added and the resulting solution is washed with a saturated aqueous solution of $NaHCO_3$ (x4). The organic layer is dried over $MgSO_4$ and the solvent is evaporated under vacuum. The reaction crude was purified by column chromatography over silica gel (EtOAc) obtaining tetrapeptide **40** as a white solid (0.055 g, 0.07 mmol, 69% yield).

Spectroscopic data for compound 40:

[α]D = -2 (c=1.0 in MeOH).

M.p: 107-110 ºC (from EtOAc).

IR (ATR): 3295, 2976, 1698, 1647, 1534 cm^{-1}.

^{1}H NMR (600 MHz, DMSO-*d*$_6$,358 K): major conformation: δ 1.38 (s,18H, *t*-Bu), 1.75 (m, 2H, H_{12}, H_{28}), 1.84 (m, 2H, $H_{12'}$, $H_{28'}$), 1.90 (m, 2H, H_{11}, H_{27}), 2.05 (m, 5H, $H_{11'}$, H_{20}, $H_{27'}$, H_{36}), 2.15 (m, 1H, $H_{36'}$), 2.90 (m, 2H, H_{13}, H_{29}), 3.19 (m, 2H, H_{17}, H_{33}), 3.60 (m, 2H, $H_{17'}$, $H_{33'}$), 3.68 (m, 2H, Me), 4.09 (m, 1H, H_{10}), 4.15 (m, 1H, H_{19}), 4.25 (m, 3H, H_{16}, H_{26}, H_{32}), 4.63 (m, 1H, H_{35}), 5.04 (m, 2H, H_7), 7.30 (m, 1H, NH9), 7.36 (m, 5H, H_{Ar}), 7.70 (m, 2H, NH_{15}, NH_{31}), 7.95 (m, 1H, NH_{25}).

^{13}C NMR (150 MHz, DMSO-*d*$_6$, 358 K): major conformation: δ 18.3 (C_{12}), 18.5 (C_{28}), 25.4 (C_{27}), 26.1 (C_{11}), 28.5 (C_{Boc}), 28.7 (C_{Boc}), 36.0 (broad, C_{36}), 37.0 (broad, C_{20}), 47.5 (C_{26}), 48.0 (C_{13}, C_{16}, C_{29}, C_{32}), 49.0 (C_{10}), 51.8 (C_{33}), 52.2 (Me, C_{17}), 58.2 (C_{35}), 59.3 (C_{19}), 66 (C_7), 79.8 ($C_{q\ tBu}$), 128.0 (C_{Ar}), 128.8 (C_{Ar}), 137.6 (C_{Ar}), 154 (broad C_{21}, C_{37}), 155.7 (C_8), 172.4 (C_{14}, C_{24}, C_{30}), 173.0 (C_{40}).

HRMS: calculated for $C_{39}H_{56}N_6O_{11}Na$ $(M+Na)^+$: 807.3830, Found: 807.3911.

(1*S*,3*R*)-3-Acetyl-2,2-dimethylcyclobutane-1-carboxylic acid, 68

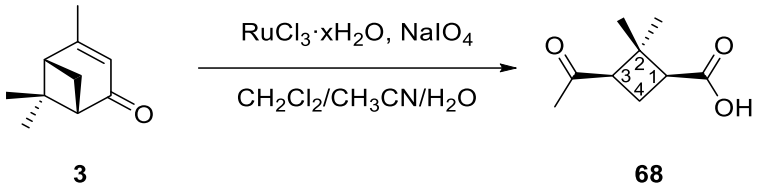

3 **68**

To a stirred solution of (-)-verbenone (2 mL, 13.0 mmol) in 2:2:3 dichloromethane-acetonitrile-water (120 mL) were added catalytic $RuCl_3$ hydrate (0.05 g, 0.02 eq) and $NaIO_4$ (11.70 g, 54.5 mmol, 4.2 eq). The mixture was stirred at room temperature for 18 h. The crude obtained was filtered through Celite® and the organic layer was extracted with dichloromethane (3x40 mL). Then, the combined organic extracts were dried over $MgSO_4$ and concentrated under vacuum to afford the (-)-*cis*-pinonic acid (2.10 g, 12.3 mmol, 86% yield) which was used in the next step without further purification.

Spectroscopic data for compound 68:

^{1}H NMR (250 MHz, $CDCl_3$): δ 0.97 (s,3H, *trans*-CH_3), 1.45 (s, 3H, *cis*-CH_3), 1.91 (m, 1H, H_{4a}), 2.07 (s, 3H, $COCH_3$), 2.62 (m, 1H, H_{4b}), 2.86 (c.a., 2H, H_1, H_3).

Spectroscopic data are consistent with those reported in reference:

Burgess, K.; Li, S, Rebenspies, J. *Tetrahedron Lett.* **1997**, *38*, 1681-1684.

tert-Butyl (1*S*,3*R*)-3-acetyl-2,2-dimethylcyclobutane-1-carboxylate, 69

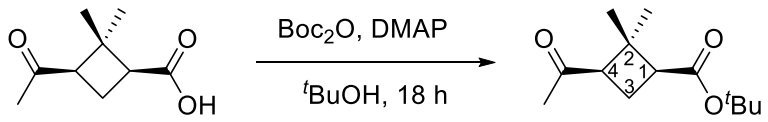

X **X**

To a stirred solution of (-)-cis-pinonic acid **68** (2.01 g, 10.91 mmol) in *tert*-butanol (20 mL) was added di-*tert*-butyl dicarbonate (5.5 g, 27.3 mmol, 2.5 eq). After stirring for 4 h at room temperature the solvent was removed at reduced pressure. The reaction crude was then purified using a flash chromatography (EtOAc-hexane, 1:3), obtaining the *tert*-butyl ester **69** (2.37 g, 96% yield).

Spectroscopic data for compound 69:

^{1}H NMR (250 MHz, $CDCl_3$): δ 0.90 (s,3H, *trans*-CH_3), 1.39 (s, 3H, *cis*-CH_3), 1.42 (s, 9H, ^{t}Bu), 1.65-2.01 (s, 1H, H_4), 2.03 (s, 3H, $COCH_3$), 2.48-2.69 (m, 1H, $H_{4'}$), 2.81 (c.a., 2H, H_1, H_3).

Spectroscopic data are consistent with those reported in reference:

Rouge, P.D.; Moglioni, A.G; Moltrasio, G.Y.; Ortuño, R.M. *Tetrahedron: Asymmetry* **2003**, *14 (2)*, 193-195.

(1*R*,3*S*)-3-(*tert*-Butoxycarbonyl)-2,2-dimethylcyclobutane-1-carboxylic acid, 49

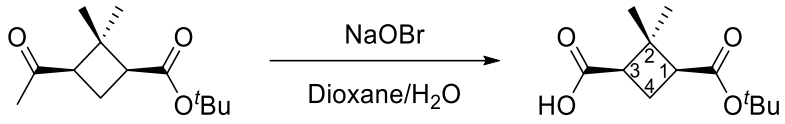

69 **49**

A solution of *tert*-Butyl ester **69** (2.00 g, 8.8 mmol) was prepared using 125 mL of a 3:1 mixture of 1,4-dioxane-water and cooled at 0 ºC. At the same time, a solution of sodium hypobromite was prepared using 10.00 g of sodium hydroxide (250.1 mmol, 28.3 eq) in 240 mL of H_2O which were cooled at 0 ºC and then 3.4 mL (65.4 mmol, 7.4 eq) of bromine were slowly added. After 10 minutes at 0 ºC, the sodium hypobromite solution was added to the other one and 80 mL of 1,4-dioxane were incorporated to the mixture which was stirred for 5 h at 0ºC. After that time, a solution of $NaHSO_4$ was added until the yellowish color is not observed. By that time, the mixture is acidified using 5 % HCl until reach pH 2 and then extracted with CH_2Cl_2 (4 x 70 mL). The combined organic extracts were dried over $MgSO_4$ and concentrated under *vacuum* to afford the acid **49** as a white solid (2.37 g, 97% yield) which was used in the next step without further purification.

Spectroscopic data for compound 49:

^{1}H NMR (250 MHz, $CDCl_3$): δ 1.01 (s,3H, *trans*-CH_3), 1.30 (s, 3H, *cis*-CH_3), 1.41 (s, 9H, ^{t}Bu), 1.90-2.05 (s, 1H, H_4), 2.39-2.55 (m, 1H, $H_{4'}$), 2.59-2.86 (c.a., 2H, H_1, H_3).

Spectroscopic data are consistent with those reported in reference:

Aguado, G.P.; Moglioni, A.G.; Brousse, B.N; Ortuño, R.M. *Tetrahedron: Asymmetry* **2003**, *14*, 2445-2451.

(1*R*,3*S*)-3-*tert*-Butoxycarbonyl-2,2-dimethylcyclobutane-1-carboxylic acid, 48

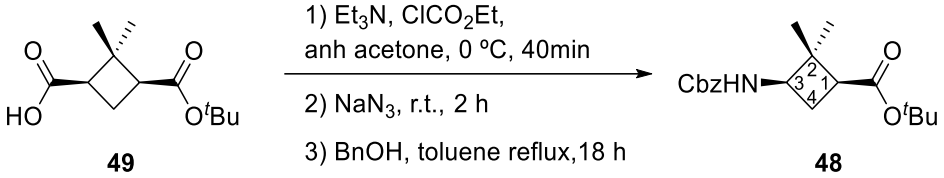

To an ice-cooled solution of half-ester **49** (1.50 g, 6.57 mmol) in anhydrous acetone (40 mL), triethylamine (1.50 mL, 10.7 mmol, 1.6 eq) and ethyl chloroformate (1.00 mL, 10.6 mmol, 1.6 eq) were subsequently added. The mixture was stirred at 0 ºC for 40 minutes. Then, sodium azide (1.11 g, 17.10 mmol, 2.6 eq) in 10 mL of water was added and the resultant solution was stirred at room temperature for 2 h. The reaction mixture was extracted with dichloromethane (4x20 mL), and the organic extracts were dried over $MgSO_4$. Solvents were removed under reduced pressure to give the corresponding acyl azide as a yellow oil, which was used in the next step without further purification. Acyl azides are instable reagents: it is very important not to heat the final product while it is being dried, and the solvent must not be removed until full dryness. The obtained acyl azide was dissolved in toluene (40 mL) and BnOH (1.45 mL, 13.8 mmol, 2.1 eq) was added and the resulting mixture was stirred for 16 h under reflux conditions. Then, solvents were removed under reduce pressure and residual BnOH was microdestilled under vacuum.

The reaction crude was then purified using a flash chromatography (EtOAc-hexane, 1:2), obtaining orthogonally protected amino acid **48** (1.55 g, 70% yield). WARNING: Acyl azides are instable reagents: it is very important not to heat the intermediate product while it is being dried, and the solvent must not be removed until full dryness.

Spectroscopic data for compound 48:

^{1}H NMR (250 MHz, $CDCl_3$): δ 0.95 (s,3H, *trans*-CH_3), 1.30 (s, 3H, *cis*-CH_3), 1.46 (s, 9H, ^{t}Bu), 2.02 (m, 1H, H_{4a}), 2.25-2.36 (m, 1H, H_{4b}), 2.51 (m, 1H, H_1), 3.90 (m, 1H, H_3), 5.13 (m, 2H, CH_2-Ph), 7.36 (m, 5H, H_{Ar}).

Spectroscopic data are consistent with those reported in reference:

Aguilera, J.; Moglioni, A.G.; Moltrasio, G.Y.; Ortuño. R.M. *Tetrahedron: Asymmetry* **2008,** *19*, 302-308.

(1*S*,3*R*)-3-Benzyloxycarbonylamino-2,2-dimethylcyclobutane-1-carboxylic acid, 70

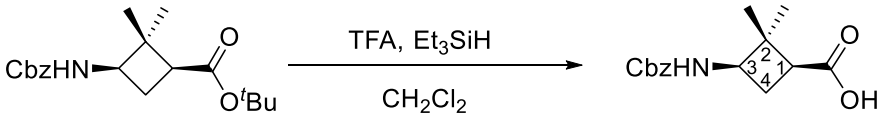

48 **70**

To a solution of orthogonally protected amino acid **48** (0.48 g, 1.32 mmol) in CH_2Cl_2 (10 mL), TFA (1,5 mL, 9.4 mmol, 7.0 eq) and Et_3SiH (1.5 mL, 9.4 mmol, 7.0 eq) were added and the reaction was stirred at room temperature for 30 h. After that, excess of reactants and solvent were removed under vacuum to afford protected amino acid **70** as a white solid (0.40 g, 1.32 mmol, quantitative yield) which was used for peptide synthesis without further purification.

Spectroscopic data for compound 70:

^{1}H NMR (250 MHz, $CDCl_3$): δ 0.98 (s,3H, *trans*-CH_3), 1.34 (s, 3H, *cis*-CH_3), 2.04 (m, 1H, H_{4a}), 2.33 (m, 1H, H_{4b}), 2.59 (m, 1H, H_1), 3.95 (m, 1H, H_3), 5.12 (m, 2H, CH_2-Ph), 7.36 (m, 5H, H_{Ar}).

Spectroscopic data are consistent with those reported in reference:

Aguilera, J.; Moglioni, A.G.; Moltrasio, G.Y.; Ortuño. R.M. *Tetrahedron: Asymmetry* **2008,** *19*, 302-308.

Dipeptide 41

70 **45** **41**

Carboxylic acid cyclobutane **70** (0.370 g, 1.30 mmol) and PyBOP (0.800 g, 1.50 mmol, 1.1 eq) were dissolved in anhydrous DMF (6 mL) in a round bottom flask under nitrogen. Then, freshly distilled DIPEA (0.900 mL, 5.20 mmol, 4 eq) was added. The solution was stirred at room temperature for 10 minutes. In another round bottom flask under nitrogen, *trans*-γ-amino- N^{α}-Boc-L-proline methyl ester hydrochloride **45** (0.420 g, 1.50 mmol, 1.1 eq) was dissolved in the minimum amount of anhydrous DMF. This solution was transferred to the flask containing the carboxylic acid derivative and was stirred at room temperature for 18 h. After this, EtOAc was added and the resulting solution was washed with a saturated aqueous solution of $NaHCO_3$ (x4). The organic layer was dried over $MgSO_4$ and the solvent was evaporated under vacuum. The reaction crude was purified by column chromatography over silica gel (EtOAc-Hexane 2:1) obtaining dipeptide **41** as a white solid (0.580 g, 1.15 mmol, 86% yield).

Spectroscopic data for compound 41:

[α]$_D$ = -9.2 (c = 1.1 in MeOH)

M.p: 94-97 ºC (from Et_2O)

IR (ATR): 3307 (NH_{st}), 2955 (CH_{st}), 1687 (C=O), 1655 (C=O).

^{1}H NMR (600 MHz, $CDCl_3$): major conformation: δ 0.79–0.96 (m, 3H, *cis*-CH_3), 1.27–1.37 (m, 3H, *trans*-CH_3), 1.45 (m, 9H, ^{t}Bu), 1.80–1.94 (m, 1H, $H_{22'}$), 2.03 – 2.19 (m, 1H, $H_{11'}$), 2.25–2.48 (c.a., 3H, H_{11}, H_{12}, H_{22}), 3.42–3.62 (m, 2H, H_{19}), 3.77 (m, 3H, CO_2Me), 3.89 (m,1H, H_{10}), 4.20–4.37 (m, 1H, H_{18}), 4.53–4.72 (m, 1H, H_{21}), 4.96–5.19 (c.a., 3H, H_7, H_9), 6.58 (c.a., 1H, NH_{17}), 7.29 – 7.38 (m, 5H, Ar).

^{13}C NMR (150 MHz, $CDCl_3$): δ 16.6 (*cis*-CH_3), 26.1 (C_{11}), 28.3 (CH_3-^{t}Bu), 29.2 (*trans*-CH_3), 34.7-37.2 (C_{22}) , 44.5 (C_{12}), 47.1-49.5 (C_{21}, 51.7 (C_{10}), 52.3-54.5 (C_{19}, CO_2Me), 57.6 (C_{18}), 66.7 (CH_2-Ph), 80.9 (C-^{t}Bu), 128.01 , 128.6, 136.4 ,153.1 (Ar), 156.1, 170.3, 171.2, 175.4 (C=O).

HRMS: calculated for $C_{24}H_{24}N_2O_6Na$ (M+Na): 526.2524, Found: 526.2544.

Dipeptide 42

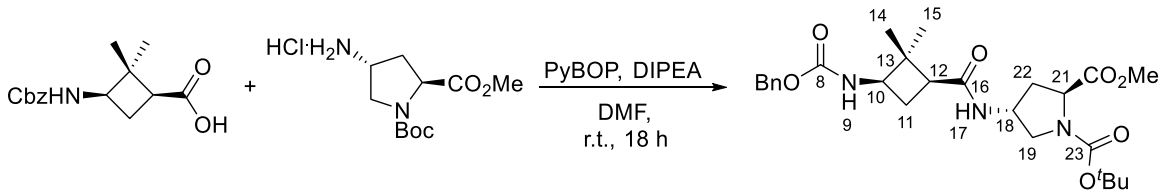

70 **46** **42**

Carboxylic acid cyclobutane **70** (0.500 g, 1.80 mmol) and PyBOP (1.50 g, 2.00 mmol, 1.1 eq) were dissolved in anhydrous DMF (9 mL) in a round bottom flask under nitrogen. Then, freshly distilled DIPEA (1.25 mL, 7.20 mmol, 4 eq) was added. The solution was stirred at room temperature for 10 minutes. In another round bottom flask under nitrogen, *trans*-γ-amino- N^{α}-Boc-L-proline methyl ester hydrochloride **46** (0.560 g, 2.00 mmol, 1.1 eq) was dissolved in the minimum amount of anhydrous DMF. This solution was transferred to the flask containing the carboxylic acid derivative and was stirred at room temperature for 18 h. After this, EtOAc was added and the resulting solution was washed with a saturated aqueous solution of $NaHCO_3$ (x4).

The organic layer was dried over $MgSO_4$ and the solvent was evaporated under vacuum. The reaction crude was purified by column chromatography over silica gel (EtOAc-Hexane 2:1) obtaining dipeptide **42** as a white solid (0.760 g, 1.50 mmol, 84% yield).

Spectroscopic data for compound 42:

$[\alpha]_D$ = -8.5 (c = 1.0 in MeOH)

M.p: 54-57 ºC (from Et_2O)

IR (ATR): 3296 (NH_{st}), 2952 (CH_{st}), 1742 (C=O), 1696 (C=O), 1656 (C=O).

^{1}H NMR (600 MHz, $CDCl_3$): major conformation: δ 0.89 (s, 3H, *cis*-CH_3), 1.28 (s, 3H, *trans*-CH_3), 1.45 (s, 9H, ^{t}Bu), 2.07-2.38 (c.a., 5H, H_{11}, H_{12}, H_{22}), 3.36 (m, 1H, $H_{19'}$), 3.73 (m, 4H, CO_2Me, H_{19}), 3.89 (m, H_{10}), 4.26 - 4.38 (m, 2H, H_{18}), 4.51 (m, 1H, H_{21}), 4.96 – 5.22 (c.a., 3H, H_7, H_9), 5.47 (m, 1H, H_{17}), 7.28 – 7.40 (m, Ar).

^{13}C NMR (150 MHz, $CDCl_3$): δ 17.0 (*cis*-CH_3), 26.1 (CH_2), 28.3, (CH_3-^{t}Bu), 29.3 (*trans*-CH_3), 35.4-37.3 (CH_2), 44.6 (C_{12}), 48.0-48.7 (C_{21}), 51.3-52.6 (C_{10}, C_{19}, CO_2Me), 57.3-57.7 (C_{18}), 66.8 (CH_2-Ph), 80.8 (C-^{t}Bu), 128.3, 128.6, 136.3, 154.33 (Ar), 156.0, 171.5, 172.7, 173.0 (C=O).

HRMS: calculated for $C_{24}H_{24}N_2O_6Na$ (M+Na): 526.2524, Found: 526.2521.

tert-Butyl (1*S*,3*R*)-3-amino-2,2-dimethylcyclobutane-1-carboxylate, 101

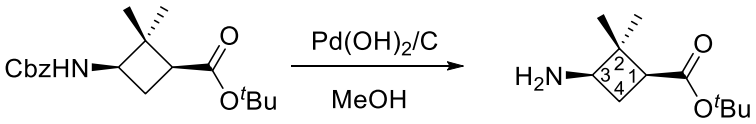

48 **101**

Diprotected amino acid **48** (1.55 g, 4.65 mmol) in MeOH (15 mL) was hydrogenated under 10 atmospheres of pressure in the presence of 20% $Pd(OH)_2/C$ (0.31 g) overnight. The reaction mixture was filtered through Celite® and solvent was removed under vacuum affording the desired protected amino acid **101** as a white solid (0.77 g, 65% yield) which was used in the next step without further purification.

Spectroscopic data for compound 101:

^{1}H NMR (250 MHz, $CDCl_3$): δ 1.08 (s,3H, *trans*-CH_3), 1.24 (s, 3H, *cis*-CH_3), 1.42 (s, 9H, ^{t}Bu), 1.95-2.34 (m, 2H, H_{4a}), 2.46 (m, 1H, CH), 3.21 (m, 1H, CH), 5.76 (br., 2H, NH).

Spectroscopic data are consistent with those reported in reference:

Gorrea, E.; Carbajo, D.; Gutiérrez-Abad, R.; Illa, O.; Branchadell, V.; Royo, M.; Ortuño, R.M. *Org. Biomol. Chem* **2012**, *10*, 4050.

tert-Butyl (1*S*,3*R*)-3-((9H-fluoren-9-ylmethoxycarbonyl)amino)-2,2-dimethylcyclobutane-1-carboxylate, 102

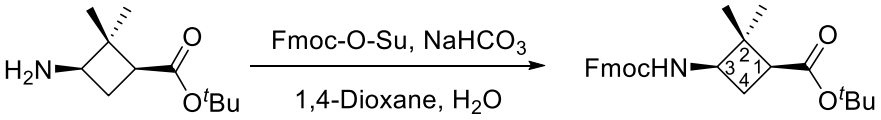

101 **102**

Protected amino acid **101** (1.10 g, 5.52 mmol) dissolved in a 1:1 mixture of 1,4-Dioxane/Water (70 mL) was cooled at 0ºC for 10 minutes. Then, $NaHCO_3$ (0.90 g, 10.7 mmol, 2.0 eq) and Fmoc-O-Su (1.9 g, 5.56 mmol, 1 eq) were added. Reaction was then heated to room temperature and it was stirred for 16 h. After that, NH_4Cl saturated solution (28 mL) was added and the reaction mixture was extracted with dichloromethane (4 x 30 mL), then the organic extracts were dried over $MgSO_4$. Solvents were removed under reduced pressure. The reaction crude was then purified using a flash chromatography (EtOAc-hexane, 1:2), obtaining orthogonally protected amino acid **102** (1.90 g, 81% yield).

Spectroscopic data for compound 102:

^{1}H NMR (250 MHz, $CDCl_3$): δ 0.96 (s,3H, *trans*-CH_3), 1.31 (s, 3H, *cis*-CH_3), 1.48 (s, 9H, ^{t}Bu), 2.06-2.25 (m, 1H, H_{4a}), 2.25-2.38 (m, 1H, H_1), 2.45-2.60 (m, 1H, H_{4b}), 3.83-3.97 (m, 1H, H_3), 4.01-4.30 (m, 1H, H_{10}), 4.36-4.61 (m, 2H, CH_2), 5.07, (br. 1H, NH), 7.28-7.77 (m, 8H, H_{Ar})

Spectroscopic data are consistent with those reported in reference:

Gorrea, E.; Carbajo, D.; Gutiérrez-Abad, R.; Illa, O.; Branchadell, V.; Royo, M.; Ortuño, R.M. *Org. Biomol. Chem* **2012**, *10*, 4050.

(1*S*,3*R*)-3-(9H-Fluoren-9-ylmethoxycarbonylamino)-2,2-dimethylcyclobutane-1-carboxylic acid, 72

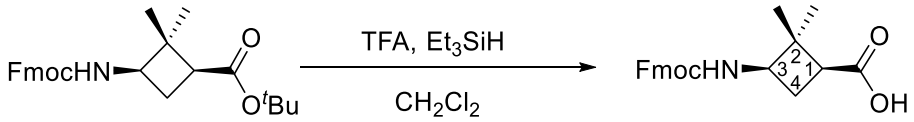

102 **72**

To a solution of orthogonally protected amino acid **102** (1.10 g, 2.60 mmol) in CH_2Cl_2 (15mL), TFA (2.40 mL, 31.2 mmol, 12 eq) and Et_3SiH (1.5 mL, 9.4 mmol, 3.6 eq) were added and the reaction was stirred at room temperature for 30 h. After that, excess of reactants and solvent were removed under vacuum to afford protected amino acid **72** as a white solid (0.93 g, quantitative yield) which was used for peptide synthesis without further purification.

Spectroscopic data for compound 72:

^{1}H NMR (250 MHz, $CDCl_3$): δ 0.99 (s,3H, *trans*-CH_3), 1.34 (s, 3H, *cis*-CH_3), 2.08 (m, 1H, H_{4a}), 2.16-2.30 (m, 1H, H_{4b}), 2.60-2.70 (m, 1H, H_1), 3.88-4.01 (m, 1H, H_3), 4.20-4.26 (m, 1H, $H_{2'}$), 4.38-4.48 (m, 2H, CH_2), 4.82, (br. 1H, NH), 7.28-7.77 (m, 8H, H_{Ar}).

Spectroscopic data are consistent with those reported in reference:

Gorrea, E.; Carbajo, D.; Gutiérrez-Abad, R.; Illa, O.; Branchadell, V.; Royo, M.; Ortuño, R.M. *Org. Biomol. Chem* **2012**, *10*, 4050.

(2*S*,4*R*)-4-9H-Fluoren-9-ylmethoxycarbonylamino-1-(allyloxycarbonyl) pyrrolidine-2-carboxylic acid, 98

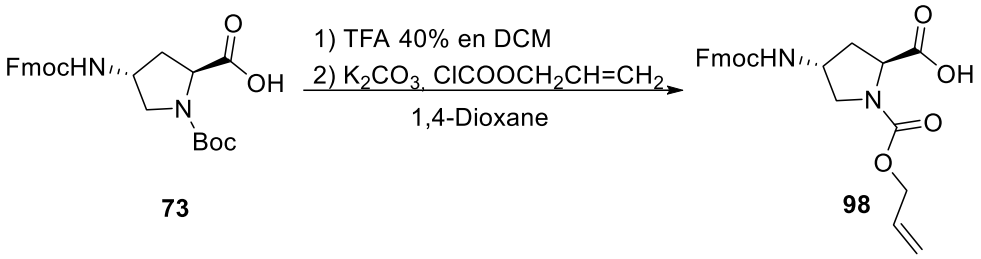

73 **98**

Commercially available carboxylic acid **73** (2.00 g, 4.42 mmol) was dissolved in 25 mL of a 40% solution of TFA in dichloromethane. The resulting mixture was stirred at room temperature for 30 minutes. The solvent and excess volatiles were evaporated under vacuum (coevaporations with 2 x 10 mL of DCM and 1 x 10 mL Et_2O). The intermediate ammonium salt (2.06 g, 4.42 mmol, quantitative yield) was obtained as a white solid. The protecting group removal was checked by nmr. Then, the ammonium salt (2.06 g, 4.42 mmol) was dissolved in dioxane (20 mL). 25% K_2CO_3 aqueous solution (48 mL) and allyl chloroformate (0.56 mL, 5.30 mmol) were added and the vessel was sealed. The reaction mixture was stirred at room temperature for 2 hours. The reaction mixture was acidified with 2 M HCl and extracted with EtOAc (3 x 30 mL). The organic layers were combined, dried over $MgSO_4$ and the solvent was evaporated under vacuum. Compound **98** (1.73 g, 3.96 mmol, 90% yield) was obtained as a white solid.

Spectroscopic data for compound 98:

[α]$_D$ = -13.8 (c=1.05 in MeOH).

M.p: 65-68 ºC (from EtOAc).

IR (ATR): 3308 (OH_{st}), 2949 (CH_{st}), 1685 (C=O), 1525 (C=O).

HRMS: calculated for $C_{24}H_{23}N_2O_6$ (M-H): 435.1551, Found: 435.1545.

(2*S*,4*S*)-4-9H-Fluoren-9-ylmethoxycarbonylamino-1-(allyloxycarbonyl) pyrrolidine-2-carboxylicacid, 99

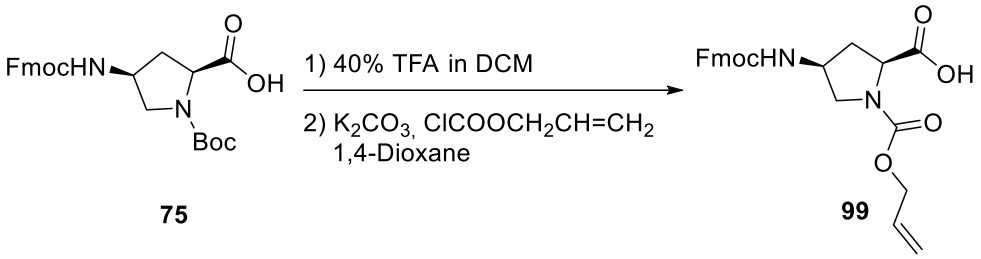

75 **99**

Commercially available carboxylic acid **75** (2.11 g, 4.68 mmol) was dissolved in a 40% solution of TFA in dichloromethane. The resulting mixture was stirred at room temperature for 30 minutes. The solvent and excess volatiles were evaporated under vacuum (coevaporations with 2 x 10 mL of DCM and 1 x 10 mL Et_2O). The intermediate ammonium salt (1.54 g, 4.68 mmol, quantitative yield) was obtained as a white solid. The protecting groupo removal was checked by nmr. Then the ammonium salt (1.9 g, 5.39 mmol) was dissolved in dioxane (22 mL). 25% K_2CO_3 aqueous solution (56 mL) and allyl chloroformate (0.71 mL, 6.65 mmol) were added and the vessel was sealed. The reaction mixture was stirred at room temperature for 2 hours. The reaction mixture was acidified with 2 M HCl and extracted with EtOAc (3 x 30 mL). The organic layers were combined, dried over $MgSO_4$ and the solvent was evaporated under vacuum. Compound **99** (2.42 g, 5.54 mmol, 90% yield) was obtained as a white solid.

Spectroscopic data for compound 99:

$[\alpha]_D$ = -14.2 (c=1.04 in MeOH).

M.p: 70-73 ºC (from EtOAc).

IR (ATR): 3304 (OH_{st}), 2945 (CH_{st}), 1679 (C=O), 1534 (C=O).

HRMS: calculated for $C_{24}H_{24}N_2O_6Na$ (M+Na): 459.1527, Found: 459.1517.

(*E*)-5-(2,3-Bis(*tert*-butoxycarbonyl)guanidino)pentanoic acid, 100

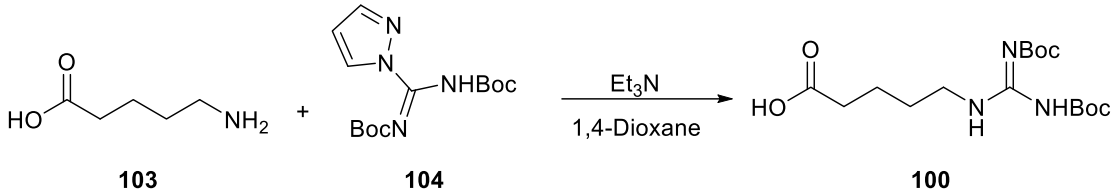

103 **104** **100**

5-amino pentanoic acid **103** (0.6 g, 5.12 mmol) was dissolved in 60 mL of a CH_3CN/H_2O mixture (55:5). Then, triethylamine (2.6 mL, 14.93 mmol, 2.9 eq) was added and the resulting mixture was cooled to 0 ºC. After that, *N,N'*–Bis(*terc*-butoxycarbonyl)-1H-pirazole-1-carboxamidine **104** (1.75 g, 5.64 mmols, 1.1 eq) was added. The reaction mixture was stirred for 16 h heating progressively to reach room temperature. Then the solvent was evaporated under vacuum. The crude was dissolved in EtOAc (30 mL) and water (10mL) and pH 2-3 was reached using HCl 1M. The organic layer was separated and washed with saturated $NaHCO_3$ (2 x 10 mL) and brine (2 x 10 mL). The organic layer was dried with $MgSO_4$ and the solvent was evaporated under reduced pressure. The crude was purified by column chromatography on silica gel using a mixture of CH_2Cl_2-MeOH 98:2. Compound **100** (1.60 g, 4.62 mmol, 87% yield) was obtained as a white solid.

Spectroscopic data for compound 100:

$[\alpha]_D$ = -14.2 (c=1.04 in MeOH).

M.p: 70-73 ºC (from EtOAc).

IR (ATR): 3304 (OH_{st}), 2945 (CH_{st}), 1679 (C=O), 1534 (C=O).

^{1}H NMR (360 MHz, $CDCl_3$): δ 1.47 (s, 18H, ^{t}Bu), 1.56-1.80 (m, 4H, CH_2), 2.37 (m, 2H, CH_2), 3.41 (m, 2H, CH_2), 8.35 (br., 1H, N*H*) 11.27 (br., 1H, N*H*).

^{13}C NMR (90 MHz, $CDCl_3$): δ 21.9, 28.0, 28.2, 28.4, 33.6, 40.4, 79.32, 83.1, 153.2, 156.2, 163.4, 178.6.

HRMS: calculated for $C_{24}H_{24}N_2O_6Na$ (M+Na): 459.1527, Found: 459.1517.

Benzyl *tert*-butyl ((1*S*,2*S*)-cyclobutane-1,2-diyl)dicarbamate, 112

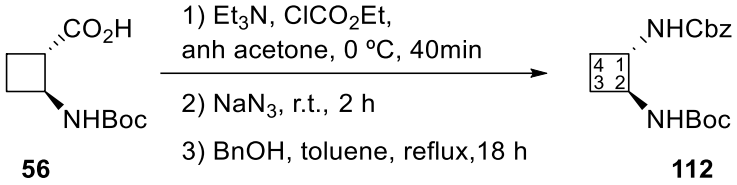

56 **112**

Carboxylic acid **56** (380 mg, 1.90 mmol) was dissolved in anhydrous acetone (40 mL) and ethyl chloroformate (0.200 mL, 2.00 mmol, 1.1 eq) and trimethylamine (0.250 mL, 1.80 mmol,1 eq) were added at 0 ºC under nitrogen atmosphere and the reaction mixture was stirred for 40 minutes. Then, NaN_3 (0.180 g, 2.75 mmol, 1.6 eq) dissolved in water (5 mL) was added and the mixture was stirred at room temperature for 2 hours. After that, the reaction mixture was extracted with DCM (3 x 30 mL) and the organic layer was dried with $MgSO_4$ and the solvent was evaporated under reduced pressure avoiding completely dryness. The acyl azide was dissolved in anhydrous toluene (76 mL) and benzyl alcohol (0.350 mL, 3.45 mmol, 2 eq) was added under nitrogen atmosphere. The mixture was refluxed for 18 hours. After that, the solvent was evaporated under vaccum and the excess of benzyl alcohol was destilled under vacuum at 110 ºC. The reaction crude was purified by column chromatography over silica gel (EtOAc-hexane 1:3) to obtain orthogonally protected diamine **112** (320 mg, 1 mmol, 55% yield). WARNING: Acyl azides are instable reagents: it is very important not to heat the intermediate product while it is being dried, and the solvent must not be removed until full dryness.

Spectroscopic data for compound 112:

^{1}H NMR (250 MHz, $CDCl_3$): δ 1.45 (s, 9H, ^{t}Bu), 1.50 (m, 2H, H_3, H_4), 2.16 (m, 2H, $H_{3'}$, $H_{4'}$), 3.88 (m, 2H, H_1, H_2), 4.93 (broad, s, 1H, N*H*), 5.10 (m, 2H, CH_{2Cbz}), 5.83 (br. s., 1H, N*H*), 7.37 (m, 5H, H_{Ar}).

Spectroscopic data are consistent with those reported in reference:

Sans, M.; Illa, O.; Ortuño, R.M. *Org. Letters* **2012**, *14*, 2431-2433.

(1*S*,2*S*)-2-(Benzyloxycarbonylamino)cyclobuta-1-amine hydrochloride, 122

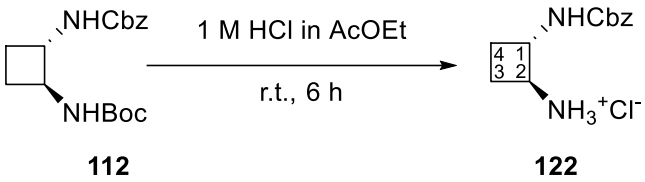

112 **122**

Orthogonally protected diamine **112** (0.230 g, 0.72 mmol) was dissolved in a 1 M HCl solution in EtOAc (15 mL). The reaction was stirred at room temperature during 6 hours. After that, excess of reactants and solvent were removed under vacuum to afford iminium salt **122** (0.180 g, 0.70 mmol, 97 % yield) as a brown oil, which was used in the next step without further purification.

Spectroscopic data for compound 122:

^{1}H NMR (MeOD, 250 MHz) δ 1.80 (m, 2H, H_3, H_4), 2.21 (m, 2H, $H_{3'}$, $H_{4'}$), 3.59 (m, 1H, H_1), 4.10 (m, 1H, H_2), 5.08 (m, 2H, CH_{2Cbz}), 7.33 (m, 5H, H_{ar}).

Spectroscopic data are consistent with those reported in reference:

Sans, M.; *PhD Thesis* **2014** *UAB*.

Dibenzyl ((1*S*,2*S*)-cyclobutane-1,2-diyl)dicarbamate, 123

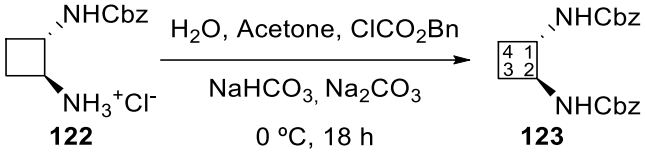

122 **123**

To an ice cooled solution of **122** (0.160 g, 0.73 mmol) in water (30 mL) and acetone (4 mL), $NaHCO_3$ (0.120 g, 1.45 mmol, 2 eq) and Na_2CO_3 (0.230 g, 2.20 mmol, 3 eq) were added. The mixture was stirred until the complete dissolution of the carbonates. Then, benzyl chloroformate (0.2 mL, 1.20 mmol, 1.6 eq) was added and the mixture was stirred at 0 ºC (reaction was monitored by TLC). After 18 h, the reaction was extracted with EtOAc (4x50 mL) and the organic layer was dried over magnesium sulfate. The solvent was removed under vacuum, and the excess of benzyl chloroformate was lyophilized. The residue was purified by column chromatography (2:1 hexane-EtOAc) to afford diprotected amine **123** (0.155 g, 0.44 mmol, 60% yield) as a white solid.

Spectroscopic data for compound 123:

[α]D = -10.0 (c=1.00 in MeOH).

M.p: 70-73 ºC (from EtOAc).

IR (ATR): 3306 (NH_{st}), 2975 (CH_{st}), 1682 (C=O)

^{1}H NMR (400 MHz, $CDCl_3$): δ 1.54 (m, 2H, H_3, H_4), 2.17 (m, 2H, $H_{3'}$, $H_{4'}$), 3.93 (m, 2H, H_1, H_2), 5.11 (m, CH_2-Ph), 5.19 (br. 2H, N*H)*, 7.37 (s, 10H, Ar)

^{13}C NMR (100 MHz, $CDCl_3$): δ 23.5 (C_3, C_4), 53.4 (C_1, C_2), 66.7 (CH_2-Ph), 128.1 (Ar), 128.5 (Ar), 136.3 (Ar), 155.6 (CO).

HRMS: calculated for $C_{24}H_{24}N_2O_6Na$ (M+Na): 377.1472, Found: 377.1466.

Di-*tert*-butyl 2,2'-((1*S*,2*S*)-cyclobutane-1,2-diyl)bis(benzyloxy carbonylazanediyl))diacetate, 125

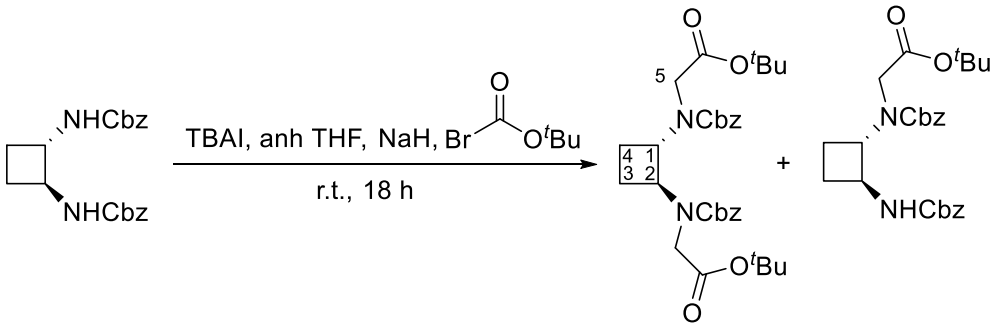

123 **125** **124**

To a solution of anhydrous THF (8 mL) containing previously washed 60% NaH in mineral oil (280 mg, 7 mmol, 10 eq), TBAI (1.55 g, 4.20 mmol, 6 eq) was added under nitrogen atmosphere. At the same time, a solution of anhydrous THF (10 mL) containing diprotected amine **123** (250 mg, 0.70 mmol) under nitrogen atmosphere was prepared. After that, the second solution was added using a cannula to the first one. Finally, AcBr^{t}Bu (0.620 mL, 4.20 mmol, 6 eq) was added ant the mixture was stirred at room temperature for 24 h (reaction was monitored by TLC). Then, the reaction was quenched by adding 10 mL of water and THF was removed under vaccum. Next, more water was added (10 mL) and the crude was extracted with DCM (3 x 30 mL) The organic layer was dried over magnesium sulfate and the solvent was removed under vacuum.

The residue was purified by column chromatography (3:1 hexane-EtOAc) to afford dialkilated diprotected amine **125** (250 mg, 62% yield) as a brown oil. At the same time, monoalkilated diprotected amine **124** (64 mg, 21% yield) was recovered.and used as starting material with similar conditions.

Spectroscopic data for compound 125:

[α]$_D$ = + 2.00 (c=1.02 in MeOH).

IR (ATR): 2978 (CH_{st}), 1743 (C=O), 1709 (C=O).

^{1}H NMR (400 MHz, Chloroform-d) δ 1.27 – 1.52 (m, 18H, ^{t}Bu), 1.52-1.73 (m, 2H, H_3, H_4), 1.94 – 2.13 (m, 2H, $H_{3'}$, $H_{4'}$), 3.68 – 4.18 (m, 4H, H_5), 4.37-4.60 (m, 2H, H_1, H_2), 5.12 (m, 4H, CH_2-Ph), 7.33 (m, 10H, Ar).

HRMS: calculated for $C_{24}H_{24}N_2O_6Na$ (M+Na): 605.2833, Found: 605.2830.

Di-tert-butyl 2,2'-(((1*S*,2*S*)-cyclobutane-1,2-diyl)bis(azanediyl)) diacetate, 126

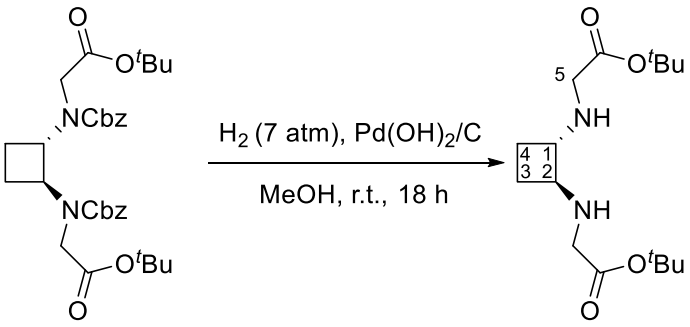

125 **126**

Dialkylated diprotected amine **125** (170 mg, 0.29 mmol) in MeOH (8 mL) was hydrogenated under 7 atmospheres of pressure in the presence of 20% $Pd(OH)_2/C$ (35.0 mg) overnight. The reaction mixture was filtered through Celite® and solvent was removed under vacuum affording the desired dialkylated amine **126** as a yellow oil (92 mg, 0.29 mmol, quantitative yield) which was used in the next step without further purification.

Spectroscopic data for compound 126:

[α]$_D$ = + 24.00 (c=1.02 in MeOH).

IR (ATR): 3331 (NH_{st}), 2978 (CH_{st}), 2936 (CH_{st}), 1733 (C=O).

^{1}H NMR (360 MHz, $CDCl_3$): δ 1.32-1.42 (m, 2H, H_3, H_4), 1.49 (s, 20H, ^{t}Bu), 1.94 – 2.11 (m, 2H, $H_{3'}$, $H_{4'}$), 2.94 – 3.09 (m, 2H, H_1, H_2), 3.34 (s, 4H, H_5).

^{13}C NMR (63 MHz, $CDCl_3$): δ 23.3 (C_3, C_4), 28.4 (CH_3-^{t}Bu), 49.7 (C_5), 61.4 (C_1, C_2), 81.4 (C-^{t}Bu), 172.0 (CO).

HRMS: calculated for $C_{24}H_{24}N_2O_6Na$ (M+Na): 315.2278, Found: 315.2270.

Methyl 6-(chloromethyl)picolinate, 119

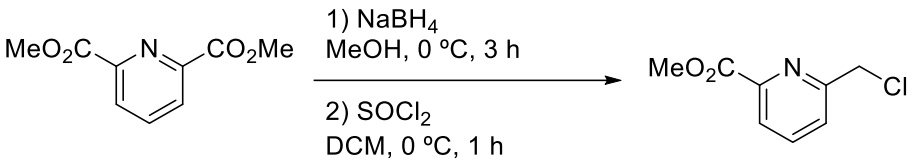

113 **119**

To a stirred solution of **113** (2.5 g, 11.5 mmol) in methanol (100 mL), was added $NaBH_4$ (1.80 g, 47.6 mmol, 4.1 eq) at 0 ºC. The solution was stirred 3 h at 0 ºC and then poured into a saturated $NaHCO_3$ aqueous solution (50 mL). The methanol was evaporated and the resulting aqueous solution was extracted with DCM (4 x 30 mL). The organic layer was dried over magnesium sulfate and evaporated under reduced pressure. The resulting residue (1.40 g, 8.4 mmol) was dissolved in DCM (25 mL), $SOCl_2$ (2.75 mL,37.8 mmol, 4.5 eq) was added at 0 ºC and the mixture was stirre for 1 h at 0ºC. After that, excess of reactants and solvent were removed under vacuum and DCM (30 mL) was added again. The solution was washed with saturated $NaHCO_3$ (2 x 20 mL) and the organic layer was dried over magnesium sulfate and evaporated under reduced pressure. The residue was purified by column chromatography over silica gel (3:1 Hexane-EtOAc) to afford **119** (1.20 g, 6.50 mmol, 57% yield) as a white solid.

Spectroscopic data for compound 119:

^{1}H NMR (360 MHz, $CDCl_3$) δ 4.03 (s, 3H, Me), 4.80 (s, 2H, CH_2), 7.75 (d, *J*= 7.2 Hz, 1H, Ar), 7.92 (t, *J*= 7.2, Hz, 1H, Ar), 8.11 (d, *J*= 7.2 Hz, 1H, Ar).

Spectroscopic data are consistent with those reported in reference:

Sun, Yan-Yan; Yi, Jun; Lu, Xi; Zhang, Zhen-Qi; Xiao, Bin; Fu, Yao. *Chem. Commun*. **2014**, *50*, 11060-11062.

Protected ligand L3, 127

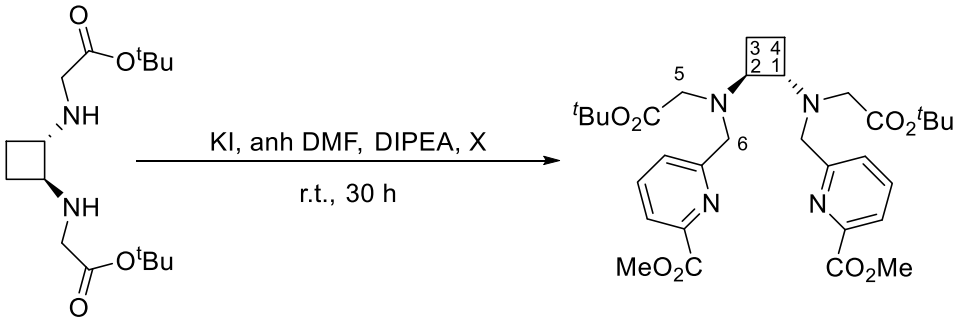

126 **127**

Dialkylated diamine **126** (230 mg, 0.73 mmol), KI (365mg, 2.20 mmol, 1.5 eq) and methyl 6-(chloromethyl)picolinate **119** (300 mg, 1.60 mmol, 1.1 eq) were dissolved in anhydrous DMF (10 mL) under nitrogen atmosphere. After that, DIPEA (0.820 mL, 4.70 mmol, 3.2 eq) was added and the reaction was stirred at room temperature for 30 hours. After that, EtOAc (30 mL) was added and washes with saturated $NaHCO_3$ (3 x 20 mL), brine (3 x 20 mL) and water (1 x 20 mL) were performed. The final organic layer was dried over magnesium sulfate and the solvent was removed under vacuum. The residue was purified by column chromatography over silica gel with a gradient of solvents (3:1 Hexane-EtOAc to 1:1 Hexane-EtOAc) to afford **127** (270 mg, 0.42 mmol, 57% yield) as a brown oil.

Spectroscopic data for compound 127:

[α]$_D$ = + 18.0 (c=1.01 in MeOH).

IR (ATR): 2977 (CH_{st}), 2951 (CH_{st}), 1721 (C=O), 1589 (C=O).

^{1}H NMR (400 MHz, $CDCl_3$): 1.39 (s, 18H, ^{t}Bu), 1.41-1.50 (m, 2H, H_{4R}, H_{3S}), 1.73 – 1.89 (m, 2H, H_{4S}, H_{3R}), 3.25 (s, 4H, H_5), 3.41 (m, 2H, H_1, H_2), 3.98 (s, 6H, Me), 4.05 (s, 4H, H_6), 7.73 (m, 2H, Ar), 7.86 (m, 2H, Ar), 7.96 (m, 2H, Ar).

^{13}C NMR (100 MHz, $CDCl_3$): δ 19.3 (C_3, C_4), 28.1 (CH_3-^{t}Bu), 52.8 (CH_3), 53.8 (C_5), 57.0 (C_6), 62.6 (C_1, C_2), 80.8 (C-^{t}Bu), 123.4 (Ar), 126.2 (Ar), 137.2 (Ar), 147.1 (Ar), 161.3 (Ar), 165.9 (CO), 170.8 (CO).

HRMS: calculated for $C_{24}H_{24}N_2O_6Na$ (M+Na): 613.3232, Found: 613.3231.

Ligand L3

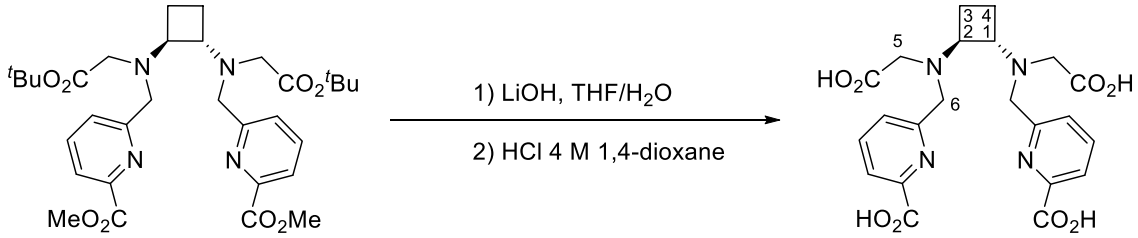

X **X**

Compound **127** (150 mg, 0.245 mmol) was dissolved in THF/H_2O (1:1, 5 mL), LiOH (31.0 mg, 0.740 mmol, 3 eq) was added and the reaction mixture was stirred at room temperature for 4 h. Then, the mixture was concentrated to dryness under reduced pressure and the resultant residue was dissolved in 4 M HCl in dioxane (3 mL) and stirred at room temperature for 18 h. Then, the solvent was evaporated under reduced pressure. A small amount of water (3 mL) was added and the mixture was evaporated to dryness. This process was repeated twice with water and twice with the addition of diethyl ether (3 mL) to afford. **L3·2HCl** (100 mg, 0.184 mmol, 75% yield) as a brown solid without need of further purification.

Spectroscopic data for compound L3:

[α]$_D$ = + 36.00 (c=1.00 in H_2O).

IR (ATR): 3377 (OH_{st}), 2945 (CH_{st}), 1720 (C=O), 1616 (C=O).

^{1}H NMR (400 MHz, D_2O): δ 1.72-1.82 (m, 2H, H_{4R}, H_{3S}), 2.04 – 2.17 (m, 2H, H_{4S}, H_{3R}), 3.71-3.91 (m, 4H, H_5), 4.16 (m, 2H, H_1, H_2), 4.46 (s, 4H, H_6), 7.76 (m, 2H, Ar), 8.04 (m, 2H, Ar), 8.17 (m, 2H, Ar).

^{13}C NMR (100 MHz, D_2O): δ 17.7 (C_3, C_4), 52.1 (C_5), 55.1 (C_6), 51.5 (C_1, C_2), 125.9 (Ar), 128.7 (Ar), 143.8 (Ar), 144.2 (Ar), 152. (Ar), 164. (CO), 171. (CO).

HRMS: calculated for $C_{24}H_{24}N_2O_6Na$ (M+Na): 495.1486, Found: 495.1478.

7.15 Solid Phase Synthesis

7.15.1 γ-CC / γ-CT Families

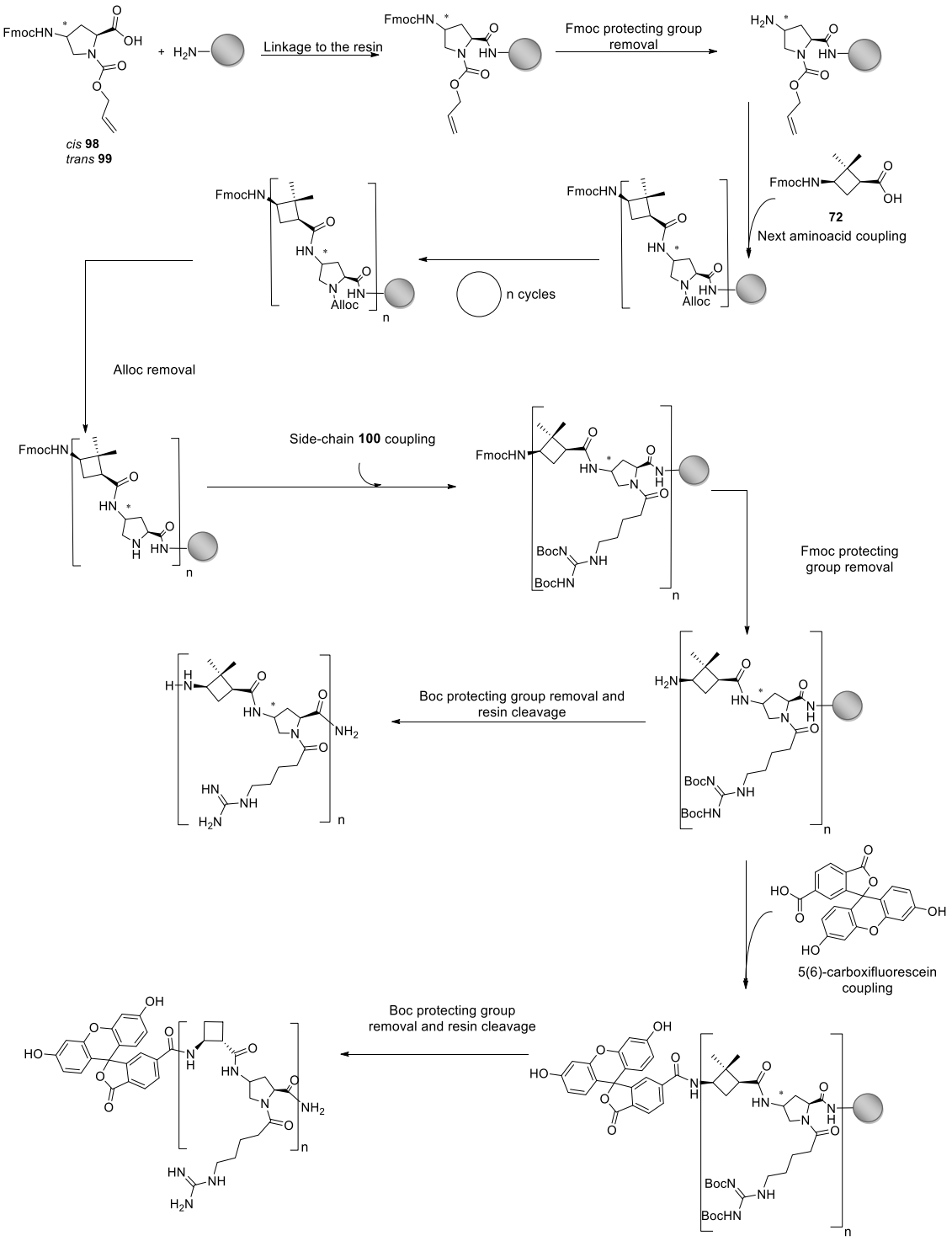

Scheme 27. Followed solid phase synthesis protocol.

Resin H-rink amide ChemMatrix® with 0.47 mmol/g functionalization, previously conditioned by several washes with DMF and DCM. The synthesis of both hybrid peptides and TAT_{58-57} was performed by using the Fmoc/Alloc strategy, although monomers for TAT_{48-57} contained other protecting groups. The protocol is summarized in Table 9.

Table 9. General protocol for the solid phase synthesis of Hybrid γ-CBAA,*cis*- or *trans*-γ-amino-L-proline peptides, by Fmoc/Alloc strategy.

Step	Reagents /Solvents	Aim	Cycles	t/cycle (min)
1	DCM	Wash	5	1
2	DMF	Wash	5	1
3	(2*SS*,4*SR*)-Fmoc-amino-proline/DIC/OxymaPure® (2.5:2.5:2.5) in DMF	Coupling	1	120
4	DMF	Wash	5	1
5	DCM	Wash	5	1
6	Ninhydrine test (-)	Coupling test	1	3
7	Piperidine/DMF (2:8, v/v)	Deprotection	3	10
8	DMF	Wash	5	1
9	DCM	Wash	5	1
10	Ninhydrine test (+)	Deprotection test	1	3
11	DMF	Wash	5	1
12	(1*S*,3*R*)-Fmoc-amino-cyclobuthane/OxymaPure®/PyBOP/ DIPEA (2.5:2.5:2.5:5) in DMF	Coupling	1	120
13	DMF	Wash	5	1
14	DCM	Wash	5	1
15	Ninhydrine test (-)	Coupling test	1	3
16	Piperidine/DMF (2:8, v/v)	Wash	3	10
17	DMF	Wash	5	1
18	DCM	Wash	5	1
19	Ninhydrine test (+)	Deprotection test	1	3

Steps from 1 to 19 were repeated n number of times in order to obtain the desired peptide longitude. N = 3 to 7 for each respectively. By the time the desired peptide was obtained, 200 mg of resin were separated for further reactions.

Once the peptide skeleton was prepared, the derivatization of the γ-amino function was performed. First of all, the Alloc protecting groups were removed by a catalytic reduction using palladium and then the guanidilated lateral chain, previously synthesized in solution, was incorporated using OxymaPure® as coupling agent. After that, the Fmoc group of the final residue was eliminated (Table 10).

Table 10. General protocol for the solid phase synthesis of the derivatization of the α-amine function.

Step	Reagents /Solvents	Aim	Cycles	t/cycle (min)
1	DCM	Wash	5	1
2	$PhSiH_3$/$Pd(PPh_3)_4$ (12:0.1) in DCM	Deprotection	2	15
3	DCM	Wash	5	1
4	DMF	Wash	5	1
5	$(Et)_2NCSSNa{\cdot}3H_2O$ (20 mM in DMF)	Palladium Wash	5	1
6	DMF	Wash	5	1
7	DCM	Wash	5	1
8	Chloranil (+)	Deprotection test	1	3
9	DMF	Wash	5	1
10	Product **100** /DIC/OxymaPure® (2.5:2.5:2.5) for each proline in DMF	Coupling	1	120
11	DMF	Wash	5	1
12	DCM	Wash	5	1
13	Chloranil (-)	Coupling test	1	3
14	Piperidine/DMF (2:8, v/v)	Deprotection	3	10
15	DMF	Wash	5	1
16	DCM	Wash	5	1
17	Ninhydrine test (+)	Deprotection test	1	3

Once the functionalization of the α-amine is finished, the resin including each peptide was divided in two parts. Half of it was used to obtain the free amine peptides and the other part was used to proceed with the incorporation of the 5(6)-carboxyfluoroscein in the *N*-terminal group (Table 11).

Table 11. General protocol for the incorporation of the 5(6)-carboxyfluorescein.

Step	Reagents /Solvents	Aim	Cycles	t/cycle (min)
1	DMF	Wash	5	1
2	CF/ OxymaPure®/PyBOP/DIPEA (4:6:4:6) in DMF	Coupling	1	120
3	DMF	Wash	5	1
4	DCM	Wash	5	1
5	Ninhydrine test (-)	Deprotection test	1	3
6	TFA/(^{i}Pr)$_3$SiH/H_2O (95:2.5:2.5)	Deprotection / Resin cleavage	1	120
7	DCM	Wash	5	1

7.15.2 $Tat_{48\text{-}57}$ and $Tat_{48\text{-}57}$-CF Peptide Synthesis

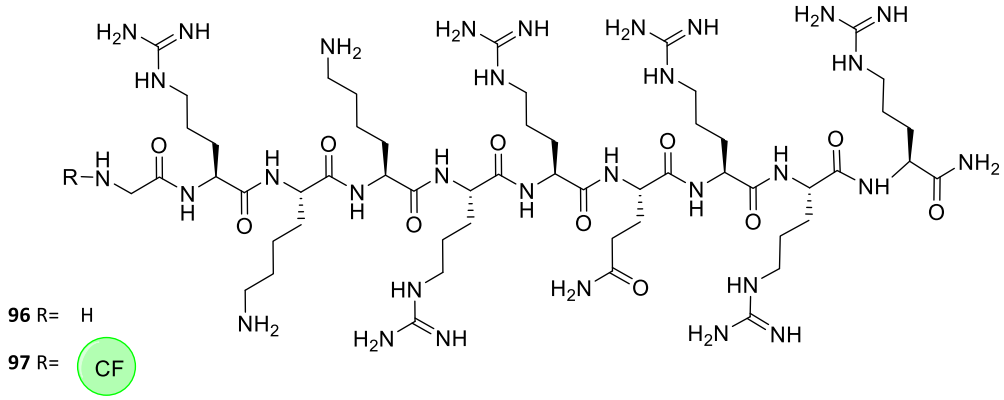

H-Rink amide-ChemMatrix® resin with 0.49 mmol/g functionalization was used. It was conditioned with successive washes with DMF and DCM. The used amino acids are protected in the N^{α} function as Fmoc and the side chains as follows: Arg (R) with (Pbf), Gln (Q) with Trt, and Lys (K) with Boc (Figure 82). The protocol of the synthesis is summarized in Table 12.

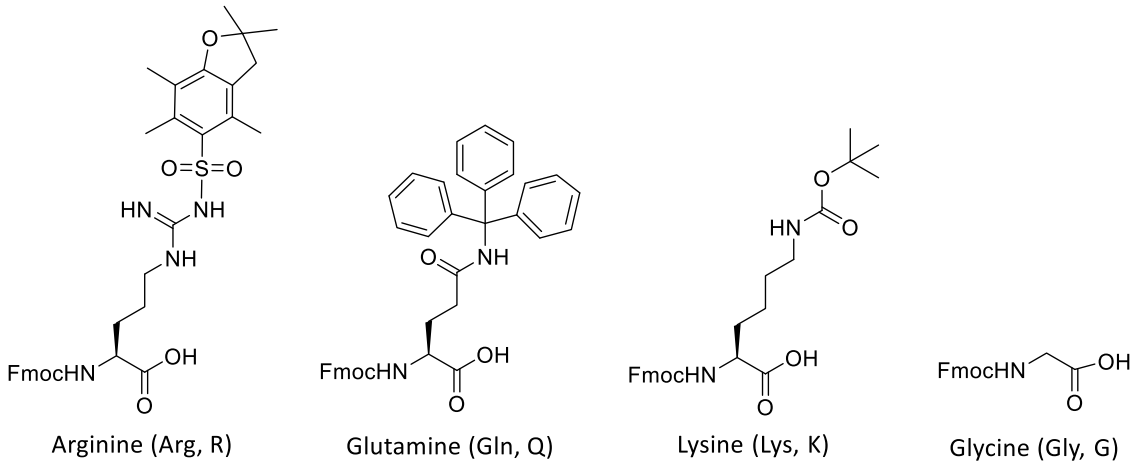

Figure 83. Protecting groups used in the synthesis of Tat_{48-57}

Table 12. General protocol for the preparation of Tat_{48-57} and Tat_{48-57}CF.

Step	Reagents /Solvents	Aim	Cycles	t/cycle (min)
1	DCM	Wash	5	1
2	DMF	Wash	5	1
3	Fmoc-L-Arg(Pbf)-OH(**R**)/OxymaPure®/DIC (3:3:3) in DMF	Coupling	1	120
4	DMF	Wash	5	1
5	DCM	Wash	5	1
6	Ninhydrine test (-)	Coupling test	1	3
7	Piperidine/DMF (2:8, v/v)	Deprotection	3	10
8	DMF	Wash	5	1
9	DCM	Wash	5	1
10	Ninhydrine test (+)	Deprotection test	1	3
11	DMF	Wash	5	1
12	Fmoc-L-Gln(Trt)-OH(**Q**)/OxymaPure®/ DIC (3:3:3) in DMF	Coupling	1	120
13	DMF	Wash	5	1
14	Fmoc-L-Lys(Boc)-OH(**K**)/OxymaPure®/ DIC (3:3:3) in DMF	Coupling	1	120
15	DMF	Wash	5	1
16	Fmoc-Gly-OH(**G**)/OxymaPure®/ DIC (3:3:3) in DMF	Coupling	1	120
Sequence: Steps 1-11 (twice), 1-13 (once), 5-10 (once), 2-10 (twice), 13-14 (once), 5-10 (once), 13-14 (once), 5-10 (once), 2-10 (once), 15-16 (once).				

Once the desired length peptide were prepared and functionalized, the resin was divided into two parts. The first one was left as amino free and the other was coupled to carboxyfluorescein (CF) through the terminal amino group (see Protocol in Table 11)

7.15.3 Cleaveage from the Aminomethyl-ChemMatrix® resin and protecting groups' removal: acid hydrolysis

The cleavage of the peptide from the resin were carried out through acid hydrolysis using TFA/TIS/H_2O (95:2.5:2.5) during 3 hours and stirring. The peptide were separated from the resin through filtration. The solid were washed with DCM (4x). The solution was concentrated under vacuum but not until dryness. Then, the peptide were precipitated through addition of cold Et_2O. The solid were filtered and centrifuged with Et_2O (3x). The resulting solid were dissolved in ACN:H_2O (1:1, v/v) and lyophilized.

7.15.4 Peptide conjugation with Doxorubicin

Once the peptides were studied in both *Leishmania* parasites and *HeLa* cells, the best ones were chosen to be conjugated with Doxorubicin. The peptides structure were reached by following the protocol in Tables 9, 10 and 12. Then the primary chain was elongated with a Cys(Trt) residue, that was protected by an acetyl group (protocol described in Table 13).

Table 13. Protocol for the elongation of peptides with a Cys residue.

Step	Reagents /Solvents	Aim	Cycles	t/cycle (min)
1	DCM	Wash	5	1
2	DMF	Wash	5	1
3	Fmoc-L-Cys(Trt)-OH(**C**)/OxymaPure®/DIC (3:3:3) in DMF	Coupling	1	120
4	DMF	Wash	5	1
5	DCM	Wash	5	1
6	Ninhydrine test (-)	Coupling test	1	3
7	Piperidine/DMF (2:8, v/v)	Deprotection	3	10
8	DMF	Wash	5	1
9	DCM	Wash	5	1
10	Ninhydrine test (+)	Deprotection test	1	3
9	DMF	Wash	5	1
11	Ac_2O, DIPEA (5:5) in DMF	Protection of NH_2	1	100
13	DMF	Wash	5	1
14	DCM	Wash	5	1
15	Ninhydrine test (-)	Coupling test	1	3
16	Piperidine/DMF (2:8, v/v)	Wash	3	10
17	DMF	Wash	5	1
18	DCM	Wash	5	1
19	Ninhydrine test (+)	Deprotection test	1	3

7.15.5 Synthesis of Doxorubicin-MCC

Doxorubicin HCl salt (3 mg, 5.17 µmols, 1.0 equiv), SMCC (2.1 mg, 6.60 µmols, 1.2 equiv) and DIPEA (5 µL, 7.75 µmols, 1.5 equiv) were added to DMF (450 µL) in a 2 mL round-bottomed flask. The reaction was allowed to run in the dark at room temperature. The reaction was followed by RP-HPLC-MS. After 1.5 h, 450 µL of PBS were added and the pH was lowered to 6-7 with 1 M HCl.

7.15.6 Coupling between Doxorubicin-MCC and Cysteine elongated peptides

1.2 equivalents of the desired peptide were added to the previous reaction mixture and the reaction time was determined by RP-HPLC-MS. After the reaction, the crude was immediately purified by RP-HPLC.

7.16 Peptide purification and characterization

The peptide crudes were purified using a system of high resolution liquid chromatography at semi-preparative scale coupled to a mass spectrometer with a reverse phase column C_{18} (Section 7.4.2.2).

Dodecamer NH_2 79:

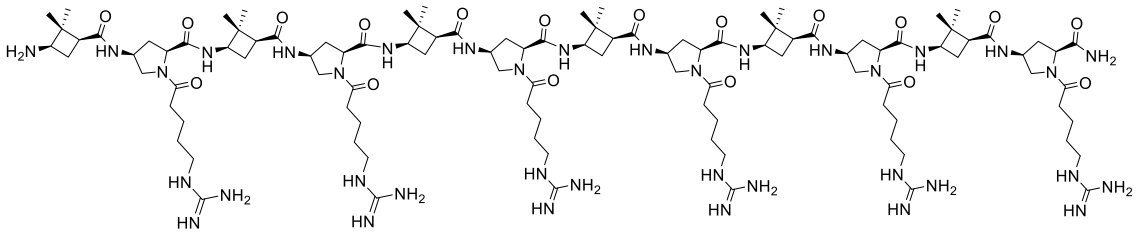

The peptide crude was purified by RP-HPLC-MS semiprep. Gradient: from 7% to 10% of CH_3CN/HCOOH in 7 minutes; from 10% to 100% of CH_3CN/HCOOH in 0.5 minutes (maintained for 2 minutes); finally initial conditions were reached in 0.5 minutes. The purified peptide was characterized by RP-HPLC and RP-HPLC-MS. The peptide **79** was more than 95% pure with a retention time of 6.0 minutes. **m/z (ESI)**: M+5/5 = 458.5 M+6/6 = 382.3, M+7/7 = 327.8.

Dodecamer CF 83:

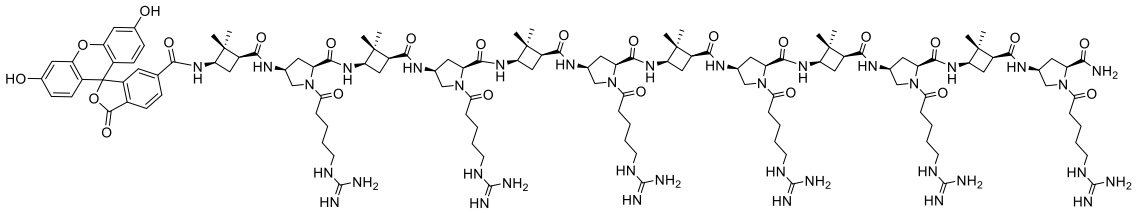

The peptide crude was purified by RP-HPLC-MS semiprep. Gradient: from 10% to 20% of CH_3CN/HCOOH in 7 minutes; from 20% to 100% of CH_3CN/HCOOH in 0.5 minutes (maintained for 2 minutes); finally initial conditions were reached in 0.5 minutes. The purified peptide was characterized by RP-HPLC and RP-HPLC-MS. The peptide **83** was more than 95% pure with a retention time of 7.7 minutes. **m/z (ESI)**: M+5/5 = 530.3 M+6/6 = 442.0, M+7/7 = 379.0.

Tetradecamer NH_2 90:

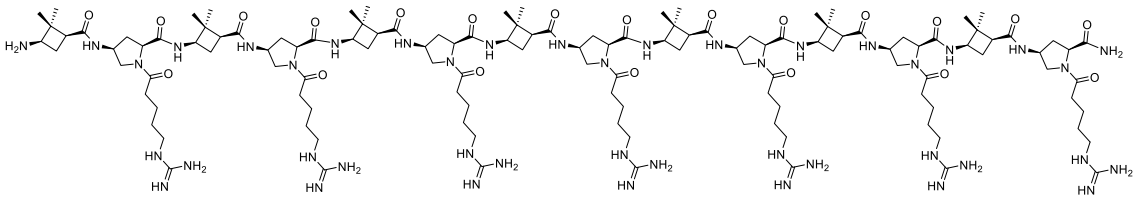

The peptide crude was purified by RP-HPLC-MS semiprep. Gradient: from 5% to 12% of CH_3CN/HCOOH in 7 minutes; from 12% to 100% of CH_3CN/HCOOH in 0.5 minutes (maintained for 2 minutes); finally initial conditions were reached in 0.5 minutes. The purified peptide was characterized by RP-HPLC and RP-HPLC-MS. The peptide **90** was more than 97% pure with a retention time of 6.2 minutes. **m/z (ESI)**: M+6/6 = 445.4 M+7/7 = 381.9, M+8/8 = 334.3.

Tetradecamer CF 91:

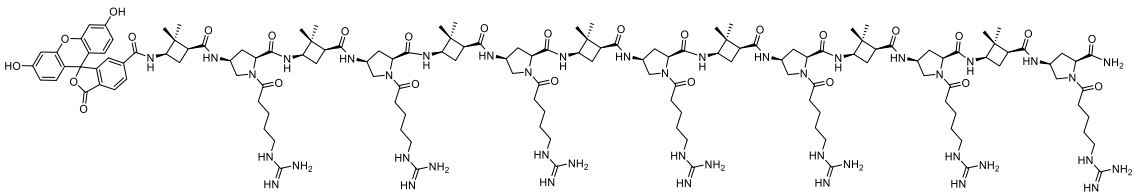

The peptide crude was purified by RP-HPLC-MS semiprep. Gradient: from 12% to 20% of CH_3CN/HCOOH in 7 minutes; from 20% to 100% of CH_3CN/HCOOH in 0.5 minutes (maintained for 2 minutes); finally initial conditions were reached in 0.5 minutes. The purified peptide was characterized by RP-HPLC and RP-HPLC-MS. The peptide **91** was more than 98% pure with a retention time of 5.1 minutes. **m/z (ESI)**: M+6/6 = 505.1 M+7/7 = 433.1, M+8/8 = 379.0.

Dodedecamer NH_2 92:

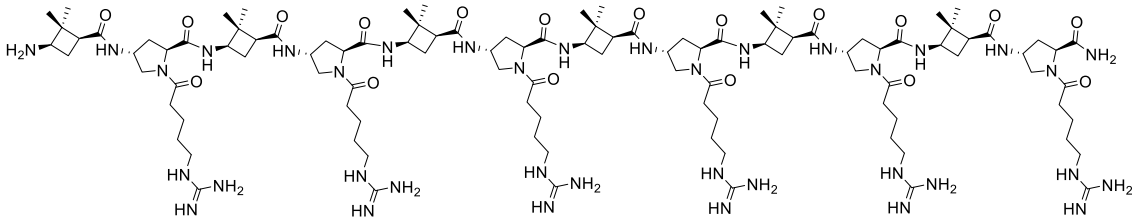

The peptide crude was purified by RP-HPLC-MS semiprep. Gradient: from 7% to 10% of CH_3CN/HCOOH in 7 minutes; from 10% to 100% of CH_3CN/HCOOH in 0.5 minutes (maintained for 2 minutes); finally initial conditions were reached in 0.5 minutes. The purified peptide was characterized by RP-HPLC and RP-HPLC-MS. The peptide **92** was more than 96% pure with a retention time of 5.8 minutes. **m/z (ESI)**: M+5/5 = 458.5 M+6/6 = 382.3, M+7/7 = 327.8.

Dodecamer CF 94:

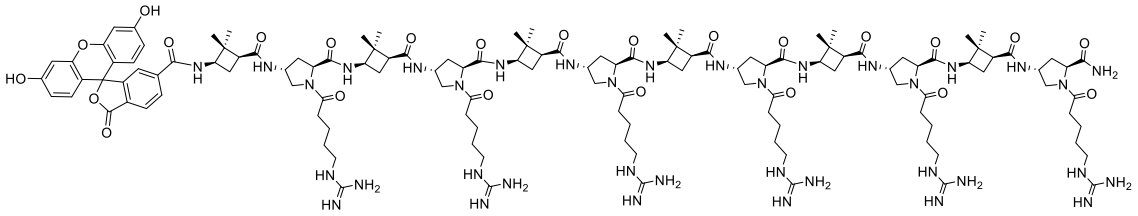

The peptide crude was purified by RP-HPLC-MS semiprep. Gradient: from 10% to 20% of CH_3CN/HCOOH in 7 minutes; from 20% to 100% of CH_3CN/HCOOH in 0.5 minutes (maintained for 2 minutes); finally initial conditions were reached in 0.5 minutes. The purified peptide was characterized by RP-HPLC and RP-HPLC-MS. The peptide **94** was more than 97% pure with a retention time of 7.4 minutes. **m/z (ESI)**: M+5/5 = 530.3 M+6/6 = 442.0, M+7/7 = 379.0.

Tetradecamer NH_2 93:

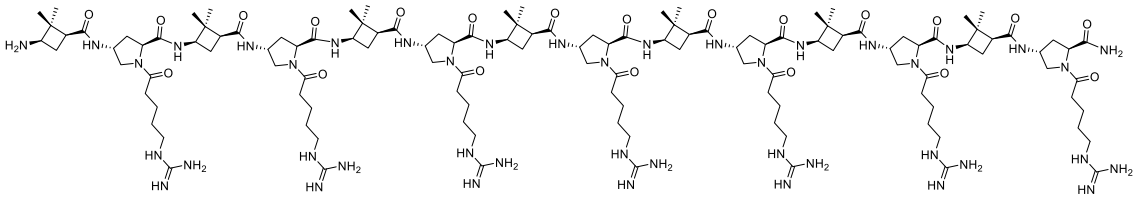

The peptide crude was purified by RP-HPLC-MS semiprep. Gradient: from 5% to 12% of CH_3CN/HCOOH in 7 minutes; from 12% to 100% of CH_3CN/HCOOH in 0.5 minutes (maintained for 2 minutes); finally initial conditions were reached in 0.5 minutes. The purified peptide was characterized by RP-HPLC and RP-HPLC-MS. The peptide **93** was more than 96% pure with a retention time of 5.9 minutes. **m/z (ESI)**: M+6/6 = 445.4 M+7/7 = 381.9, M+8/8 = 334.3.

Tetradecamer CF 95:

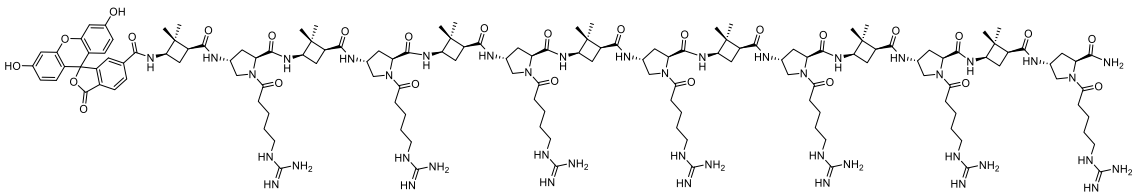

The peptide crude was purified by RP-HPLC-MS semiprep. Gradient: from 12% to 20% of CH_3CN/HCOOH in 7 minutes; from 20% to 100% of CH_3CN/HCOOH in 0.5 minutes (maintained for 2 minutes); finally initial conditions were reached in 0.5 minutes. The purified peptide was characterized by RP-HPLC and RP-HPLC-MS. The peptide **95** was more than 99% pure with a retention time of 7.9 minutes. **m/z (ESI)**: M+6/6 = 505.1 M+7/7 = 433.1, M+8/8 = 379.0.

$TAT_{48\text{-}57}$ 96:

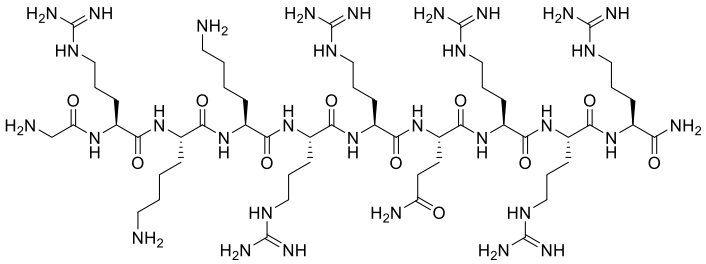

The peptide crude was purified by RP-HPLC-MS semiprep. Gradient: 0% of CH_3CN/HCOOH for 4 minutes, from 0% to 4% of CH_3CN/HCOOH in 3 minutes; from 4% to 100% of CH3CN/HCOOH in 0.5 minutes (maintained for 2 minutes); finally initial conditions were reached in 0.5 minutes. The purified peptide was characterized by RP-HPLC and RP-HPLC-MS. The peptide **96** was more than 97% pure with a retention time of 4.6 minutes. **m/z (ESI)**: M+4/4 = 349.9, M+5/5 = 280.0, M+6/6 = 233.5.

$TAT_{48\text{-}57}$ CF 97:

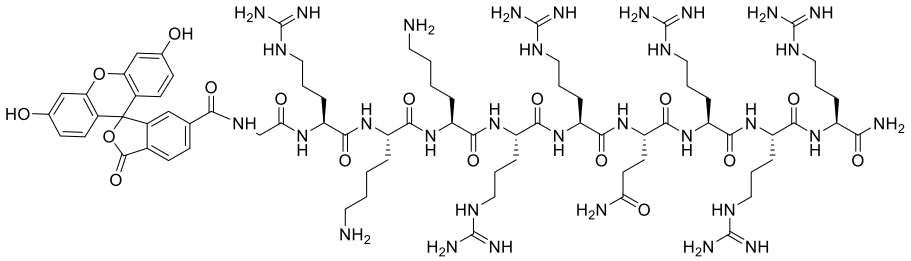

The peptide crude was purified by RP-HPLC-MS semiprep. Gradient: from 0% to 7% of CH_3CN/HCOOH in 7 minutes; from 7% to 100% of CH_3CN/HCOOH in 0.5 minutes (maintained for 2 minutes); finally initial conditions were reached in 0.5 minutes. The purified peptides was characterized by RP-HPLC and RP-HPLC-MS. The peptide **97** was more than 99% pure with a retention time of 6.9 minutes. **m/z (ESI)**: M+4/4 = 439.4, M+5/5 = 351.8, M+6/6 = 293.2.

Tetradecamer Cys-MCC-DOXO 108:

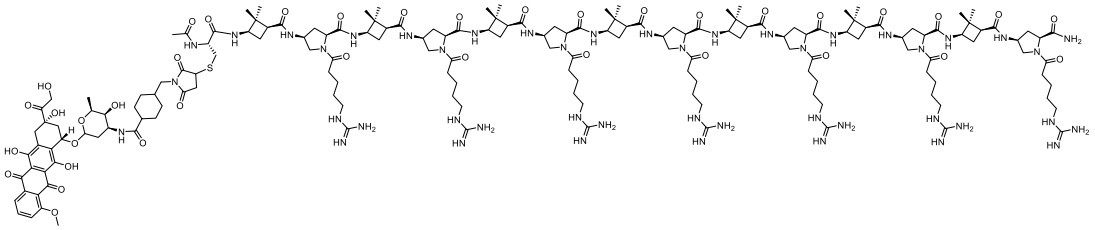

The peptide crude containing the cysteine elongated peptides was purified by RP-HPLC-MS semiprep. Gradient: from 5% to 12% of CH_3CN/HCOOH in 7 minutes; from 12% to 100% of CH_3CN/HCOOH in 0.5 minutes (maintained for 2 minutes); finally initial conditions were reached in 0.5 minutes. After that, the peptide was coupled to the DOXO-MCC using the procedure described in section 7.15.6. The purification of the peptide was performed using RP-HPLC with a gradient: from 0% to 50% of CH_3CN/HCOOH in 11 minutes, from 50% to 100% of CH_3CN/HCOOH in 0.5 minutes (maintained for 2 minutes); finally initial conditions were reached in 0.5 minutes. The purified peptide was characterized by RP-HPLC and RP-HPLC-MS. The peptide **108** was more than 95% pure with a retention time of 8.9 minutes. **m/z (ESI)**: M+4/4 = 894.1 M+5/5 = 715.7, M+6/6 = 596.8.

Tetradecamer Cys-MCC-DOXO γ 109:

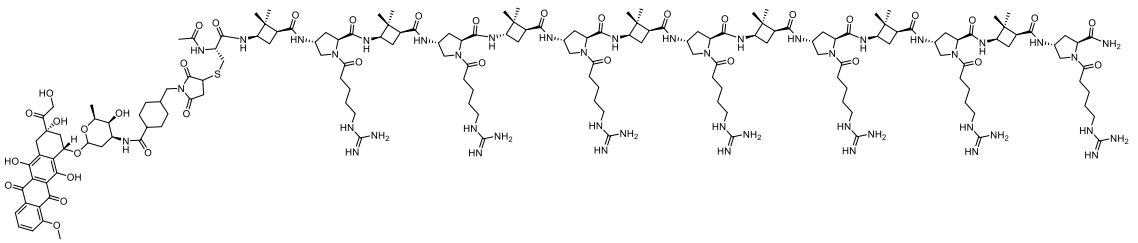

The peptide crude containing the cysteine elongated peptides was purified by RP-HPLC-MS semiprep. Gradient: from 5% to 12% of CH_3CN/HCOOH in 7 minutes; from 12% to 100% of CH_3CN/HCOOH in 0.5 minutes (maintained for 2 minutes); finally initial conditions were reached in 0.5 minutes. After that, the peptide was coupled to the DOXO-MCC using the procedure described in section 7.15.6. The purification of the peptide was performed using RP-HPLC with a gradient: from 0% to 50% of CH_3CN/HCOOH in 11 minutes, from 50% to 100% of CH_3CN/HCOOH in 0.5 minutes (maintained for 2 minutes); finally initial conditions were reached in 0.5 minutes. The purified peptide was characterized by RP-HPLC and RP-HPLC-MS. The peptide **109** was more than 95% pure with a retention time of 9.0 minutes. **m/z (ESI)**: M+5/5 = 715.7, M+6/6 = 596.7, M+7/7 = 511.5.

$TAT_{48\text{-}57}$ Cys-MCC-DOXO, 110:

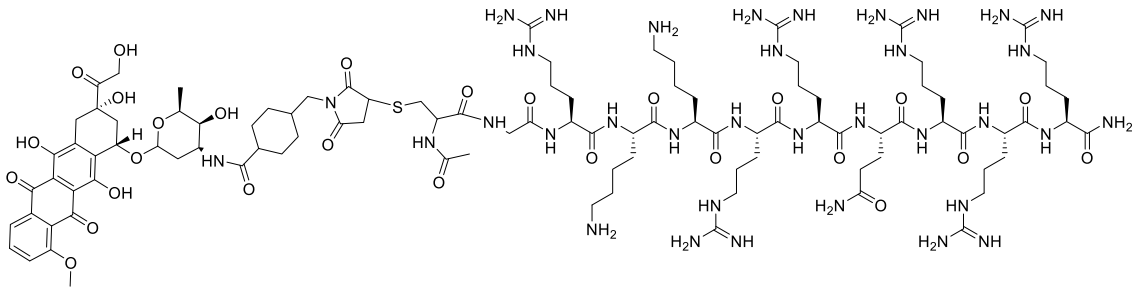

The peptide crude was purified by RP-HPLC-MS semiprep. Gradient: 0% of CH_3CN/HCOOH for 4 minutes, from 0% to 4% of CH_3CN/HCOOH in 3 minutes; from 4% to 100% of CH3CN/HCOOH in 0.5 minutes (maintained for 2 minutes); finally initial conditions were reached in 0.5 minutes. After that, the peptide was coupled to the DOXO-MCC using the procedure described in section 7.15.6.

The purification of the peptide was performed using RP-HPLC with a gradient: from 0% to 50% of CH_3CN/HCOOH in 11 minutes, from 50% to 100% of CH_3CN/HCOOH in 0.5 minutes (maintained for 2 minutes); finally initial conditions were reached in 0.5 minutes. The purified peptide was characterized by RP-HPLC and RP-HPLC-MS. The peptide **110** was more than 93% pure with a retention time of 8.8 minutes. **m/z (ESI)**: M+3/3 = 768.7, M+4/4 = 576.8, M+5/5 = 461.6.

8. Bibliography

[1] Izquierdo, S.; Rúa, F.; Sbai, A.; Parella, T.; Álvarez-Larena, A.; Branchadell, V.; Ortuño, R.M. (+)- and (-)-2-Aminocyclobutane-1-carboxylic Acids and Their Incorporation Into Highly Rigid β-peptides: Stereoselective Synthesis and a Structural Study. *J. Org. Chem.* **2005**, *70*, 7963-7971.

[2] Sans, M.; Illa, O.; Ortuño, R.M. Stereoselective Synthesis of All Stereiosiomers of Orthogonally Protected Cyclobutane-1,2-Diamine and Some Chemeoselective Tranformations. *Org. Lett.* **2012**, *14*, 2431-2433.

[3] Aguilera, J.; Moglioni, A.G.; Moltrasio, G.Y.; Ortuño, R.M. Stereodivergent and efficient synthesis of the first bis(cyclobutane) gamma-dipeptides and mixed gamma-oligomers. *Tetrahedron: Asymmetry* **2008**, *19*, 302-308.

[4] Yang, H.; Xiang, J.; Wang, N.; Zhao, Y.; Hyman, J.; Li, S.; Jiang, J.; Chen, J.K.; Yang, Z.; Lin, S. Converse Conformational Control of Smoothened Activity by Structurally Related Small Molecules. *J. Biol Chem*. **2009**, *284*, 201876-20884.

[5] Lawson, A. D. G. Antibody-Enabled Small-Molecule Drug Discovery. *Nat. Rev. Drug Discov.* **2012**, *11*, 519-525.

[6] *Small Molecule Medicinal Chemistry*; Czechtizky, W., Hamley, P.; John Wiley & Sons, 2015.

[7] Fernández, D.; Torres, E.; Avilés, F. X.; Ortuño, R.M.; Vendrell, J. Cyclobutane-Containing Peptides: Evaluation as Novel Metallocarboxypeptidase Inhibitors and Modelling of Their Mode of Action. *Bioorganic Med. Chem*. **2009**, *17*, 3824-3828.

[8] Mayans, E.; Gargallo, A.; Álvarez-Larena, Á.; Illa, O.; Ortuño, R.M. Diastereodivergent Synthesis of Chiral Vic-Disubstituted-Cyclobutane Scaffolds:1,3-Amino Alcohol and 1,3-Diamine Derivatives – Preliminary Use in Organocatalysis. Eur. *J. Org. Chem*. **2013**, *8*, 1425-1433.

[9] Sans, M.; Illa, O.; Ortuño, R.M. Organobridged Silsesquioxanes Based on Cyclobutane Diamines: Influence of the Stereochemistry on the Morphology of the Materials. *Tetrahedron* **2016**, *72*, 2913-2919.

[10] Celis, S.; Nolis, P.; Illa, O.; Branchadell, V.; Ortuño, R.M. Low-molecular-weight Gelators Consisting of Hybrid Cyclobutane-based Peptides. *Org. Biomol. Chem*. **2013**, *11*, 2839-2846.

[11] Sorrenti, A.; Illa, O.; Ortuño, R. M.; Pons R. Chiral Cyclobutane β-Amino Acid-Based Amphiphiles: Influence of cis/trans Stereochemistry on Condensed Phase and Monolayer Structure. *Langmuir* **2016**, *32*, 6977-6984.

[12] Pi-Boleda, B.; Sorrenti, A.; Sans, M.; Illa, O.; Pons, R.; Branchadell, V.; Ortuño, R.M. *Cyclobutane* Scaffold in Bolaamphiphiles: Effect of Diastereoisomerism and Regiochemistry on Their Surface Activity Aggregate Structure. *Langmuir* **2018**, 10.1021/acs.langmuir.8b01462.

[13] Aguilera, J.; Favier, I.; Sans, M.; Mor, À.; Álvarez-Larena, Á.; Illa, O.; Gómez, M.; Ortuño, R. M. Synthesis of chiral functionalised-cyclobutyl pyrrolidines and amino alcohols from (-)-(*S*)-verbenone. Applications in the stabilisation of ruthenium nanocatalysts. *Eur. J. Org. Chem*. **2015**, 810-819.

[14] Ospina, J.; Sorrenti, A.; Illa, O.; Pons, R.; Ortuño, R.M. New Chiral Polyfunctional Cyclobutane Derivatives from (-)-Verbenone: Possible Surfactant Behaviour. *Tetrahedron: Asymmetry* **2013**, *24*, 713-718.

[15] Illa, O.; Porcar-Tost, O.; Robledillo, C.; Elvira, C.; Nolis, P.; Reiser, O.; Branchadell, V.; Ortuño, R.M. Stereoselectivity of Proline/Cyclobutane Amino-Acid Containing Peptide Organocatalyst for Asymmetric Aldol Additions: A Rationale. *J. Org. Chem.* **2018**, *83*, 350-363.

[16] Gutiérrez-Abad, R.; Illa, O.; Ortuño, R.M. Synthesis of Chiral Cyclobutane Containing *C*3-Symmetric Peptide Dendrimers. *Org. Lett*. **2010**, *12*, 3148-3151.

[17] Chang, Y.S.; Graves, B.; Guerlavais, V.; Tovar, C.; Packman, K.; To, K.H.; Olson, K.A.; Kesavan, K.; Gangurde, P.; Mukherjee, A.; Baker, T.; Darlak, K.; Elkin, C.; Filipovic, Z.; Qureshi, F.Z.; Cai, H.; Berry, P.; Feyfant, E.; Shi, X.E.; Horstick, J.; Annis, D.A.; Manning, A.M.; Fotouhi, N.; Nash, H.; Vassilev, L.T.;

Sawyer, T.K. Stapled a-helical Peptide Drug Development: A Potent Dual Inhibitor of MDM2 and MDMX for p53-Dependent Cancer Therapy. *Proc. Natl. Acad. Sci. U.S.A* **2013**, *110*, E3445-54.

[18] Bock, J.E.; Gavenonis, J.; Kritzer, J.A. Getting in Shape: Controlling Peptide Bioactivity and Bioavailability using Conformational Constraints. *ACS Chem. Biol.* **2013**, *8*, 488−499.

[19] Di, L. Strategic Approaches to Optimizin Peptide ADME Properties. *The AAPS Journal* **2015**, *17*, 134-143.

[20] Tsomaia, N. Peptide Therapeutics: Targeting the Undruggable Space. *Eur. J. Med. Chem.* **2015**, *94*, 459-470.

[21] Seebach, D.; Matthews, J.L. β-Peptides: a Surprise at Every Turn. *Chem. Commun.* **1997**, 2015-2022.

[22] Gellman, S.H. Foldamers: A Manifesto. *Acc. Chem. Res.* **1998**, *31*, 173–180.

[23] Guichard, G.; Huc, I. Synthetic Foldamers. *Chem. Commun.* **2011**, *47*, 5933–5941.

[24] *Organic Foldamers and Helices in Supramolecular Chemistry: From Molecules to Nanomaterials*. Huc, I.; Jiang, H. Edited by P. A. Gale and J.W. Steed, John Wiley & Sons 2012, *5*, 2183-2206.

[25] Martinek, T.A.; Fülöp, F. Peptidic Foldamers: Ramping up Diversity. *Chem. Soc. Rev.* **2012**, *41*, 687–702.

[26] Cheng, R.P.; Gellman, S.H.; DeGrado, W.F. β-Peptides: From Structure to Function. *Chem. Rev.* **2001**, *101*, 3219–3232.

[27] Martinek, T.A.; Fülöp, F. Side-chain Control of β-Peptide Secondary Structures. *Eur. J. Biochem.* **2003**, *270*, 3657-3666.

[28] Seebach, D.; Hook, D.F.; Glättli, A. Helices and other Secondary Structures of Beta- and Gamma-Peptides. *Biopolymers* **2006**, *84*, 23–37.

[29] Epand, R.F; Umezawa, N.; Porter, E.A.; Gellman, S.H.; Epand, R.M. Interactions of the Antimicrobial β-Peptide β-17 with phospholipid vesicles differ from membrane interactions of magainins. *Eur. J. Biochem.* **2003**, *270*, 1240-1248.

[30] García-Echevarría, C.; Ruetz, S. β-Homolysine Oligomers: A New Class of Trojan Carriers. *Bioorg. Med. Chem. Lett*. **2003**, *13*, 247-251.

[31] Hanessian, S.; Luo, X.; Schaum. R. Synthesis and Folding Preferences of γ-Amino Acid Oligopeptides: Stereochemical Control in the Formation of a Reverse Turn and α-Helix. *Tetrahedron Lett.* **1999**, *40*, 4925-4929.

[32] Woll, M.G.; Lai, J.R.; Guzei, I.A.; Taylor, S.J.C.; Smith, M.E.B.; Gellman, S.H. Parallel Sheet Secondary Structure in γ-Peptides. *J. Am. Chem. Soc.* **2001**, *123*, 11077-11078.

[33] Farrera-Sinfreu, J.; Zaccaro, L.; Vidal, D.; Salvatella, X.; Giralt, E.; Pons, M.; Albericio, F; Royo, M. A New Class of Foldamers Based on *cis*-γ-Amino-L-proline. *J. Am. Chem. Soc.* **2004**, *126*, 6048-6057.

[34] Jordan, S.; Schwemler, C.; Kosch, W.; Kretschmer, A.; Schwenner, E.; Stropp, U.; Mielke, B. Synthesis of New Building Blocks for Peptide Nucleic Acids Containing Monomers with Variations in the Backbone. *Bioorg. Med. Chem. Lett.* **1997**, *7*, 681-686.

[35] Jordan, S.; Schwemler, C.; Kosch, W.; Kretschmer, A.; Stropp, U.; Schwenner, E.; Mielke, B. New Hetero-Oligomeric Peptide Nucleic Acids with Improved Binding Properties to Complementary DNA. *Bioorg. Med. Chem. Lett.* **1997**, *7*, 687-690.

[36] Balamurugan, D.; Muraleedharan, K.M. Conformational Switching in Hetereochiral α,$\beta^{2,3}$-Hybrid Peptides in Response to Solvent Polarity. *Eur. J. Org. Chem.* **2015**, 5321-5325.

[37] Grison, C.M.; Robin, S.; Aitken, D.J. 13-Helix Folding of a β/γ-Peptide Manifold Designed from a "Minimal-constraint" Blueprint. *Chem.Commun*. **2016**, *52*, 7802-7805.

[38] Grison CM, Miles JA, Robyn S, Wilson AJ, Aitken DJ. An α-Helix Mimicking 12, 13-Helix: Designed α/β/γ-Foldamers as Selective Inhibitors of Protein-Protein Interactions. *Angew. Chem. Int. Ed.* **2016**, *55*, 11096-11100.

[39] Thodupunuri P, Katukuri S, Ramakrishna KVS, Sharma GVM, Kunwar AC, Sarma AKS, Hofmann HJ. Solvent-Directed Switch of a Left-Handed 10/12-Helix into a Right-Handed 12/10-Helix in Mixed β-Peptides. *J. Org. Chem.* **2017**, *82*, 2018–2031.

[40] Szefczyk M, Weglarz-Tomczak E, Fortuna P, Krzyszton A, Rudzinska-Szostak E, Berlicki Ł. Controlling the Helix Handedness of α,α,β-Peptide Foldamers through Sequence Shifting. *Angew. Chem. Int. Ed.* **2017**, *56*, 2087 –2091.

[41] Chou, K.C. Prediction of Tight Turns and Their Types in Proteins. *Anal Biochem.* **2000**, *286*, 1-16.

[42] Chatterjee, S.; Roy, R.S.; Balaram, P. Expanding the Polypeptide Backbone: Hydrogen-bonded Conformations in Hybrid Polypeptides containing the higher homologues of α-amino acids. *J. R. Soc. Interface* **2007**, *4*, 587-606.

[43] Rúa, F.; Boussert, S.; Parella, T.; Díez-Pérez, I.; Branchadell, V.; Giralt, E.; Ortuño, R.M. Self-assembly of a Cyclobutane β-Tetrapeptide to Form Nanosized Structures. *Org. Lett.* **2007**, *9*, 3643-3645.

[44] Torres, E.; Gorrea, E.; Burusco, K.K.; Da Silva, E.; Nolis, P.; Rúa, F.; Boussert, S.; Díez-Pérez, I.; Dannenberg, S; Izquierdo, S.; Giralt, E.; Jaime, C.; Branchadell, V.; Ortuño, R.M. Folding and Self-assembling with beta-Oligomers Based on (1*R*,2*S*)-2-Aminocyclobutane-1-carboxylic acid. *Org. Biomol. Chem*. **2010**, *8*, 564-575.

[45] Fernandes, C.; Faure, S.; Pereire, E.; Théry, V.; Declerck, V.; Guillot, R.; Aitken D.J. 12-Helix Folding of Cyclobutane β-Amino Acid Oligomers. *Org. Lett.* **2010**, *12*, 3606-3609.

[46] Torres, E.; Gorrea, E.; Da Silva E.; Nolis, P.; Branchadell, V.; Ortuño, R.M. Prevalence of eight-Membered Hydrogen-bonded Rings in some bis(cyclobutane)beta-Dipeptides with trans Stereochemistry. *Org. Lett.* **2009**, *11*, 2301-2304.

[47] Gorrea, E.; Pohl, G.; Nolis, P.; Celis, S.; Burusco, K.K.; Branchadell, V.; Perczel, A.; Ortuño, R.M. Secondary Structure of Short beta-Peptides as the Chiral Expression of Monomeric Building Units: a Rational and Predictive Model. *J. Org. Chem.* **2012**, *77*, 9795-9806.

[48] Pohl, G.; Gorrea, E.; Branchadell, V.; Ortuño, R.M.; Perczel, A.; Tarczay, G. Foldamers of β-Peptides: Conformational Preference of Peptides Formed by Rigid Building Blocks. The first MI-IR spectra of a triamide nanosystem. *Amino Acids* **2013**, *45*, 957-973.

[49] Celis, S.; Gorrea, E.; Nolis, P.; Illa, O.; Ortuño, R.M. Designing Hybrid Foldamers: The Effect on the Peptide Conformational Bias of beta- versus alpha- and gamma-Linear Residues in Alternation with (1*R*,2*S*)-2-Aminocyclobutane-1-carboxylic acid. *Org. Biomol. Chem.* **2012**, *10*, 861–868.

[50] Torres, E.; Puigmartí, L.J.; Pérez del Pino, A.; Ortuño, R.M.; Amabilino, D.B. Use of Unnatural β-Peptides as a Self-Assembling Component in Functional Organic Fibers. *Org. Biomol. Chem*. **2010**, *8*, 1661-1665.

[51] Gorrea, E.; Nolis, P.; Torres, E.; Da Silva, E.; Amabilino, D.B.; Branchadell, V.; Ortuño, R.M. Self-assembly of Chiral Cyclobutane-containing beta-Dipeptides into Ordered Aggregates. *Chem. Eur. J.* **2011**, *17*, 4588 – 4597.

[52] Berlicki, Ł.; Kaske, M.; Gutiérrez-Abad, R.; Bernhardt, G.; Illa, O.; Ortuño, R.M.; Cabrele, C.; Buschauer, A.; Reiser, O. Replacement of Thr32 and Gln34 in the C-terminal Neuropeptide Y fragment 25-36 by *cis*-Cyclobutane and *cis*-Cyclopentane β-amino acids Shifts Selectivity toward Y4 Receptor. *J. Med. Chem.* **2013**, *56*, 8422–8431.

[53] Sorrenti, A.; Illa, O.; Pons, R.; Ortuño, R.M. Chiral Cyclobutane β-Amino Acid-Based Amphiphiles: Influence of cis/trans Stereochemistry on Solution Self-aggregation and Recognition. *Langmuir* **2015**, *31*, 9608–9618.

[54] Aguilera, J.; Cobos, J.A.; Gutiérrez-Abad, R.; Acosta, C.; Nolis, P.; Illa, O.; Ortuño, R.M. The Role of the Chiral *cis*-1,3-Disubstituted 2,2-Dimethylcyclobutane Motif in the Conformational Bias of Several Types of γ-Peptides. *Eur. J. Org. Chem.* **2013**, 3494-3503.

[55] De Zotti, M.; Formaggio, F.; Crisma, M.; Peggion, C.; Moretto, A.; Toniolo, C. Handedness Preference and Switching of Peptide Helices. Part I: Helices based on protein amino acids. *J. Pept. Sci.* **2014**, *20*, 307–322

[56] Nagel, Y.A.; Raschle, P.S.; Wennemers, H. Effect of Preorganized Charge-Display on the Cell-Penetrating Properties of Cationic Peptides. *Angew. Chem. Int. Ed.* **2017**, *56*, 122-126.

[57] Gutiérrez-Abad, R.; Carbajo, D.; Nolis, P.; Acosta-Silva, C.; Cobos, J.A.; Illa, O.; Royo, M.; Ortuño, R.M. Syntheis and Structural Study of Highly Constrained Hybrid Cyclobutane-Proline gamma, gamma-Peptides. *Amino Acids* **2011**, *41*, 673-686.

[58] Martín-Vilà.; Muray, E; P. Aguado, G.; Alvarez-Larena, A.; Branchadell, V.; Minguillón, C.; Giralt, E.; and Ortuño, R.M. Enantioselective Synthetic Approaches to Cyclopropane and Cyclobutane β-Amino Acids: Synthesis and Structural of a Conformationally Constrained β-Dipeptide. *Tetrahedron Asymmetry* **2000**, *11*, 3569-3584.

[59] Fernandes, C.; Gauzy, C.; Yang, Y.; Roy, O.; Pereira, E.; Faure, S.; Aitken, D.J. [2+2] Photocycloadditions with Chiral Uracil Derivatives: Access to All Four Stereoisomers of 2-Aminocyclobutanecarboxylic Acid. *Synthesis* **2007**, *14*, 2222-2232.

[60] Izquierdo, S.; Kogan, M.J. Parella, T.; Moglioni, A.G.; Branchadell, V.; Giralt, E.; Ortuño, R.M. 14-Helical Folding in a Cyclobutane-Containing β-Ttrapeptide. *J. Org. Chem.* **2004**, *69*, 5093-5099.

[61] Sabbioni, G.; Jones, J. B. Enzymes in organic synthesis. 39. Preparations of Chiral Cyclic Acid Esters and Bicyclic Lactones Via Stereoselective Pig Liver Esterase Catalyzed Hydrolyses of Cyclic Meso Diesters. *J. Org. Chem*. **1987**, *52*, 4565.

[62] Fernandes, C.; Pereira, E.; Faure, S.; Aitken, D.J. Expedient Preparation of All Isomers of 2-Aminocyclobutanecarboxylic Acid in Enantiomerically Pure Form. *J. Org. Chem.* **2009**, *74*, 3217-3220.

[63] Harayama, T.; Riezman, H. Understanding the Diversity of Membrane Lipid Composition. *Nature Reviews Molecular Cell Biology*, **2018**, *19*, 281-296.

[64] Löscher, W.; Potschka, H. Role of Drug Efflux Transporters in the Brain for Drug Diposition and Treatment of Brain Diseases. *Prog. Neurobiol.* **2005**, *76*, 22-76.

[65] Pereira, C.D.; Martins, F.; Wiltfang, J.; da Cruz e Silva, O.A.B.; Rebelo, S. ABC Transporters Are Key Players in Alzheimer's Disease. *Journal of Alzheimer's Disease*, **2018**, *61*, 463-485.

[66] Yang, N.J.; Hinner, M.J. Getting Across the Cell Membrane: An Overview for Small Molecules, Peptides and Proteins. *Methods Mol. Biol.* **2015**, *1266*, 29-53.

[67] Zhang, M.; Liu, J.; Zhou, M-M.; Wu, H.; Hou, Y.; Li, Y-F.; Yin, Y.; Zheng, L.; Cai, J.; Liao, F-F.; Liu, F-Y.; Yi, M.; Wan, Y. Anxiolytic Effects of Hippocampal Neurostereoids in Normal and Neuropathic Rats with Spared Nerve Injury. *J. Neurochem.* **2017**, *141*, 137-150.

[68] Sözer, E.B.; Pocetti, C.F.; Vernier, P.T. Asymmetric Patters of Small Molecule Transport After Nanosecond and Microsecond Electropermebilization. *J. Membrane Biol.* **2018**, *251*, 197-210.

[69] Majumder, S.; Garamella, J.; Wang, Y-L.; DeNies, M.; Noireaux, V.; Liu, A.P. Cell-sized Mechanosensitive and Biosensing Compartment Programmed with DNA. *Chem. Commun.* **2017**, *53*, 7349-7352.

[70] Copolovici, D.M.; Langel, K.; Eriste, E.; Langel, Ü. Cell-Penetrating Peptides: Design, Synthesis, and Applications. *ACS Nano* **2014**, *8*, 1972-1994.

[71] *The World of Peptides: A Brief History of Peptide Chemistry*. Weiland, T.; Bodanszky, M. Springer Verlag: Berlin-Heidelberg, **1991**.

[72] *Handbook of Biologically Active Peptides*. Kastin, A. 2nd ed.; Academic Press: Cambridge, MA, **2013**.

[73] Reissmann, S. Cell Penetration: Scope and Limitations by the Application of Cell-Penetrating Peptides. *J. Pept. Sci.* **2014**, *20*, 760-784.

[74] Tashima, T. Intelligent Substance Delivery into Cells using Cell-Penetrating Peptides. *Bioorganic. Med. Chem. Lett.* **2017**, *27*, 121-130.

[75] Nguyen, T.V.; Shin, M.C.; Min, K.A.; Huang, Y.; Oh, E. Moon, C. Cell-Penetrating Peptide-based Non-invasive Topical Delivery Systems. *J. Pharm. Invest.* **2018**, *48*, 77-87.

[76] *Handbook of Cell-Penetrating Peptides.* Langel, Ü. CRC press, Boca Raton, 2006.

[77] Wang, F.; Wang, Y.; Zhang, X.; Zhang, W.; Guo, S.; Jin, F. Recent Progress of Cell-Penetrating Peptides as New Carries for Intracellular Cargo Delivery. *J. Biol. Chem.* **2014**, *174*, 126-163.

[78] Bayshal, S.; Noh, S.; Keum, T.; Choi, T.W.; Lee, S. Cell Penetrating Peptides as an Innovative Approach for Drug Delivery; Then, Present and the Future. *J. Pharm. Invest.* **2016**, *46*, 205-220.

[79] Kim, C.H.; Lee, S.G.; Kang, M.J.; Lee, S.; Choi, Y.W. Surface Modification of Lipid-Based Nanocarriers for Cancer Cell-Specific Drug Targeting. *J. Pharm. Invest.* **2017**, *47*, 203-227.

[80] Frankel, A.D.; Pabo, C.O. Cellular Uptake of the TAT Protein from Human Immunodeficiency Virus. *Cell* **1988**, *55*, 1189-1193.

[81] Green, M.; Loewenstein, P.M.; Autonomous Functional Domains of Chemically Synthesized Human Immunodeficiency Virus TAT Trans-Activator Protein. *Cell* **1988**, *55*, 1179-1188.

[82] Elliot, G.; O'Hare, P. Intercellular Trafficking and Protein Delivery by a Herpesvirus Structural Protein. *Cell* **1997**, *88*, 223-233.

[83] Joliot, A.; Pernelle, C.; Deagostini-Bazin, H.; Prochiantz, A. Antennapedia Homeobox Peptide Regulates Neural Morphogenesis. *Natl. Acad. Sci.* **1991**, *88*, 1864-1868.

[84] Derossi, D.; Joliot, A.H.; Chassaing, G.; Prochiantz, A. The Third Helix of the Antennapedia Homeodomain Translocates through Biological Membranes. *J. Biol. Chem.* **1994**, *269*, 10444-10450.

[85] Pooga, M.; Hällbrink, M.; Zorko, M. Cell Penetration by Transportan. *Fertil Steril* **1998**, *12*, 67-77.

[86] Wender, P.A.; Mitchell, D.J.; Pattabiraman, K.; Pelkey, E.T.; Steinman, L.; Rothbard, J.B. The Design, Synthesis, and Evaluation of Molecules that Enable or Enhance Cellular Uptake: Peptoid Molecular Transporters. *Proc. Natl. Acad. Sci.* **2000**, *97*, 13003-13008.

[87] Oehlke, J.; Scheller, A.; Wiesner, B.; Krause, E.; Beyermann, M.; Klauschenz, E.; Melzig, M.; Bienert, M. Cellular Uptake of an a-helical Amphipathic Model Peptide with the Potential to Deliver Polar Compounds into the Cell Interior Non-endocytically. *Biochim. Biophys. Acta* **1998**, *1414*, 127-139.

[88] Marks, J.R.; Placone, J.; Hristova, K.; Wimley, W.C. Spontaneous Membrane-Translocating Peptides by Orthogonal High-throughput Screening. *J. Am. Chem. Soc.* **2011**, *133*, 8995-9004.

[89] Bolhassani, A.; Jafarzade, B.S.; Mardani, G. *In vitro* and *In Vivo* Delivery of Therapeutic Proteins Using Cell-Penetrating Peptides. *Peptides* **2017**, *87*, 50-63.

[90] Milletti, F. Cell-Penetrating Peptides: Classes, Origin, and current landscape. *Drug Dicov. Today* **2012**, *17*, 850-860.

[91] Rothbard, J.B.; Jessop, T.C.; Lewis, R.S.; Murray, B.A.; Wender, P.A. Role of Membrane Potential and Hydrogen Bonding in the Mechanism of Translocation of Guanidinium-rich Peptides into Cells. *J. Am. Chem. Soc.* **2004**, *126*, 9506-9507.

[92] Tian, Y.; Zeng, X.; Li, J.; Jiang, Y.; Zhao, H.; Wang, D.; Huang, X.; Li, Z. Achieving Enhanced Cell Penetration of Short Conformationally Constrained Peptides Through Amphiphilicity Tuning. *Chem. Sci.* **2017**, *8*, 7576-7581.

[93] Marks, J.R.; Placone, J. Hristova K, Wimley, W.C. Spontaneous Membrane-Translocating Peptides by Orthogonal High-Throughput Screening. *J. Am. Chem Soc.* **2011**, *133*, 8995-9004.

[94] Rabanal, F.; Ludevid, M.D.; Pons, M.; Girals, E. CD of Proline-rich Polypeptides: Application to the Study of the Repetitive Domain of Maize Glutelin-2. *Biopolymers* **1993**, *33*, 1010-1028.

[95] Morgan, A.A.; Rubenstein, E. Proline: the Distribution, Frequency, Positioning, and Common Functional Roles of Proline and Polyproline Sequences in the Human Proteome. *PLoS One* **2013**, *8*, e53785.

[96] Kuemin, M.; Nagel, Y.A.; Schweizer, S.; Monnard, F.W.; Ochsenfeld, C.; Wennemers, H. Tuning the *cis*/*trans* Conformer Ratio of Xaa-Pro Amide Bonds by Intramolecular Hydrogen Bonds: the Effect on PPII Helix Stability. *Angew. Chem. Int. Ed.* **2010**, *49*, 6324-6327.

[97] McCafferty, D.G.; Friese, D.A.; Danielson, E.; Wall, C.G.; Saderholm, M.J.; Erickson, B.W.; Meyer, T.J. Photochemical Energy Conversion in a Helical Oligoproline Assembly. *Proc. Natl. Acad. Sci. U.S.A.* **1996**, *93*, 8200-8204.

[98] Pujals, S.; Giralt, E. Proline-rich, Amphipathic Cell-Penetrating Peptides. *Adv. Drug Deliv. Rev.* **2008**, *60*, 473-484.

[99] Kuriakose, J.; Hernandez-Gordillo, V.; Nepal, M.; Brezden, A.; Pozzi, V.; Seleem, M.N.; Chmielewski, J. Targeting Intracellular Pathogenic Bacteria with Unnatural Proline-rich Peptides: Coupling Antibacterial Activity with Macrophage Penetration. *Angew. Chem. Int. Ed.* **2013**, *52*, 9664-9667.

[100] Fillon, Y.A.; Anderson, J.P.; Chmielwski, J. Cell Penetrating Agents Based on a Polyproline Helix Scaffold. *J. Am. Chem. Soc.* **2005**, *127*, 11798-11803.

[101] Farrera-Sinfreu, J.; Giralt, E.; Castel, S.; Albericio, F.; Royo, M. Cell-Penetrating *cis*-γ-Amino-L-Proline-Derived Peptides. *J. Am. Chem. Soc.* **2005**, *127*, 9459-9468.

[102] Dobitz, S.; Aronoff, M.R.; Wennemers, H. Oligoprolines as Molecular Entities for Controlling Distance in Biological and Materials Sciences. *Acc. Chem. Res.* **2017**, *50*, 2420-2428.

[103] Lindgren, M.E.; Hällbrink, M.M.; Elmquist, A.M.; Langel, Ü. Passage of Cell-Penetrating Peptides Across a Human Epithelial Cell Layer *in vitro*. *Biochem. J.* **2004**, *377*, 69-76.

[104] Carbajo, D. *γ-Peptides based on proline derivates: novel applications and secondary structure*. PhD Thesis. Universidad de Barcelona. **2012**.

[105] Pulido-Villamil, X. *Péptidos miméticos con capacidad de atravesar barreras biológicas.* PhD Thesis. Universidad de Barcelona. **2014**.

[106] Skotland, T.; Iversen, T.G.; Torgersen, M.L.; Sandvig, K. Cell-Penetrating Peptides: Possibilities and Challenges for Drug Delivery *in Vitro* and *in Vivo*. *Molecules* **2015**, *20*, 13313-13323.

[107] Kristensen, M.; Birch, D.; Nielsen, H.M. Applications and Challenges for Use of Cell-Penetrating Peptides as Delivery Vectors for Peptide and Protein Cargos. *Int. J. Mol. Sci.* **2016**, *17*, 185-201.

[108] Âmand, H.L.; Rydberg, H.A.; Fornander, L.H.; Lincoln, P.; Nordén, B.; Esbjörner, E.K. Cell Surface Binding and Uptake or Arginine-and Lysine-rich Penetratin Peptides in Absence and Presence of Proteoglycans. *Biochim. Biophys. Acta* **2015**, *1818*, 2669-2678.

[109] Futaki, S.; Nakase, I. Cell-Surface Interactions on Arginine-Rich Cell-Penetrating Peptides Allow for Multiplex Modes of Internalization. *Acc. Chem. Res.* **2017**, *50*, 2449-2456.

[110] Layek, B.; Lipp, L.; Singh, J. Cell Penetrating Peptide Conjugated Chitosan for Enhanced Delivery of Nucleic Acid. *Int. J.Mol. Sci.* **2015**, *16*, 28912-28930.

[111] Nakase, I.; Niwa, M.; Takeuchi, T.; Sonomura, K.; Kawabata, N.; Koike, Y.; Takehashi, M.; Tanaka, S.; Ueda, K.; Simpson, J. Cellular Uptake of Arginie-Rich Peptides: for Macropinocytosis and Actin Rearrangement. *J. Mol. Ther* **2004**, *10*, 1011-1022.

[112] Nakase, I.; Tadokoro, A.; Kawabata, N.; Takeuchi, T.; Katoh, H.; Hiramoto, K.; Negishi, M.; Nomizu, M.; Sugiura, Y.; Futaki, S. Interaction of Arginine-Rich Peptides with Membrane-Associated Proteoglycans Is Crucial for Induction of Actin Organization and Macropinocytosis. *Biochemistry* **2007**, *46*, 492-501.

[113] Stanzl, E.G.; Trantow, B.M.; Vargas, J.R.; Wender, P.A. Fifteen Years of Cell-Penetrating, Guanidinium-Rich Molecular Transporters: Basic Science, Research Tools, and Clinical Applications. *Acc. Chem. Res.* **2013**, *46*, 2944-2954.

[114] Fretz, M.M.; Penning, N.A.; Al-Taei, S.; Futaki, S.; Takeuchi, T.; Nakase, I.; Storm, G.; Jones, A.T. *Biochem. J.* **2007**, *403*, 335-342.

[115] Borrelli, A.; Tornesello, A.L.; Tornesello, M.L.; Buonaguro, F.M. Cell Penetrating Peptides as Molecular Carriers for Anti-Cancer Agents. *Molecules* **2018**, *23*, 295-324.

[116] Rahbari, R.; Sheahan, T.; Modes, V.; Collier, P.; Macfarlane, C.; Badge, R.M. A Novel L1 Retrotransposon Marker for HeLa Cell Line Identification. *BioTechniques.* **2009**, *46*, 277-284.

[117] Scherer, W.F.; Syverton, J.T.; Gey, G.O. Studies on the Propagation *In Vitro* of Poliomyelitis Viruses. IV. Viral Multiplication in a Stable Strain of Human Malignant Epithelial Cells (Strain *HeLa*) Derived from and Epidermoid Carcinoma of the Cervix. *J. Exp. Med.* **1953**, *97*, 695-710.

[118] Capes-Davis, A.; Theodosopoulos, G.; Atkin, I.; Drexler, H.G.; Kohara A.; MacLeod, R.A.; Masters, J.R.; Nakamura, Y.; Reid, Y.A.; Reddel, R.R.; Freshney, R.I. Check Your Cultures! A list of Cross-Contaminated or Misidentified Cell Lines. *Int. J. Cancer* **2010**, *127*, 1-8.

[119] *The Immortal Life of Henrietta Lacks.* Skloot, R. Crown/Random House. **2010**.

[120] Banaei, M.; Salami-Kalajah, M. A "Grafting to" Approach to Synthesize Low Cytotoxic Poly(aminoamide)-Dendrimer-grafted Fe_3O_4 Magnetic Nanoparticles. *Adv. Polym. Tech.* **2018**, *37*, 943-948.

[121] Ramaker, K.; Henkel, M.; Krause, T.; Röckendorf, N.; Frey, A. Cell Penetrating Peptides: A Comparative Transport Analysis for 474 Sequence Motifs. *Drug Delivery*, **2018**, *25*, 928-937.

[122] Jain, K.; Jain, N.K. Vaccines for Visceral Leishmaniasis: A Review. *J. Immunol. Methods* **2015**, *422*, 1-12.

[123] WHO. Control of the Leishmaniases. *WHO Tech. Rep. Ser.* **2010**, Nº 949, 22-26 March.

[124] WHO. Leishmaniasis. http://www.who.int/en/news-room/fact-sheets/detail/leishmaniasis. June **2018**.

[125] Shirian, S.; Oryan, A.; Hatam, G.R.; Panahi, S.; Daneshbod, Y. Comparison of Conventional, Molecular, and Immunohistochemical Methods in Diagnosis of Typical and Atypical Cutaneous Leishmaniasis. *Arch. Pathol. Lab. Med.* **2014**, *138*, 235-240.

[126] Oryan, A.; Akbari, M. Worldwide Risk Factors in Leishmaniasis. *Asian Pac. J. Trop. Med.* **2016**, *9*, 925-932.

[127] Alvar, A.; Vélez, I.D.; Bern, C.; Herrero, M.; Desjeux, P.; Cano, J.; Jannin, J.; den Boer, M. WHO Leishmaniasis Control Team. Leishmaniasis Worlwide and Global Estimates on Its Incidence. *PLoS One*, **2012**, *7*: e35671.

[128] Alver, J.; Aparicio, P.; Aselfa, A.; Den Boer, M.; Cañavate, C.; Dedet, J.P.; Gradoni, L.; Ter Horst, R.; López-Vélez, R.; Moreno, J. The Relationship Between Leishmaniasis and AIDS: the Second 10 Years. *Clin. Microbiol. Rev.* **2008**, *21*, 334-359.

[129] Kaye, P.; Scott, P. Leishmaniasis: Complexity at the Host-Pathogen Interface. *Nat. Rev. Microbiol.* **2011**, *9*, 604-615.

[130] Oryan, A. Plant-Derived Compounds in Treatment of Leishmaniasis. *Iran J. Vet. Res.* **2015**, *16*, 1-19.

[131] Akuffo, H.; Costa, C.; van Griensven, J.; Burza, S.; Moreno, J.; Herrero, M. New Insights Into Leishmaniasis in the Immunosupressed. *PLoS Negl Trop Dis* **2018**, *12*, e0006375.

[132] Reveiz, L.; Maia-Elkhoury, A.N.; Nicholls, R.S.; Romero, G.A.; Yadon, Z.E. Interventions for American Cutaneous and Mucocutaneous Leishmaniasis: A Systematic Review Update. *PLos One*, **2013**, *8*: e61843.

[133] WHO. Urbanization: An Increasing Risk Factor for Leishmaniasis. *Wkly. Epidemiol. Rec.* **2002**, *77*:365.

[134] Assimina, Z.; Charilaos, K.; Fotoula, B. Leishmaniasis: An Over-looked Public Health Concern. *Health Sci. J.* **2008**, *2*, 196-205.

[135] Maia, C.; Altet, L.; Serrano, L.; Cristóvão, J.M.; Tabar, M.D.; Francino, O.; Cardoso, L.; Campino, L.; Roura, X. Molecular Detection of *Leishmania Infantum*, *Filariae and Wolbachia* spp. In Dogs from Souther Portugal. *Parasites & Vectors* **2016**, 9:170.

[136] Gutiérrez, V.; Seabra, A.B.; Reguera, R.M.; Khandare, J.; Calderón, M. New Approaches from Nanomedicine for Treating Leishmaniasis. *Chem. Soc. Rev.* **2016**, *45*, 152-168.

[137] Gershkovich, P.; Wasan, E.K.; Sivak, O.; Li, R.; Zhu, X.; Werbovetz, K.A.; Tidwell, R.R.; Clement, J.G.; Thornton, S.J.; Wasan, K.M. Visceral Leishmaniasis Affects Liver and Spleen Concentrations of Amphotericin B Following Administration to Mice. *J. Antimicrob. Chemother.* **2010**, *65*, 535-537.

[138] Beattie, L.; Sawtell, A.; Mann, J.; Frame, T.C.M.; Teal, B.; de Labastida Rivera, F.; Brown, N.; Walwyn-Brown, K.; Moore, J.W.J.; MacDonald, S.; Lim, E.K.; Dalton, J.E.; Engwerda, C.R.; MacDonald, K.P.; Kaye, P.M. Bone Marrow-Derived and Resident Liver Macrophages Display Unique Transcriptomic Signatures but Similar Biological Functions. *J. Hepatol*. **2016**, *65*, 758-768.

[139] Esch, K.J.; Petersen, Christine, A. Transmision and Epidemiology of Zoonotic Protozoal Diseases of Companion Animals. *Clin. Microbiol. Rev.* **2013**, *26*, 58-85.

[140] Akbari, M.; Oryan, A.; Hatam, G. Application of Nanotechnology in Treatment of Leishmaniasis: A Review. *Acta Tropica* **2017**, *172*, 86-90.

[141] Bezerra, D.M.J.; Sampaio, C.; Alameida, A.; Mothé, D.; Tavares, P. Advances in Development of New Treatment for Leishmaniasis. *Biomed. Res. Int.* **2015**, 1-11.

[142] De Oliveira Guerra, J.A.; Prestes, S.R.; Silveira, H.; Coelho, L.I.D.A.R.C.; Gama, P.; Moura, A.; Amato, V.; Barbosa, M.D.G.V.; de Lima Ferreira, L.C. Mucosal Leishmaniasis Caused by *Leishmania (Viannia) Braziliensis* and *Leishmania (Viannia) Guyanensis* in the Brazilian Amazon. *PLoS Negl. Trop. Dis.* **2011**, *5*, e980.

[143] Alvar, J.; Yactayo, S.; Bern, C. Leishmaniasis and Poverty. *Trends Parasitol.* **2006**, *22*, 552-557.

[144] Rijal, S.; Koirala, S.; Van der Stuyft, P.; Boelaert, M. The Economic Burden of Visceral Leishmaniasis for Households in Nepal. *Trans. R. Soc. Trop. Med. Hyg.* **2006**, *100*, 838-841.

[145] Kedzierski, L.; Sakthianandeswaren, A.; Curtis, J.M.; Andrews, P.C.; Junk, P.C.; Kedzierska, K. Leishmaniasis: Current Treatment and Prospects for New Drugs and Vaccines. *Curr. Med. Chem.* **2009**, *16*, 599-614.

[146] Igbineweka, O.; Aghedo, F.; Idusuyi, O.; Hussain, N. Evaluating the Efficacy of Topical Silver Nitrate and Intramuscular Antimonial Drugs in the Treatment of Cutaneous Leishmaniasis in Sokoto, Nigeria. *Afr. J. Clin. Exp. Microbiol.* **2012**, *13*, 90-97.

[147] Uliana, S.R.B.; Trinconi, C.T.; Coelho, A.C. Chemotherapy of Leishmaniasis: Present Challenges. *Parasitology* **2018**, *145*, 464-480.

[148] Lindoso, J.A.; Costa, J.M.; Queiroz, I.T.; Goto, H. Review of the Current Treatments for Leishmaniases. *Res. Rep. Trop. Med.* **2012**, *3*, 69-77.

[149] Gamboa-Leon, R.; Vera-Ku, M.; Peraza-Sanchez, S.R.; KuChulim, C.; Horta-Baas, A.; Rosado-Vallado, M. Antileishmanial Activity of a Mixture of Tridax Procumbensand Allium Sativumin Mice. *Parasite* **2014**, *21*, 15.

[150] Chávez-Fumagalli, M.A.; Ribeiro, T.G.; Castilho, R.O.; Fernandes, S.O.; Cardoso, V.N.; Coelho, C.S.; Mendonça, D.V.; Soto, M.; Tavares, C.A.; Faraco, A.A.; Coelho, E.A. New Delivery Systems for Amphotericin B Applied to the Improvement of Leishmaniasis *Treatment* **2015**, *48*, 235-242.

[151] Das, S.; Khan, W.; Mohsin, S.; Kumar, N. Miltefosine Loaded Albumin Microparticles for Treatment of Visceral Leishmaniasis: Formulation Development and in Vitro Evaluation. *Polym. Adv. Technol.* **2010**, *22*, 172-179.

[152] Fernandez, O.L.; Diaz-Toro, Y.; Ovalle, C.; Valderrama, L.; Muvdi, S.; Rodriguez, I.; Gomez, M.A.; Saravia, N.G. Miltefosine and Antimonial Drug Susceptibility of *Leihsmania/Viannia* Species and Populations in Regions of High Transmission in Colombia. *PLoS Negl. Trop. Dis.* **2014**, *8*, e2871.

[153] de Carvalho, R.F.; Ribeiro, I.F.; Miranda-Vilela, A.L.; de Souza Filho, J.; Martins, O.P.; Cintra e Silva Dde, O.; Tedesco, A.C.; Lacava, Z.G.; Báo, S.N.; Sampaio, R.N. Leishmanicidal Activity of Amphotericin B Encapsulated in PLGA-DMSA Nanoparticles to Treat Cutaneous Leishmaniasis in C57BL/6 Mice. *Exp. Parasitol.* **2013**, *135*, 217-222.

[154] Askarizadeh, A.; Jaafari, M.R.; Khamesipour, A.; Badiee, A. Liposomal Adjuvant Development for Leishmaniasis Vaccines. *Ther. Adv. Vaccines* **2017**, *5*, 85-101.

[155] Collado Camps, E.; Brock, R. An Opportunistic Route to Success: Towards a Change of Paradigm to Fully Exploit the Potential of Cell-Penetrating Peptides. *Bioorganic Med. Chem.* **2018**, *26*, 2780-2787.

[156] Fosgerau, K.; Hoffmann, T. Peptide Therapeutics: Current Status and Future Directions. *Drug Discov. Tod.* **2015**, *20*, 122-128.

[157] Gomes, B.; Augusto, M.T.; Felício, M.R.; Hollmann, A.; Franco, O.L.; Gonçalves, S.; Santos, N.C. Designing Improved Active Peptides for Therapeutic Approaches Against Infectious Diseases. *Biotech. Adv.* **2018**, *36*, 415-429.

[158] De la Torre, B.G.; Hornillos, V.; Luque-Ortega, J.R.; Abengozar, M.A.; Amat-Guerri, F.; Ulises Acuna, A.; Rivas, L.; Andreu, D. A BODIPY-embedding Miltefosine Analog Linked to Cell-Penetrating Tat (48-60) Peptides Favors Intracellular Delivery and Visualization of the Antiparasitic Drug. *Amino Acids* **2014**, *46*, 1047-1058.

[159] Ruiz-Santaquiteria, M.; Sánchez-Murcia, P.A.; Toro, M.A.; de Lucio, H.; Gutiérrez, K.J.; de Castro, S.; Carneiro, F.A.C.; Gago, F.; Jiménez-Ruiz, A.; Camarasa, M.J.; Velázquez, S. First Example of Peptides Targeting the Dimer Interface of Leishmania Infantum Trypanothione Reductase with Potent In Vitro Antileishmanial Activity. *Eur. J. Med. Chem.* **2017**, *135*, 49-59.

[160] Gorrea, E.; Carbajo, D.; Gutiérrez-Abad, R.; Illa, O.; Branchadell, V.; Royo, M.; Ortuño, R.M. Searching for New Cell-Penetrating Agents: Hybrid Cyclobutane-Proline γ,γ-peptides. *Org. Biomol. Chem.* **2012**, *10*, 4050-4057.

[161] Ospina, J.A. *Nuevas Plataformas Quirales de Alta Versatilidad: Síntesis y Aplicaciones.* PhD Thesis. Universitat Autónoma de Barcelona. **2016**.

[162] Tacar, O.; Sriamornsak, P.; Dass, CR. Doxorubicin: An Update on Anticancer Molecular Action, Toxicity and Novel Drug delivery Systems. *J. Pharm Pharmaco.* **2013**, *65*, 157-170.

[163] Gamo, F-J.; Sanz, L.M.; Vidal, J.; de Cozar, C.; Alvarez, E.; Lavandera, J-L.; Vanderwall, D.E.; Green, D.V.S.; Kumar, V., Hasan, S.; Brown, J.R.; Peishoff, C.E.; Cardo, L.R.; Garcia-Bustos, J.F. Thousands of Chemical Starting Points for Antimalarial Lead Identification. *Nature* **2010**, *465*, 305-310.

[164] Futaki, S. Membrane-Permeable Arginie-Rich Peptides and the Translocation Mechanisms. *Adv. Drug. Deliv. Rev.* **2005**, *57*, 547-558.

[165] Duchardt, F.; Fotin-Mleczek, M.; Schwarz, H.; Fischer, R.; Brock, R. A Comprehensive Model for the Cellular Uptake of Cationic Cell-Penetrating Peptides. *Traffic* **2008**, *8*, 848-866.

[166] Gräslund, A.; Madani, F.; Lindberg, S.; Langel, Ü.; Futaki, S. Mechanisms of Cellular Uptake of Cell-Penetrating Peptides. *J. Biophys.* **2011**, *article ID 414729*, 1-10.

[167] Deshayes, S.; Plénat, T.; Aldrian-Herrada, G.; Divita, G.; Le Grimellec, C.; Heitz, F. Primary Amphipathic Cell-Penetrating Peptides: Structural Requirements and Interactions with Model Membranes. *Biochemistry* **2004**, *43*, 7698-7706.

[168] Ziegler, A. Thermodynamic Studies and Binding Mechanisms of Cell-Penetrating Peptides with Lipids and Glycosaminoglycans. *Adv.Drug Deliv. Rev.* **2008**, *60*, 580-597.

[169] Zaro, J.L.; Vckich, J.E.; Tran, T.; Shen, W.C. Nuclear Localization of Cell-Penetrating Peptides is Dependent on Endocytosis Rather than Cytosolic Delivery in CHO Cells. *Mol. Pharm.* **2009**, *6*, 337-344.

[170] Jiao, C.Y.; Delaroche, D.; Durlina, F.; Alves, I.D.; Chassaing, G.; Sagan, S. Translocations and Endocytosis for Cell-Penetrating Peptide Internalization. *J. Biol. Chem.* **2009**, *284*, 33957-33965.

[171] Pae, J.; Liivamägi, L.; Lubenets, D.; Arukuusk, P.; Langel, Ü.; Pooga, M. Glycosaminoglycans are Required for Translocation of Amphipathic Cell-Penetrating Peptides Across Membranes. *Biochim. Biophys. Acta*, **2016**, *1858*, 1860-1867.

[172] Gautam, A.; Sharma, M.; Vir, P.; Chaudhary, K.; Kapoor, P.; Kumar, R.; Nath, S.K.; Raghava, G.P.S. Identification and Characterization of Novel Protein-derived Arginine-rich Cell-Penetrating Peptides. *Eur. J. Pharm. Biopharm.* **2015**, *89*, 93-106.

[173] *The Chemistry of Contrast Agents in Medical Magnetic Resonance Imaging*, second Ed.; Merbach, A.; Helm, L.; Tóth, É., Eds.; Wiley, **2013**.

[174] *Theranostics and Image Guided Drug Delivery*, Thanou, M. Eds.; The Royal Society of Chemistry, 2018.

[175] Bloch, F.; Hansen, W.W.; Packard, M. Nuclear Induction. *Phys. Rev.* **1946**, *69*, 127.

[176] Bloembergen, N.; Purcell, E.M.; Pound, R.V. Relaxation Effects in Nuclear Magnetic Resonance Absorption. *Phys. Rev.* **1948**, *73*, 679.

[177] Lauterbur, P.C. Image Formation by Induced Local Interactions: Examples Employing Nuclear Magnetic Resonance. *Nature*, **1973**, *242*, 190-191.

[178] *An Introduction to Biomedical Nuclear Magnetic Resonance*, Petersen, S.B.; Muller, R.N.; van As, H.; Rinck, P.A.; Eds.; Georg Thieme Verlag, **1985**.

[179] Ananta, J.S.; Godin, B.; Sethi, R.; Moriggi, L.; Liu, X.; Serda, R.E.; Krishnamurthy, R.; Muthupillai, R.; Bolskar, R.D.; Helm, L.; Ferrari, M.; Wilson, L.J.; Decuzzi, P. Geometrical Confinement of Gadolinium-Based Contrast Agents in Nanoporous Particles Enhances T_1 contrast. *Nat. Nanotechnol.* **2010**, *5*, 815-821.

[180] *Contrast Agents for MRI: Experimental Methods*. Pierre, V.C.; Allen, M.J. The Royal Society of Chemistry, **2018**.

[181] *Lanthanide and Actinide Chemistry*, Cotton, S.; Ed.; John Wiley & Sons: Uppingham, Rutland, UK, **2006**.

[182] *Principles of Neural Science*; Kandel, E.R.; Schawartz, J.H.; Jessel, T.M.; Eds.; McGraw-Hill: New York, **2000**.

[183] Lanthanide Probes in Life, Chemical and Earth Science: Theory and Practice; Bünzli, J.C.G.; Choppin, G.R.; Eds.; Elsevier: Amsterdam, **1989**.

[184] Caravan, P. Strategies for Increasing the Sensitivity of Gadolinium based MRI Contrast Agents. Chem. Soc. Rev. **2006**, 35, 512-523.

[185] Weinmann, H.J.; Brasch, R.C.; Press, W.R. Characteristics of Gadolinium-DTPA Complex: A Potential NMR Contrast Agent. *Am. J. Roentgenol.* **1984**, *142*, 625-630.

[186] Pierre, V.C.; Allen, M.J.; Caravan, P. Contrast Agents for MRI: 30+ Years and Where Are We Going? *J. Biol. Inorg. Chem.* **2014**, *19*, 127-131.

[187] Surman, A.J.; Bonnet, C.S.; Lowe, M.P.; Kenny, G.D.; Bell, J.D.; Tóth, É.; Vilar, R. A Pyrophosphate-Responsive Gadolinium (III) MRI Contrast Agent. *Chem. Eur. J.* **2011**, *17*, 223-230.

[188] Aime, S.; Caravan P. Biodistribution of Gadolinium-Based Contrast Agents, Including Gadolinium Deposition. *J. Magn. Reson. Imaging* **2009**, *30*, 1259-1267.

[189] Baker, J.F.; Kratz, L.C.; Stevens, G.R.; Wible, J.H Jr. Pharmacokinetics and Safety of the MRI Contrast Agent Gadoversetamide Injection (OptiMARK) in Healthy Pediatric Subjects. *Invest. Radiol.* **2004**, *39*, 334-339.

[190] Uggeri, F.; Aime, S.; Anelli, P.L.; Botta, M.; Brocchetta, M.; de Haeen, C.; Ermondi, G.; Grandi, M.; Paoli, P. Novel Contrast Agents for Magnetic Resonance Imaging. Synthesis and Characterization of the Ligand BOPTA and Its Ln(III) Complexes (Ln=Gd, La, Lu). *Inorg. Chem.* **1995**, *34*, 633-643.

[191] Cowper, S.E. Nephrogenic Systemic Fibrosis: A review and Exploration of the Role of Gadolinium. *Adv. Dermatol.* **2007**, *23*, 131-154.

[192] Ramalho, M.; Ramalho, J.; Burke, L.M.; Semelka, R.C. Gadolinium Retention and Toxicity-An Update. *ACKD* **2017**, *24*, 138-146.

[193] Malikova, H.; Holesta, M. Gadolinium Contras Agents – Are They Really Safe? *J. Vasc. Access* **2017**, *18*, 51-57.

[194] Frenzel, T.; Lengsfeld, P.; Schirmer, H.; Hütter, J.; Weinmann, H.J. Stability of Gadolinium-Based Magnetic Resonance Imaging Contrast Agents in Human Serum at 37 Degrees C. *Invest. Radiol.* **2008**, *43*, 817-828.

[195] Yang, L.; Krefting, I.; Gorovets, A.; Marzella, L.; Kaiser, K.; Boucher, R.; Rieves, D. Nephrogenic Systemic Fibrosis and Class Labeling of Gadolinium-Based Contrast Agents by the Food and Drug Administration. *Radiology* **2012**, *265*, 248-253.

[196] Sarka, L.; Burai, L.; Brücher, E. The Rates of the Exchange Reactions Between $[Gd(DTPA)]^{2-}$ and the Endogenous Ions Cu^{2+} and Zn^{2+}: A Kinetic Model for the Prediction of the Magnetic Resonance Imaging. *Chem. Eur. J.* **2000**, *6*, 719-724.

[197] Pálinkás, Z.; Roca-Sabio, A.; Mato-Iglesias, M.; Esteban-Gómez, D.; Platas-Iglesias, C.; De Blas, A.; Rodríguez-Blas, T.; Tóth, E. Stability, Water Exchange, and Anion Binding Studies on Lanthanide(III) Complexes with a Macrocyclic Ligand Based on 1.7-Diaza-12-Crown-4: Extremely Fast Water Exchange on the Gd^{3+} Complex. *Inorg. Chem.* **2009**, *48*, 8878-8889.

[198] Rodríguez-Rodríguez, A.; Esteban-Gömez, D.; Tripier, R.; Tircsö, G.; Garda, Z.; Töth, I.; De Blas, A.; Rodríguez-Blas, T.; Platas-Iglesias, C. Lanthanide(III) Complexes with a Reinforced Cyclam Ligand Show Unprecedented Kinetic Inertness. *J. Am. Chem. Soc.* **2014**, *136*, 17954-17957.

[199] Kálman, F.K.; Végh, A.; Regueiro-Figueroa, M.; Tóth, E.; Platas-Iglesias, C.; Tircsó, G. H4octapa: Highly Stable Complexation of Lanthanide(III) Ions and Copper(II). *Inorg. Chem.* **2015**, *54*, 2345-2356.

[200] Tircsó, G.; Regueiro-Figueroa, M.; Nagy, V.; Garda, Z.; Garai, T.; Kálmán, F.K.; Esteban-Gõmez, D.; Tóth, É, Platas-Iglesias, C. Approaching the Kinetic Inertness of Macrocyclic Gadolinium(III)-Based MRI Contrast Agents with Highly Rigid Open-Chain Derivatives. *Chem Eur. J.* **2016**, *22*, 896-901.

[201] Pellegatti, L.; Zhang, J.; Dharos, B.; Villete, S.; Suzenet, F.; Guillaumet, G.; Petoud, S.; Tóth, É. Pyridine-Based Lanthanide Complexes: Towars Bimodal Agents Operating as near Infrared Luminiscent and MRI Reporters. *Chem. Commun.* **2008**, *60*, 6591-6593.

[202] Gale, E.M.; Kenton, N.; Caravan, P. $[Gd(CyPic3A)(H_2O)_2]^-$: A Stable, Bis(aquated) and High-Relaxiviy Gd(III) Complex. *Chem. Commun.* **2013**, *49*, 8060-8062.

[203] Bonnet, C.S.; Laine, S.; Buron, F.; Tircso, G.; Pallier, A.; Helm, L.; Suzenet, F.; Tóth, É. A Pyridine-Based Ligand with Two Hydrazine Functions for Lanthanide Chelation: Remarkable Kinetic Inertness for a Linear, Byshydrated Complex. *Inorg. Chem.* **2015**, *54*, 5991-6003.

[204] Bloembergen, N.; Morgan, L.O. Proton Relaxation Times in Paramagnetic Solutions. Effects of Electron Spin Relaxation. *J. Chem. Phys.* **1961**, *34*, 842.

[205] Micksei, K.; Helm, L.; Brucher, E.; Merbach, A.E. Oxygen-17 NMR Study of Water Exchange on Gadolinium Polyaminopolyacetates $[Gd(DTPA)(H_2O)]^{2-}$ and $[Gd(DOTA)(H_2O)]^-$ Related to NMR Imagin. *Inorg. Chem.* **1993**, *32*, 3844-3850.

[206] Fries, P.H.; Belorizky, E. Electronic Relaxation of Paramagnetic Metal Ions and NMR Relaxivity in Solution: Critial Analysis of Various Approaches and Application to Gd(III)-Based Contrast Agent. *J. Chem. Phys.* **2005**, *123*, 124510-124515.

[207] Jacques, V.; Dumas, S.; Sun, W-C. Troughtin, J.S.; Greenfield, M.T.; Caravan P. High-Relaxivity Magnetic Resonance Imaging Contrast Agents Part 2. Optimization of Inner- and Second-Sphere Relaxivity. *Invest. Radiol.* **2010**, *45*, 613-624.

[208] Bonnet, C.S.; Fries, P.H.; Crouzy, S.; Delangle, P. Outer-Sphere Investigation of MRI Relaxation Contrast Agents. Example of a Cyclodecapeptide Gadolinium Complex with Second-Sphere Water. *J. Phys. Chem.* **2010**, *114*, 8770-8781.

[209] Caravan, P.; Greenfield, M.T.; Li, X.; Sherry, A.D. The Gd^{3+} Complex of a Fatty Acid Analogue of DOTP Binds to Multiple Albumin Sites with Variable Water Relaxivities. *Inorg. Chem.* **2001**, *40*, 6580-6587.

[210] Lebdusková, P.; Hermann, P.; Helm, L.; Tóth, É, Kotek, J.; Binnemans, K.; Rudovský, J.; Lukes, I.; Merbach, A.E. Gadolinium(III) Complexes of Mono- and Diethyl Esters of Monophosphonic Acid Analogues of DOTA as Potential MRI Contrast Agents: Solution Structures and Relaxometric Studies. *Dalton Trans.* **2007**, *4*, 493-501.

[211] Aime, S.; Calabi, L.; Cavallotti, C.; Gianolio, E.; Giovenzana, G.B.; Losi, P.; Maiocchi, A.; Palmisano, G.; Sisti, M. [Gd-AAZTA]$^-$: A New Structural Entry for an Improved Generation of MRI Contrast Agents. *Inorg. Chem.* **2004**, *43*, 7588-7890.

[212] Datta, A.; Raymond, K.N. Gd-HOPO Based High Relaxivity MRI Contrast Agents. *Acc. Chem. Res.* **2009**, *42*, 938-497.

[213] Baranyai, Z.; Botta, M.; Fekete, M.; Giovenzana, G.B.; Negri, R.; Tei, L.; Platas-Iglesias, C. Ligand Denticity Leading to Improved Thermodynamic and Kinetic Stability of the Gd^{3+} Complex: The Strange Case of OBETA. *Chem. Eur. J.* **2012**, *18*, 7680-7685.

[214] Boros, E.; Caravan, P. Probing the Structure-Relaxivity Relationship of Bis-Hydratated Gd(DOTAla) Derivaties. *Inorg. Chem.* **2015**, *54*, 2403-2410.

[215] Boros, E.; Karimi, S.; Kenton, N.; Helm, L.; Caravan, P. Gd(DOTAlap): Exploring the Boundaries of Fast Water Exchange in Gadolinium-Based Magnetic Resonance Imaging Contrast Agents. *Inorg. Chem.* **2014**, *53*, 6985-6994.

[216] Granato, L.; Elst, L.V.; Henoumont, C.; Muller, R.N.; Laurent, S. Optimizing Water Exchange Rates and Rotational Mobility for High-Relaxivity of a Novel Gd-DO3A Derivative Complex Conjugated to Inulin as Macromolecular Contrast Agents for MRI. *Chem. Biodiversity* **2018**, *15*, e1700487.

[217] Elhabiri, M.; Abada, S.; Sy, M.; Nonat, A.; Choquet, P.; Esteban-Gómez, D.; Cassino, C.; Platas-Iglesias, C.; Botta, M.; Charbonnière, L. Importante of Outer-Sphere and Aggregation Phenomena in the Relaxation Properties of Phosphonated Gadolinium Complexes with Potential Application as MRI Contrast Agents. *Chem. Eur. J.* **2015**, *21*, 6535-6546.

[218] Diaferia, C.; Gianolio, E.; Accardo, A.; Morelli, G. Gadolinium Containing Telechelic PEG-Polymers end-Capped by di-Phenylalanine Motives as Potential Supramolecular MRI Contrast Agents. *J. Pept. Sci.* **2017**, *23*, 122-130.

[219] Porcar, O. Chiral Cyclobutane Scaffolds: Their Application in the Development of New Funcitonalized Organogelators, Organocatalysts and MRI Contrast Agents. PhD Thesis. Universitat Autónoma de Barcelona. **2017**.

[220] Salvatore, R.N.; Shin, S.I.; Flanders, V.L.; Woon Jung, K. Efficient and Selective *N*-Alkylation of Carbamates in the Presence of Cs_2CO_3 and TBAI. *Tetrahedron Lett.* **2001**, *42*, 1799-1801.

[221] Baranyai, Z.; Palinkas, Z.; Uggeri, F.; Brücher, E. Equilibrium Studies on the Gd^{3+}, Cu^{2+} and Zn^{2+} Complexes of BOPTA, DTPA and DTPA-DMA Ligands: Kinetics of Metal-Exchange Reactions of $[Gd(BOPTA)]^{2-}$. *Eur. J. Inor. Chem.* **2010**, 1948-1956.

[222] Garw, P.; Sabatini, A.; Vacca, A. Investigation of Equilibria in Solution. Determination of Equilibrium Constant with the HYPERQUAD Suite of Programs. *Talanta* **1996**, *43*, 1739-1753.

[223] *Biochemistry of the Lanthanides*; Evans, C.H., Ed.; Springer US, **1990**.

[224] Cacheris, W.P.; Quay, S.C.; Rocklage, S.M. The Relationship between Thermodynamics and Toxicity of Gadolinium Complexes. *Magn. Reson. Imaging* **1990**, *8*, 467-481.

[225] Alderighi, L.; Gans, P.; Ienco, A.; Peters, D.; Sabatini, A.; Vacca, A. Hyperquad Simulation and Speciation (HySS): A Utility Program for the Investigation of Equilibria Involving Soluble and Partially Soluble Species. *Coord. Chem. Rev.* **1999**, *184*, 311-318.

[226] Wei, C.; Ma, L.; Wei, H.; Liu, Z.; Bian, Z.; Huang, C. Advances in Luminescent Lanthanide Complexes and Applications. *Sci. China Tech. Sci.* **2018**, *61*. https://doi.org/10.1007/s11431-017-9212-7.

[227] Haas, Y.; Stein, G. Pathways of Radiative and Radiationless Transitions in Europium (III) Solutions. Role of Solvents and Anions. *J. Phys. Chem.* **1971**, *75*, 3668-3677.

[228] William De, W.H.; Sudnick, D.R. Lanthanide Ion Probes of Structure in Biology. Laser-Induced Luminescence Decay Constants Provide a Direct Measure of the Number of Metal-Coordinated Water Molecules. *J. Am. Chem. Soc.* **1979**, *101*, 334-340.

[229] Horrocks, W.D.; Sudnick, D.R. Lanthanide Ion Luminescence Probes of the Structure of Biological Macromolecules. *Acc. Chem. Res.* **1981**, *14*, 384-392.

[230] Beeby, A.; Clarkson, I.M.; Dickins, R.S.; Faulkner, S.; Parker, D.; Royle, L.; de Sousa, A.S.; Williams, J.A.G.; Woord, M. Non-Radiative Deactivation of the Excited States of Europium, Terbium and Ytterbium Complexes by Proximate Energy-Matched OH, NH and CH Oscillators: An Improved Luminescence Method for Establishing Solution Hydration States. *J. Chem. Soc. Perkin Trans. 2* **1999**, *2*, 493-504.

[231] Supkowski, R.M. Horrocks, W.D. On the Determination of the Number of Water Molecules, Q. Coordinated to Europium (III) Ions in Solution from Luminescence Decay Lifetimes. *Inorganica Chim. Acta* **2002**, *340*, 44-48.

[232] Aime, S.; Barge, A.; Botta, M.; Howard, J.A.J.; Kataky, R.; Lowe, M.P.; Moloney, J.M.; Parker, D.; de Sousa, A.S. Dependence of the Relaxivity and Luminescence of Gadolinium and Europium Amino-Acid Complexes on Hydrogencarbonate and pH. *Chem. Commun.* **1999**, *2*, 1047-1048.

[233] Botta, M.; Aime, S.; Barge, A.; Bobba, G.; Dickins, R.S.; Parker, D.; Terreno, E. Ternary Complexes between Cationic GdIII Chelates and Anionic Metabolites in Aqueous Solution: An NMR Relaxometric Study. *Chem. Eur. J.* **2003**, *9*, 2102-2109.

[234] Aime, S.; Gianolio, E.; Terreno, E.; Giovenzana, G.B.; Pagliarin, R.; Sisti, M.; Palmisano, G.; Botta, M.; Lowe, M.P.; Parker, D. Ternary Gd(III)L-HAS Adducts: Evidence for the Replacement of Inner-Sphere Water Molecules by Coordinating Groups of the Protein. Implications for the Design of Contrast Agents for MRI. *J. Biol. Inorg. Chem.* **2000**, *5*, 488-497.

[235] Aime, S.; Terreno, E.; Botta, M.; Bruce, J.I.; Parker, D.; Mainero, V. Modulation of the Water Exchange Rates in [Gd-DO3A] Complex by Formation of Ternary Complexes with Carboxylate Ligands. *Chem. Commun.* **2001**, *1*, 115-116.

[236] de Sousa, P.L.; Livramento, J.B.; Helm, L.; Merbach, A.E.; Même, W.; Doan, B.T.; Beloeil, J.C.; Prata, M.I.M.; Santos, A.C.; Geraldes, C.F.G.; Tóth, E. In Vivo MRI Assesment of a Novel GdIII-Based Contrast Agents Designed for High Magnetic Field Applications. *Contrast Media Mol. Imaging* **2008**, *3*,78-85.

[237] Mato-Iglesias, M.; Roca-Sabio, A.; Pálinkás, Z.; Esteban-Gomez, D.; Platas-Iglesias, C.; Tóth, É, De Blas, A.; Rodríguez-Blas, T. Complexes Based on a 1,7-Diaza-12-Crown-4 Platform Containing Picolinate Pendants: A New Structural Entry for the Design of Magnetic Resonance Imaging Contrast. *Inorg. Chem.* **2008**, *47*, 7840-7851.

[238] Mosnann, T. Rapid Colorimetric Assay for Cellular Growth and Survival: Application to Proliferation and Cytotoxicity Assays *J. Immunol. Methods* **1983**, *65*, 55-63.

[239] Corsi, D.M. Platas-Iglesias, C.; Van Bekkum, H.; Peters, J.A. Determination of Paramagnetic Lanthanide(III) Concentrations from Bulk Magnetic Susceptibility Shifts in NMR Spectra. *Magn. Reson. Chem.* **2001**, *39*, 723-726.

[240] *Determination and Use of Stability Constants*; Martell, A.E.; Motekaitis, R.J., Eds.; VCH: New York, **1992**.

[241] Gans, P.; O'Sullivan, B. Glee, A New Computer Program for Glass Electrode Calibration. *TalantaTalanta* **2000**, *51*, 33.

[242] Smith, R.M.; Motekaitis, R.J.; Martell, A.E. NIST Standar Reference Database. *Natl. Inst. Stand. Technol.* **1997**.

[243] Beeby, A.; Clarkson, I.M.; Dickins, R.S.; Faulkner, S.; Parker, D.; Royle, L.; de Sousa, A.S.; Williams, J.A.G.; Woord, M. Non-Radiative Deactivation of the Excited States of Europium, Terbium and Ytterbium Complexes by Proximate Energy-Matched OH, NH and CH Oscillators: An Improved Luminescence Method for Establishing Solution Hydration States. *J. Chem. Soc. Perkin Trans. 2* **1999**, *2*, 493-504.

[244] Supkowski, R.M. Horrocks, W.D. On the Determination of the Number of Water Molecules, Q. Coordinated to Europium (III) Ions in Solution from Luminescence Decay Lifetimes. *Inorganica Chim. Acta* **2002**, *340*, 44-48.

[245] Yerly, F. VISUALISEUR 2.3.5; Lausanne, Switzerland, **1999**.

[246] Yerly, F. OPTIMISEUR 2.5.5; Lausanne, Switzerland, **1999**.

[247] Solomon, I. Relaxation Processes in a System of Two Spins. *Phys. Rev.* **1955**, *99*, 559.

[248] Solomon, I.; Bloembergen, N. Nuclear Magnetic Interactions in the HF Molecule. *J. Chem. Phys.* **1956**, *25*, 261.

[249] Bloembergen, N. Proton Relaxation Times in Paramagnetic Solutions. *J. Chem. Phys. Phys.* **1957**, *27*, 572.

[250] Luz, Z.; Meiboom, S. Proton Relaxation in Dilute Solutions of Cobalt (II) and Nickel (II) Ions in Methanol and the Rate of Methanol Exchange of the Solvation Sphere. *J. Chem. Phys.* **1964**, *40*, 2686.

[251] Fries, P.H.; Gateau, C.; Mazzanti, M. Practical Route to Relative Diffusion Coefficients and Electronic Relaxation Rated of Paramagnetic Metal Complexes in Solution by Model-Independent Outer-Sphere NMRD. Potentiality for MRI Contrast Agents. *J. Am. Chem. Soc.* **2005**, *127*, 15801-15814.

[252] Borel, A.; Laus, S.; Ozarowski, A.; Gateau, C.; Nonat, A.; Mazzanti, M.; Helm, L. Multiple-Frequency EPR Spectra of Two Aqueous Gd^{3+} Polyamino Polypyridine Carboxylate Complexes: A Study of High Field Effects. *J. Chem. Phys.* **2007**, *111*, 5399-5407.

[253] Freed, J.H. Dynamic Effects of Pair Correlation Functions on Spin Relaxation by Translational Diffusion in Liquids. Finite Jumps and Independent T1 Processes. *J. Chem. Phys.* **1978**, *68*, 4034-4037.

[254] Koenig, S.H.; Brown III, R.D. Field-Cycling Relaxometry of Protein Solutions and Tissue: Implications for MRI. *Prog. Nucl. Magn. Reson. Spectrosc.* **1990**, *22*, 487-567.

[255] Raiford, D.S.; Fisk, C.L.; Becker, E.D. Calibration of Methanol and Ethylene Glycol Nuclear Magnetic Resonance Thermometers. *Anal. Chem.* **1979**, *51*, 2050-2051.

[256] Meiboom, S.; Gill, D. Modified Spin-Echo Method for Measuring Nuclear Relaxation Times. *Rv. Sci. Instrum.* **1958**, *29*, 688-691.

[257] Hugi, A.D.; Helm, L.; Merbach, A.E. Water Exchange on Hexaaquavanadium(III): A Variable-Temperature and Variable-Pressure ^{17}O-NMR Study at 1.4 and 4.7 Tesla. *Helv. Chim. Acta* **1985**, *68*, 508-521.

[258] *Purification of laboratory chemicals*, W.L.F. Armarego and D.D. Perrin, 4th edition, Butterworth-Heinemann, UK, **1999**.

9. Annex

Table of contents

NMR spectra for the characterization of hybrid peptides

β-*cis*,γ-*cis* 33

^{1}H-NMR (600 MHz, DMSO-d_6, 298 K)

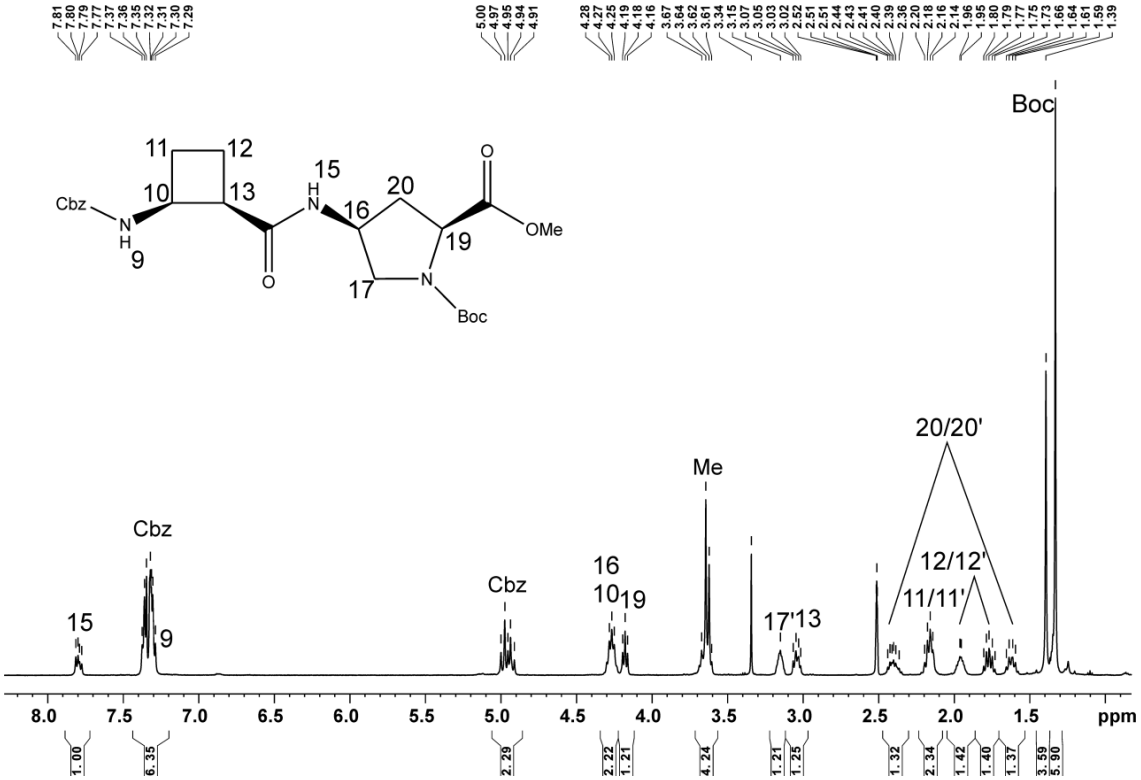

^{1}H-NMR (600 MHz, $CDCl_3$, 298 K)

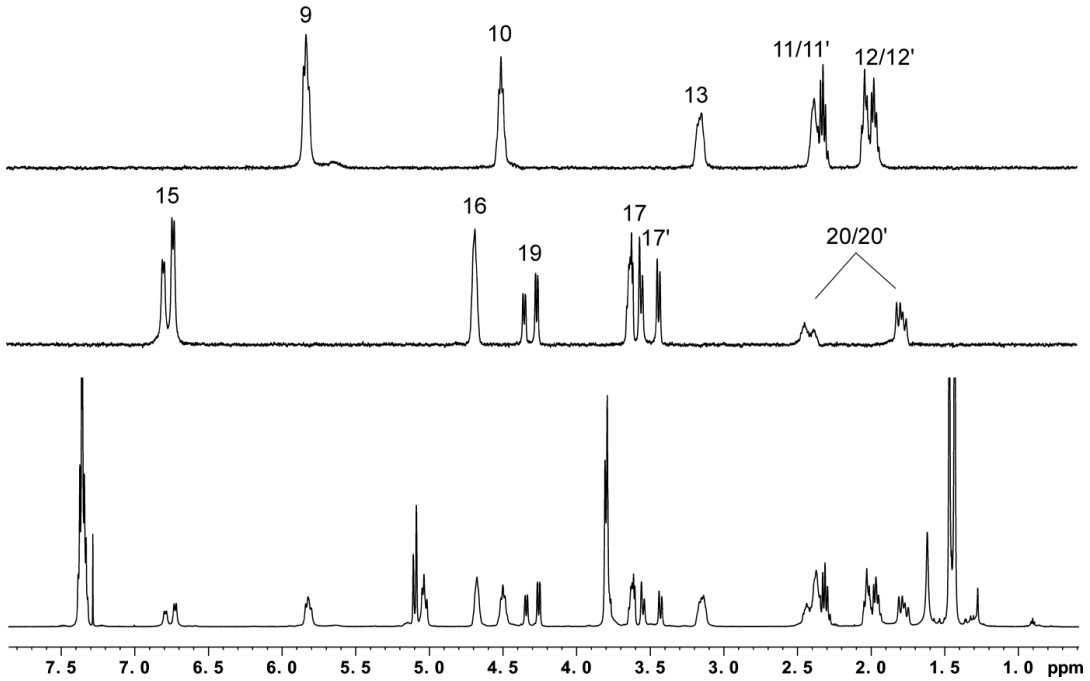

^{13}C-NMR (150 MHz, DMSO-*d*$_6$, 298 K)

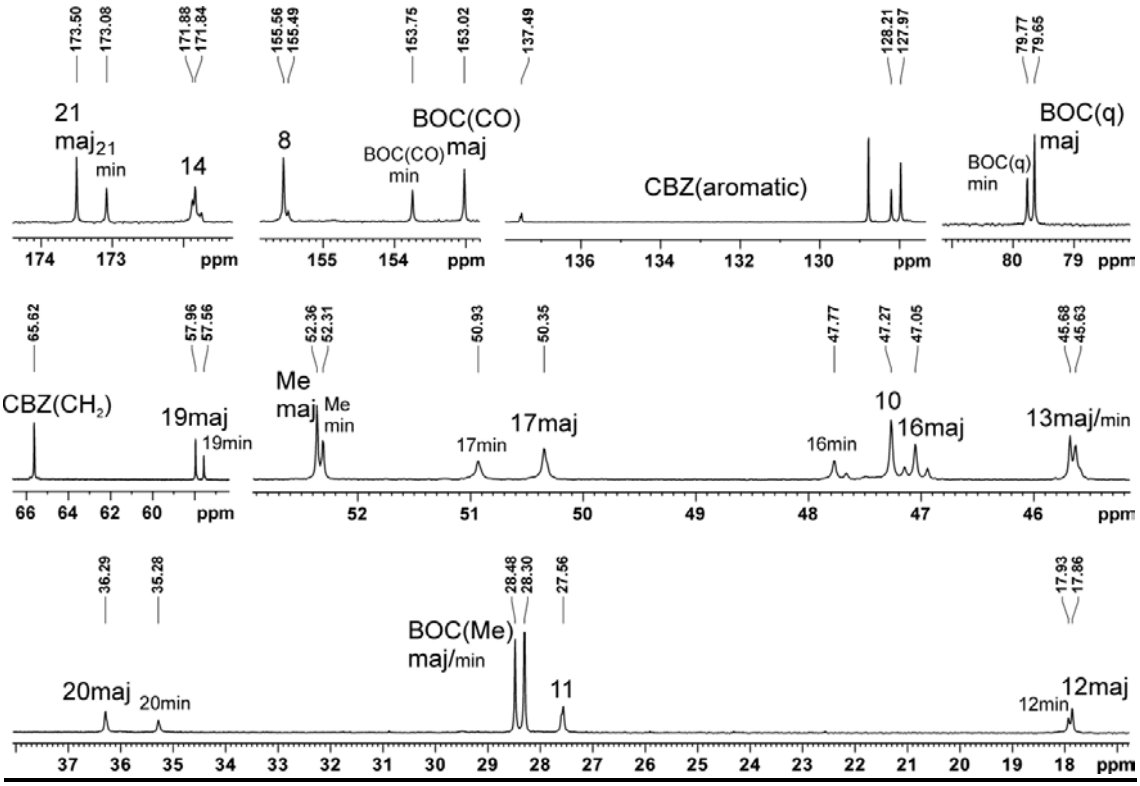

Multiplicity Edited HSQC (600 MHz, DMSO-*d*$_6$, 298 K)

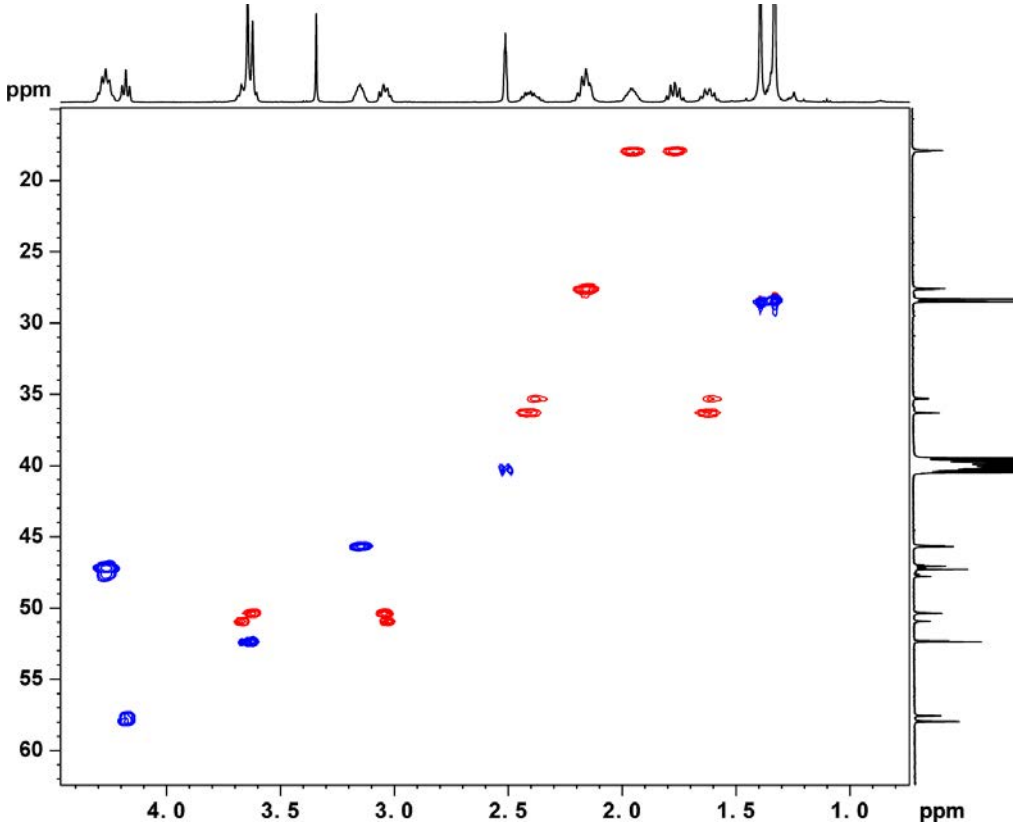

β-*cis*,γ-*trans*, 35

^{1}H-NMR (600 MHz, DMSO-d_6, 298 K)

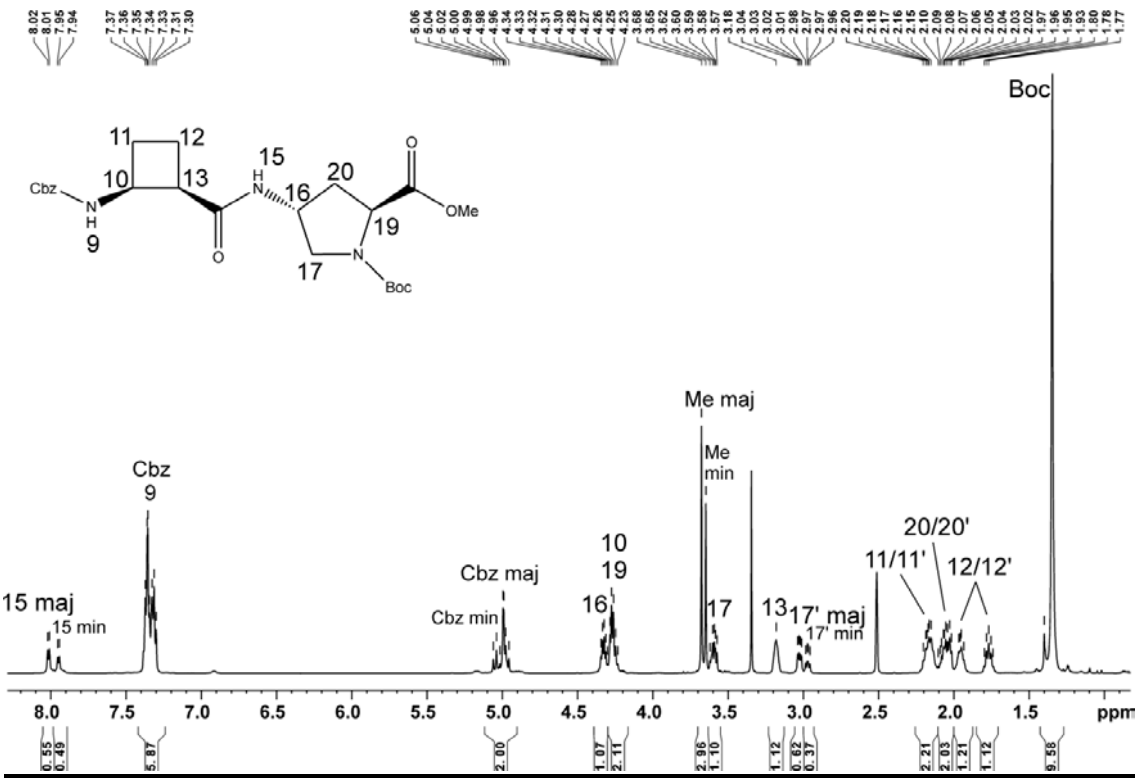

^{1}H-NMR (600 MHz, $CDCl_3$, 298 K)

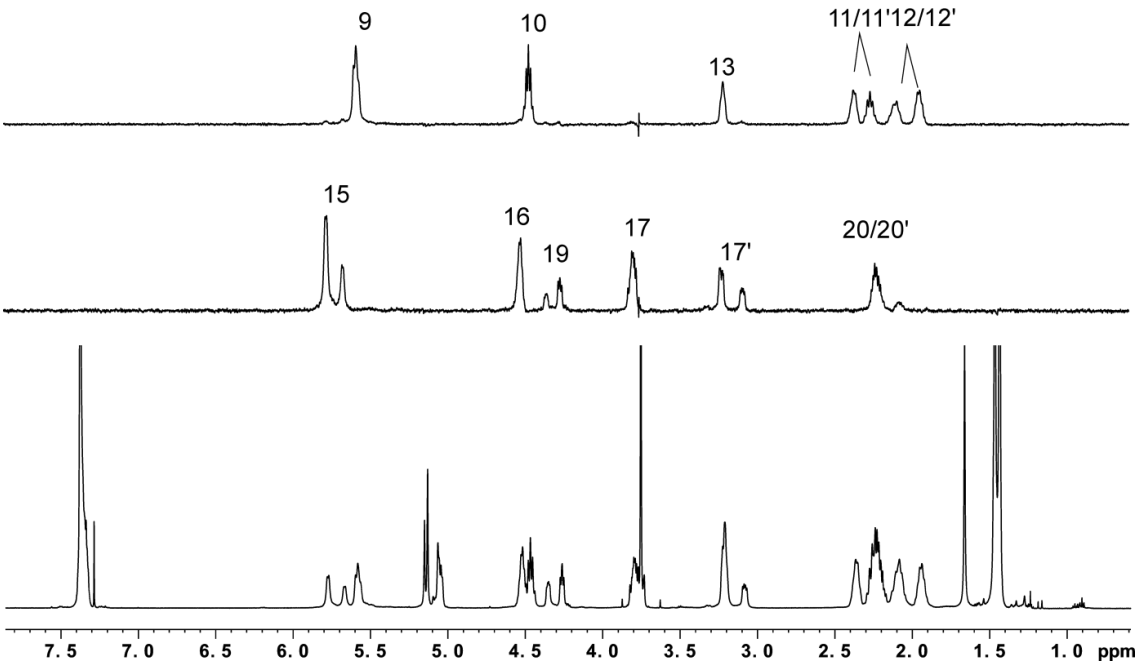

^{13}C-NMR (150 MHz, DMSO-d_6, 298 K)

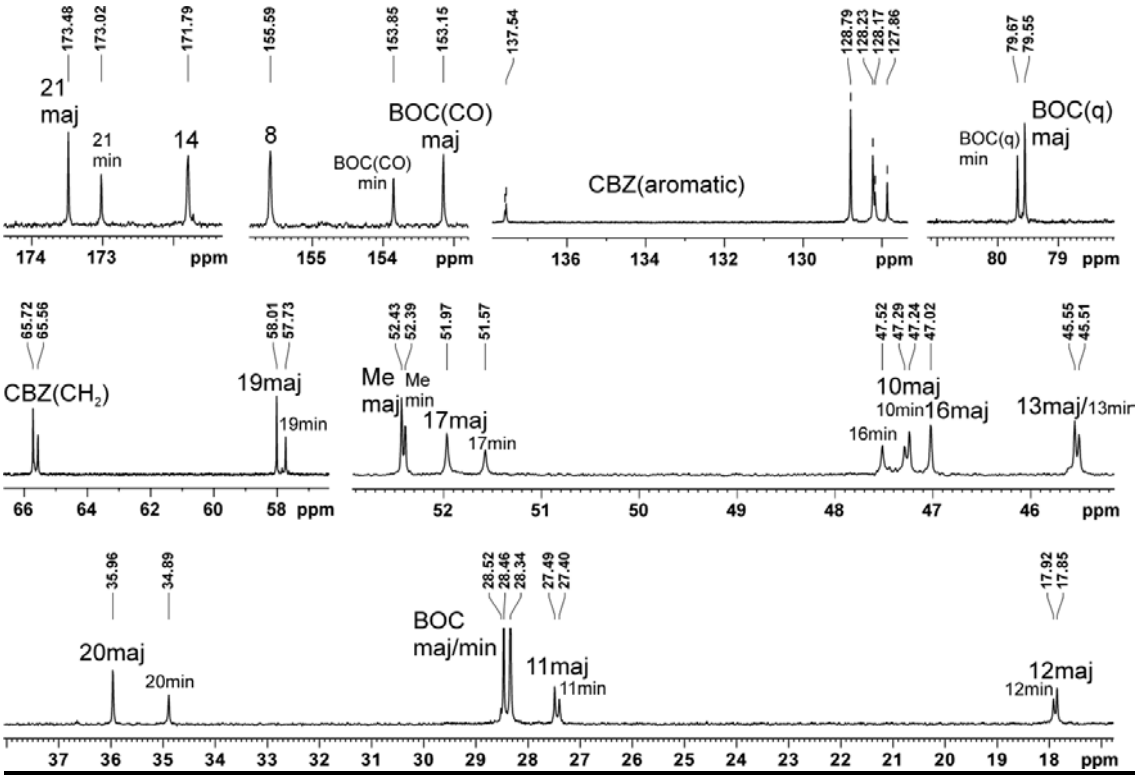

Multiplicity Edited HSQC (600 MHz, DMSO-d_6, 298 K)

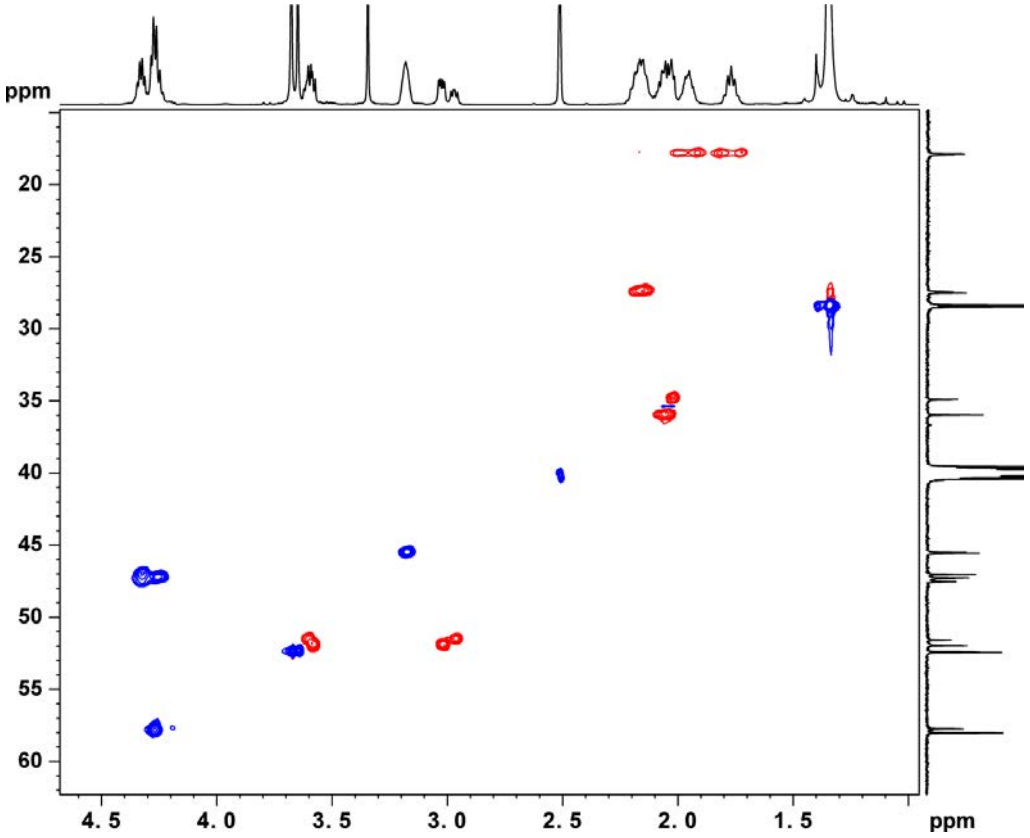

β-*trans*,γ-*cis*, 37

^{1}H-NMR (600 MHz, DMSO-d_6, 298 K)

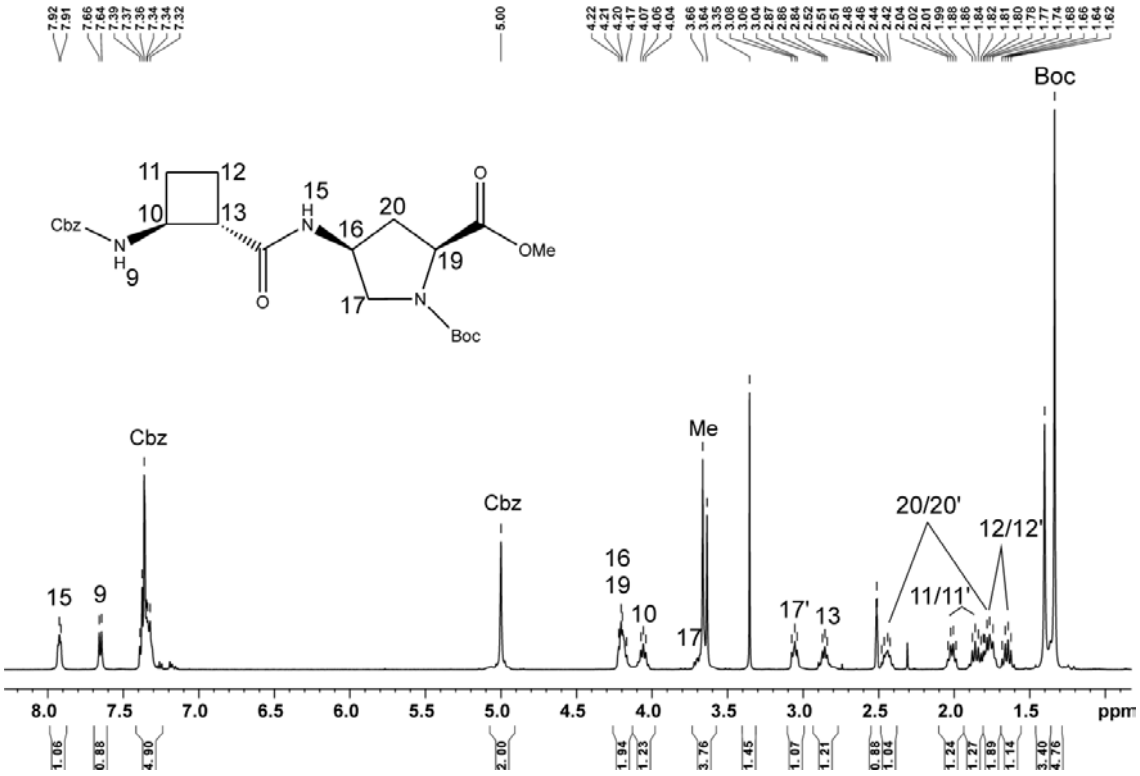

^{1}H-NMR (600 MHz, $CDCl_3$, 298 K)

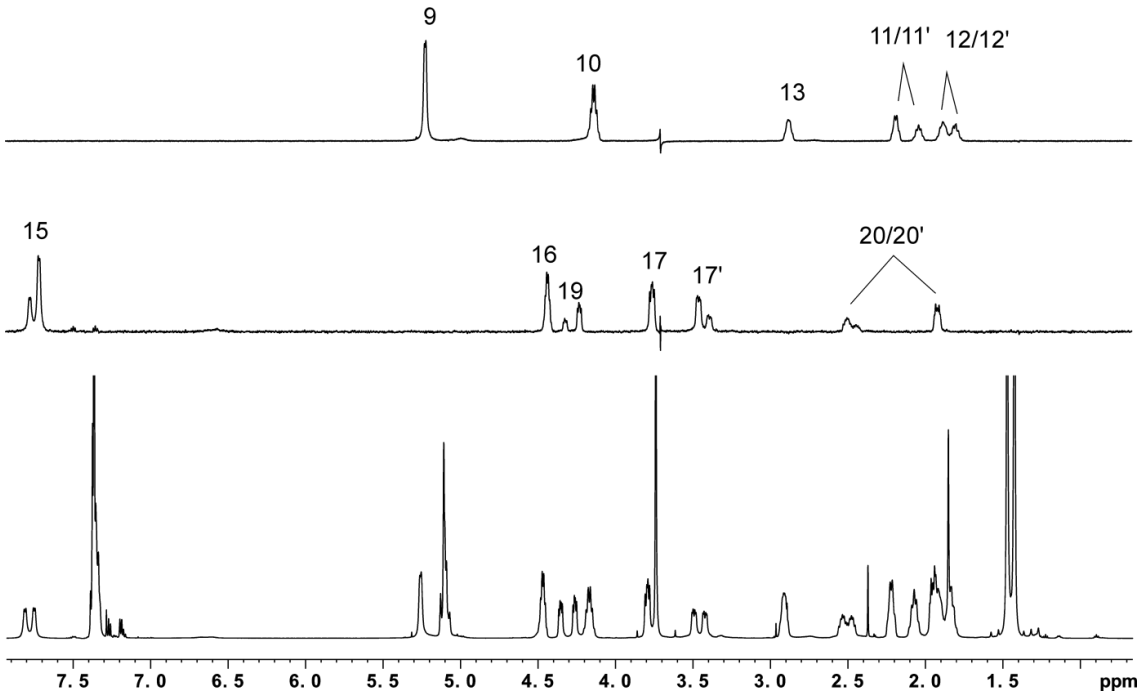

^{13}C-NMR (150 MHz, DMSO-d_6, 298 K)

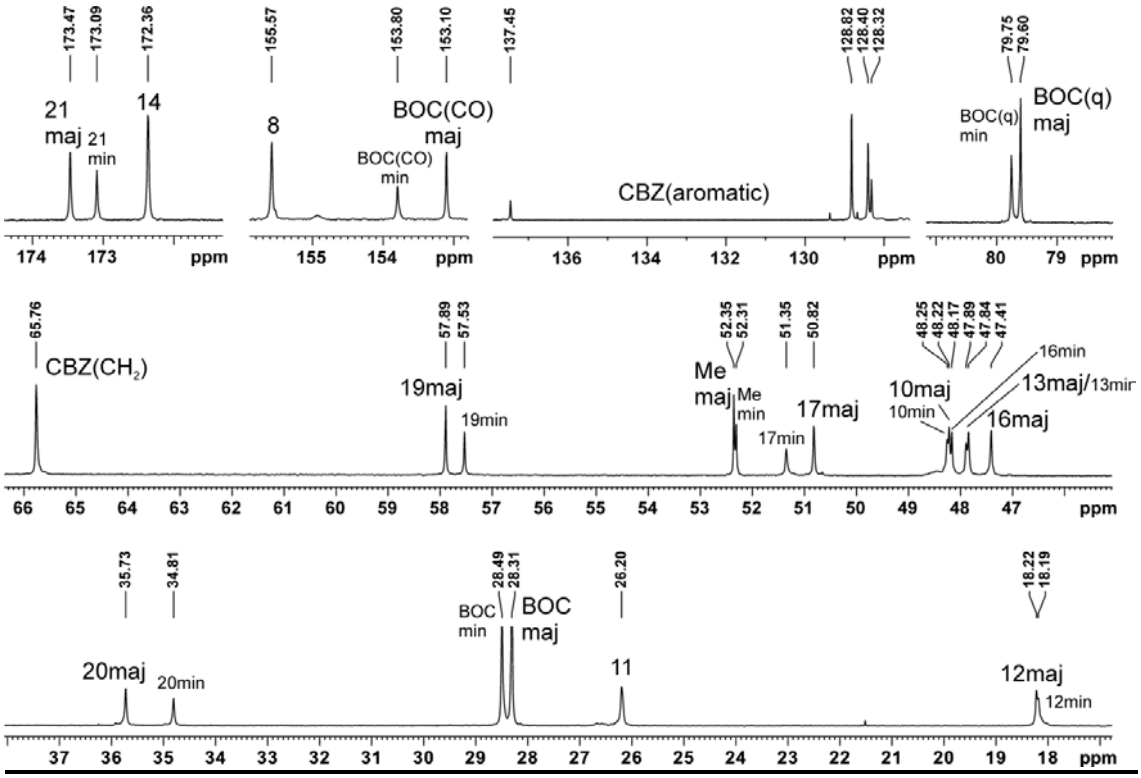

Multiplicity Edited HSQC (600 MHz, DMSO-d_6, 298 K)

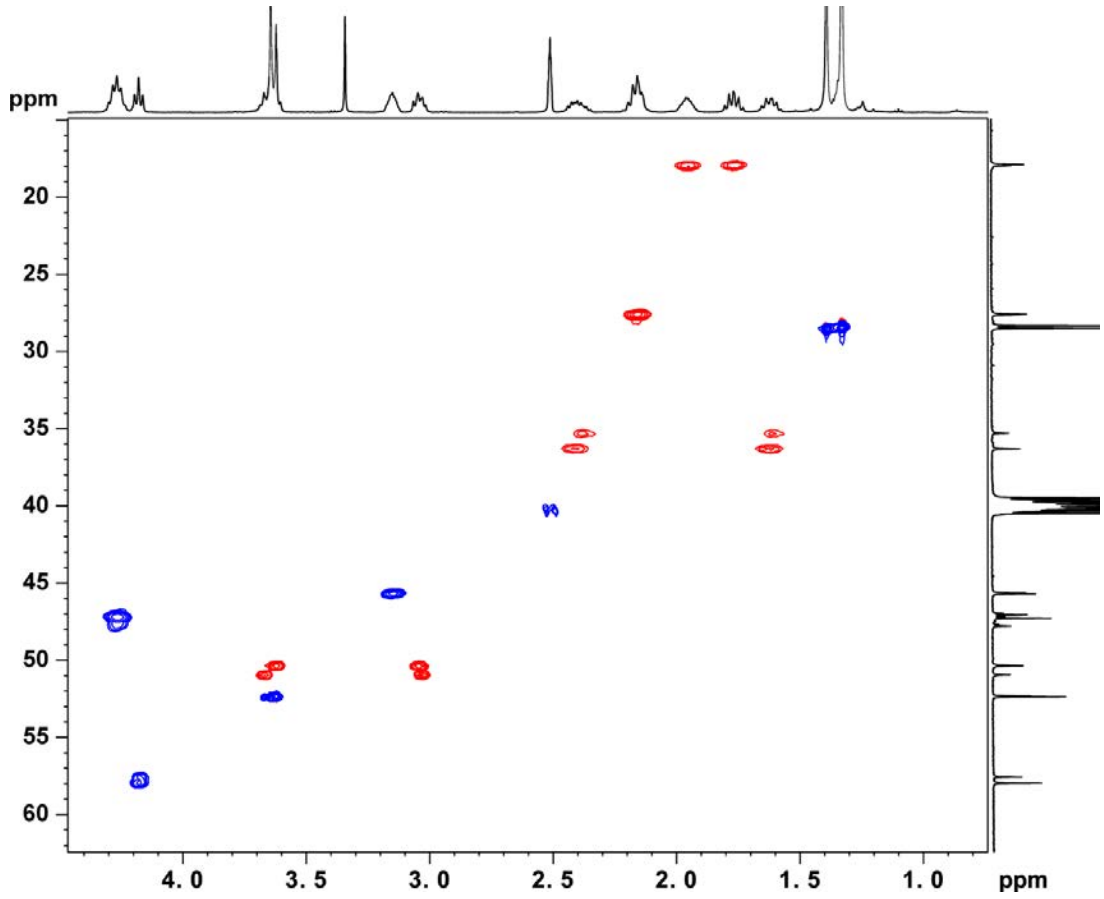

β-*trans*,γ-*trans*, 39

^{1}H-NMR (600 MHz, DMSO-d_6, 298 K)

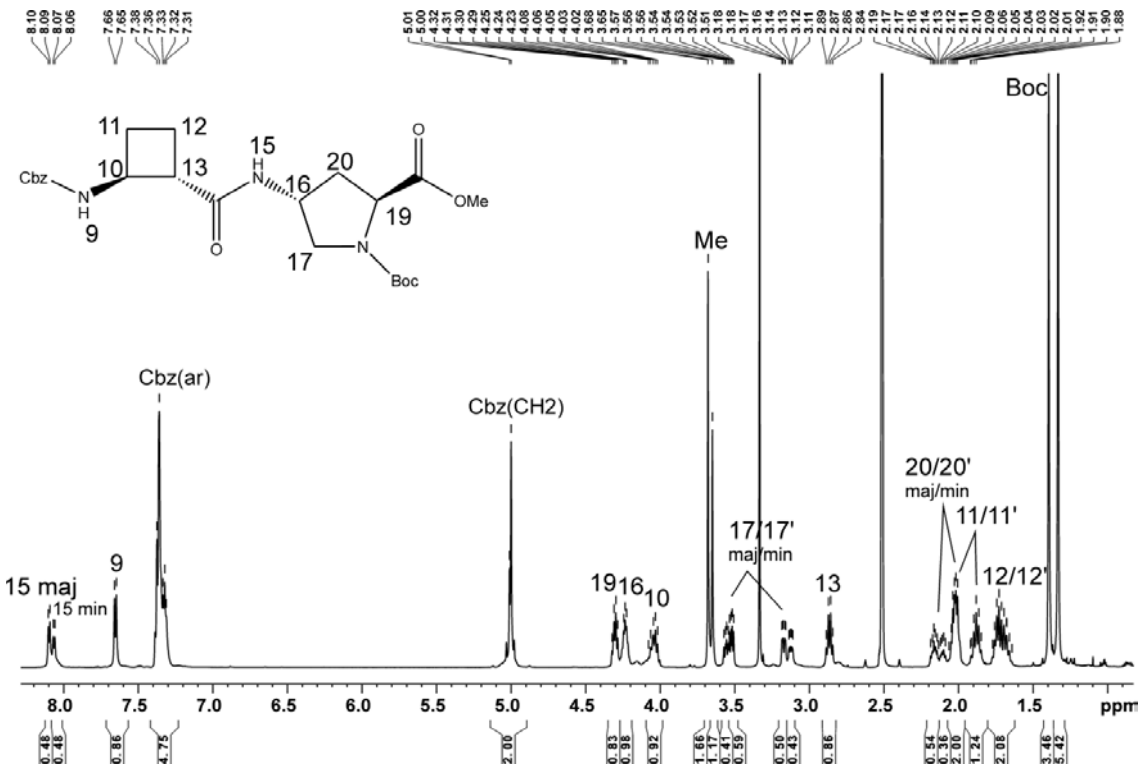

^{1}H-NMR and SELTOCSY (600 MHz, $CDCl_3$, 298 K)

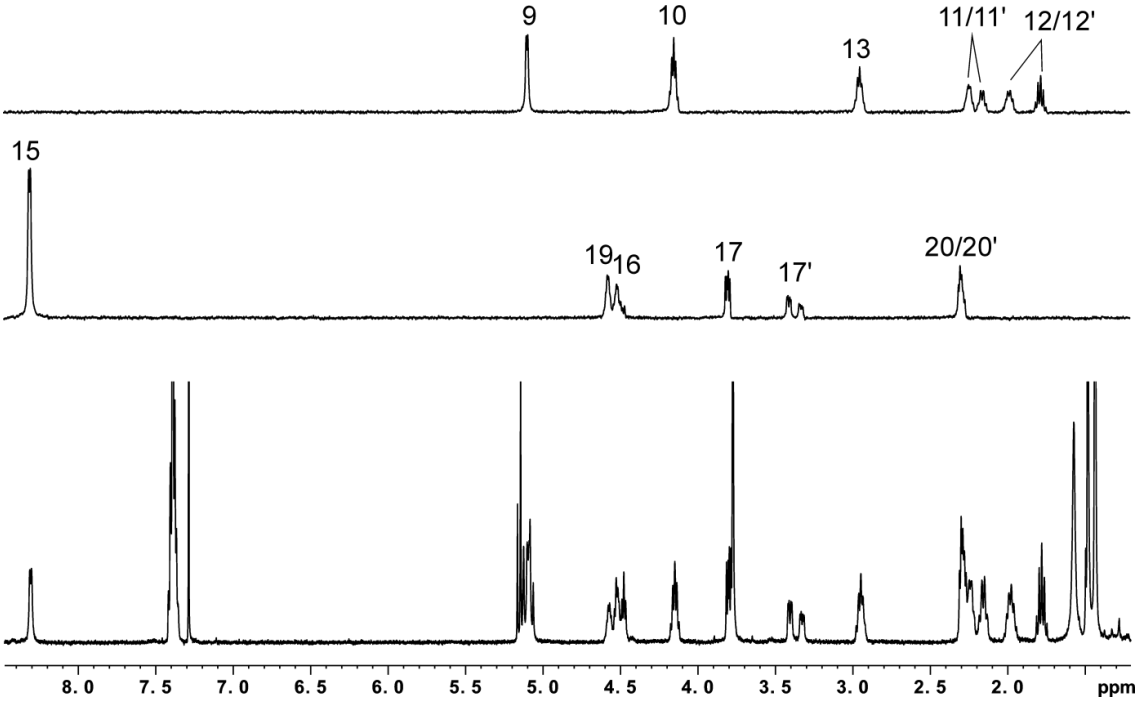

^{13}C-NMR (150 MHz, DMSO-d_6, 298 K)

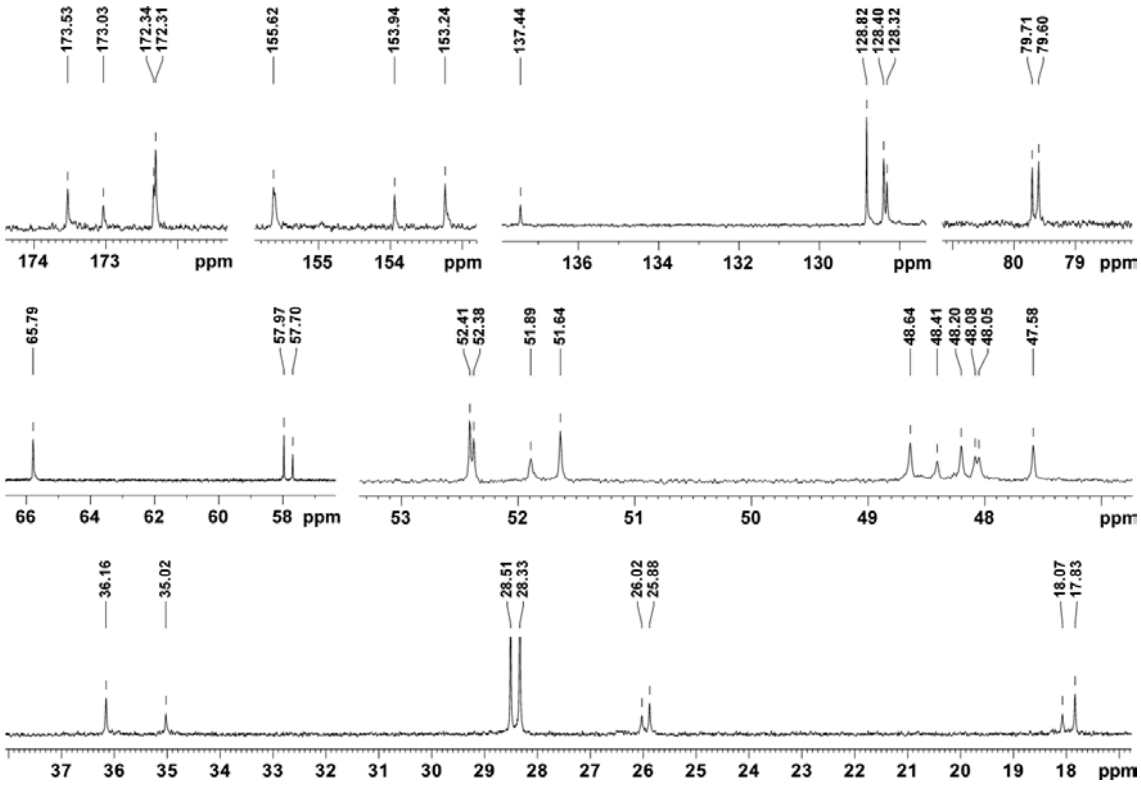

Multiplicity Edited HSQC (600 MHz, DMSO-d_6, 298 K)

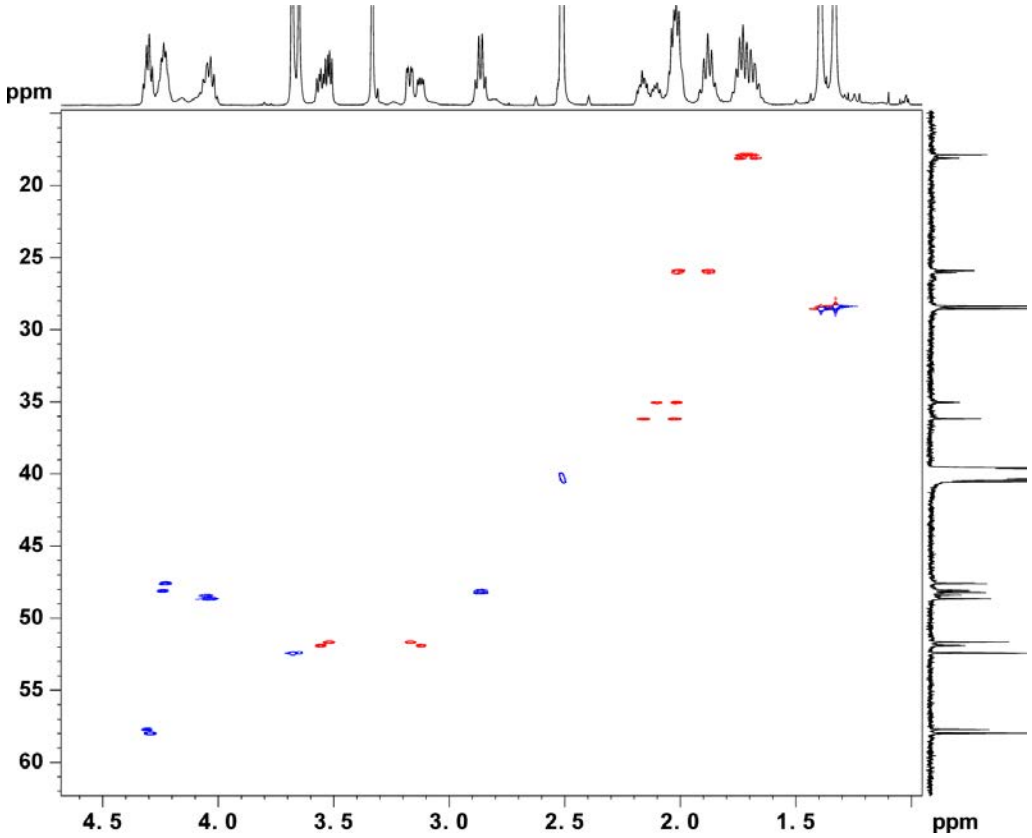

β-*cis*,γ-*cis*, 34

^{1}H-NMR (600 MHz, DMSO-d_6, variable temperatures)

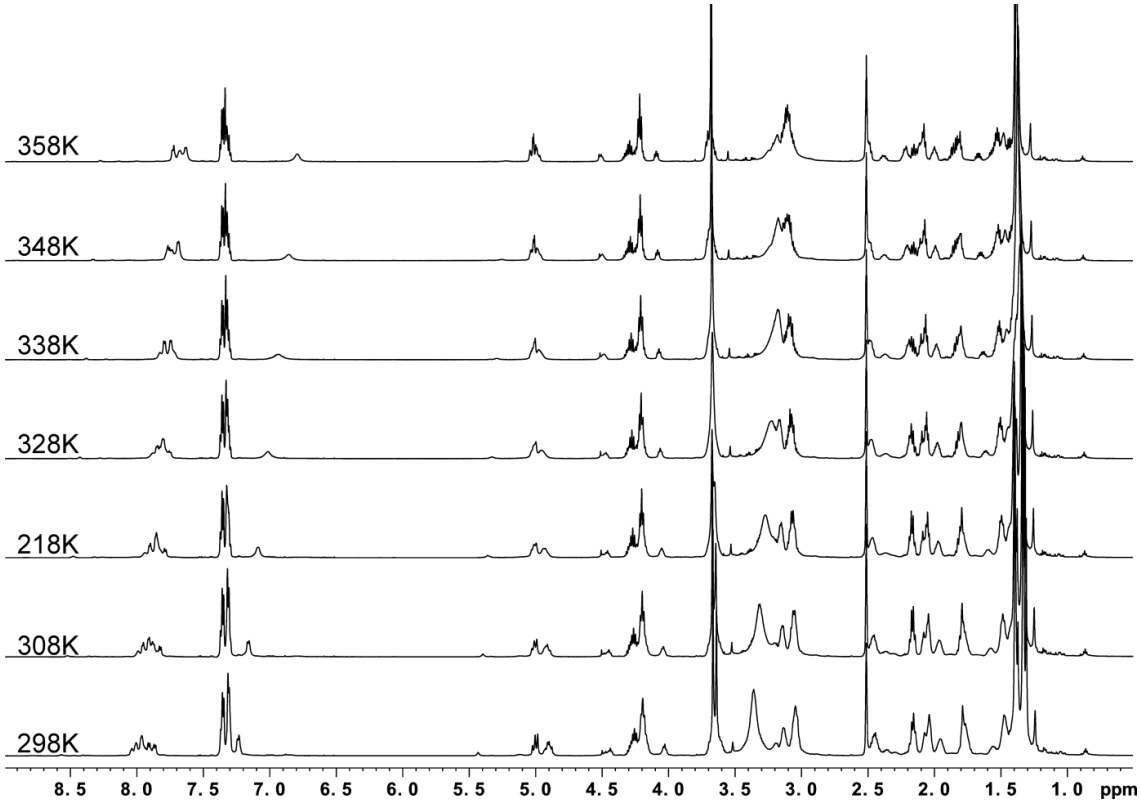

SELTOCSY (600 MHz, DMSO-d_6, 358 K)

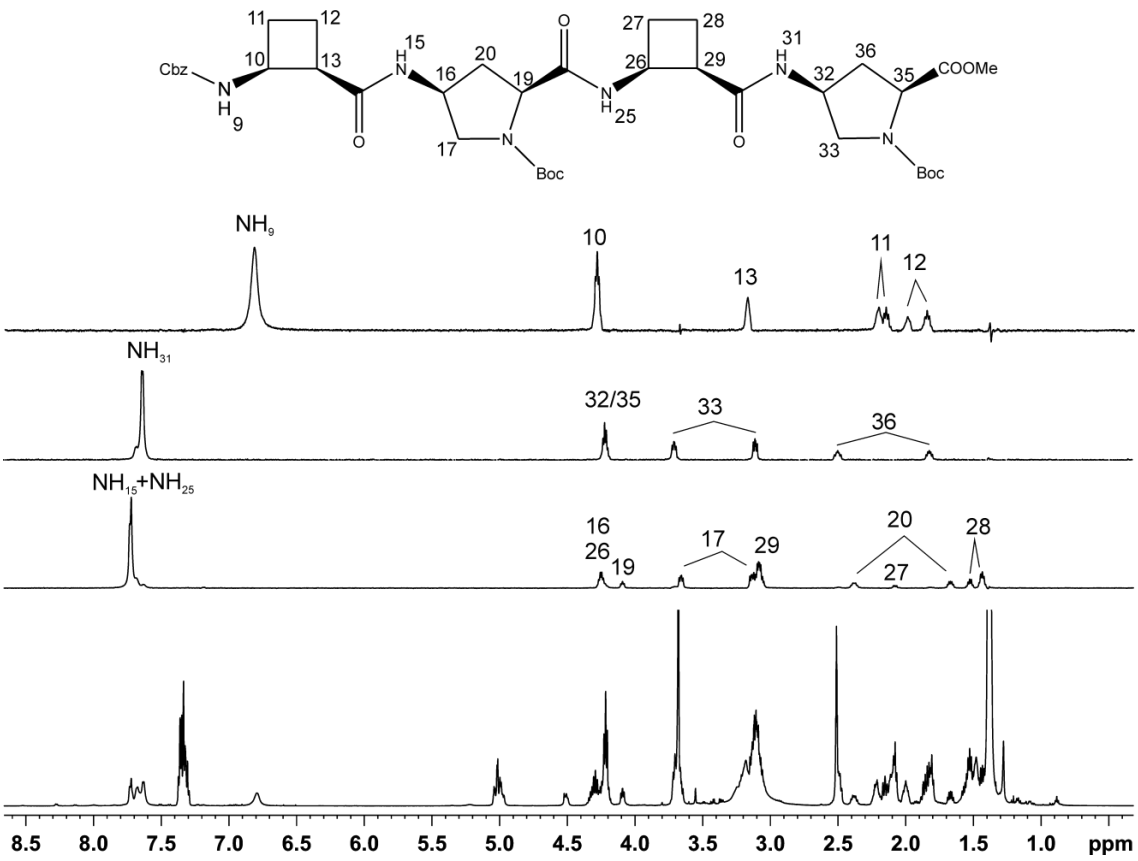

^{13}C-NMR (150 MHz, DMSO-d_6, 358 K)

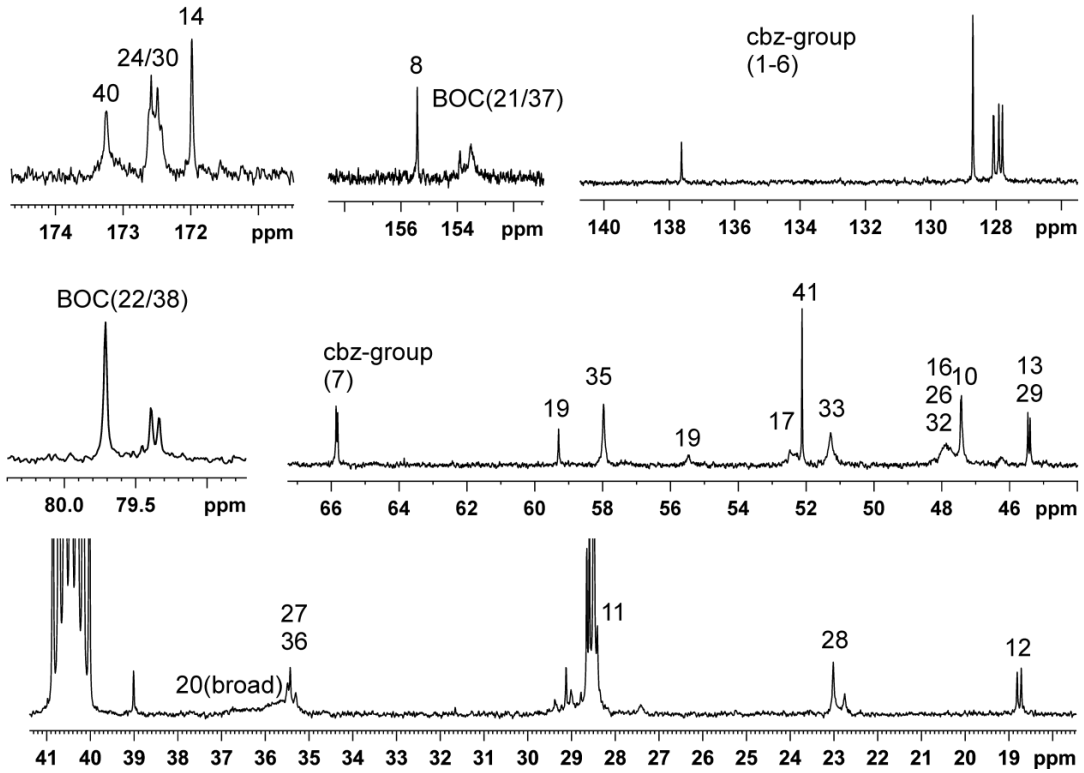

COSY (600 MHz, DMSO-d_6, 358 K)

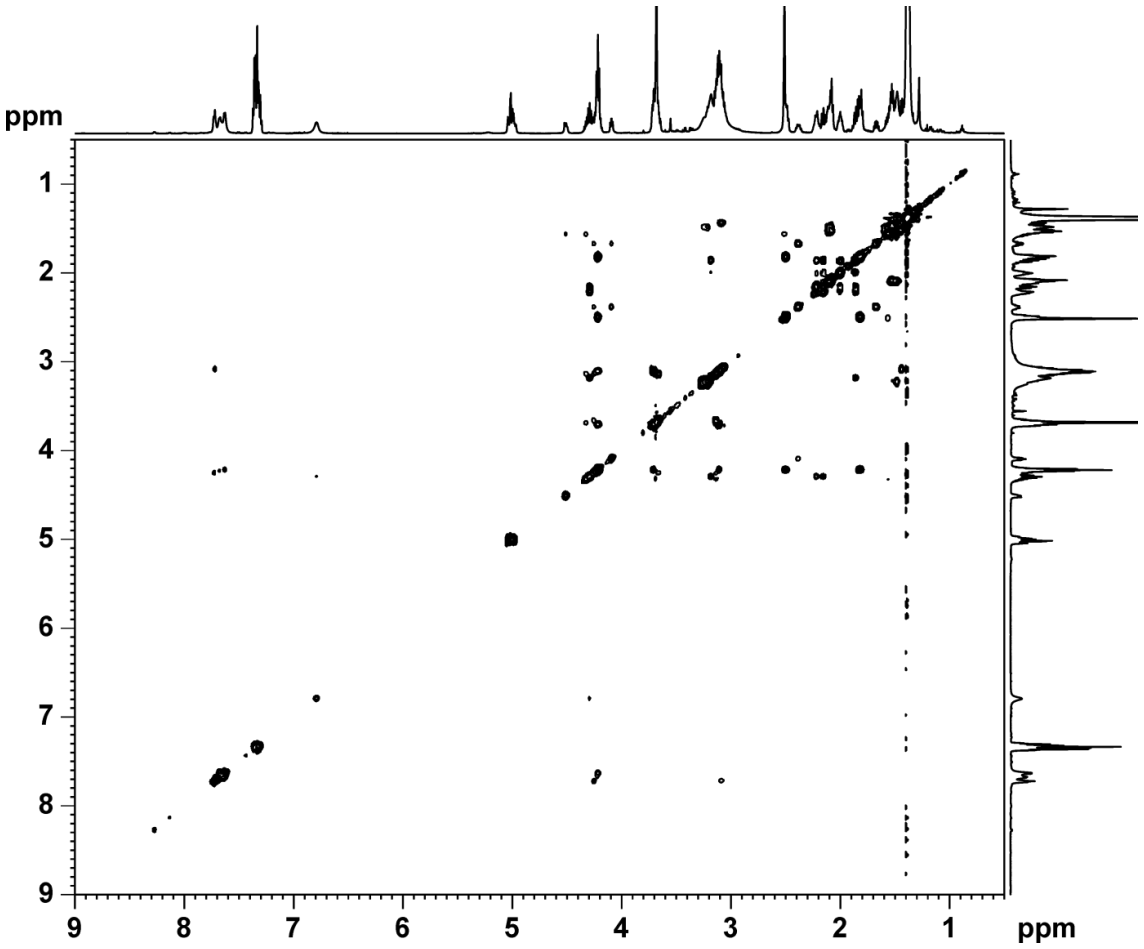

Multiplicity edited HSQC (600 MHz, DMSO-d_6, 358 K)

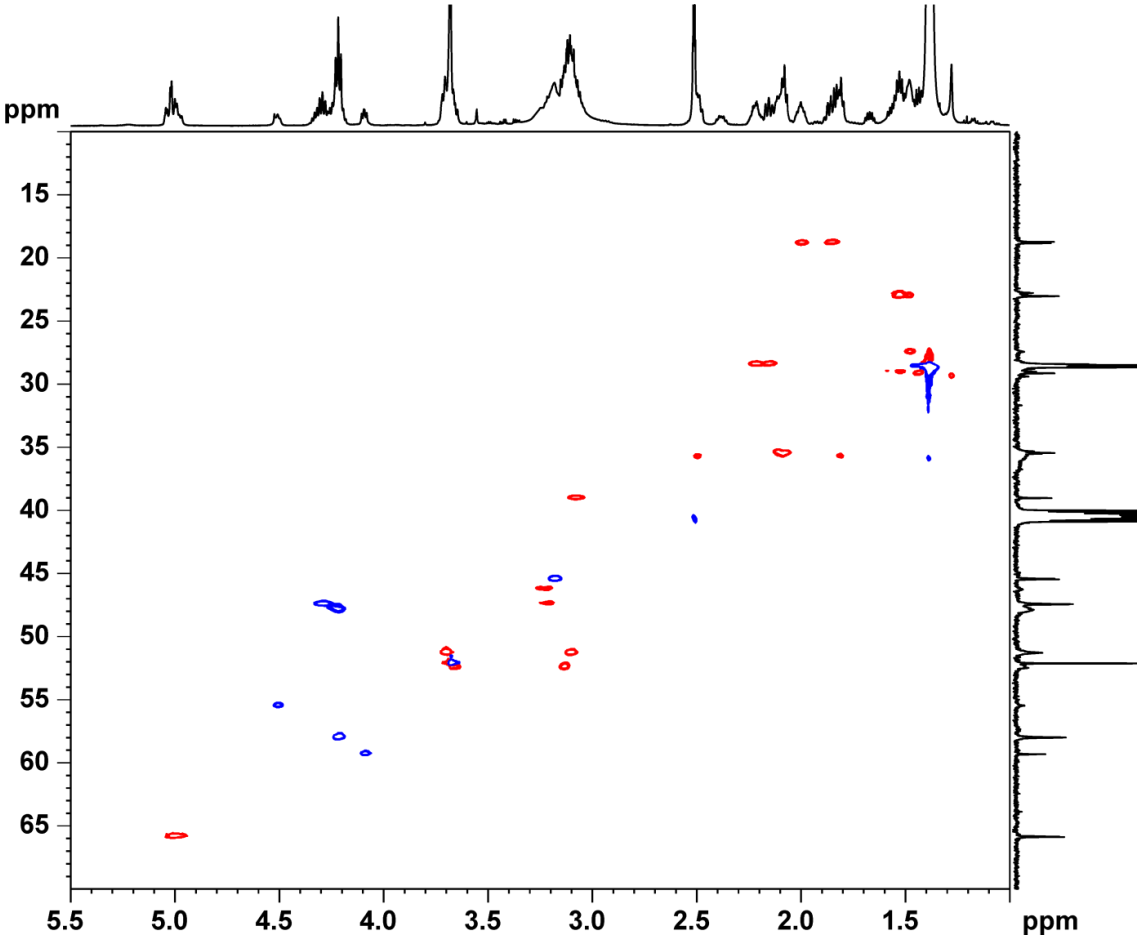

β-*cis*,γ-*trans*, 36

^{1}H-NMR (600 MHz, DMSO-d_6, variable temperatures)

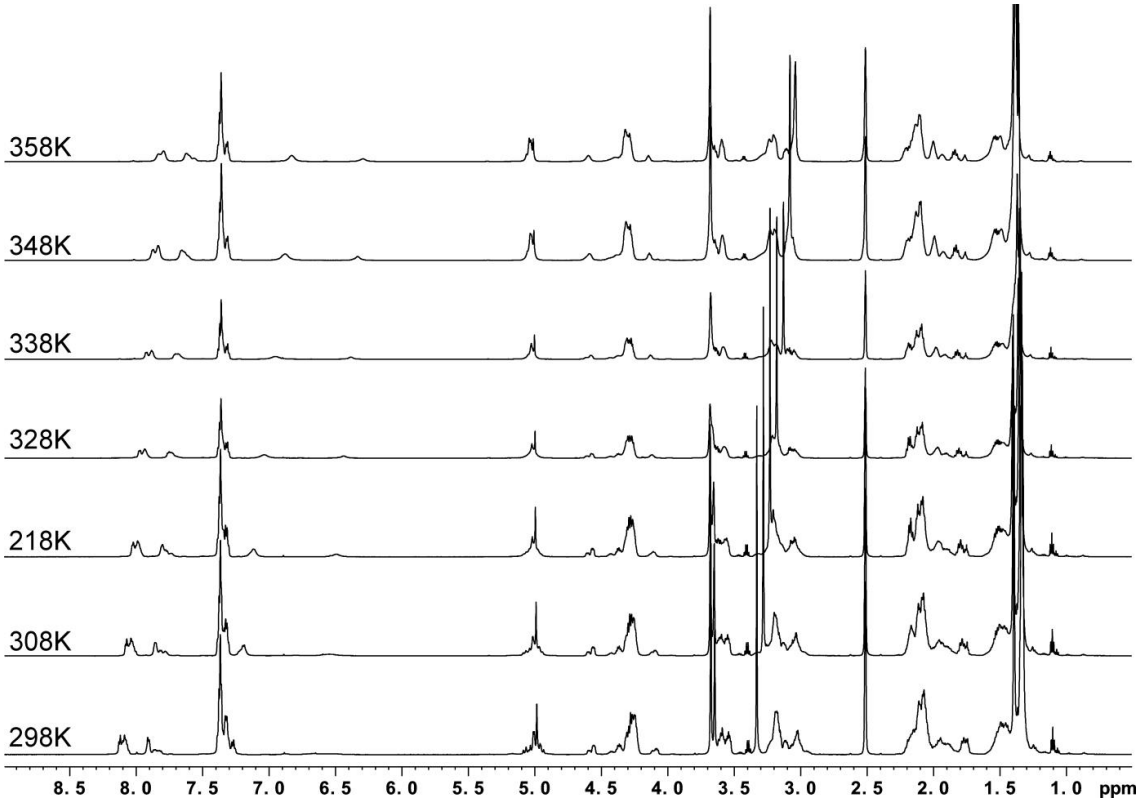

^{13}C-NMR (150 MHz, DMSO-d_6, 358 K)

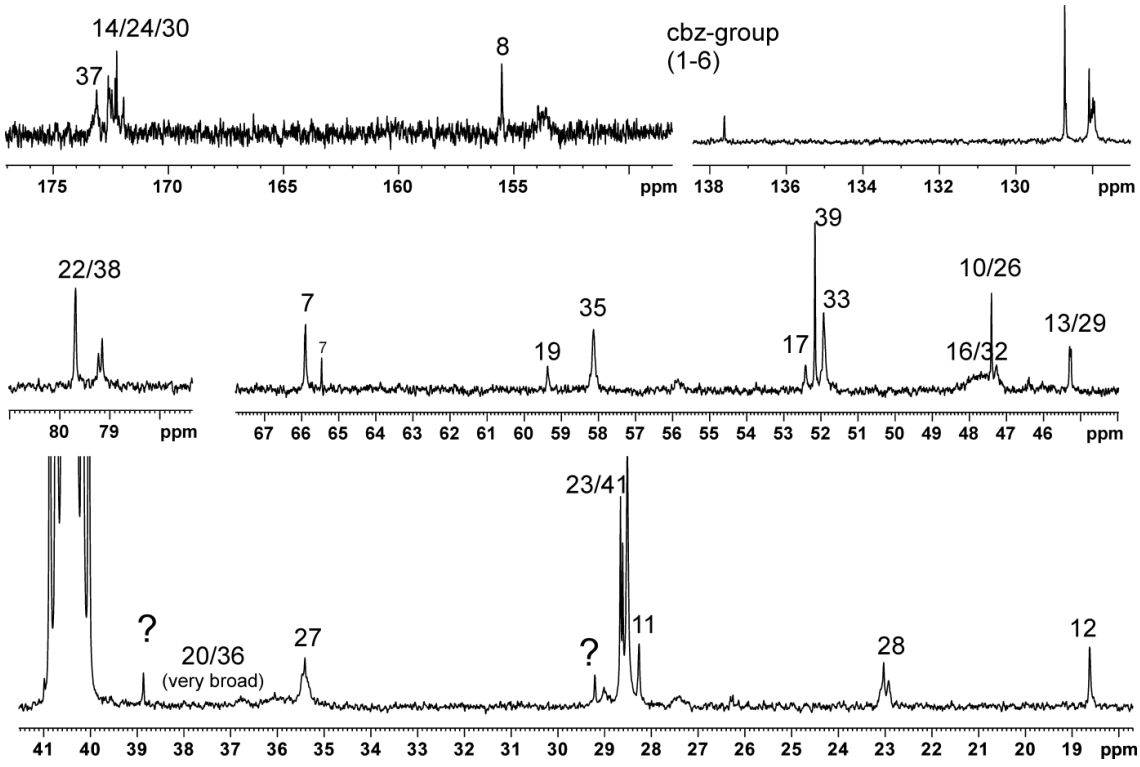

SELTOCSY (600 MHz, DMSO-d_6, 358 K)

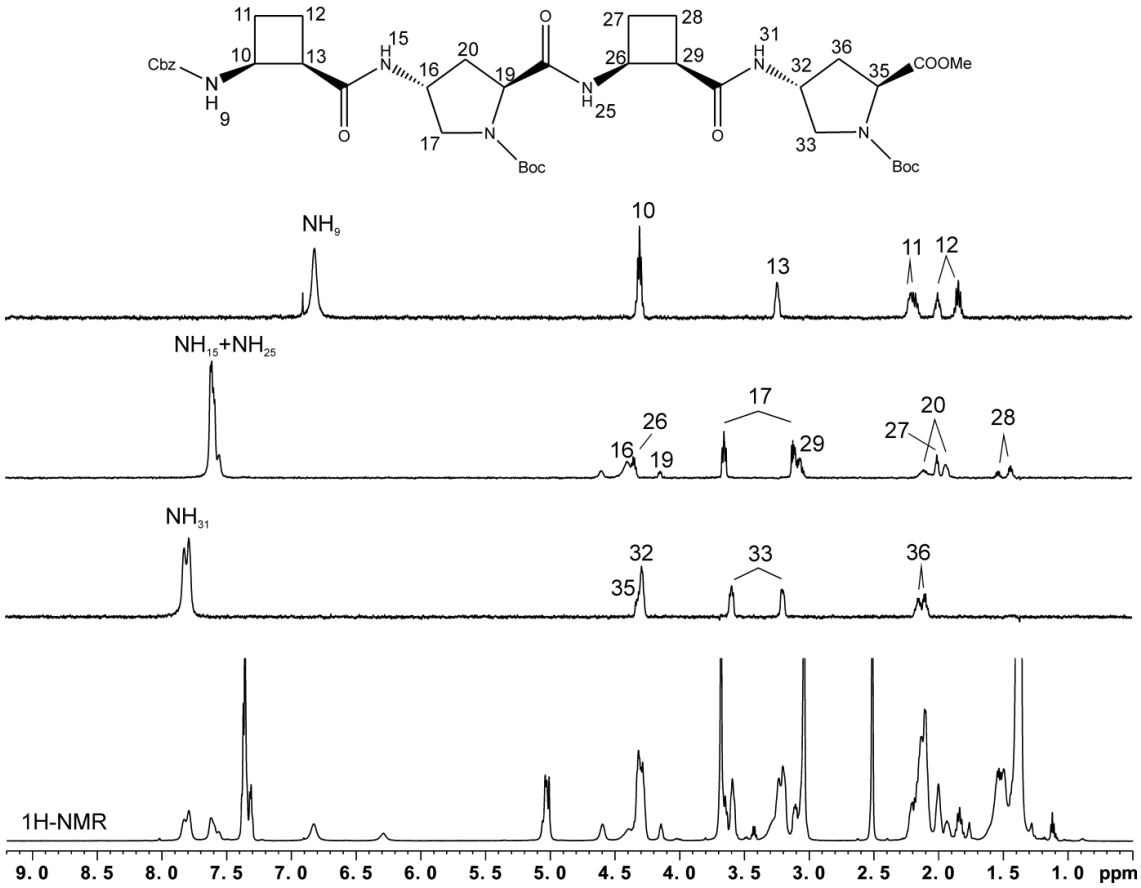

COSY (600 MHz, DMSO-d_6, 358 K)

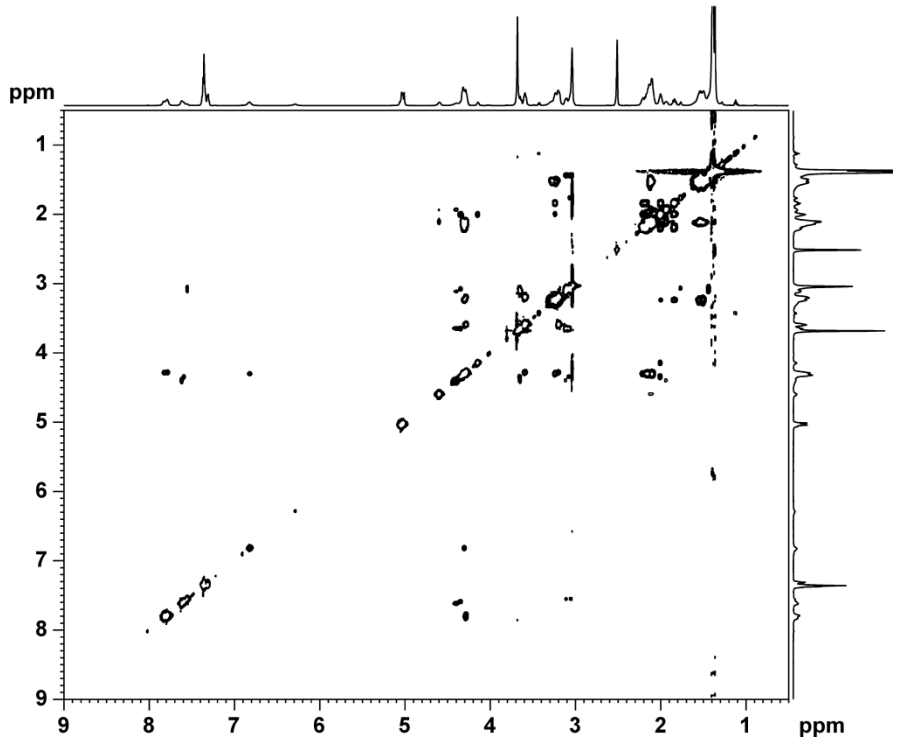

Multiplicity Edited HSQC (600 MHz, DMSO-d_6, 358 K)

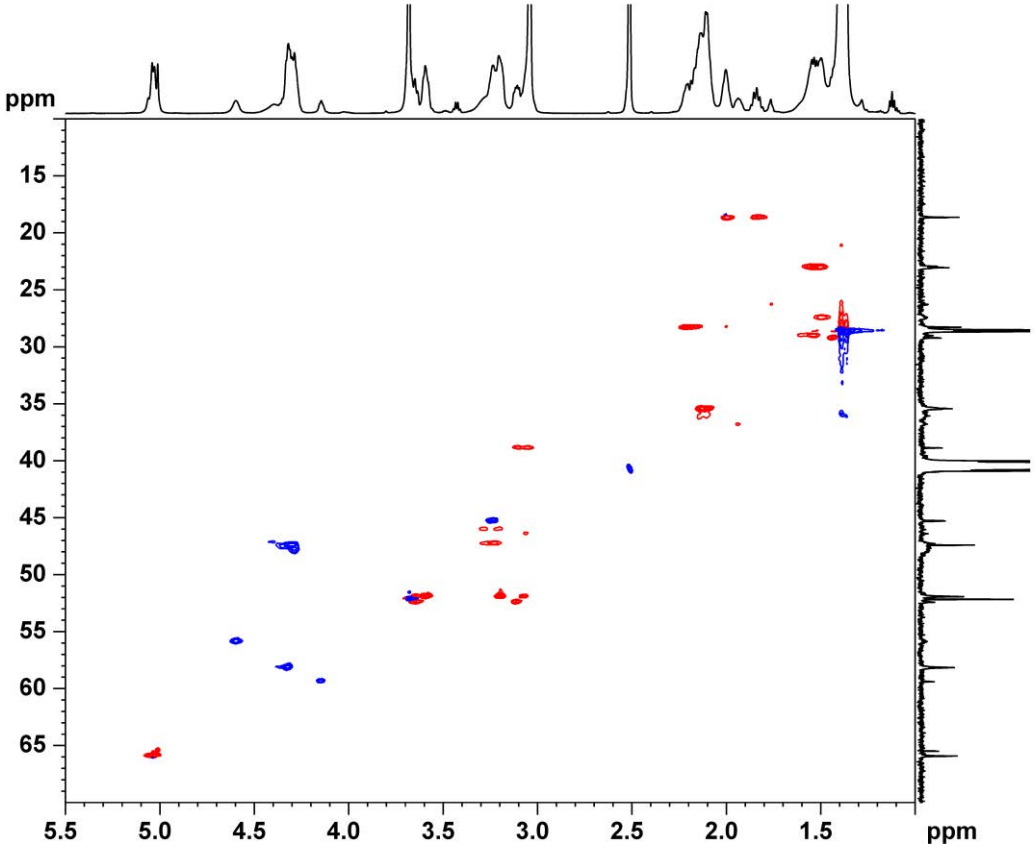

β-*trans*,γ-*cis*, 38

^{1}H-NMR (600 MHz, DMSO-d_6, variable temperatures)

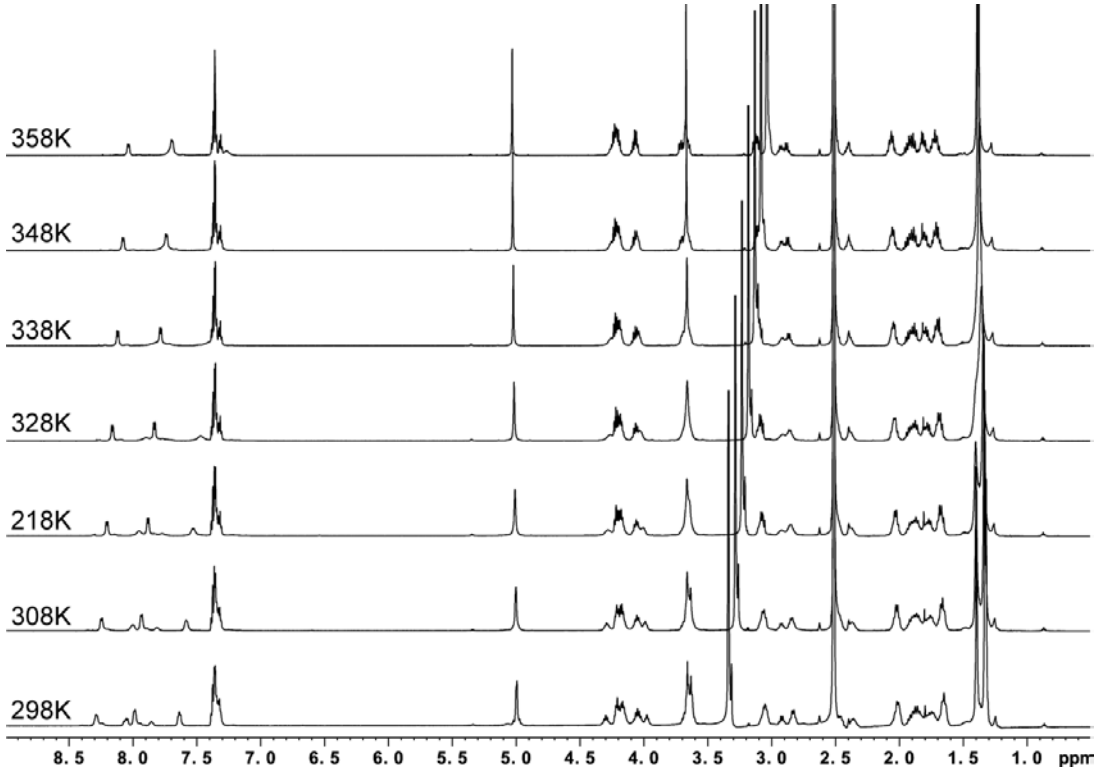

^{13}C-NMR (150 MHz, DMSO-d_6, 358 K)

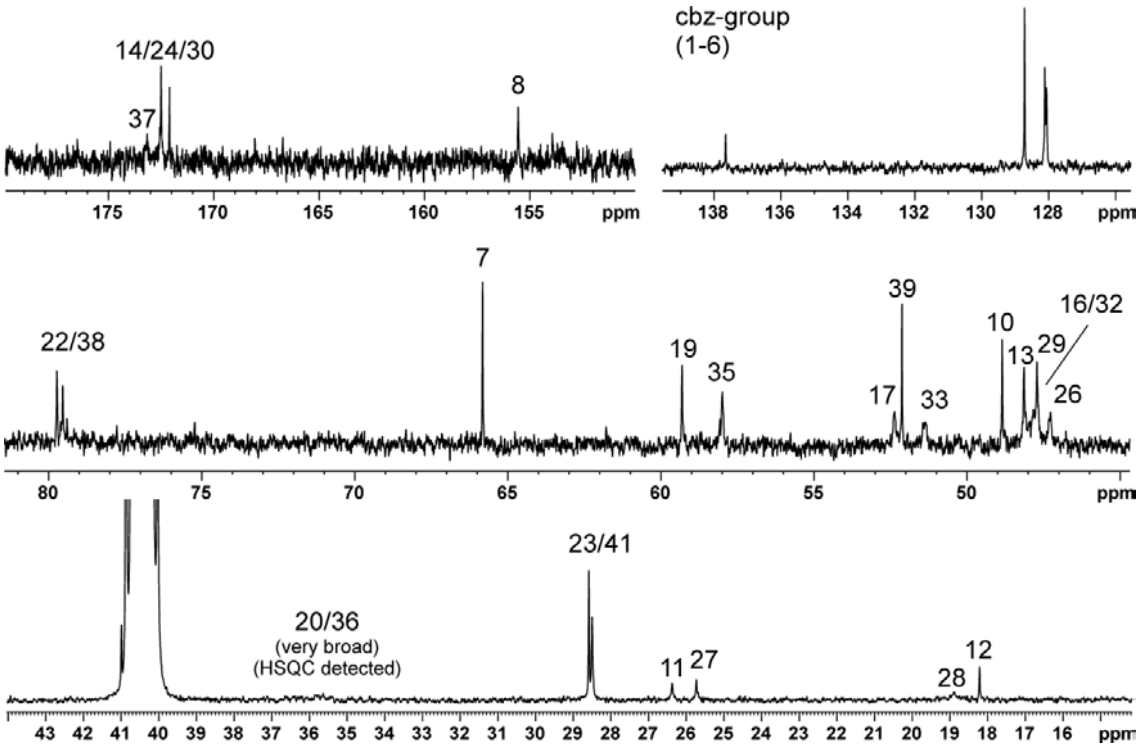

SELTOCSY (600 MHz, DMSO-d_6, 358 K)

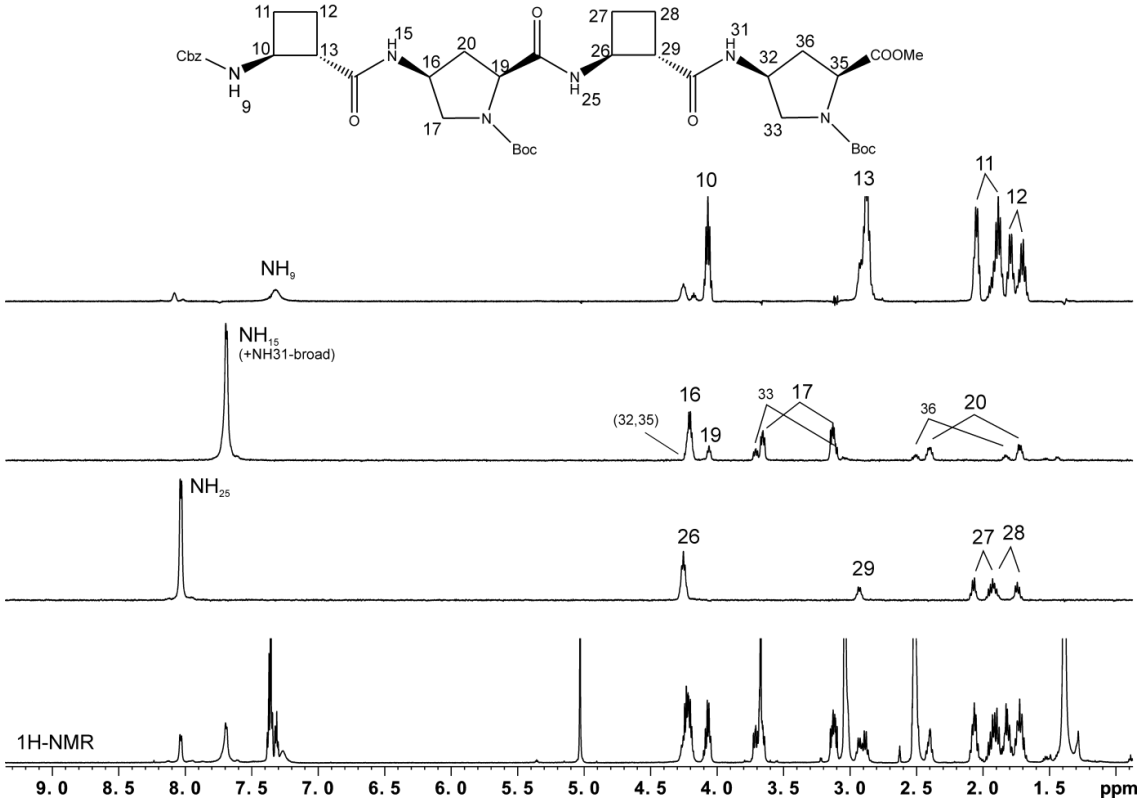

SELROESY (600 MHz, DMSO-d_6, 358 K)

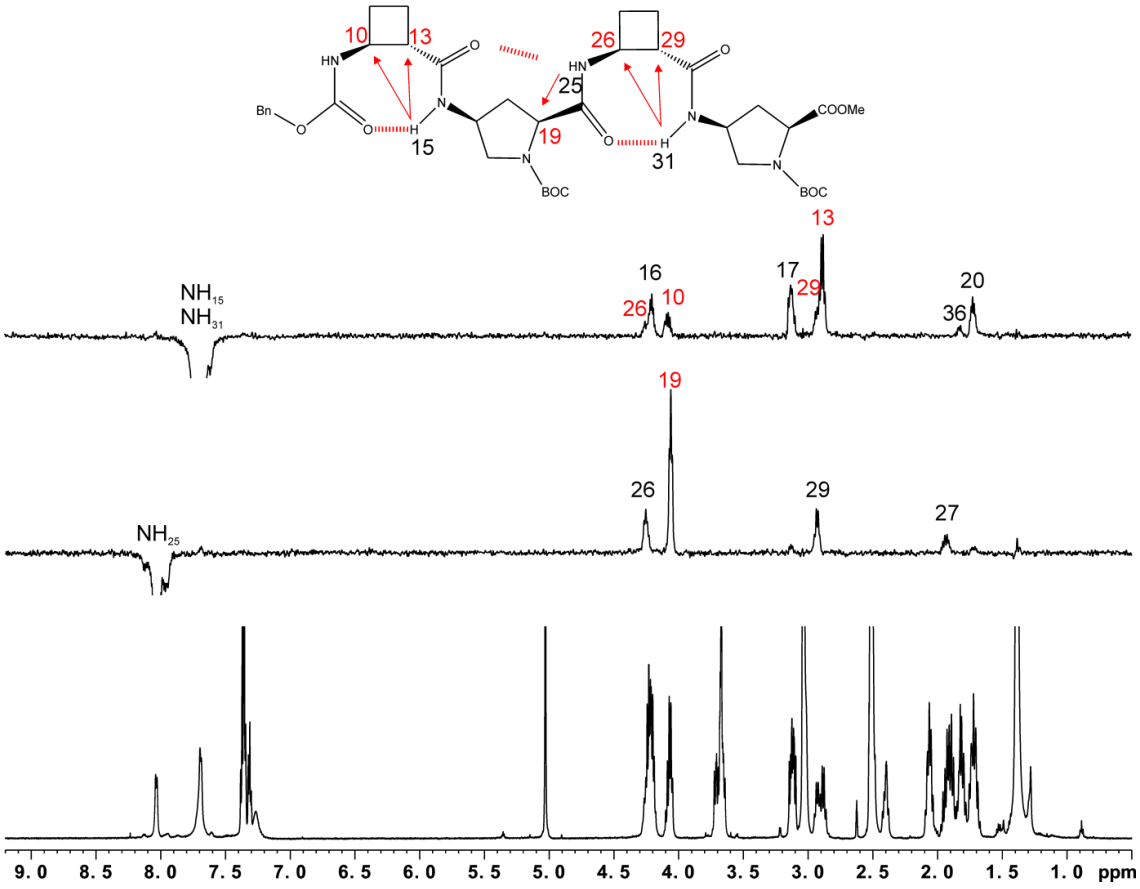

COSY (600 MHz, DMSO-d_6, 358 K)

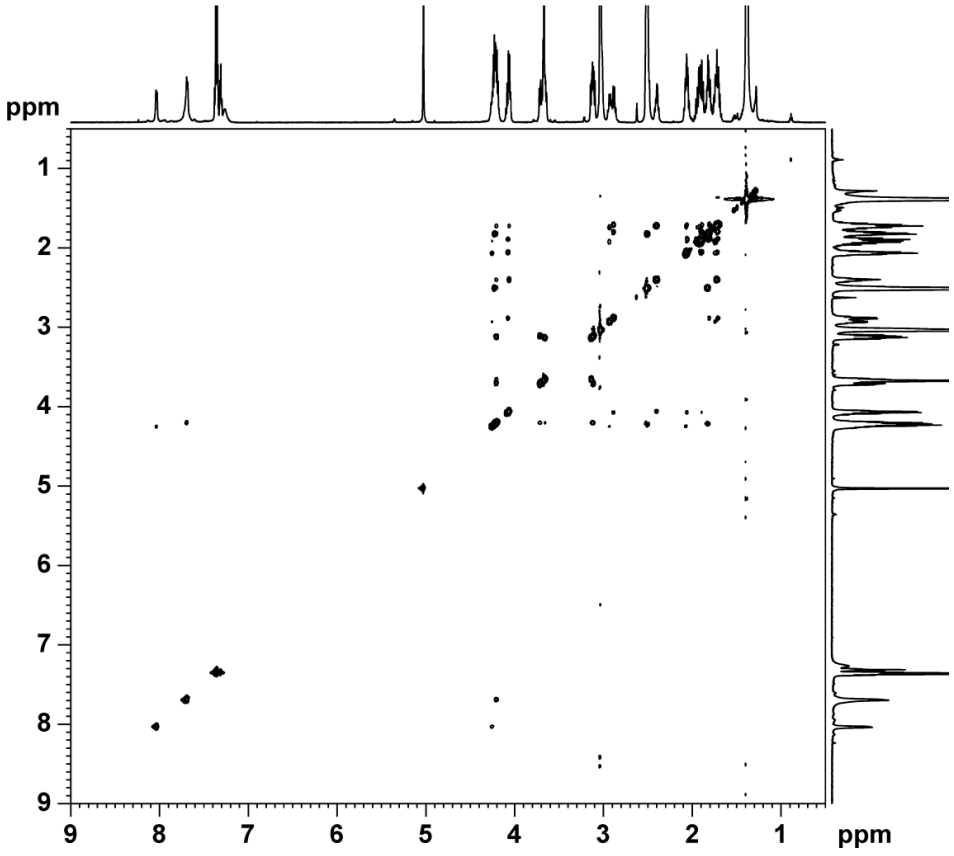

Multiplicity Edited HSQC (600 MHz, DMSO-d_6, 358 K)

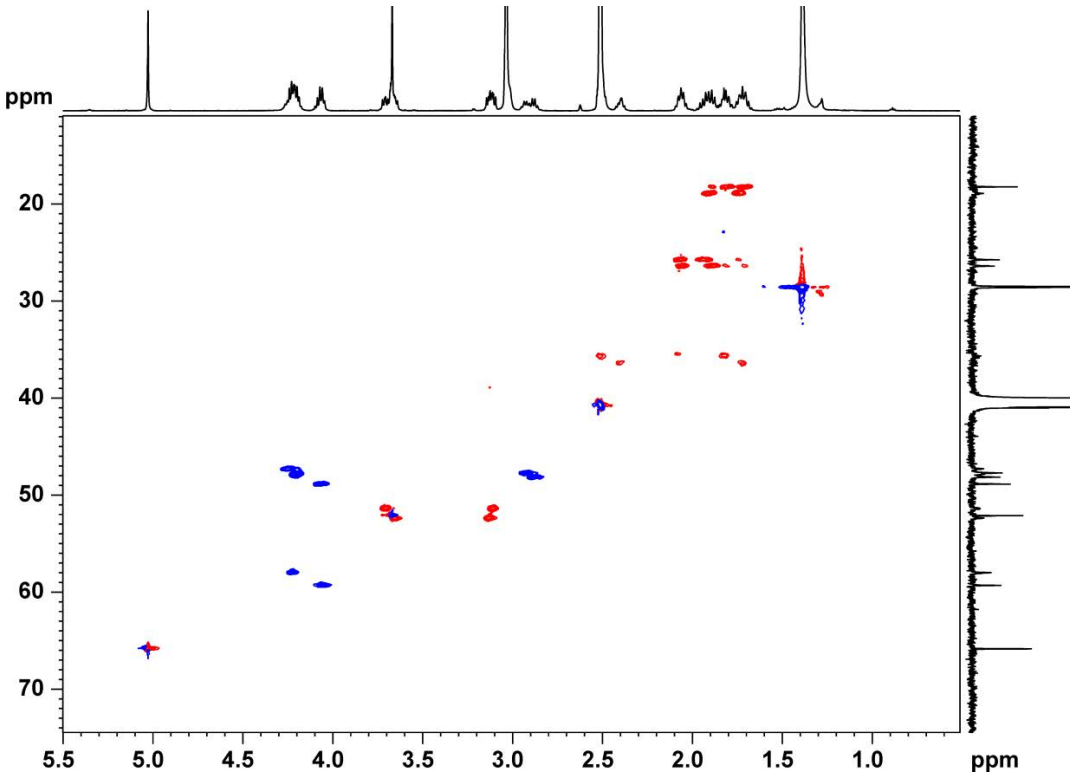

β-*trans*,γ-*trans*, 40

^{1}H-NMR (600 MHz, DMSO-d_6, variable temperatures)

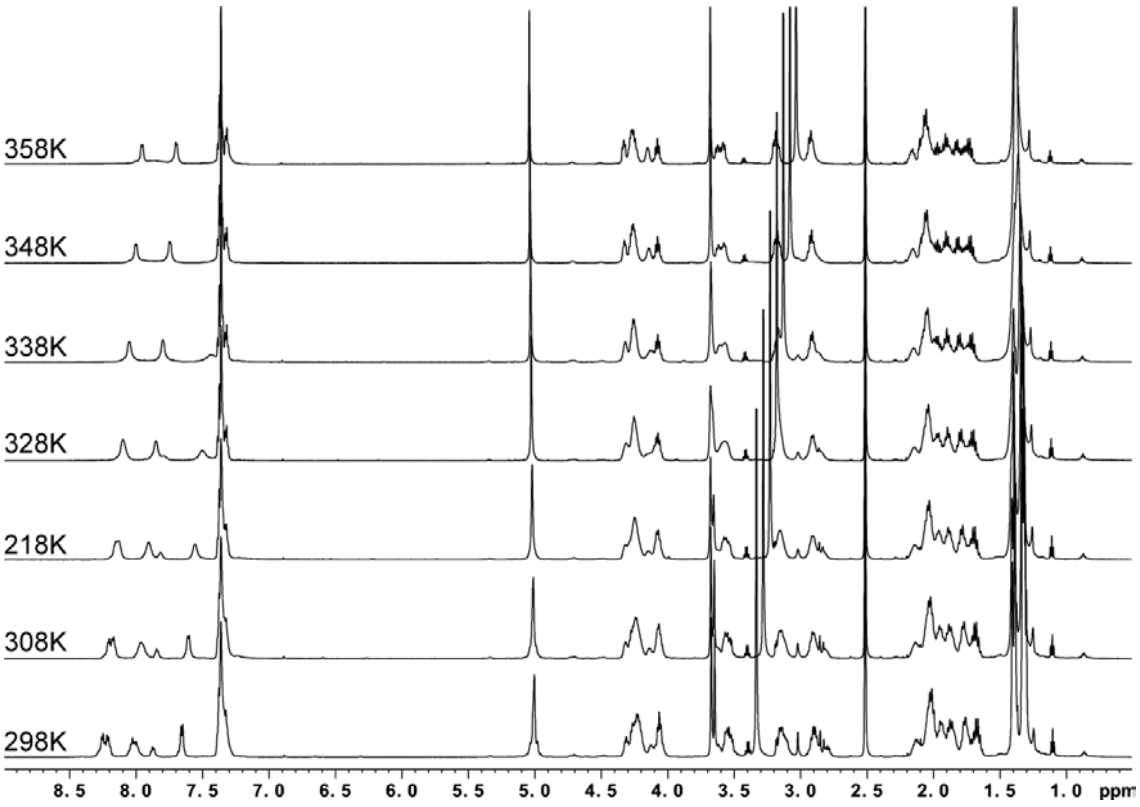

^{13}C-NMR (150 MHz, DMSO-*d*$_6$, 358 K)

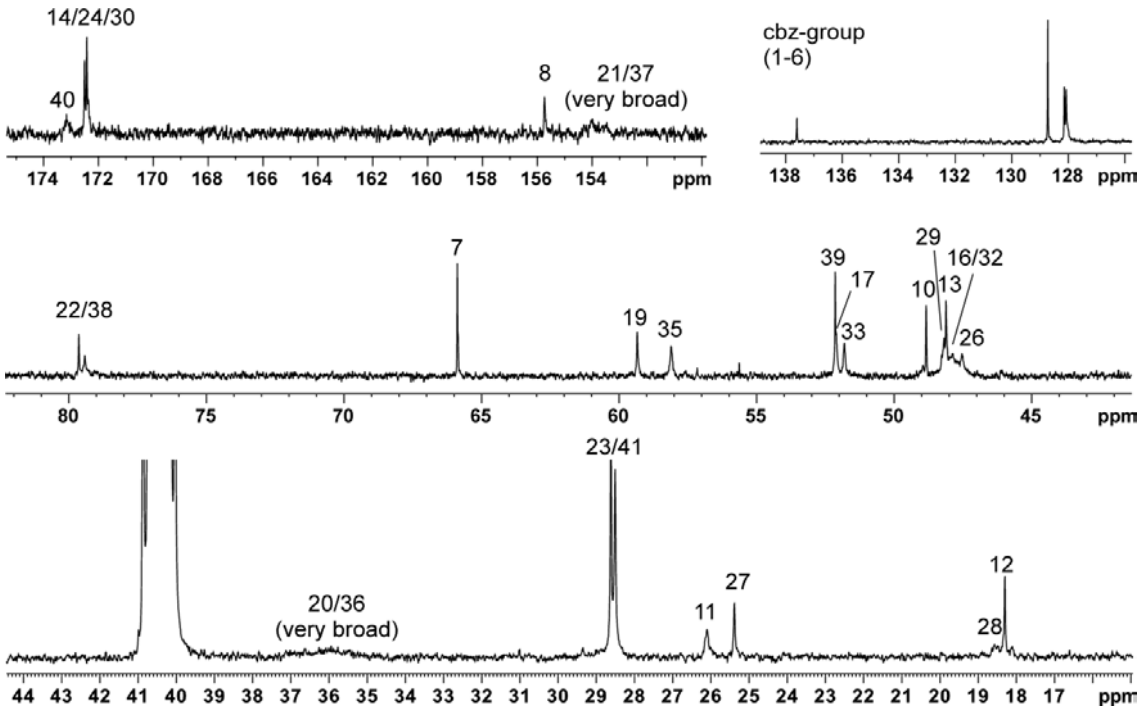

SELTOCSY (600 MHz, DMSO-*d*$_6$, 358 K)

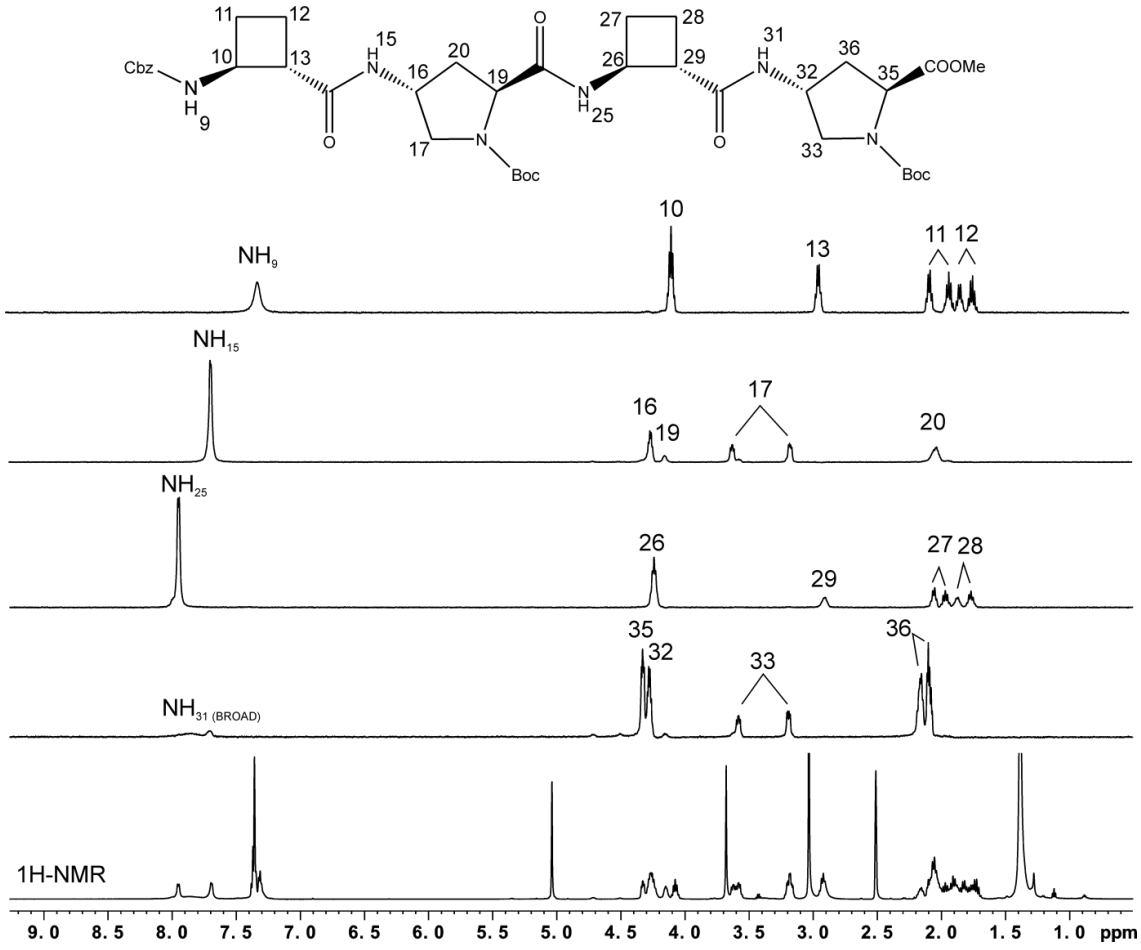

SELROESY (600 MHz, DMSO-*d*$_6$, 358 K)

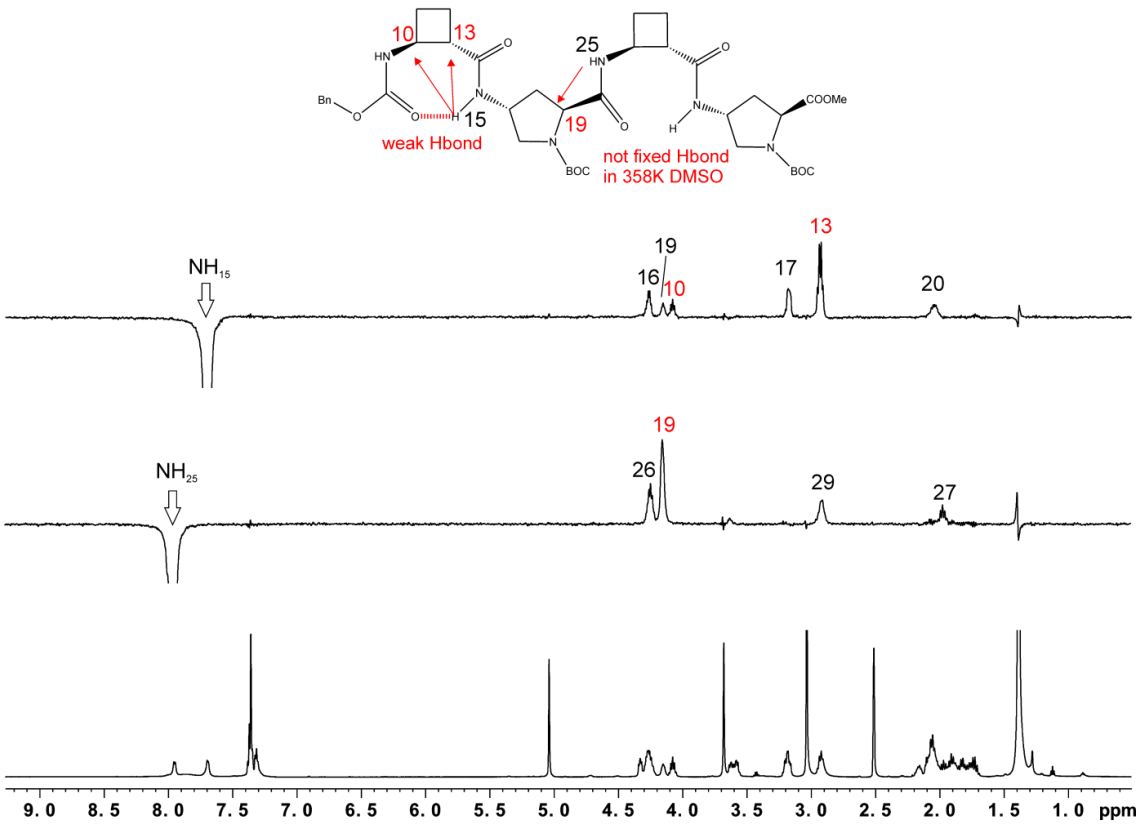

COSY (600 MHz, DMSO-*d*$_6$, 358 K)

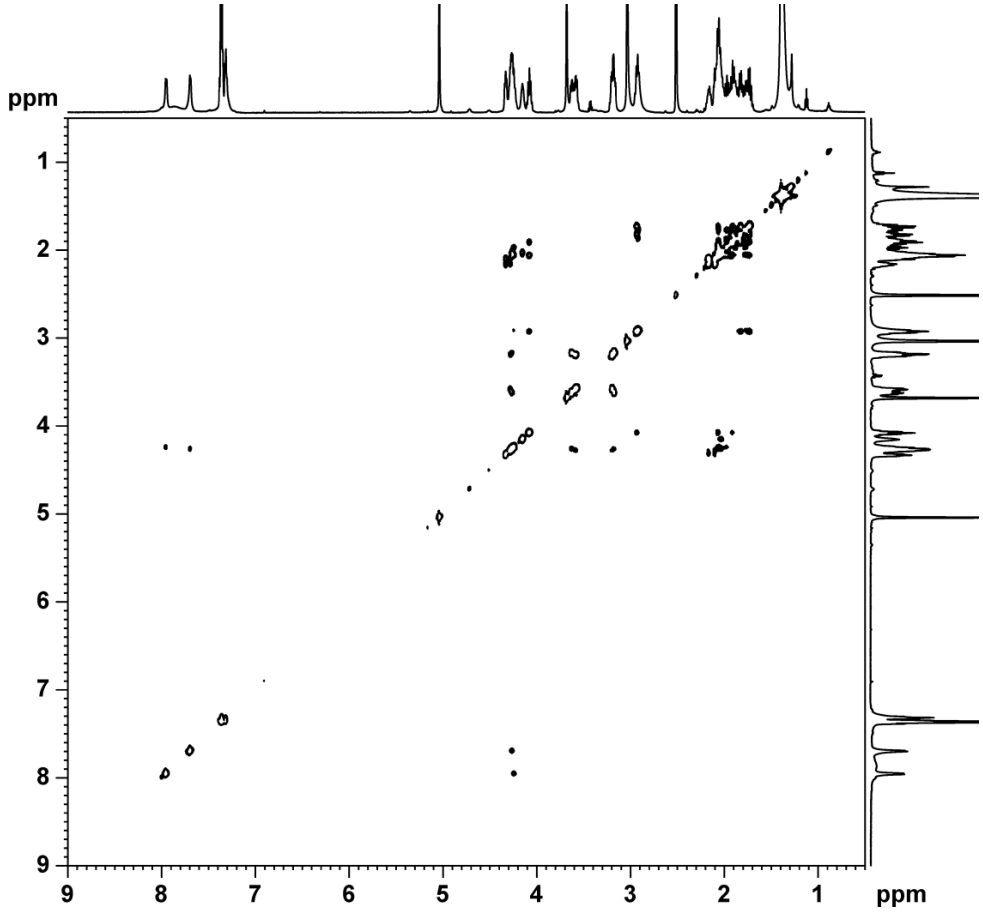

Multiplicity Edited HSQC

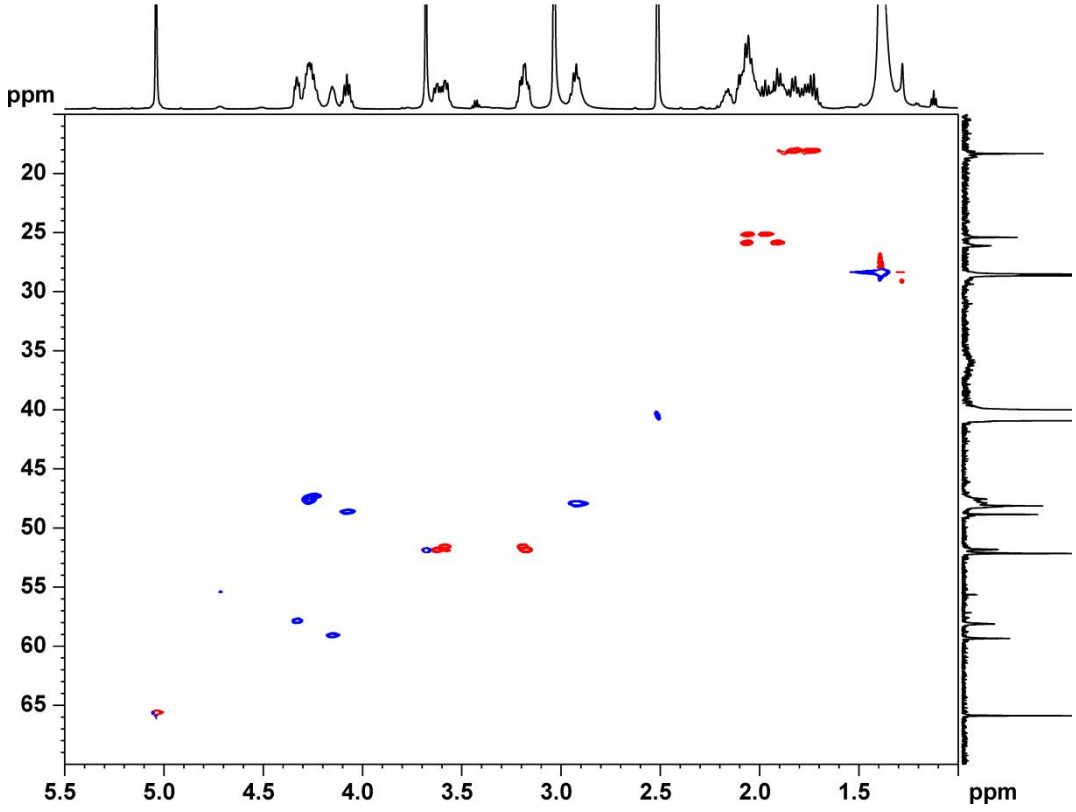

Comparison of N*H* signals region in the $^{1}H/^{15}N$-HSQC spectra (600 MHz, DMSO-d_6, 358 K) of tetrapeptides 34, 36, 38 and 40

CC: β-*cis*,γ-*cis*-**34**; **CT**: β-*cis*,γ-*trans*-**36**; **TC**: β-*trans*,γ-*cis*-**38**; **TT**: β-*trans*,γ-*trans*-**40**

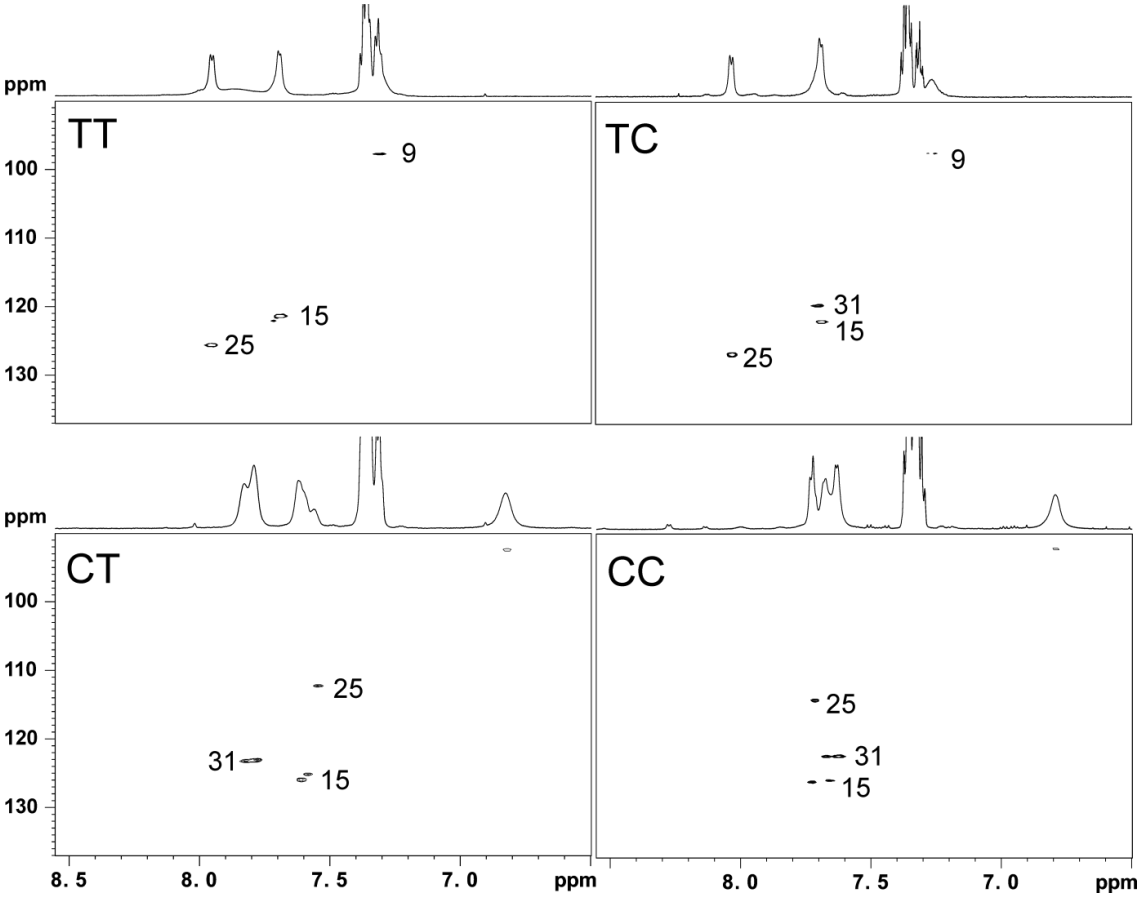

γ-*cis*,γ-*cis*, 41

^{1}H-NMR (600 MHz, $CDCl_3$, 298 K)

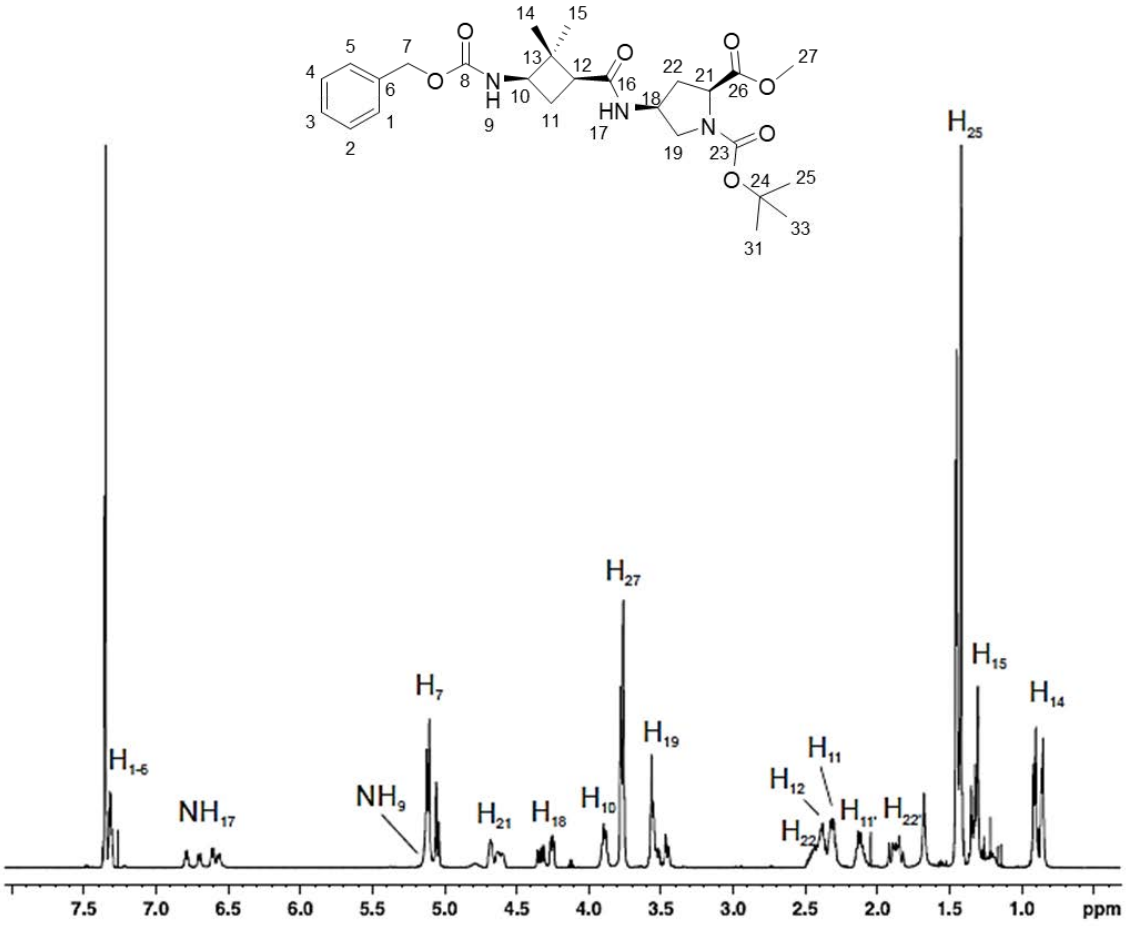

^{1}H-NMR and SELTOCSY (600 MHz, $CDCl_3$, 273 K)

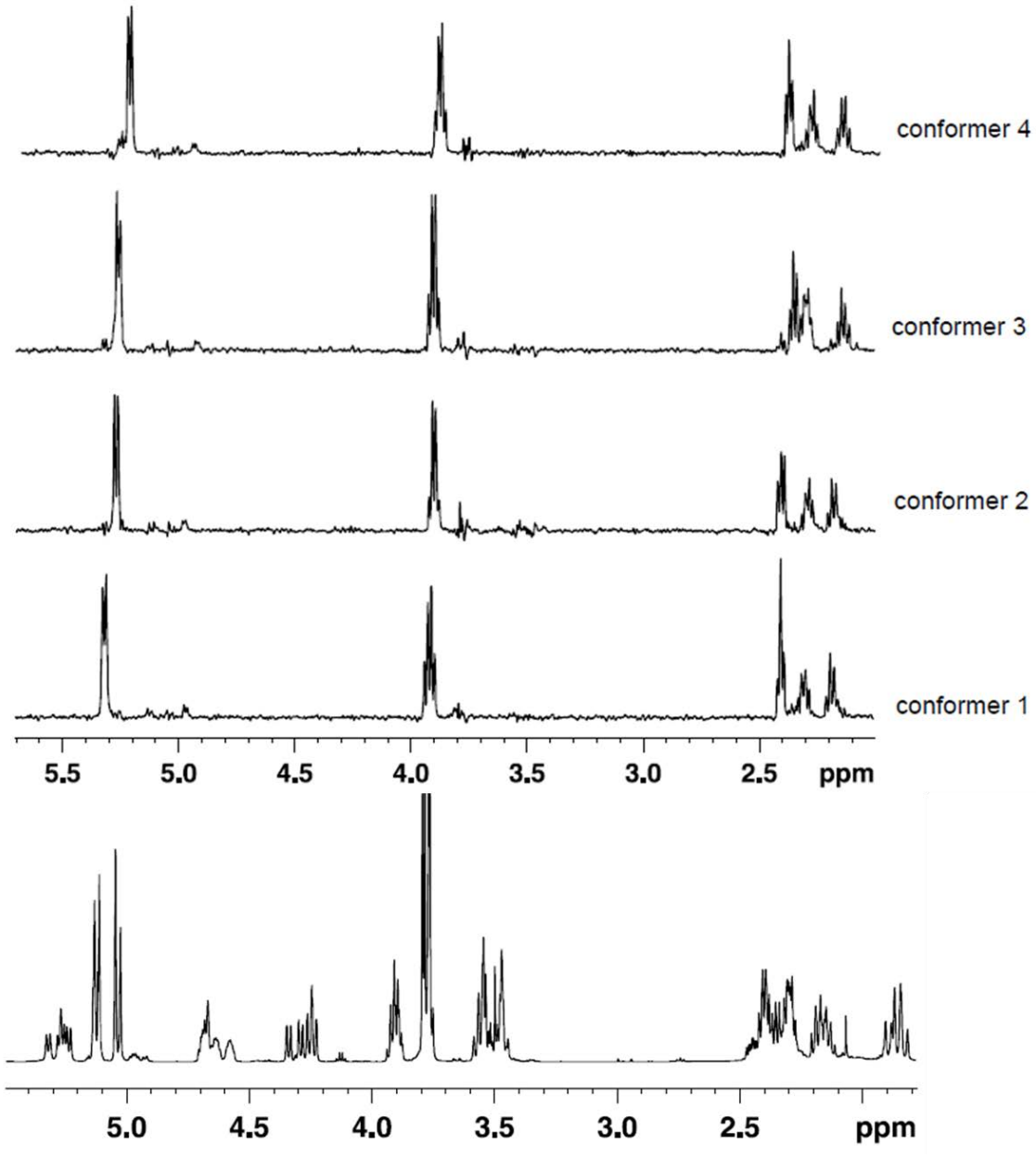

^{13}C-NMR (150 MHz, $CDCl_3$, 298 K)

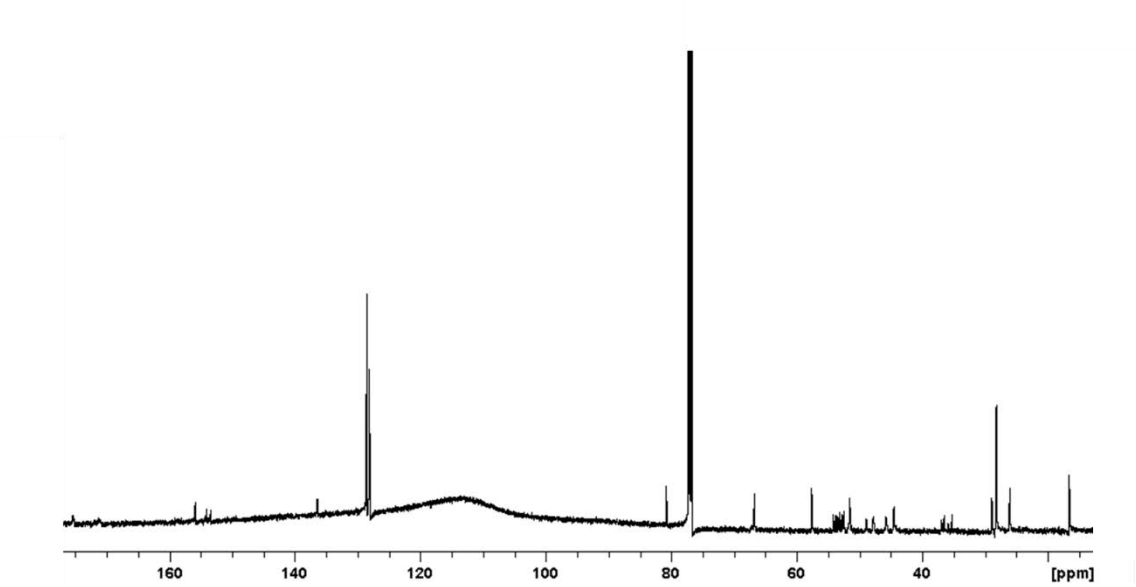

Multiplicity Edited HSQC (600 MHz, $CDCl_3$, 298 K)

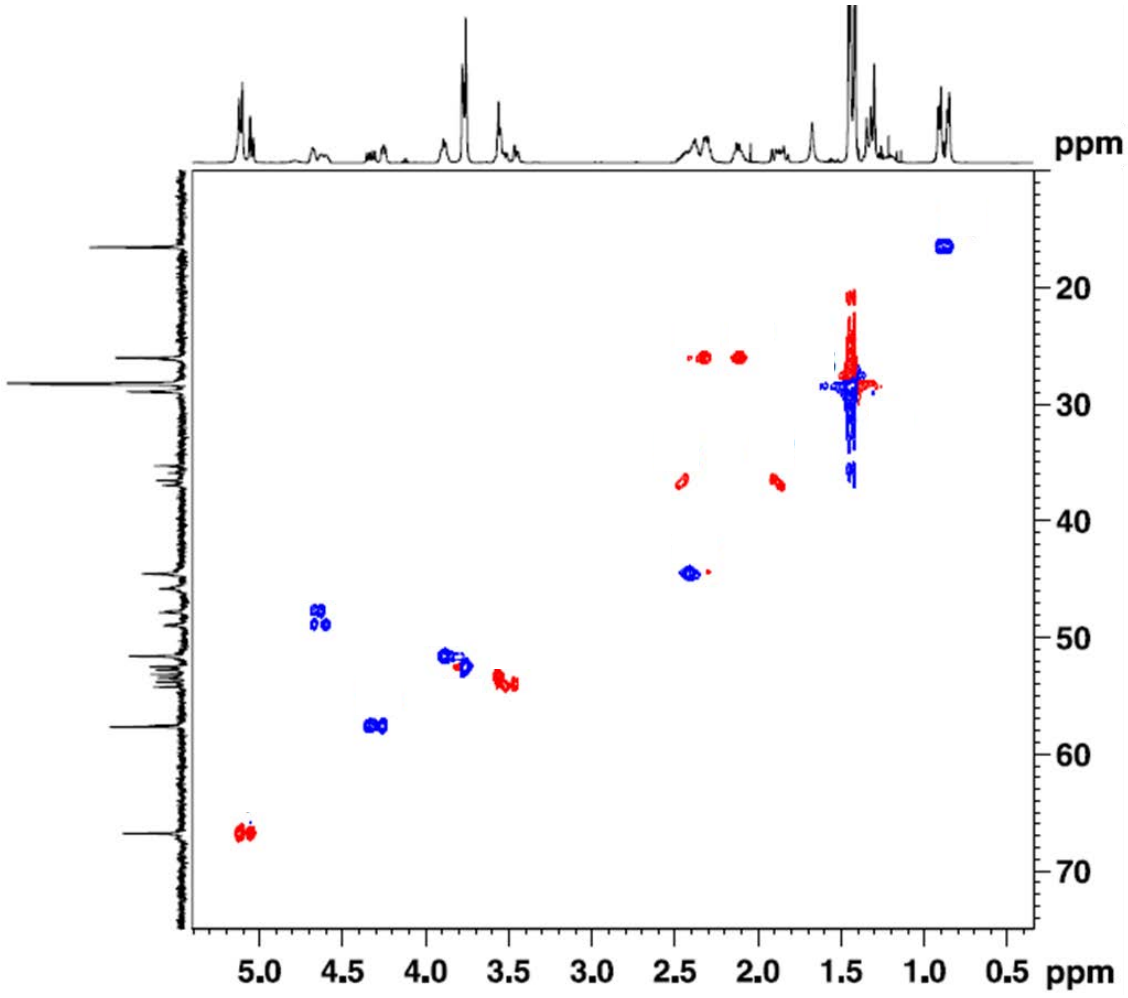

γ-*cis*,γ-*trans*, 42

^{1}H-NMR (600 MHz, $CDCl_3$, 298 K)

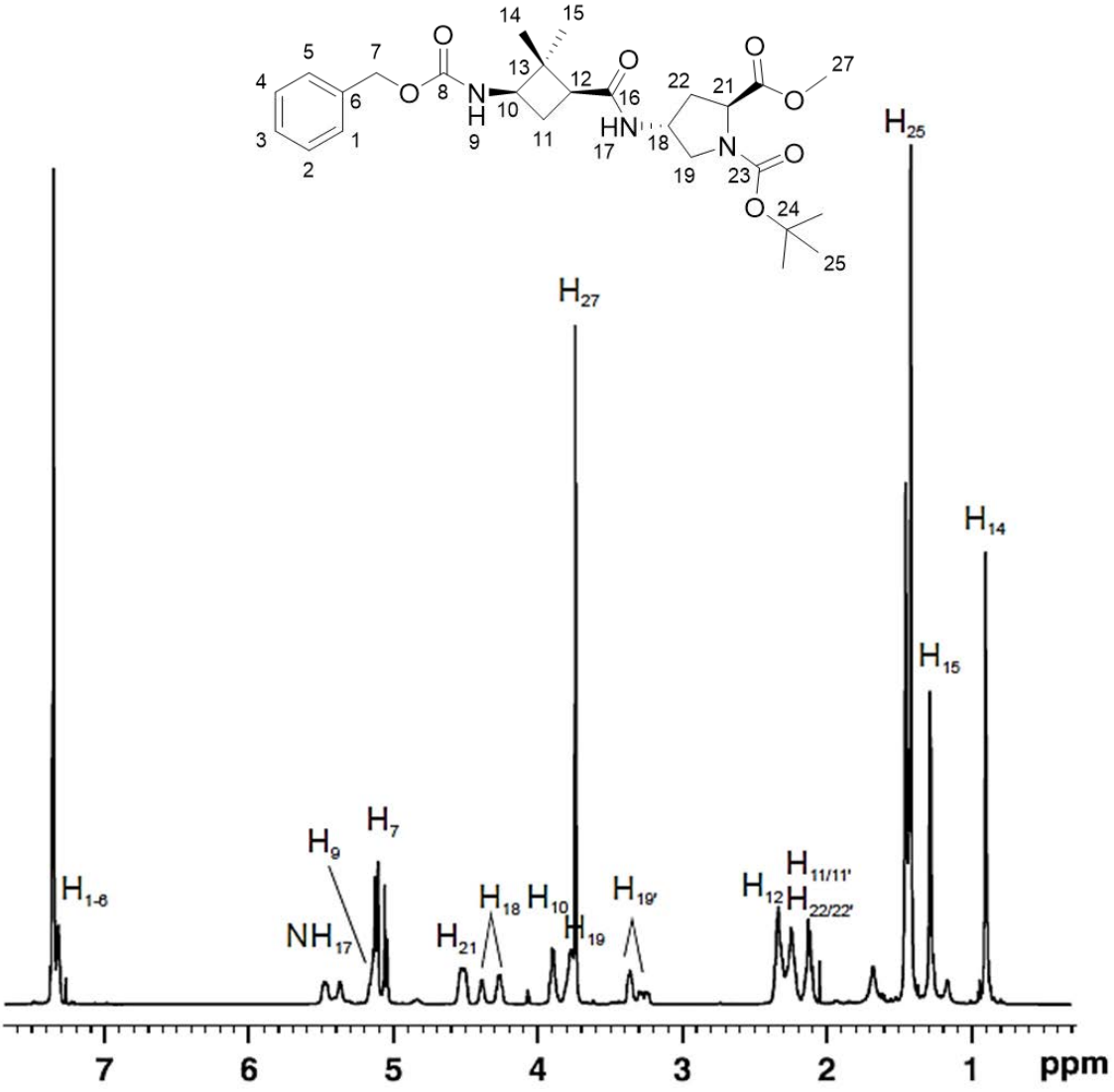

^{13}C-NMR (150 MHz, $CDCl_3$, 298 K)

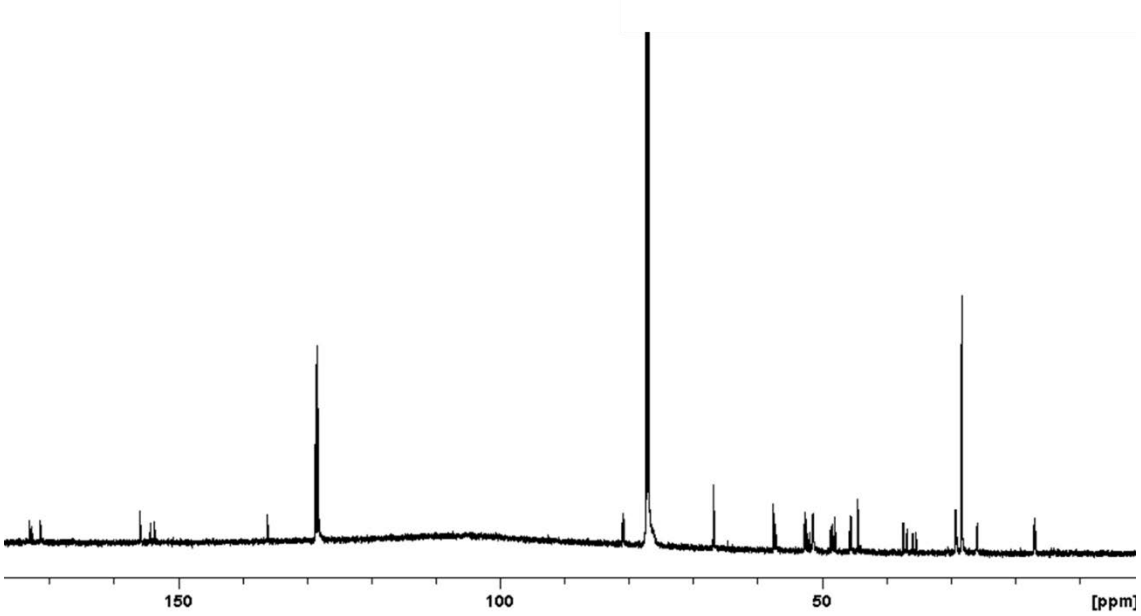

Multiplicity Edited HSQC (600 MHz, $CDCl_3$, 298 K)

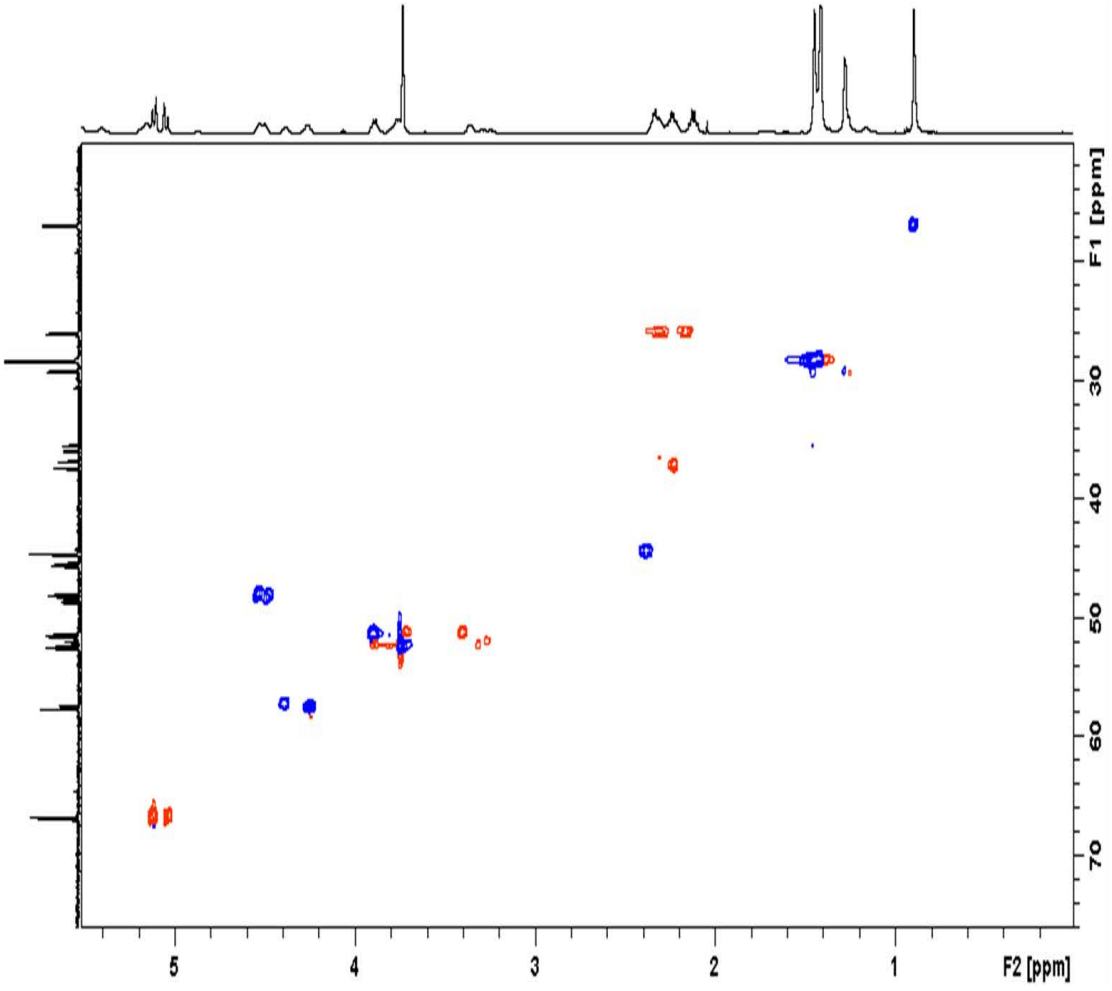

NMR spectra for the characterization of L3 and its precursors

Compound 123

^{1}H-NMR (400 MHz, $CDCl_3$, 298 K)

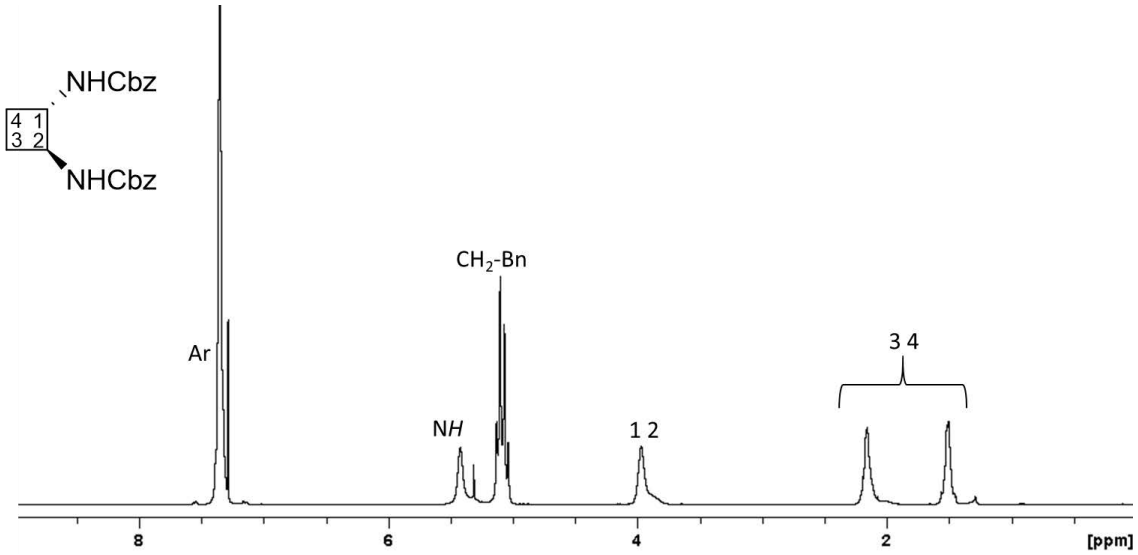

^{13}C-NMR (100 MHz, $CDCl_3$, 298 K)

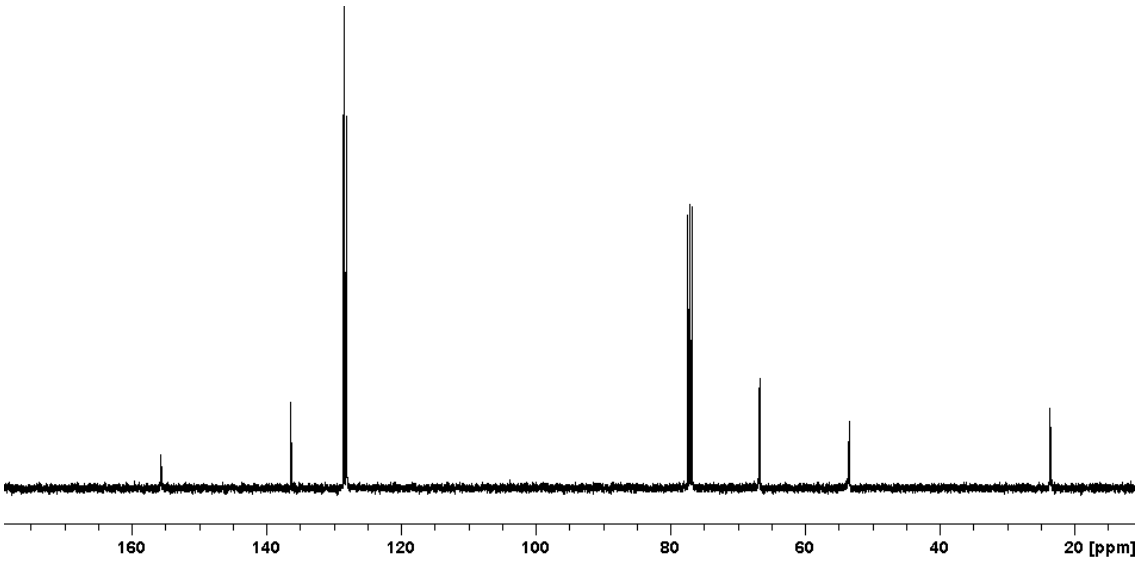

Compound 125

^{1}H-NMR (400 MHz, $CDCl_3$, 298 K)

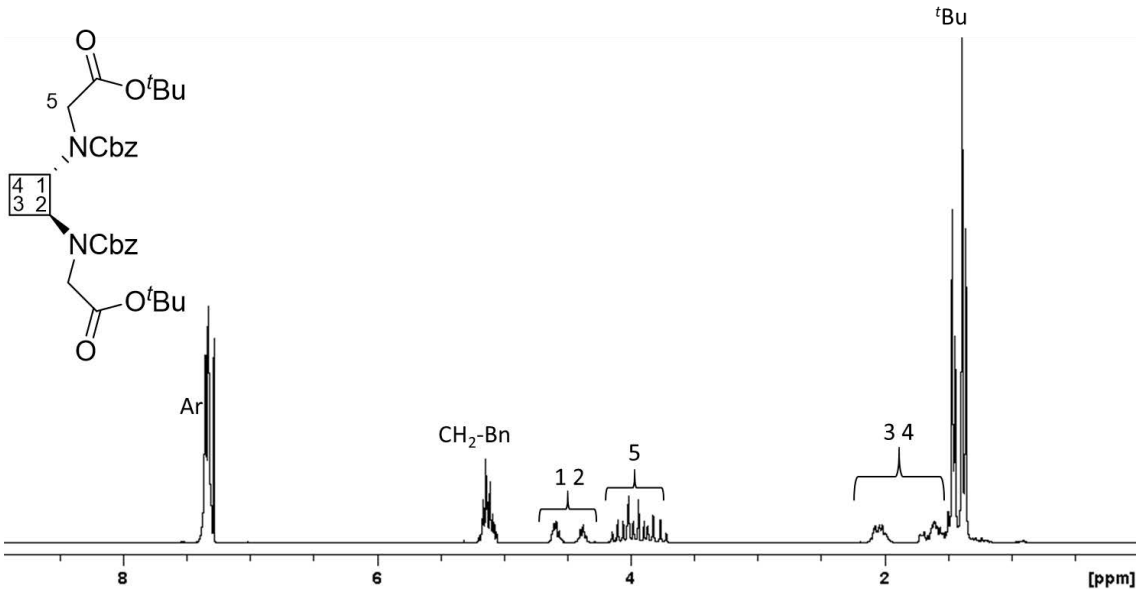

^{13}C-NMR (100 MHz, $CDCl_3$, 298 K)

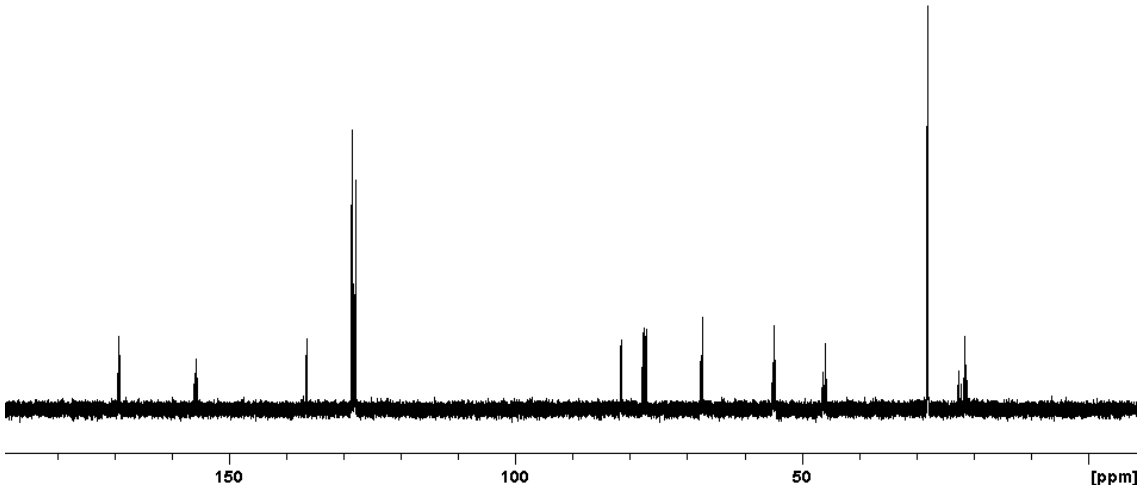

Multiplicity Edited HSQC (400 MHz, $CDCl_3$, 298 K)

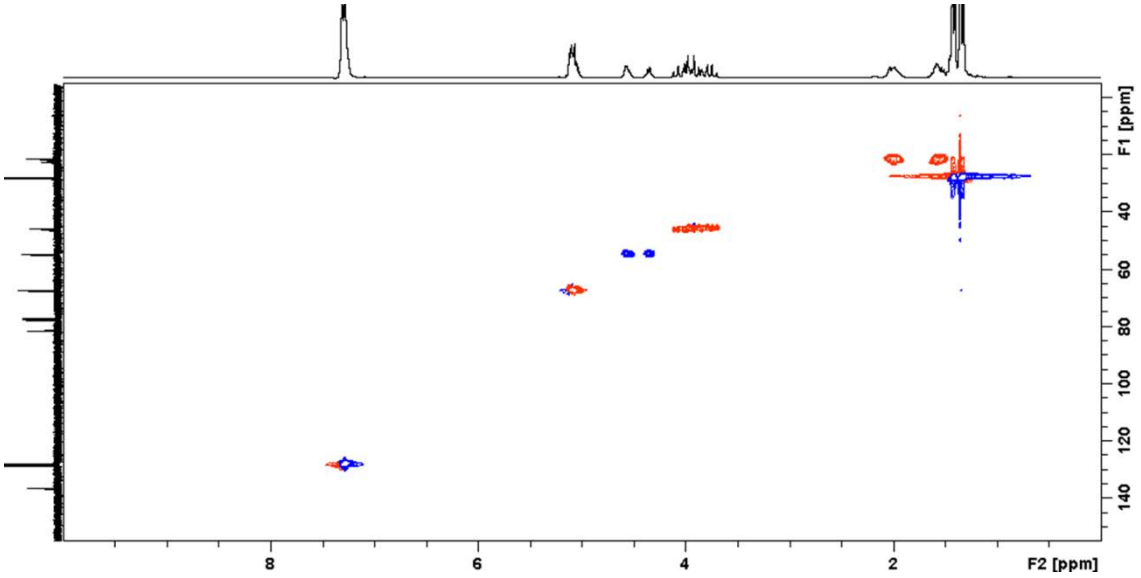

Compound 126

^{1}H-NMR (360 MHz, $CDCl_3$, 298 K)

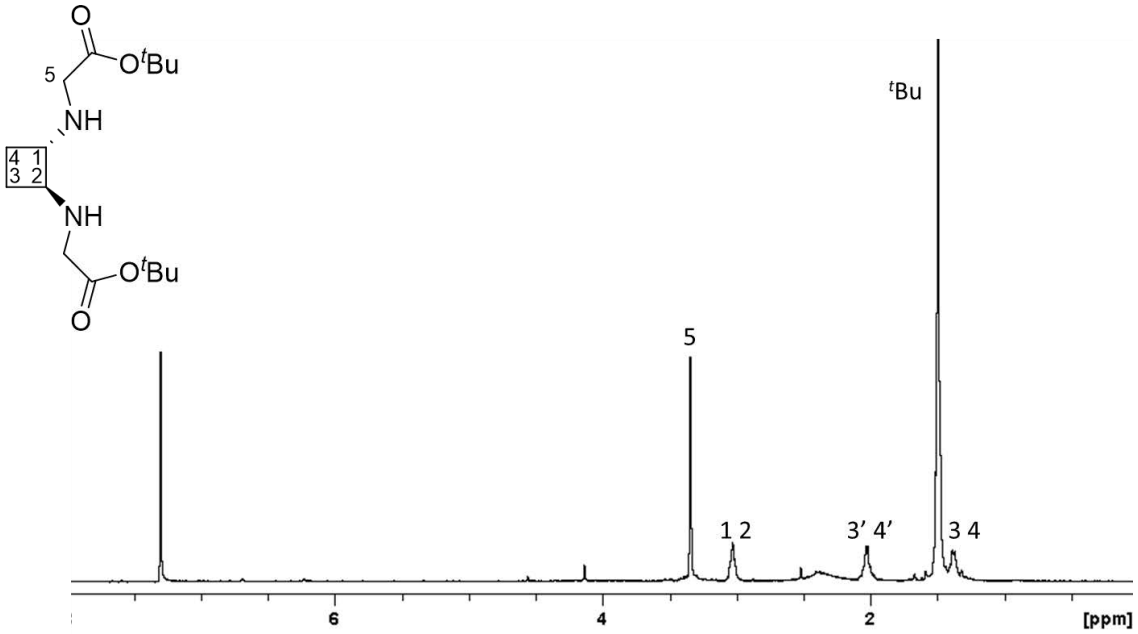

^{13}C-NMR (62.5 MHz, $CDCl_3$, 298 K)

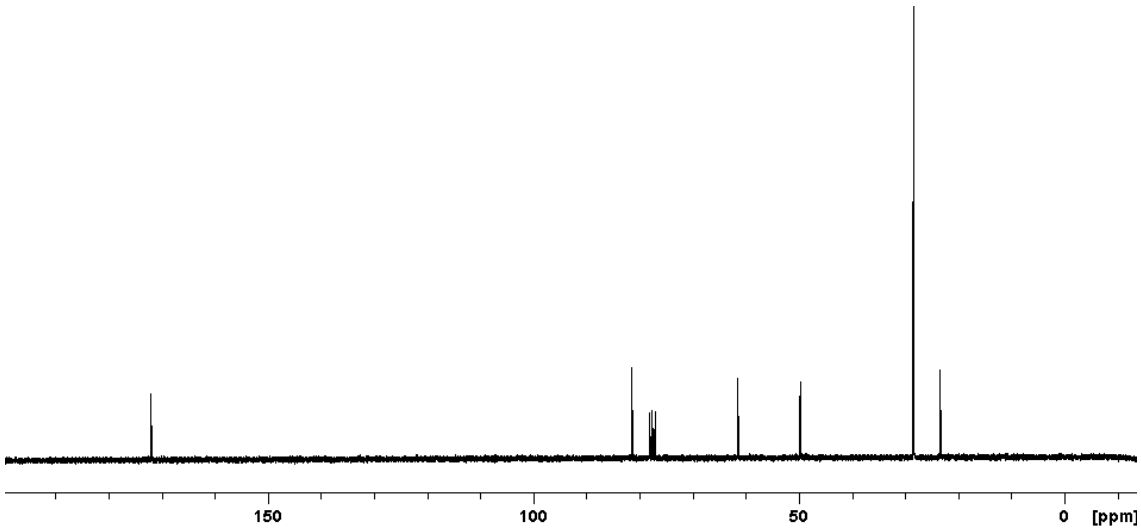

Compound 127

^{1}H-NMR (360 MHz, $CDCl_3$, 298 K)

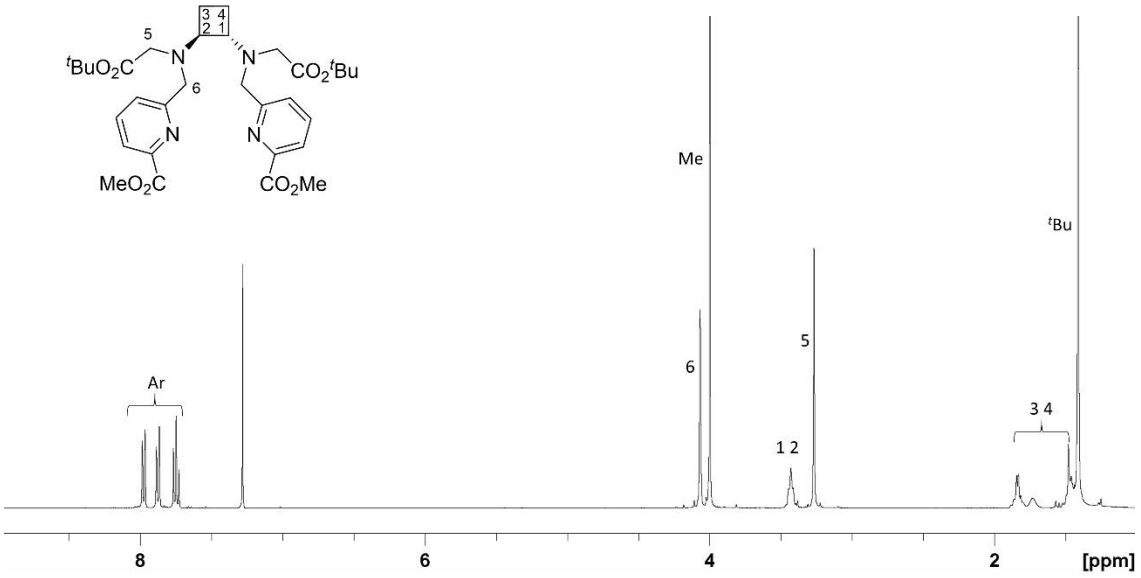

^{13}C-NMR (90 MHz, $CDCl_3$, 298 K)

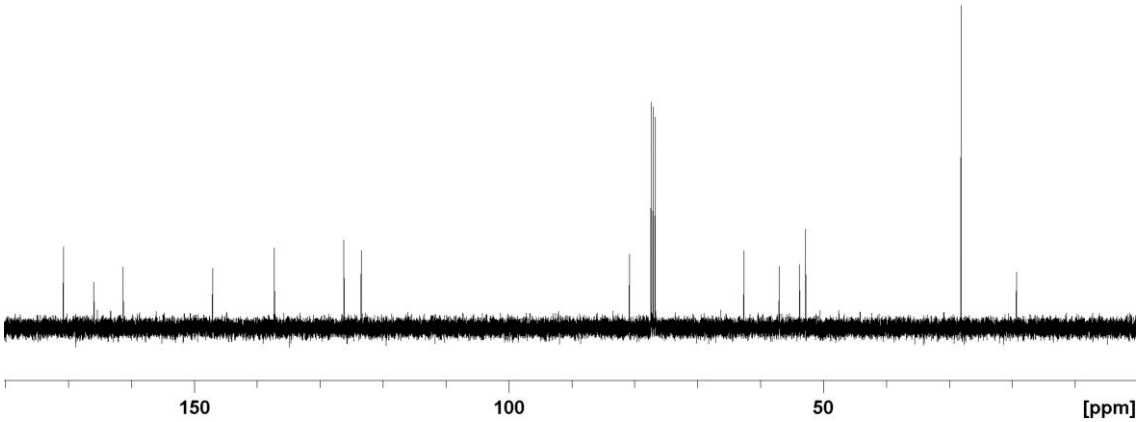

Multiplicity Edited HSQC (360 MHz, $CDCl_3$, 298 K)

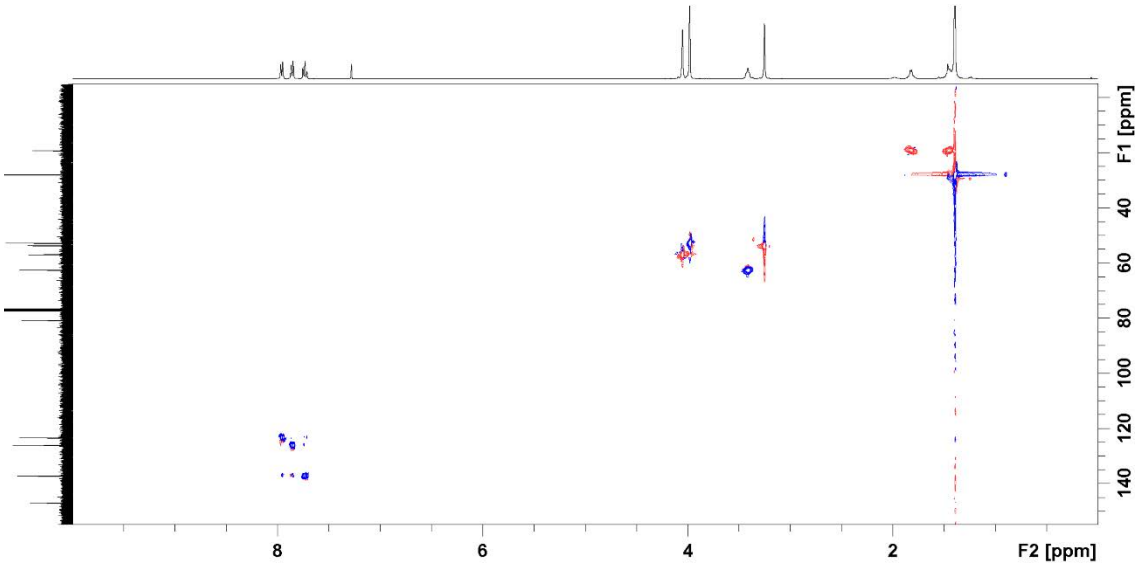

L3

^{1}H-NMR (360 MHz, D_2O, 298 K)

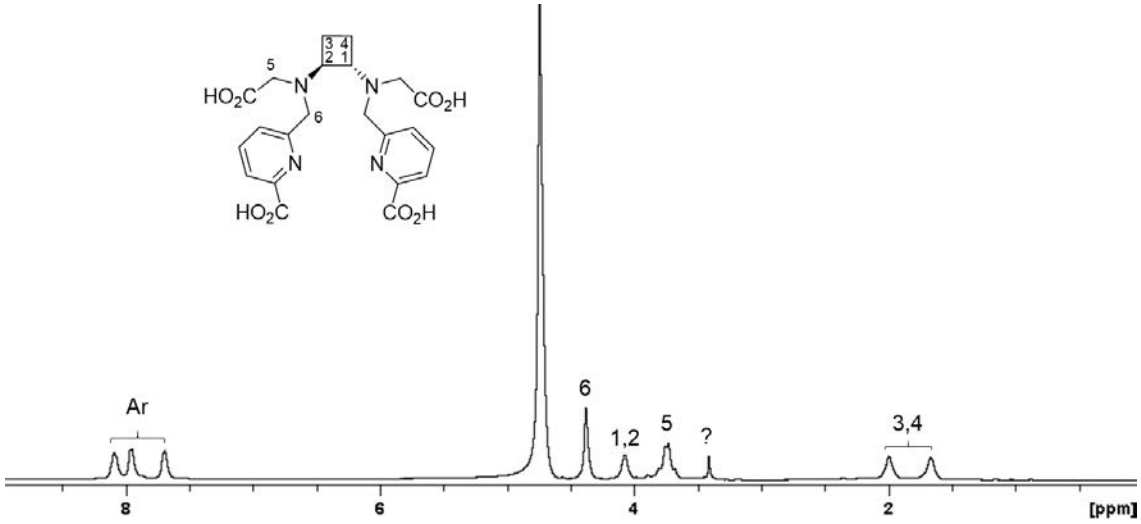

^{13}C-NMR (90 MHz, D_2O, 298 K)

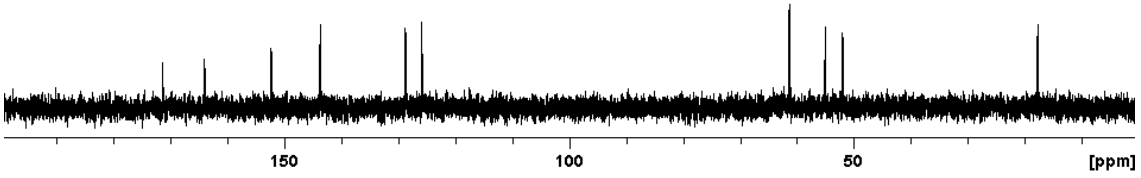

Multiplicity Edited HSQC (360 MHz, D_2O, 298 K)